NUI MAYNOOTH

Ollscoil na hÉireann Má Nuad

Optimal control of wave energy converters

Giorgio Bacelli

A thesis submitted to the National University of Ireland for the degree of
Doctor of Philosophy

in the
Faculty of Science and Engineering
Electronic Engineering Department

Supervisor: Prof. John V. Ringwood
Head of Department: Dr. Ronan Farrell

February 2014

Table of Contents

Abstract

Wave Energy Converters (WECs) are devices designed to absorb energy from ocean waves. The particular type of Wave Energy Converter (WEC) considered in this thesis is an oscillating body; energy conversion is carried out by means of a structure immersed in water which oscillates under forces exerted by waves. This thesis addresses the control of oscillating body WECs and the objective of the control system is to optimise the motion of the devices that maximises the energy absorption. In particular, this thesis presents the formulation of the optimal control problem for WECs in the framework of direct transcription methods, known as spectral and pseudospectral optimal control. Direct transcription methods transform continuous time optimal control problems into Non Linear Programming (NLP) problems, for which the literature (and the market) offer a large number of standard algorithms (and software packages). It is shown, in this thesis, that direct transcription gives the possibility of formulating complex control problems where realistic scenarios can be taken into account, such as physical limitations and nonlinearities in the behaviour of the devices. Additionally, by means of spectral and pseudospectral methods, it is possible to find an approximation of the optimal solution *directly* from sampled frequency and impulse response models of the radiation forces, obviating the need for finite order approximate models. By implementing a spectral method, convexity of the NLP problem, associated with the optimal control problem for a single body WEC described by a linear model, is demonstrated analytically. The solution to a nonlinear optimal control problem is approximated by means of pseudospectral optimal control. In the nonlinear case, simulation results show a significant difference in the optimal behaviour of the device, both in the motion and in the energy absorption, when the quadratic term describing the viscous forces are dominant, compared to the linear case. This thesis also considers the comparison of two control strategies for arrays of WECs. A Global Control strategy computes the optimal motion by taking into account the complete model of the array and it provides the global optimum for the absorbed energy. In contrast, an Independent Control strategy implements a control system on *each* device which is independent from all the other devices. The final part of the thesis illustrates an approach for the study of the effects of constraints on the total absorbed energy. The procedure allows the feasibility of the constrained energy maximisation problem to be studied, and it provides an intuitive framework for the design of WECs relating to the power take-off operating envelope, thanks to the geometrical interpretation of the functions describing both the total absorbed energy and the constraints.

Declaration of authorship

I, Giorgio Bacelli, declare that this thesis titled 'Optimal control of wave energy converters' and the work presented in it are my own. I confirm that:

- This work was done wholly or mainly while in candidature for a research degree at this University.
- Where any part of this thesis has previously been submitted for a degree or any other qualification at this University or any other institution, this has been clearly stated.
- Where I have consulted the published work of others, this is always clearly attributed.
- Where I have quoted from the work of others, the source is always given. With the exception of such quotations, this thesis is entirely my own work.
- I have acknowledged all main sources of help.
- Where the thesis is based on work done by myself jointly with others, I have made clear exactly what was done by others and what I have contributed myself.

Signed: _____ Date: _____

Acknowledgment

I would like to express my most sincere gratitude to my supervisor Professor John Ringwood for the opportunity he gave me to engage in postgraduate studies and for his continuous support and advice. I would like to thank the administrative, technical and academic staff of the Electronic Engineering Department and, in particular, the past and present members of the wave energy research group: Ronan, Iain, Tom, Simone, Andrej, Josh, Davide, Paula, Francesco P., Marco, Francesco F., Jochem, Philip, Jan and Jean-Christophe. I would also like to thank my colleagues and friends with whom I have shared office and time during my studies in Maynooth: Tue, Paul, Ken, Niall, Gary, Violeta, Shane B. and Shane L. .

Finally, I would like to thank my parents and my sister for their patience and support.

Acronyms

PTO Power Take Off

WEC Wave Energy Converter

DoF Degrees of Freedom

AWS Archimedes Wave Swing

ODE Ordinary Differential Equation

MPC Model Predictive Control

IDE Integro-Differential Equation

PMP Pontryagin's Minimum Principle

NLP Non Linear Programming

GC Global Control

IC Independent Control

List of symbols

A general convention adopted in this thesis is the use of the italic font style for variables (e.g. velocity and force) and the roman font style for parameters and constants (mass, hydrostatic restoring coefficient). Additionally, bold font style is used for multidimensional variables, such as matrices (e.g. radiation impedance matrix) and vectors (e.g state vector of dynamical system).

Symbol	**Description**
$\mathbf{M}$	Mass matrix
$\mathbf{B}$	Matrix of linear damping coefficients
$\mathbf{S}$	Matrix of hydrostatic restoring coefficients
$\mathbf{Z}(\omega)$	Radiation impedance matrix
$\mathbf{R}(\omega)$	Radiation resistance
$\mathbf{X}(\omega)$	Radiation reactance
$\mathbf{m}(\omega)$	Added mass
$\mathbf{m}_\infty$	Asymptotic value of the added mass for $\omega \rightarrow \infty$
$\mathbf{H}(\omega)$	Vector of the excitation force coefficient
$\mathbf{K}(t)$	Matrix of the radiation impulse responses
$\mathbf{h}(t)$	Vector of the excitation impulse responses
$\boldsymbol{f}_e$	Excitation force (vector)
$\boldsymbol{f}_r$	Radiation force (vector)
$\boldsymbol{f}_{pto}$	Power Take Off force (vector)
$\boldsymbol{F}(\omega)$	Fourier transform of the force vector $\boldsymbol{f}(t)$
ζ	Wave elevation
$\boldsymbol{\eta}$	Position (vector) of a rigid body $\boldsymbol{\eta} = [x, y, z, \varphi, \theta, \psi]^T$
$\boldsymbol{v}$	Velocity (vector) of a rigid body $\boldsymbol{v} = \dot{\boldsymbol{\eta}}$
$\boldsymbol{P}$	Power
$\boldsymbol{x}$	State variable of a dynamical system ($\dot{\boldsymbol{x}} = f(\boldsymbol{x}, \boldsymbol{u}, t)$)
$\boldsymbol{u}$	Control input

x_i	i-th state variable
x_i^N	Approximated i-th state variable ($x_i \approx x_i^N = \Phi(t)\,\hat{\boldsymbol{x}}_i$)
$\hat{\boldsymbol{x}}_i$	Vector of coefficients for the approximation of the i-th state variable
$\Phi(t)$	Vector of basis functions used for the approximation of the state variables: $\Phi(t) = \left[\phi_1(t), \phi_2(t), \ldots, \phi_N(t)\right]$
$\hat{\boldsymbol{u}}_i$	Vector of coefficients for the approximation of the i-th control input
D_ϕ	Differentiation matrix
$\mathbf{F}_P$	Power Take Off configuration matrix

"The deep structure of change is decay. What decays is not the quantity but the quality of energy. I shall explain what is meant by high quality energy, but for the present think of it as energy that is localized, and potent to effect change. In the course of causing change it spreads, becomes chaotically distributed like a fallen house of cards, and loses its initial potency. Energy's quality, but not its quantity, decays as it spreads in chaos.

Harnessing the decay results not only in civilizations but in all the events in the world and the universe beyond. It accounts for all discernible change, both animate and inanimate. The quality of energy is like a slowly unwinding spring. The quality spontaneously declines and the spring of the universe unwinds. The quality spontaneously degrades, and the spontaneity of the degradation drives the interdependent processes webbed around and within us, as through the interlocked gear wheels of a sophisticated machine. Such is the complexity of the interlocking that here and there chaos may temporarily recede and quality flare up, as when cathedrals are built and symphonies are performed. But these are temporary and local deceits, for deeper in the world the spring inescapably unwinds. Every thing is driven by decay. Everything is driven by motiveless, purposeless decay.

As we have said, by 'quality' of energy is meant the extent of its dispersal. High-quality, useful energy, is localized energy. Low quality, wasted energy, is chaotically diffuse energy. Things can get done when energy is localized; but energy loses its potency to motivate change when it has become dispersed. The degradation of quality is chaotic dispersal.

I shall now argue that such dispersal is ultimately natural, motiveless, and purposeless. It occurs naturally and spontaneously, and when it occurs it causes change. When it is precipitate it destroys. When it is geared through chains of events it can produce civilizations."

Peter Atkins [1]

Chapter 1

Introduction

Availability of energy supplies is undoubtedly one of the most critical priorities for the functioning of a modern economy. Fossil fuels have played the central role in the energy supply since the era of industrial revolution because of their favourable properties, among which are the high energy density (energy per unit volume), the fact that they can be easily stored and distributed, and that, up until recently, they have been relatively cheap to extract. However, in the last few decades, countries have been putting large efforts into the diversification of their energy supply chains with the objective of strengthening their energy security. Renewable energy is a key factor in the diversification of the energy supply chain, and some technologies, e.g. wind and solar power, have reached commercial maturity. Wave energy conversion, on the other hand, has not arrived at being commercially viable yet, although several companies have developed advanced prototypes and pre-commercial demonstration devices.

One of the reasons for the slower pace at which research in wave energy conversion is moving, compared to wind and solar, is due to the nature of the source itself. In fact, waves are generated by wind flowing on the water surface; wind, in turn, is generated by the atmospheric pressure differential caused by the radiation from the sun. The transformation of energy from solar radiation into waves results in a significant increase of the energy density, as the amount of wave energy per square meter on the surface of the ocean can be one order of magnitude larger than the amount of solar energy on the same area. The benefit of a higher energy density, however, is also associated with the necessity to build more robust devices, that can withstand

the harshness of the sea environment. Additionally, the largest amount of resources are often available in remote areas and far away form the coast, causing large cost of installation (e.g. moorings and submarine power transmission cables), and operation and maintenance.

A number of concept devices for wave energy conversion are being studied and developed (see [2], [3], [4] for reviews), and they can be grouped into three main categories based on their conversion principle: oscillating bodies, oscillating water columns and overtopping devices. Oscillating body WECs absorb energy carried by waves through the mechanical work done by the force that waves exert on a structure immersed in the water. The oscillating nature of waves induces an alternating motion on the structure; part of the kinetic energy associated with its motion is then recovered by applying an external force to the oscillating body, usually by means of electrical or hydraulic machinery. The part of the WEC which exerts this external force is known as the Power Take Off (PTO). Oscillating water column WECs use air as the working medium for conversion of energy: in particular, the oscillating motion of water compresses air enclosed in a chamber. Compressed air then flows through a turbine which can be connected directly to an electrical generator. The conversion principle of overtopping WECs exploits the hydraulic head between a reservoir and the mean water level. The reservoir is filled by waves propagating up a ramp leading into the reservoir itself, and electricity is generated by low head water turbines activated by the water flowing from the reservoir back to the sea.

In summary, this thesis focuses only on oscillating body WECs. Specifically, it presents a method for the optimal control of this type of devices, where for optimal control it is intended the calculation of the force generated by the PTO which maximises a given criteria.

1.1 Motivation

Oscillating body WECs absorb energy by means of the mechanical work done by the wave forces on the oscillating structure, and because of the oscillation, there is a continuous exchange between kinetic and potential energy within the oscillating body. The PTO, by applying a force on the body, does mechanical work, thus it converts part of the kinetic energy into a different form, such as electricity. The control system influences the wave energy conversion process by acting on the PTO force. Ideally, in the simplest situation, the controller would be designed with the sole objective of maximising the energy absorption, although in practice other requirements should often be considered, as will be discussed in chapter 3.

Theoretical results regarding the optimal control which maximises the energy absorption are common knowledge in the wave energy community [5]; however, in many situations, they are not applicable because the control law is not causal and the resulting motion and forces are well beyond the physical limitations of the device. Moreover, since the optimal control law is formulated in the frequency domain, the inclusion of the physical limitations of the device

(constraints) in the formulation of the optimal control problem is not straightforward. Time domain techniques allow the inclusion of constraints in the formulation of the control problem, and chapter 3 of this thesis shows that they have been implemented in a variety of forms.

Independently of the domain where the control problem is formulated, the quality of the results depend on the accuracy of the model used for the calculation of the control signal. The model of a WEC includes a part describing the interaction between the fluid (water) and the oscillating body, which is generally obtained by means of laboratory experiments or hydrodynamic software. Both solutions provide a description of the fluid-structure interaction with a set of data points in the frequency domain (frequency response) or in the time domain (impulse response). Although both sampled frequency responses and sampled impulse responses can be used for the simulation of the behaviour of a device, these forms are not the most convenient for the design of a control system. To obviate this issue, it is a common approach to fit the sampled responses with parametric models by performing system identification [6] to obtain transfer functions or linear state space models [7], [8], which can then be used to implement standard control techniques available in the literature.

When the WEC is allowed to oscillate in several Degrees of Freedom (DoF) or when a number of interacting WECs are considered, system identification has to be carried out (in the worst case) for each oscillating mode, and for all the combinations between any two oscillating modes[1], a task that can be tedious and prone to mistakes if the number of oscillating modes/devices is large. Although the procedure could be automated, the fitting errors may be non-negligible for some complex geometries and, in some cases, by increasing the order of the model in the attempt to improve the fitting, system identification may produce unstable models.

The issue introduced by the need for system identification is particularly critical when the control law design has to be implemented within a WEC optimisation loop. At present, in fact, significant effort in the wave energy research community is focussed on the studies to select the *best* device concepts [9]. Among the many factors that will influence the economic success of a WEC, the amount of absorbed energy is clearly one of the most important, although not the only one. The absorbed energy depends on the PTO force, the optimal value of which is calculated by the control system. Furthermore, the control law depends on the model of the WEC which, in turns, depends on the shape of the device because the fluid-body interaction depends on the geometry of the submerged structure of the WEC. Thus, since the study of the *best* WEC concepts also involves the shape of the device, the implementation of a control-informed geometric optimisation of a WEC as in [10] requires the online implementation of the control algorithm.

An additional motivation for the research presented in in this thesis is that most studies,

[1] i.e., when symmetry cannot be exploited, system identification has to be carried out $n + n(n-1)/2$ times, where n is the number of oscillating modes of each device multiplied by the number of devices.

academic and commercial, focus on the use of linear WEC's models; their appeal is mainly due to the possibility of developing analytical solutions for the control problems and analysis of performance [5]. However, a variety of effects introduce nonlinearities in the model of WECs, from the PTO [11], [12] to the fluid-body interactions. While it is often reasonable to assume a linear approximation for the radiation [13], some studies have shown the wide disparity between linear and nonlinear models of excitation forces [14], viscous forces [15] and hydrostatic restoring forces [16]. Although some work has already been presented for the nonlinear optimal control of WECs [17], [18], [19], in all cases the control strategy either relies on a linear state space model for the fluid-body interaction [17], [18] or introduces a significant approximation by considering the fluid-body interaction being frequency-independent [19].

1.2 Objectives

If the main objective of the control problem of a WEC is defined as the maximisation of the energy absorbed by the device, then the control problem can be formulated within the framework of optimal control. The optimal control of a WEC can be solved analytically only for special cases, such as when the WEC's model is linear and constraints are not being considered.

For more complex control problems, which cannot be solved analytically, the literature indicates two general approaches for the approximation of the optimal solution [20]: indirect transcription and direct transcription. The indirect transcription consists of formulating the necessary conditions for optimality (for example by applying Pontryagin's Minimum Principle (PMP)), and then solve numerically the resulting two-point boundary value problem, as described for example in [21] by Eidsmoen. The direct transcription method, on the other hand, consists of transforming the optimal control problem into a finite dimensional optimisation problem, by approximating the state and control variables with linear combinations of "simple" functions.

The main objective of this thesis is to formulate the direct transcription of the optimal control problem (energy maximisation) of a generic WEC directly using the sampled frequency or impulse responses describing the fluid-body interactions, thus obviating the need for system identification. A further objective of this thesis is to demonstrate how the direct transcription approach for the optimal control of WECs can be applied to several types of device, including devices composed of multiple bodies, arrays of WECs and devices described by nonlinear models.

1.3 Contributions

1. The primary contribution of this thesis is the formulation of the optimal control problem of WECs in the framework of the direct transcription methods known as spectral and pseudospectral optimal control. Direct transcription methods transform a continuous time optimal control problem into a NLP problem, the solution of which approximates the solution of the original optimal control problem. In this thesis it is shown that:

   - Direct transcription allows approximated solutions to difficult optimal control problems describing realistic situations to be found, where nonlinearities and physical limitations (constraints) of WECs' components are also taken into account.
   - The proposed direct transcription methods can be implemented directly from the impulse (or frequency) response models describing the fluid-body interaction, thus obviating the need for the identification of finite order approximations.
   - Thanks to the good approximating properties of both spectral and pseudospectral methods, the NLP problem resulting from the direct transcription is relatively small in both dimension and computational load, making the approach presented in this thesis a suitable candidate for the real-time control of WECs.
   - The modularity of the framework allows the same formulation of the control problems to be seamlessly applied to a number of multi body/multi WEC configurations

2. A further contribution of this thesis is the comparison of two antithetical strategies for the control of arrays of WECs, namely Global Control (GC) and Independent Control (IC). The GC strategy consists of the calculation of the optimal control law based on the complete model of the array, whereas the IC strategy calculates the control law neglecting the interaction between the devices composing the array. The comparison helps the designer to make an informed decision regarding the best approach for the control of the array, with respect to a number of factors, among which are the array layout, the device geometry, the wave climate and the restrictions on the device motion and forces.

3. Finally, a method for the feasibility analysis of the constrained optimal control is also presented. The approach is based on the spectral method, and it provides a geometrical interpretation of the equations describing the absorbed energy and constraints on the PTO force and oscillation amplitude. In some special cases, the procedure allows the study of the sensitivity of the absorbed energy with respect to the force and position constraints permitting its use as a design framework.

List of publications

Journal articles

- Bacelli, G. and Ringwood, J.V., "Constrained control of arrays of wave energy devices," *Int. Journal of Marine Energy*, Vol. 3–4, pp. e53–e69, Dec. 2013.
- Bacelli, G., Balitsky, P. and Ringwood, J.V., "Coordinated control of arrays of wave energy devices – benefits over independent control," *IEEE Trans. on Sustainable Energy*, Vol. 4, no. 4, pp. 1091–1099, Oct. 2013.
- Bacelli, G. and Ringwood, J.V., "A geometric tool for the analysis of position and force constraints in wave energy converters," *Ocean Engineering*, Vol. 65, pp. 10–18, June 2013.

Conference articles

- Bacelli, G. and Ringwood, J.V., "Constrained control of arrays of wave energy devices," In *Proc. 10th European Wave and Tidal Energy Conf. EWTEC2013*, Aalborg, DK, Sept. 2013.
- Westphalen, J., Bacelli, G., Balitsky, P. and Ringwood, J.V., "Control strategies for arrays of wave energy devices," In *Proc. 9th European Wave and Tidal Energy Conf. EWTEC2011*, Southampton, UK, Sept. 2011.
- Bacelli, G. and Ringwood, J.V., "A geometrical interpretation of force and position constraints in the optimal control of wave energy devices," In *Proc. 9th European Wave and Tidal Energy Conf. EWTEC2011*, Southampton, UK, Sept. 2011.
- Bacelli, G., Ringwood, J.V. and Gilloteaux, J.-C., "A control system for a self-reacting point absorber wave energy converter subject to constraints," In *Proc. 18th IFAC World Congr.*, Milan, IT, Aug./Sept. 2011.
- Bacelli, G., Ringwood, J.V. and Gilloteaux, J.-C., "Control of a wave energy device for potable water production," In *Proc. European Control Conf. ECC'09*, Budapest, HU, Aug. 2009.
- Bacelli, G., Gilloteaux, J.-C. and Ringwood, J.V., "State space model of a hydraulic power take off unit for wave energy conversion employing bondgraphs," In *Proc. World Renewable Energy Congr. WREC X*, Glasgow, UK, July 2008.

Accepted

- Bacelli, G. and Ringwood, J.V., "Nonlinear optimal wave energy converter control with application to a flap-type device," Submitted to *19th IFAC World Congr.*, Cape Town, ZA, Aug. 2014.

In preparation

- Bacelli, G. and Ringwood, J.V., "Pseudospectral nonlinear optimal control of wave energy converters with application to a flap-type device," Submitted to *IEEE Trans. on Sustainable Energy*.
- Bacelli, G. and Ringwood, J.V., "Numerical optimal control of wave energy converters," Submitted to *IEEE Trans. on Sustainable Energy*.

1.4 Organisation of the thesis

The thesis is composed of six additional chapters, the subjects of which are outlined in the following part of this section.

Chapter 2 summarises the background theory and fundamental results in wave energy conversion. The first part of the chapter provides a description of the structure of an oscillating body WEC, including the most common configurations and PTO units. The second part provides a concise overview of the derivation of the equations of motion of a generic oscillating body WEC, starting from the conservation of mass (continuity equation) and momentum (Navier-Stokes equation), with the additional purpose of illustrating the fundamental assumptions at the basis of linear wave theory, and its range of validity. The last part of the chapter covers the main results regarding energy transported by water waves and energy absorption by an oscillating body WEC.

Chapter 3 provides a literature survey covering the control of oscillating body WECs. The literature is organised into groups based on the type of control approach, starting from the classical results of reactive control, linear PTO damping and latching control, documented in sec.3.1–3.3, respectively. The description of the three control approaches is also integrated with numerical and graphical examples, in addition to a discussion about their advantages and limitations. Sections 3.5 and 3.6 review the control of constrained WECs and arrays of WECs, respectively. The last section of the chapter considers the literature that compares the different control strategies for WECs.

Chapter 4 provides the fundamental contribution of this thesis, which is the formulation of the optimal control problem of WECs in the framework of the direct transcription methods known as spectral and pseudospectral optimal control. The chapter is divided into three

main parts. The first part provides a concise overview of numerical optimal control, spanning the definition of a general continuous time optimal control problem to the enunciation of the fundamental results in the field of NLP, including also a brief description of the most common methods for both direct and indirect transcription of optimal control problems. The second part of the chapter focusses on the direct transcription of the absorbed energy maximisation problem of a generic WEC described by a linear model, and it also provides a numerical example of a heaving buoy WEC where the discretisation is carried out by means of a spectral method. The last part of the chapter illustrates the implementation of pseudospectral optimal control on a flap type WEC, the model of which includes a nonlinear term describing viscous forces.

In chapter 5, two strategies for the control of arrays of WECs are compared. Both strategies are based on spectral optimal control, although they are diametrically opposite in the control approach. The Global Control strategy is based on the complete knowledge of the (linear) hydrodynamic interactions between the devices composing the array for the calculation of the optimal control. In the Independent Control strategy, however, each WEC is controlled independently, and the control signal of each device is calculated by completely neglecting the inter-body hydrodynamic interactions. The comparison is carried out for a number of device geometries, array configurations and wave climates, also considering constraints on the PTO force and oscillation amplitude.

Chapter 6 illustrates a method for the feasibility analysis of the constrained energy maximisation problem. The approach is based on the geometrical interpretation of the equations describing the PTO force and position constraints, and of the energy absorbed by the WEC. The chapter also illustrates the application of the procedure by providing numerical examples concerning two types of WECs which highlight, by means of a visual feedback due to the geometrical interpretation, the interplay between the wave climate (excitation force) and the constraints, keeping in the background the energy absorbed by the WEC.

The thesis is concluded in chapter 7 with a summary and a discussion on the contributions and results, as well as a discussion on future work.

Chapter 2

Wave energy conversion: Background

> *"It is easy to make a device that will respond vigorously to the action of sea waves. Indeed it is quite hard to make one that will not. However the conversion of the slow, random, reversing energy flows with very high extreme values into phase-locked synchronous electricity with power quality acceptable to a utility network is very much harder."* Salter, Taylor and Caldwell [22]

Wave Energy Converters (WECs) interact with water waves to absorb part of the energy they transport. The interaction depends on the physical properties of the device as well as on its motion. This chapter describes the basic principles of the interaction between an oscillating body and water. The first part (section 2.1) provides a brief description of the structure of the most common types of oscillating body WECs. The section also includes a description of several configurations of oscillating bodies and the most common technologies for converting the energy associated with the alternating motion of the devices into electricity. Section 2.2 provides a concise overview of the procedure for the linear approximation of the hydrodynamic interaction; the final objective is to derive the equations of motion which describe the behaviour of oscillating body WECs. In section 2.3 the interaction is considered from the point of view of energy, starting from the energy transported by waves and then studying the motion which maximise the energy absorbed by the WEC.

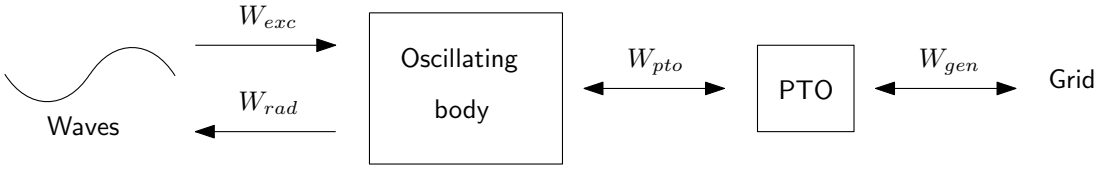

Figure 2.1: Energy transfer through an oscillating body wave energy converter.

2.1 Structure of an oscillating body wave energy converter

The process of converting energy carried by ocean waves into a different usable form of energy can be achieved in a number of ways, although the conversion process always begins by absorption from an reciprocating source, which arises from the oscillatory nature of waves. The oscillating body WECs, which are the types of devices considered in this thesis, are among the most common types of devices. The distinguishing characteristic of oscillating body WECs, compared to other types of WECs, is that the interaction between the device and water is due to the oscillation of a structure or a combination of structures, usually named *prime mover(s)* or *primary hydrodynamic absorber(s)*. The first part of this section covers the several common configurations of prime movers (section 2.1.1). The energy associated with the oscillation of the prime mover is then converted into usable energy (generally electricity) by the PTO. The PTO may be composed of several stages; for example, the energy associated with the alternating motion of the prime mover may be converted into kinetic energy associated with the rotating motion of a flywheel before being converted into electricity. Some typical basic configurations of PTOs are described in section 2.1.2.

Figure 2.1 depicts the main stages of the energy transfer through a WEC (losses are neglected): the energy is transferred from waves to the prime mover by means of the work done by the force exerted by the incoming wave (W_{exc}), which is called excitation force. Neglecting losses, part of the energy is returned to the sea by means of radiation effects (W_{rad}) and part is absorbed by the PTO. In turn, a fraction of the energy absorbed by the PTO is delivered to the electrical grid by means of the work performed by the electrical generator (W_{gen}), and the other fraction may be returned to the oscillating body.

The description presented in this section is aimed at providing a basic overview of the principles involved in the energy conversion process of oscillating body WECs. A comprehensive description of wave energy conversion technologies can be found in books [5] [23] and review papers [24] [25] [4] [3]; comparative studies between different technologies have also been published [9] and a special issue of the Philosophical Transactions of the Royal Society has been dedicated to the field of wave energy [26].

2.1.1 Primary hydrodynamic absorption

In this section, several configurations for the primary hydrodynamic energy conversion by commercial WEC devices and prototypes are considered. The simplest case is where the oscillating body reacts against a fixed reference such as the seabed, or a floating structure the size of which is so large that can be considered to be fixed by nature of its considerable inertia. The diagram in figure 2.2 depicts a heaving WEC which reacts against the seabed, where the PTO exerts a force between the seabed and the primary hydrodynamic absorber. Examples of commercial devices based on this principle are the first version of Archimedes Wave Swing (AWS)[1] and the device developed by Seabased[2]. The device in figure 2.3 also reacts against the seabed, but it exploits the combination of pitch and surge modes; the Oyster [3], developed by Aquamarine Power, is an example of a commercial WEC of this type.

Self-reacting WECs are devices composed of multiple oscillating bodies which react against each other by means of the force exerted by the PTO. The example in figure 2.4 portrays a self-reacting WEC composed of two bodies oscillating in heave, in which the PTO applies a force between M_1 and M_2 and the power transferred from the primary movers (M_1 and M_2) to the PTO is, excluding losses, the PTO force times the relative velocity between M_1 and M_2. Commercial devices such as Wavebob [4] and PowerBUOY [5] are based on this principle. The Pelamis[6] and the McCabe wave pump are also self-reacting WECs, but energy is absorbed from the relative rotation (pitching) of the prime movers[7], as depicted in figure 2.6. These type of devices are also known in the literature as attenuators.

The devices depicted in figure 2.4 and 2.6 are composed of multiple oscillating bodies, all of which interact with the surrounding water. A special case of self-reacting WECs consists of devices with an internal moving mass; in this case, the hydrodynamic interaction takes place between the water and an oscillating body that completely encloses an internal mass which is constrained to move in a specified mode. Figure 2.5 depicts an example of this type of device and the SEAREV [27] is a prototype WEC which is based on this principle.

2.1.2 The power take off unit

The PTO is designed to transform the energy associated with the oscillation of the primary hydrodynamic absorbers to a smooth flow of energy suitable for being delivered to the electrical grid. A number of difficulties are involved in the transformation process due to the very differ-

[1] en.openei.org/wiki/MHK_Technologies/Archimedes_Wave_Swing
[2] www.seabased.com
[3] www.aquamarinepower.com
[4] en.openei.org/wiki/MHK_Technologies/Wavebob
[5] www.oceanpowertechnologies.com
[6] www.pelamiswave.com
[7] In reality, the Pelamis WEC converts energy by relative pitch and yaw.

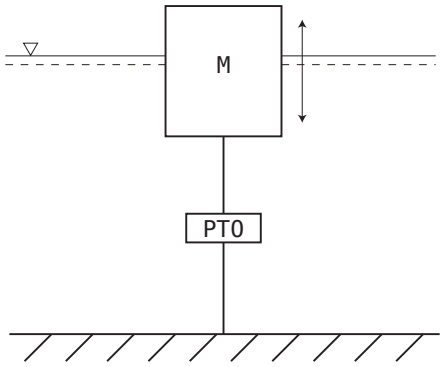

Figure 2.2: Seabed referenced heaving wave energy converter

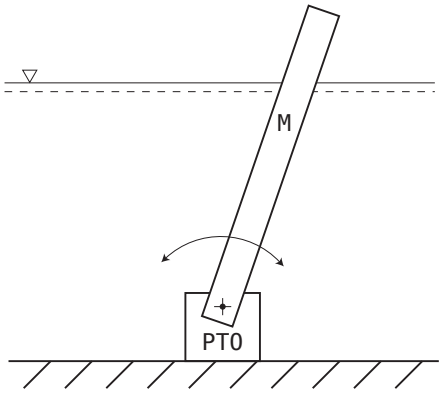

Figure 2.3: Seabed referenced pitching-surging wave energy converter

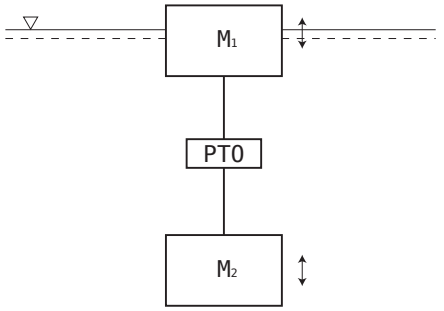

Figure 2.4: Self-reacting heaving wave energy converter

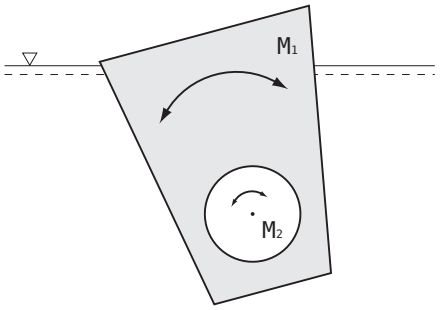

Figure 2.5: Self-reacting wave energy converter with internal mass

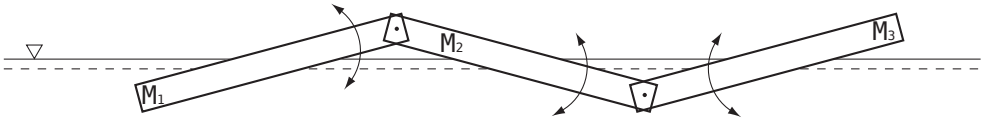

Figure 2.6: Self-reacting pitching wave energy converter (a.k.a. attenuators)

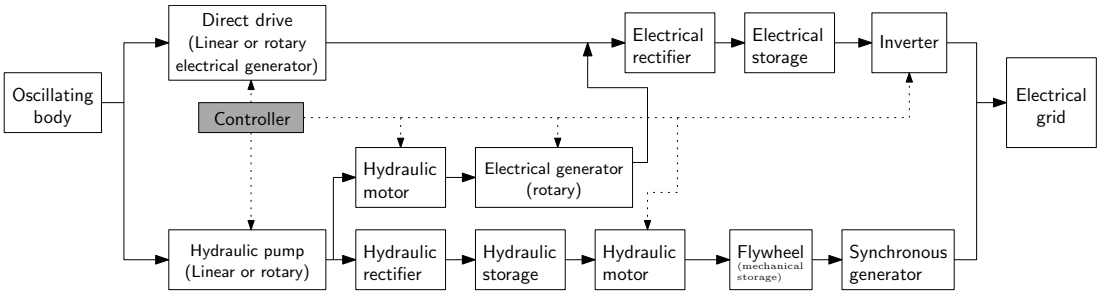

Figure 2.7: Block diagram of common PTO configurations

ent power flow characteristics between the source (wave energy) and the destination (the grid). In fact, the wave power is variable both in time and in amplitude, while power delivered to the electrical grid is required to satisfy stringent requirements (power quality). More particularly, wave power is oscillatory by nature, where the frequency and amplitude of oscillations (wave spectra) depend on meteorological factors, thus they are non-deterministic. As a direct consequence, PTOs always include at least a rectifier and a storage element: the rectifier compensates for the alternating nature of wave power producing a unidirectional energy flow with variable intensity, while the storage acts as a decoupling element between the random source (waves) and the (ideally) deterministic destination (grid).

The block diagram in figure 2.7 provides a summary of the most common structures of PTOs. The objective of the PTO is to transform the slow alternating motion of the oscillating body (left side of the figure) into an electric signal with constant voltage and frequency required for grid connection (right side of the figure). Depending on the mode of oscillation of the prime movers, the alternating motion could be linear or rotary. For example, devices in figure 2.2 and 2.4 produce a linear alternating motion, whereas devices in depicted in figures 2.3 and 2.6 generate a rotary alternating motion.

The energy associated with the oscillating motion can be converted directly into an alternating current with variable amplitude and frequency by using linear or rotary electrical generators. In this case, the electrical rectifier and storage produce a smooth DC signal, and the inverter generates the AC signal suitable for grid connection. The direct conversion of the mechanical energy into electricity is generally known as *direct drive*; the advantage is that fewer components are required, which improves reliability and efficiency. However, the slow oscillating motion of the primary hydrodynamic absorber requires generators with many poles and large dimensions to generate the necessary PTO forces.

An alternative approach is to use hydraulic components to transform the alternating mechanical motion into an alternating flow of fluid (oil), which is then smoothed and rectified by hydraulic accumulators and valves, respectively, to drive an hydraulic motor at a constant or variable speed. If the hydraulic motor is controlled to rotate at constant speed, then the motor

can be linked directly to a synchronous electrical generator connected to the grid. Additional smoothing is provided by the inertia of rotor of the synchronous generator and, in some cases, by including a flywheel. An example of this configuration is the PTO depicted in figure 2.9; the pressure in the hydraulic circuit is kept constant and the power delivered to the grid is controlled by acting on the displacement of the hydraulic motor and/or on the current in the generator.

Variable pressure/speed hydraulic PTOs are also common, and a typical configuration is illustrated in figure 2.8. The hydraulic pump is connected directly to the hydraulic motor which, in turn, is connected to the electrical generator. By using this solution, the hydraulic motor can drive the electrical generator at a higher speed than the direct drive, acting effectively as a gearbox; consequently, the dimension of the electrical generator is smaller than for a direct drive PTO.

Hydraulic PTOs are characterised by good efficiency in situations involving large forces and slow motion, as in wave energy. In addition, cost is generally lower than direct drive solutions because components are often available off-the-shelf.

2.1.2.1 Reaction force

An important property for the classification of PTOs is their capability in terms of the force that they can generate; in fact, the amount of energy absorbed by a WEC is related to the mechanical work performed by the PTO force. Therefore, the amount of energy transferred by the primary absorber to PTO can be controlled by acting on the PTO force; furthermore, the PTO force also influences the motion of the primary absorber in the water, thus affecting the amount of wave energy absorbed by the prime mover. If a WEC is equipped with a control system which optimise the energy flow through the device[8], the control system usually acts on the PTO force in order to pursue this objective. Thus, the force characteristics of PTOs are important for the energy absorption performance of WECs. In particular, the controllability of the PTO is a fundamental factor for the implementation of sophisticated control algorithms, where controllability describes the capability of the PTO to exert the exact force requested by the control system. When the PTO is also capable of reaching the force set point generated by the control system with a fast response, then it is said to exhibit good dynamical properties.

Direct drive solutions are characterised by good controllability and dynamical properties. In fact, the force/torque exerted by an electrical generator can be controlled by acting on the current flowing through the coils, and the control of torque/force in electrical motors and generators is a widely studied problem and a large number of well established commercial solutions are available.

Variable pressure/speed hydraulic PTOs in the configuration depicted in figure 2.8 also ex-

[8]The objective is generally, but not necessarily, to maximise the absorbed energy

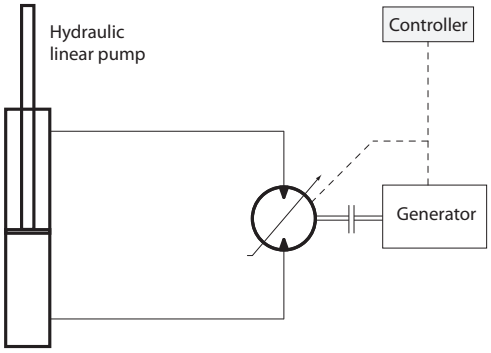

Figure 2.8: Variable speed/pressure hydraulic PTO

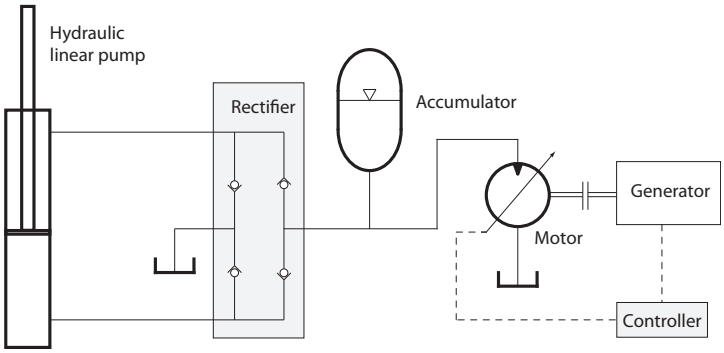

Figure 2.9: Constant pressure hydraulic PTO

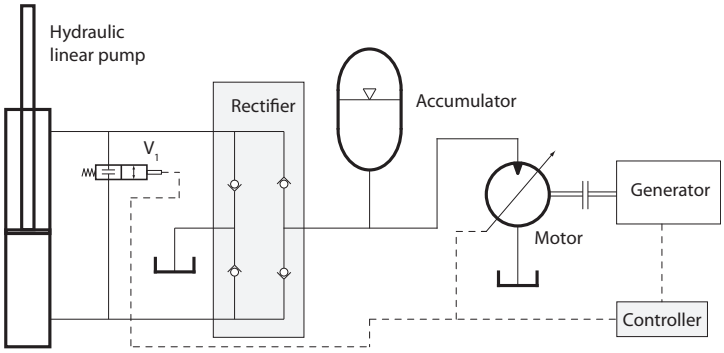

Figure 2.10: Constant pressure hydraulic PTO with de-clutching capability

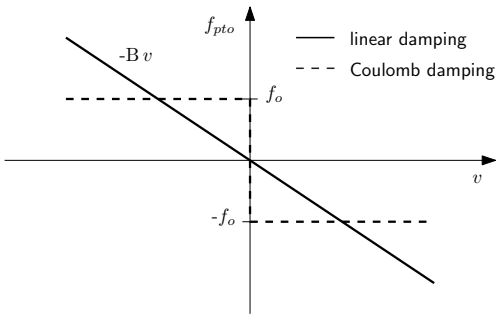

Figure 2.11: Linear and Coulomb damping

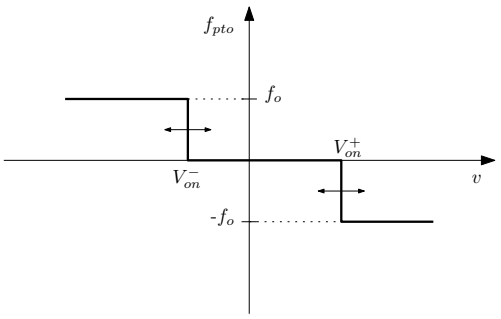

Figure 2.12: De-clutching damping profile

hibit good dynamic properties, because the force exerted by the hydraulic pump is, to a first approximation, linearly proportional to the torque of the electrical generator. Thus, the PTO force can be controlled by controlling the torque on the generator in the same manner as a rotary direct drive solution.

A simple law for the control of WECs is linear damping, where the PTO force (f_{pto}) is linearly proportional to the velocity (v) of the oscillating body, that is $f_{pto} = -\mathrm{B}\, v$ (fig. 2.11).

Direct drive PTOs and variable pressure PTOs (fig. 2.8) are also capable of bidirectional power, that is to reverse the energy flow from the PTO to the primary mover, and back to the water. The reversed energy flow is commonly known as *reactive* power. This property is required by some control techniques for improving wave energy absorption, as will be described in section 2.3.2 and in chapter 3. When the PTO is capable of returning energy to the oscillating body it is called an *active* PTO; a *passive* PTO is instead a PTO which is not capable of returning energy to the oscillating body, and not capable of generating reactive power.

Passive PTOs are generally simpler than active PTOs, thus less expensive; furthermore, when using passive PTOs, the absorbed energy is less sensitive to the efficiency of the PTO components because the ratio between the converted energy over the total energy flowing through the PTO[9] is larger. Controllability of the PTO force is not available with passive hydraulic PTOs of the type depicted in fig. 2.9, since they are designed as constant pressure systems. This effect is sometimes referred to as Coulomb damping [28] [29] and the PTO force characteristic is plotted in figure 2.11: the pressurised hydraulic circuit causes the hydraulic piston to exert a constant force $f_{pto} = \pm f_o$, and the oscillating body is prevented from moving until the external force acting on it exceeds the PTO force. The advantage of this configuration is its simplicity from both the mechanical point of view and the control system.

Limited controllability can be achieved by adding a control valve as depicted in fig. 2.10: this configuration makes possible the implementation of a control law termed *unlatching* [22] or *de-clutching* [29], the force characteristic of which is plotted in figure 2.12. The PTO force is zero as long as the control valve V_1 is open and the body is free to move under the effect of

[9] Energy absorbed plus energy returned

external forces; when the valve V_1 is closed the PTO exerts the force $f_{pto} = \pm f_o$ and the absorbed power is $P = f_o v$. The absorbed energy can be controlled by acting on the thresholds V_{on}^+ and V_{on}^-, where $V_{on}^+ \geq 0$ and $V_{on}^- \leq 0$ because this configuration is passive, that is $P = f_{pto} v \leq 0$. Bidirectional power can also be achieved with the configuration in fig. 2.9 by replacing the check valves with controlled valves and by increasing the complexity of the control system [30]; in fact, this modification makes it possible to accelerate the oscillating body by allowing $V_{on}^+ < 0$ and $V_{on}^- > 0$.

2.2 Theory of wave-body interaction and model of oscillating-body wave energy converter

The theory of wave energy conversion has its roots in the field of marine hydrodynamics. The equations of motion commonly used to describe the behaviour of a WEC were, in fact, originally devised around 1950s–'60s for the purpose of *predicting* [10] the motion of ships when subject to waves. A detailed and interesting account of the intense efforts dedicated to the field of marine hydrodynamics during this period is presented in [31].

The model of a WEC is essential for the development of the work presented in this thesis, and this section provides a concise summary of the model derivation and the assumptions which characterise its validity. The detailed derivation can be found in textbooks of marine hydrodynamics, such as [32], or in [5], which is specific to wave energy conversion.

The WEC is modelled as a floating rigid body, the motion of which is described by six components corresponding to the six DoF, also called modes of motion, and it is assumed that the body is free to oscillate in all six modes. The coordinate system is oriented as in fig. 2.13, and the modes are labelled as in table. 2.1.

The equations of motion are in the form of a harmonic oscillator with a frequency dependent damping. The frequency domain formulation is

$$\left(i\omega \mathbf{M} + \mathbf{Z}(\omega) + \mathbf{B} + \frac{\mathbf{S}}{i\omega} \right) \boldsymbol{v}(\omega) = \mathbf{H}(\omega)\zeta(\omega) + \boldsymbol{F}(\omega), \tag{2.1}$$

where $\boldsymbol{v}(\omega)$ is the Fourier transform of the velocity vector of the floating body and $\zeta(\omega)$ is the Fourier transform of the wave elevation; the corresponding time domain model is

$$\widetilde{\mathbf{M}}\ddot{\boldsymbol{\eta}}(t) + \int_{-\infty}^{t} \mathbf{K}(t-\tau)\dot{\boldsymbol{\eta}}(\tau)\, d\tau + \mathbf{B}\dot{\boldsymbol{\eta}}(t) + \mathbf{S}\boldsymbol{\eta}(t) = \int_{-\infty}^{+\infty} \mathbf{h}(t-\tau)\zeta(\tau)\, d\tau + \boldsymbol{f}(t), \tag{2.2}$$

[10] The term *prediction* was intended, in the context of marine hydrodynamic, to indicate the ability of a model to accurately describe the motion of a floating body when compared to experimental results [31]; this clarification is necessary to avoid ambiguity since, in different context, such as control theory, prediction refers to the temporal aspect, that is the ability of a model to describe the future evolution.

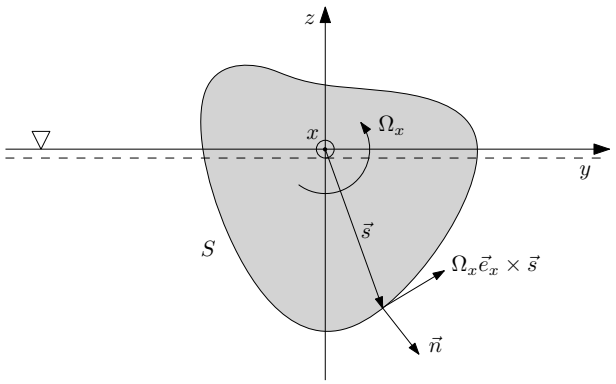

Figure 2.13: Floating body

where $\boldsymbol{\eta}(t)$ is the displacement vector. The equations of motion are linear with respect to the wave amplitude and to the velocity of the floating body. Section 2.2.1 provides an overview of the derivation of the mathematical model describing the hydrodynamic forces acting on the body under the effect of water waves. We start from a general formulation and we illustrate the simplifications introduced to obtain the linear models in (2.1) and (2.2). By means of the superposition principle, which was hypothesised in [33] and validated by experiments in the following years as reported in [31], the body motion in irregular seas can be considered as a linear combination of motions, each resulting from a sinusoidal wave (a.k.a. regular wave). Sinusoidal waves are assumed to be described by linear wave theory (Airy theory) which is briefly introduced in sec. 2.2.1.1. The terms composing equations (2.1) and (2.2) are described in section 2.2.2, in addition to a discussion on the relation between the two formulations.

2.2.1 Hydrodynamic notions and wave-body interaction

The forces acting on floating body depend on the behaviour of the fluid in which the body is immersed, and the behaviour of the fluid is described by pressure and flow velocity. The equations describing pressure and flow velocity in the fluid are derived by the conservation principles for mass and momentum.

For incompressible fluids (fluids with constant density ρ), the conservation of mass is ex-

MODE	COMPONENT	DIRECTION	NAME
1	x	x axis	surge
2	y	y axis	sway
3	z	z axis	heave
4	φ	rotation about x axis	roll
5	θ	rotation about y axis	pitch
6	ψ	rotation about z axis	yaw

Table 2.1: Modes of motion

pressed by the continuity equation

$$\nabla \cdot \vec{v} = 0, \tag{2.3}$$

where $\vec{v} = \vec{v}(x, y, z, t)$ is the fluid flow velocity vector, which states that the rate at which mass enters a systems is equal to the rate at which mass leaves the system. The conservation of momentum is described by the Navier-Stokes equations

$$\rho \left(\frac{\partial \vec{v}}{\partial t} + \vec{v} \cdot \nabla \vec{v} \right) = \vec{f} - \nabla p + \mu \nabla^2 \vec{v}, \tag{2.4}$$

where $\vec{f} = [0, 0, -\rho g]^T$ is the gravitational force per unit volume, p is the pressure and μ is the viscosity. Pressure and flow velocity can be obtained by solving the Navier-Stokes equations (2.4) together with the continuity equation (2.3), but it is a difficult problem and it is necessary to introduce some simplifications.

If the viscosity is neglected ($\mu = 0$) and the fluid is considered to be irrotational ($\nabla \times \vec{v} = 0$), then there exists a scalar function $\Phi(x, y, z, t)$ called velocity potential, such that

$$\vec{v} = \nabla \Phi. \tag{2.5}$$

By substituting (2.5) into the continuity equation (2.3), the velocity potential can be obtained by solving the Laplace equation

$$\nabla^2 \Phi = 0, \tag{2.6}$$

and the velocity $\vec{v}$ can be calculated form the velocity potential Φ by using (2.5).

Following from the assumption that the fluid is inviscid ($\mu = 0$), the last term of the Navier-Stokes equation (2.4) vanishes; the Bernoulli equation is then obtained by integrating (2.4) along a streamline of the velocity field:

$$\frac{p}{\rho} + \frac{\partial \Phi}{\partial t} + \frac{1}{2} (\nabla \Phi)^2 + g z = C, \tag{2.7}$$

where C is a constant of integration.

The calculation of the velocity potential and pressure from (2.6) and (2.7) requires the definition of boundary conditions. The floating body is considered to be impermeable; thus the velocity of a fluid particle on the surface of the body must be zero in the direction normal to the body surface. If the body is moving with a velocity $\vec{v}_b$, the kinematic boundary condition on the body surface is

$$\frac{\partial \Phi}{\partial n} = \vec{v}_b \cdot \vec{n} \tag{2.8}$$

where $\vec{n}$ is the unit normal vector on the body surface directed into the fluid domain. If the body is not moving, the boundary condition (2.8) reduces to $\partial \Phi / \partial n = 0$.

An additional kinematic boundary condition can be specified on the free surface. The free surface can be defined as

$$z = \zeta(x, y, t), \tag{2.9}$$

where ζ is the wave elevation. By also defining the function

$$F(x, y, z, t) = z - \zeta(x, y, t), \tag{2.10}$$

the kinematic free-surface condition, stating that a fluid particle on the free surface is assumed to remain on the free surface, can be formulated as

$$F(x, y, z, t) = 0 \qquad \text{and} \qquad \frac{\mathrm{D}}{\mathrm{D}t} F(x, y, z, t) = 0. \tag{2.11}$$

The operator D/Dt is the substantial derivative defined as

$$\frac{\mathrm{D}}{\mathrm{D}t} F = \frac{\partial F}{\partial t} + \vec{v} \cdot \nabla F, \tag{2.12}$$

and it describes the rate of change of the function F with respect to time t when following a fluid particle moving along a path with velocity $\vec{v}$. An explicit version of the kinetic free surface boundary condition (2.11) is obtained by substituting (2.5) and (2.10) into (2.12), resulting in

$$\frac{\partial \zeta}{\partial t} + \frac{\partial \Phi}{\partial x}\frac{\partial \zeta}{\partial x} + \frac{\partial \Phi}{\partial y}\frac{\partial \zeta}{\partial y} - \frac{\partial \Phi}{\partial z} = 0 \qquad \text{on} \qquad z = \zeta(x, y, t). \tag{2.13}$$

The water pressure p is considered to be equal to the constant atmospheric pressure p_{atm} on the free surface ($z = 0$); if the fluid is assumed to be motionless and the surface tension at the air-fluid interface is neglected, the constant of integration C in the Bernoulli equation (2.7) is $C = p_{\text{atm}}/\rho$, and the dynamic free surface boundary condition is defined as

$$g\zeta + \frac{\partial \Phi}{\partial t} + \frac{1}{2}\left(\left(\frac{\partial \Phi}{\partial x}\right)^2 + \left(\frac{\partial \Phi}{\partial y}\right)^2 + \left(\frac{\partial \Phi}{\partial y}\right)^2\right) = 0 \qquad \text{on} \qquad z = \zeta(x, y, t). \tag{2.14}$$

2.2.1.1 Linear wave theory

The final objective of this section is to obtain a model in which the motion and forces acting on the floating body are proportional to the wave amplitude. The Laplace equation (2.6) describing the velocity potential is linear, but the free surface conditions (2.13) and (2.14) are nonlinear and some simplification is required. The intermediate step toward the final linear model is to find an expression for the velocity potential which is proportional to the wave elevation.

A linearisation can be performed by neglecting the higher order terms in (2.13) and (2.14), and by considering the mean free surface at $z = 0$ instead of the free surface $z = \zeta(x, y, t)$; the

resulting linearised free surface boundary conditions are

$$\frac{\partial \zeta}{\partial t} = \frac{\partial \Phi}{\partial z} \qquad \text{on} \quad z = 0, \tag{2.15}$$

$$g\zeta + \frac{\partial \Phi}{\partial t} = 0 \qquad \text{on} \quad z = 0, \tag{2.16}$$

which can be combined as

$$\frac{\partial^2 \Phi}{\partial t^2} + g\frac{\partial \Phi}{\partial z} = 0 \qquad \text{on} \quad z = 0. \tag{2.17}$$

Plane Harmonic Waves If the velocity potential is oscillating harmonically in time with angular frequency ω, that is

$$\Phi(x, y, z, t) = \mathrm{Re}\left\{\hat{\Phi}(x, y, z)\, e^{i\omega t}\right\}, \tag{2.18}$$

the free surface boundary condition (2.17) becomes

$$-\omega^2\hat{\Phi} + g\frac{\partial \hat{\Phi}}{\partial z} = 0 \qquad \text{on} \quad z = 0. \tag{2.19}$$

In addition, if the sea bottom is planar and horizontal, it is possible to introduce the boundary condition

$$\frac{\partial \Phi}{\partial t} = 0 \qquad \text{on} \quad z = -h, \tag{2.20}$$

where h is the water depth.

The velocity potential can be calculated by solving the Laplace equation $\nabla^2\hat{\Phi} = 0$ using the method of separation of variables; it can be shown [5] that for planar waves of infinite horizontal extent, a particular solution using the boundary conditions (2.19) and (2.20) is[11]

$$\hat{\Phi} = -\frac{g}{i\omega}\zeta_a \frac{\cosh(kz + kh)}{\cosh(kh)} e^{-ikx}. \tag{2.21}$$

The wave number $k = 2\pi/\lambda$, where λ is the wavelength, is related to the angular frequency ω by means of the dispersion relation

$$\omega^2 = gk\tanh(kh), \tag{2.22}$$

while the wave elevation $\zeta(x, t)$ can be calculated by reformulating (2.16) as $\hat{\zeta} = -\frac{i\omega}{g}\hat{\Phi}\big|_{z=0}$, the result of which is

$$\hat{\zeta}(x) = \zeta_a e^{-ikx}, \tag{2.23}$$

[11] To simplify notation, it has been assumed that the wave propagates in the x direction only.

where ζ_a is the amplitude of the wave elevation.

The fluid flow velocity vector $\vec{v}$ can be calculated by using the definition of the velocity potential $\hat{\vec{v}} = \nabla\hat{\Phi}$ (2.5), and the result is:

$$\hat{v}_x = \frac{\partial\hat{\Phi}}{\partial x} = \omega\zeta_a \frac{\cosh(kz+kh)}{\sinh(kh)} e^{-ikx} \tag{2.24}$$

$$\hat{v}_z = \frac{\partial\hat{\Phi}}{\partial z} = i\omega\zeta_a \frac{\sinh(kz+kh)}{\sinh(kh)} e^{-ikx} \tag{2.25}$$

The pressure is obtained by the Bernoulli equation (2.7); in particular, (2.7) can be linearised by neglecting the second order term $(\nabla\Phi)^2$, and the result is composed of two terms representing the hydrodynamic (hdyn) and the hydrostatic (hstat) pressure:

$$p - p_{\text{atm}} = -\underbrace{\rho\frac{\partial\Phi}{\partial t}}_{\text{hdyn}} - \underbrace{\rho g z}_{\text{hstat}}. \tag{2.26}$$

Thus, the hydrodynamic pressure in complex form as function of the velocity potential $\hat{\Phi}$ and of the wave elevation amplitude ζ_a, respectively, is

$$\hat{p} = -i\omega\rho\hat{\Phi} = \rho g\zeta_a \frac{\cosh(kz+kh)}{\cosh(kh)} e^{-ikx}. \tag{2.27}$$

Equation (2.21) fulfils the intermediate objective of finding a linear relationship between the velocity potential and the wave elevation; in addition, (2.27) provides a linear relation between the wave amplitude and the hydrodynamic pressure.

Dispersive waves Water waves are dispersive, which means that the velocity of propagation of waves depends on the frequency. In other words, waves at different frequencies travel with different velocities. The velocity of propagation of each frequency component is the phase velocity, denoted as v_p and defined as

$$v_p = \frac{\omega}{k}.$$

The group velocity v_g is the velocity of propagation of the envelope modulating the amplitude of the dispersive wave, defined as

$$v_g = \frac{d\omega}{dk}.$$

Considering the dispersion relation (2.22) and a constant water-depth h, the phase velocity and the group velocity are

$$v_p = \frac{\omega}{k} = \sqrt{\frac{g}{k}\tanh(kh)} = \frac{g}{\omega}\tanh(kh) \tag{2.28}$$

$$v_g = \frac{D(kh)}{2\tanh(kh)} v_p = \frac{g}{2\omega} D(kh) \tag{2.29}$$

respectively, where

$$D(kh) = \left(1 + \frac{2kh}{\sinh(2kh)}\right)\tanh(kh) = 2k\int_{-h}^{0}\left(\frac{\cosh(kz+kh)}{\cosh(kh)}\right)^2 dz. \tag{2.30}$$

2.2.1.2 Forces acting on the floating body

The forces and moments acting on the body are calculated by integrating the pressure over the wetted surface as

$$\boldsymbol{F} = -\iint_S p\,\mathbf{n}\,dS,$$

where the six-dimensional generalized force vector $\boldsymbol{F}$ is defined as

$$\boldsymbol{F} = \begin{bmatrix} \vec{F} \\ \vec{M} \end{bmatrix}; \tag{2.31}$$

$\vec{F}$ and $\vec{M}$ are, respectively, the three-dimensional vectors of the hydrodynamic force and moment applied on the body. The six-dimensional vector $\mathbf{n}$ is the normal vector defined as

$$\mathbf{n} = \begin{bmatrix} \vec{n} \\ \vec{s} \times \vec{n} \end{bmatrix} \tag{2.32}$$

where $\vec{s}$ is the position of the infinitesimal surface element dS with respect to the chosen reference system, as depicted in Figure 2.13. The velocity of the element dS is $\vec{v} = \vec{U} + \vec{\Omega} \times \vec{s}$, where $\vec{U}$ and $\vec{\Omega}$ are, respectively, the linear velocity and the angular velocity of the floating body. It is convenient to define also the six-dimensional generalised velocity vector $\boldsymbol{v}$ as

$$\boldsymbol{v} = \begin{bmatrix} \vec{U} \\ \vec{\Omega} \end{bmatrix}. \tag{2.33}$$

When the motion of the floating body is small compared to the wave amplitude, the velocity potential Φ is generally considered the sum of two contributions, named *radiation* (Φ_R) and *excitation* (Φ_E), that is

$$\Phi = \Phi_R + \Phi_E.$$

The radiation component describes the radiated waves due to the motion of the body while the excitation component describes the effect due to the presence of the body, and it is independent of the body motion, because linearity is assumed.

The hydrodynamic force can also be calculated from the velocity potential by considering

the hydrodynamic part of the linearised Bernoulli equation, that is the first element on the right hand side of (2.26). If the velocity potential is a harmonic function of time, the complex generalized force vector $\hat{\boldsymbol{F}}$ can be calculated as

$$\hat{\boldsymbol{F}} = i\omega\rho \iint_S \hat{\Phi}\,\mathbf{n}\,dS = \underbrace{i\omega\rho \iint_S \hat{\Phi}_R\,\mathbf{n}\,dS}_{\text{Radiation force}} + \underbrace{i\omega\rho \iint_S \hat{\Phi}_E\,\mathbf{n}\,dS}_{\text{Excitation force}}. \tag{2.34}$$

Radiation force The floating body is considered to be free to oscillate in all of its modes. Because of linearity, the velocity potential associated with the radiated wave $\hat{\Phi}_R$ is the linear combination of potentials associated with the waves radiated by the oscillation in each mode; furthermore, the radiation potential associated with each mode is linearly proportional to the oscillation amplitude. Thus, assuming that there are no incident waves, $\hat{\Phi}_R$ can be written as

$$\hat{\Phi}_R = \sum_{j=1}^{6} \phi_j\,\hat{v}_j = \boldsymbol{\phi}\cdot\hat{\boldsymbol{v}}, \tag{2.35}$$

where ϕ_j is a function of position but it is independent of time, that is $\phi_j = \phi_j(x, y, z)$, and $\hat{v}_j$ is the j-th component of the generalised velocity vector $\hat{\boldsymbol{v}}$, defined in (2.33). The coefficients ϕ_j may be interpreted as the radiated velocity potential when the body oscillates in the mode j with unit velocity.

The *radiation problem* is defined as finding the radiation coefficients ϕ_j and it is solved by considering that the radiated velocity potential $\hat{\Phi}_R$ must satisfy the Laplace equation (2.6) together with the boundary conditions (2.8), (2.19) and (2.20). For the uniqueness of the solution, the radiated potential must satisfy an additional boundary condition at infinite distance which comes from the conservation of energy, defined as

$$\hat{\Phi}_R \propto R^{-1/2} e^{-ikR},$$

where R is the distance from the floating body. From the linearity of the Laplace equation and the boundary conditions it also follows that the radiated velocity potential coefficients ϕ_j must satisfy the Laplace equation and the boundary conditions, thus the radiation problem results in solving

$$\nabla^2\phi_i = 0, \tag{2.36}$$

with the boundary conditions

$$\frac{\partial\phi_j}{\partial n} = n_j \qquad \text{on } S \qquad\qquad \text{(body surface bound. cond.)}, \tag{2.37}$$

$$\frac{\partial \phi_j}{\partial z} = 0 \Big|_{z=-h} \qquad \text{(sea bottom bound. cond.)}, \tag{2.38}$$

$$-\omega^2 \phi_j + g \frac{\partial \phi_j}{\partial z} = 0 \Big|_{z=0} \qquad \text{(free surface bound. cond.)}, \tag{2.39}$$

$$\phi_j \propto R^{-1/2} e^{-ikR} \qquad \text{(radiation bound. cond. at infinity)}, \tag{2.40}$$

where n_j are the elements of the normal vector $\mathbf{n}$ defined in (2.32).

When the body is forced to oscillate and no incident waves are present, the body radiates waves; the forces and moments describing the wave-body interaction in this case are called radiation forces and moments, and are denoted by the six-dimensional generalized force vector $\boldsymbol{F}_R$ defined consistently with (2.31). If the body is forced to oscillate in mode j only, the j'-th component of the radiation force $\boldsymbol{F}_R$ is

$$\hat{F}_{R,j'} = i\omega\rho \iint_S \phi_j \hat{v}_j n_{j'} \, dS, \tag{2.41}$$

which is obtained by substituting (2.35) into the radiation component of (2.34). The elements of the generalised velocity vector $\hat{\boldsymbol{v}}$ defined in (2.33) are constant when integrating over the body surface because the body is rigid, thus (2.41) may be written as

$$\hat{F}_{R,j'} = -Z_{j'j} \, \hat{v}_j, \qquad \text{with} \quad Z_{j'j} = -i\omega\rho \iint_S \phi_j n_{j'} \, dS.$$

that is, the radiation force is linearly proportional to the body velocity and the constant of proportionality is $Z_{j'j}$, which is an element of the radiation impedance matrix $\mathbf{Z}$. Considering the boundary condition (2.37), $Z_{j'j}$ can be calculated as

$$Z_{j'j} = -i\omega\rho \iint_S \phi_j \frac{\partial \phi_{j'}}{\partial n} \, dS. \tag{2.42}$$

The negative sign is to indicate that the radiation force opposes the motion of the body. The radiation impedance matrix is complex and frequency dependent, that is $\mathbf{Z}(\omega) = \mathbf{R}(\omega) + i\mathbf{X}(\omega) = \mathbf{R}(\omega) + i\omega\mathbf{m}(\omega)$; the real part $\mathbf{R}(\omega)$ is generally known as *radiation resistance* (or radiation damping) matrix, the imaginary part $\mathbf{X}(\omega)$ as *radiation reactance* matrix, and $\mathbf{m}(\omega)$ as the *added mass* matrix.

In summary, the radiation force $\hat{\boldsymbol{F}}_R$ is calculated as the product between the velocity of the body $\hat{\boldsymbol{v}}$ and the radiation impedance matrix $\mathbf{Z}$, which is obtained by solving the radiation problem (2.36)–(2.41), and then using the solution ϕ_j to calculate the integrals in (2.42). In

matrix form, the radiation force can be expressed as

$$\hat{\boldsymbol{F}}_R = -\mathbf{Z}(\omega)\,\hat{\boldsymbol{v}}. \tag{2.43}$$

Excitation force If the body is held fixed, the wave-body interaction is described by the excitation velocity potential $\hat{\Phi}_E$, which is decomposed into two components ($\hat{\Phi}_E = \hat{\Phi}_I + \hat{\Phi}_D$) describing the effect due to the unperturbed incident wave ($\hat{\Phi}_I$) and the diffraction effect ($\hat{\Phi}_D$), which is the disturbance to the incident wave due to the presence of the body. The resulting excitation force is the second term on the right hand side of (2.34), that is

$$\hat{\boldsymbol{F}}_E = i\omega\rho \iint_S \hat{\Phi}_E\,\mathbf{n}\,dS = i\omega\rho \iint_S \hat{\Phi}_I\,\mathbf{n}\,dS + i\omega\rho \iint_S \hat{\Phi}_D\,\mathbf{n}\,dS$$

If the body is very small with respect to the wavelength, the diffraction term can be neglected and the resulting force is called the Froude-Krylov force.

Both $\hat{\Phi}_I$ and $\hat{\Phi}_D$ must satisfy the boundary conditions of the free surface (2.19) and on the sea bottom (2.20); the boundary condition on the body surface in this case is

$$-\frac{\partial\hat{\Phi}_D}{\partial n} = \frac{\partial\hat{\Phi}_I}{\partial n} \qquad \text{on } S. \tag{2.44}$$

The diffraction problem is defined similarly to the the radiation problem, in that $\hat{\Phi}_D$ must satisfy the Laplace equation (2.6) with the free surface (2.19) and the sea bottom (2.20) boundary conditions, in addition to the boundary condition at infinity (2.40); the only difference is the boundary condition on the body surface (2.44). The diffraction potential can be considered as the disturbance resulting from a forced motion of the body, the normal velocity of which is equal and opposite to the velocity of the incident wave; this interpretation can be seen more clearly by considering the boundary condition (2.44) in conjunction with the definition of the velocity potential in (2.5), that is $\vec{v} = \nabla\Phi$. Assuming that the velocity potential of the incident wave is proportional to the wave amplitude (linear wave theory), then the velocity potential of the diffracted wave is also linearly proportional to the wave amplitude. Therefore, the excitation force can be written as function of the wave elevation:

$$\hat{\boldsymbol{F}}_E = \mathbf{H}(\omega)\,\hat{\zeta}. \tag{2.45}$$

The vector of the frequency dependent excitation force coefficients $\mathbf{H}(\omega)$ can be calculated as

$$\mathbf{H} = i\omega\rho \iint_S \left(\hat{\Phi}_I^o + \hat{\Phi}_D^o\right)\,\mathbf{n}\,dS \tag{2.46}$$

where $\hat{\Phi}_I^o$ and $\hat{\Phi}_D^o$ are the incident wave and diffracted wave velocity potentials per unit amplitude of the incident wave. The velocity potential of the incident wave $\hat{\Phi}_I^o$ is provided by the description of the waves with no interactions with bodies; for example, in the case of plane waves as in sec. 2.2.1.1, the velocity potential can be calculated by normalising (2.21) w.r.t. the wave amplitude. The velocity potential due to diffraction $\hat{\Phi}_D^o$ can be determined by solving the boundary value problem given by the Laplace equation (2.6) and the boundary conditions (2.19), (2.20), (2.40) and (2.44), as mentioned above.

An alternative approach for calculating the excitation force $\hat{\boldsymbol{F}}_E$ is to use the solution of the radiation problem and the Haskind's relations [34], resulting in:

$$\hat{F}_{E,j} = i\omega\rho \iint_S \left(\hat{\Phi}_I \frac{\partial \phi_j}{\partial n} - \phi_j \frac{\partial \hat{\Phi}_I}{\partial n} \right) dS. \tag{2.47}$$

The excitation force depends also on the direction of the incoming wave, that is the vector of the excitation force coefficient is $\mathbf{H} = \mathbf{H}(\omega, \beta)$, where β is the angle of the incoming wave. In the case where the wave elevation is described by multiple waves $\hat{\zeta}_k$ at different frequencies ω_k and heading angles β_k, because of linearity, the total excitation force can be computed by applying the principle of superposition:

$$\hat{\boldsymbol{F}}_E = \sum_k \mathbf{H}(\omega_k, \beta_k)\, \hat{\zeta}_k.$$

Hydrostatic force The linearised Bernoulli equation (2.26), as previously described, is composed of two terms; the first term gives rise to the hydrodynamic forces (radiation and excitation) while the second term describes the hydrostatic component of the pressure, which is $p = -\rho g z$ (the atmospheric pressure p_{atm} is a constant value and it is generally considered as zero). The hydrostatic force ($\vec{F}_H$) and moment ($\vec{M}_H$) can be calculated by integrating the hydrostatic pressure over the body surface S:

$$\boldsymbol{F}_H = \begin{bmatrix} \vec{F}_H \\ \vec{M}_H \end{bmatrix} = \rho g \iint_S z\, \mathbf{n}\, dS. \tag{2.48}$$

$\boldsymbol{F}_H$ is the generalised hydrostatic force vector defined consistently with (2.31).

The integral in (2.48) depends non-linearly on the body position and orientation (attitude) with respect to a fixed coordinate system. For small perturbations around the equilibrium configuration $\boldsymbol{\xi}_0$, the hydrostatic force can be linearised with respect to the displacement vector $\boldsymbol{\eta}$; in more detail, the six-dimensional vector $\boldsymbol{\xi}$ describe the configuration of the body with respect to a fixed coordinate system that is defined as $\boldsymbol{\xi} = [x, y, z, \varphi, \theta, \psi]^T$, while $\boldsymbol{\eta}$ is the displacement

from the equilibrium position $\boldsymbol{\xi}_0$, that is $\boldsymbol{\eta} = \boldsymbol{\xi} - \boldsymbol{\xi}_0$. The hydrostatic force may be expressed as

$$\boldsymbol{F}_H = -\mathbf{S}_h \, \boldsymbol{\eta}, \tag{2.49}$$

where $\mathbf{S}_h$ is the positive semidefinite ($\mathbf{S}_h \geq 0$) [6] hydrostatic restoring coefficients matrix; the complete description of the linearisation can be found in [32].

2.2.1.3 Multiple bodies

The analysis of the forces acting on a floating structure that has been presented in so far in this section is specific to the situation where only one body is present. The extension to the case of an arbitrary number N of interacting bodies can be derived from the special case of a single body, and the structure of the resulting equation is identical. It is only necessary to redefine the generalized vectors for force, velocity and displacement, and to modify the boundary condition of the body surface for solving the radiation problem and the diffraction problem.

With regard to the radiation problem, the velocity potential associated with the radiated wave is still linearly proportional to the complex velocity, that is

$$\hat{\Phi}_R = \sum_{p=1}^{6} \boldsymbol{\phi}_p^T \hat{\boldsymbol{v}}_p,$$

but the generalised velocity vector $\hat{\boldsymbol{v}}$ is now $6N$-dimensional and defined as

$$\hat{\boldsymbol{v}} = \left[\hat{\boldsymbol{v}}_1^T, \dots, \hat{\boldsymbol{v}}_p^T, \dots, \hat{\boldsymbol{v}}_N^T\right]^T$$

where $\hat{\boldsymbol{v}}_p$ is the 6-dimensional generalised velocity vector of the body p defined as in (2.33). The vector $\boldsymbol{\phi}$ is defined as $\boldsymbol{\phi} = \left[\boldsymbol{\phi}_1^T, \dots, \boldsymbol{\phi}_p^T, \dots, \boldsymbol{\phi}_N^T\right]^T$, where $\boldsymbol{\phi}_p = [\phi_{p,1}, \dots, \phi_{p,6}]$ and $\phi_{p,j}$ is the radiation velocity potential associated with the oscillation of body p in mode j with unitary velocity amplitude. In practice, the system is now composed of $6N$ oscillators, because each of the N bodies can oscillate in 6 modes.

The solution of the radiation problem are the functions $\phi_{p,j}$ which satisfy the Laplace equation (2.36) with the boundary conditions (2.38)–(2.40); however, the body surface boundary condition has to be replaced with

$$\frac{\partial \phi_{p,j}}{\partial n} = \begin{cases} n_{p,j} & \text{on } S_p \\ 0 & \text{on } S_{p'} \text{ with } p \neq p' \end{cases}$$

where S_p is the surface of body p and $n_{p,j}$ is j-th component of the normal vector on body p,

defined as in (2.32). Finally, the radiation impedance matrix $\mathbf{Z}$ can be calculated as

$$\mathbf{Z} = -i\omega\rho \iint_S \frac{\partial \boldsymbol{\phi}}{\partial n} \boldsymbol{\phi}^T \, dS, \tag{2.50}$$

and the radiation force $\hat{\boldsymbol{F}}_R$ as

$$\hat{\boldsymbol{F}}_R = -\mathbf{Z}(\omega)\, \hat{\boldsymbol{v}}, \tag{2.51}$$

where $\hat{\boldsymbol{F}}_R$ has been redefined as $\hat{\boldsymbol{F}}_R = \left[\hat{\boldsymbol{F}}_{R,1}^T, \ldots, \hat{\boldsymbol{F}}_{R,N}^T\right]^T$.

A similar procedure is followed for the excitation force: the vector of the excitation force coefficient $\mathbf{H}(\omega)$ is calculated as for the single body case from (2.46), with the only difference being that the normal vector $\mathbf{n}$ is defined as

$$\mathbf{n} = \left[\mathbf{n}_1^T, \ldots, \mathbf{n}_p^T, \ldots, \mathbf{n}_N^T\right]^T$$

where $\mathbf{n}_p$ is defined as in (2.32), and the boundary condition on the body surface (2.44) is redefined as

$$\frac{\partial}{\partial n}\left(\hat{\Phi}_I + \hat{\Phi}_D\right) = 0 \qquad \text{on all } S_p.$$

The excitation force vector on all the bodies is then calculated as

$$\hat{\boldsymbol{F}}_E = \mathbf{H}(\omega)\, \hat{\xi},$$

with $\hat{\boldsymbol{F}}_E$ redefined as $\hat{\boldsymbol{F}}_E = \left[\hat{\boldsymbol{F}}_{E,1}^T, \ldots, \hat{\boldsymbol{F}}_{E,N}^T\right]^T$.

The hydrostatic force is simply

$$\boldsymbol{F}_H = -\mathbf{S}_h\, \eta,$$

where $\boldsymbol{F}_H = \left[\boldsymbol{F}_{H,1}^T, \ldots, \boldsymbol{F}_{H,N}^T\right]^T$, the displacement vector is $\boldsymbol{\eta} = \left[\boldsymbol{\eta}_1^T, \ldots, \boldsymbol{\eta}_N^T\right]^T$ and the hydrostatic restoring coefficient matrix $\mathbf{S}_h$ is the block diagonal matrix

$$\mathbf{S}_h = \begin{bmatrix} \mathbf{S}_1 & 0 & \ldots & 0 & \ldots & 0 \\ 0 & \mathbf{S}_2 & \ldots & 0 & \ldots & 0 \\ \vdots & \vdots & \ddots & \vdots & & \vdots \\ 0 & 0 & \ldots & \mathbf{S}_p & \ldots & 0 \\ \vdots & \vdots & & \vdots & \ddots & \vdots \\ 0 & 0 & \ldots & 0 & \ldots & \mathbf{S}_N \end{bmatrix}$$

in which $\mathbf{S}_p$ is the matrix of the hydrostatic restoring coefficients of body p.

Following the definitions provided in this section, the equations for multiple bodies and the single body take the same form and no distinction between them will be made in the rest of this thesis.

2.2.2 Equation of motion

Considering a single unconstrained floating body, its motion is described by six equations, which can be derived by applying Newton's second law $\sum \boldsymbol{F}_i = \mathbf{M}\,\mathbf{a}$, where $\boldsymbol{F}_i$ are the vectors of forces and moments acting on the body, consistent with the definition in (2.31), and $\mathbf{a}$ its acceleration. When the origin of the coordinate system is the centre of gravity G, the generalized mass matrix $\mathbf{M}$ is

$$\mathbf{M} = \begin{bmatrix} m\mathbf{I}_3 & \mathbf{0}_3 \\ \mathbf{0}_3 & \mathbf{I}^G \end{bmatrix},$$

where m is the mass of the floating body. The matrix $\mathbf{I}^G$ indicates the inertia tensor with respect to the coordinate system centred in G while $\mathbf{I}_3$ and $\mathbf{0}_3$ are, respectively, the identity matrix of size three and the zero matrix of size three.

The forces acting on a floating body due to the interaction with water, in the linear case, have been described in Section 2.2.1.2; they are the excitation force $\boldsymbol{F}_E$, the radiation force $\boldsymbol{F}_R$ and the hydrostatic force $\boldsymbol{F}_H$. For the simplest case of a sinusoidal wave, the forces and motion are also sinusoidal, and the equation of motion is

$$\hat{\boldsymbol{F}}_E + \hat{\boldsymbol{F}}_R + \hat{\boldsymbol{F}}_H = \mathbf{M}\,\hat{\mathbf{a}},$$

which results in

$$\mathbf{M}\, i\omega\, \hat{\boldsymbol{v}} + \mathbf{Z}(\omega)\, \hat{\boldsymbol{v}} + \mathbf{S}_h \frac{\hat{\boldsymbol{v}}}{i\omega} = \left(i\omega\, (\mathbf{M} + \mathbf{m}(\omega)) + \mathbf{R}(\omega) + \frac{\mathbf{S}_h}{i\omega} \right) \hat{\boldsymbol{v}} = \mathbf{H}(\omega)\, \hat{\zeta} \tag{2.52}$$

when using (2.45), (2.43) and (2.49), and where $\hat{\mathbf{a}} = i\omega\hat{\boldsymbol{v}}$ and $\hat{\boldsymbol{\eta}} = \hat{\boldsymbol{v}}/i\omega$. If the angular frequency of the incident wave is $\omega = \omega_0$, then the equation of motion can be written as a second order differential equation with frequency dependent coefficients:

$$\left(\mathbf{M} + \mathbf{m}(\omega_0)\right) \ddot{\boldsymbol{\eta}}(t) + \mathbf{R}(\omega_0)\, \dot{\boldsymbol{\eta}} + \mathbf{S}\, \boldsymbol{\eta} = \mathrm{Re}\left\{ \mathbf{H}(\omega_0)\, \hat{\zeta} e^{i\omega_0 t} \right\}. \tag{2.53}$$

Equation (2.53) is valid only for the description of the steady state response caused by a sinusoidal wave elevation $\zeta(t) = \zeta_0 \cos(\omega_0 t + \gamma)$; it is a frequency domain description, as discussed in [35] and [36], and it provides no information regarding the transient response. However, equation (2.53) is useful for the calculation of the radiation impedance matrix and excitation coefficients from experiments, as described in [31].

The problem with equation (2.53) is that it does not provide the description of the memory effects in the interaction between the body and the fluid due to radiation. The first time-domain model capable of describing the transient response was derived by Cummins [36], by using a test function for the solution of the radiation problem which contains two terms describing

the instantaneous and memory effects of fluid velocity. In particular, Cummins considered a candidate solution for the radiation problem, identified by the Laplace equation (2.6) together with the boundary conditions (2.8), (2.19) and (2.20), of the type:

$$\Phi_R(t) = \sum_{j=1}^{6} \phi_j \, \dot{\eta}_j(t) + \sum_{j=1}^{6} \int_{-\infty}^{t} \chi_j(t-\tau)\, \dot{\eta}_j(\tau)\, d\tau.$$

The instantaneous response of the fluid due to the motion of the floating body is described by the potentials ϕ_j, while the convolution integral represents the memory term and $\chi_j(t)$ are the responses of the fluid due to an impulse of the body velocity. The resulting radiation force is

$$\boldsymbol{f}_r(t) = -\boldsymbol{\mu}\, \ddot{\boldsymbol{\eta}}(t) - \int_{-\infty}^{t} \mathbf{K}(t-\tau)\, \dot{\boldsymbol{\eta}}(\tau)\, d\tau, \tag{2.54}$$

where $\boldsymbol{\mu} \in \mathbb{R}^{6\times6}$ is a constant matrix and $\mathbf{K}(t) \in \mathbb{R}^{6\times6}$ is a symmetric matrix of impulse responses, the elements of which are $\mathrm{K}_{jk}(t) = 0$ for $t < 0$, i.e. the radiation force is a causal function of the body velocity.

Similarly to the expression of the radiation force in (2.54), the excitation force can also be described, in the time-domain, by a convolution integral as

$$\boldsymbol{f}_e(t) = \int_{-\infty}^{+\infty} \mathbf{h}(t-\tau)\, \zeta(\tau)\, d\tau. \tag{2.55}$$

In this case, the function in (2.55) is non-causal, as discussed in [37], that is the excitation force at the time $t = t_0$ depends also on future values of the wave elevation ($\zeta(t)$ for $t > t_0$), and the impulse response vector $\mathbf{h}(t) \in \mathbb{R}^6 \times \mathbb{R}$ is such that $\mathbf{h}(t) \neq 0$ for $t < 0$.

The equation of motion is obtained once again by applying Newton's second law and considering the excitation force in (2.55), the radiation force in (2.54) and the hydrostatic restoring force in (2.49):

$$(\mathbf{M} + \boldsymbol{\mu})\, \ddot{\boldsymbol{\eta}}(t) + \int_{-\infty}^{t} \mathbf{K}(t-\tau)\, \dot{\boldsymbol{\eta}}(\tau)\, d\tau + \mathbf{S}_h\, \boldsymbol{\eta}(t) = \int_{-\infty}^{+\infty} \mathbf{h}(t-\tau)\zeta(\tau)\, d\tau. \tag{2.56}$$

2.2.2.1 Relation between time-domain and frequency domain models

Since the impulse responses $\mathbf{K}(t)$ and $\mathbf{h}(t)$ describe physical quantities, it is reasonable to assume that they are finite energy functions, i.e. square integrable:

$$\int_{-\infty}^{+\infty} |\mathbf{K}(t)|^2 dt \leq \infty \qquad \text{and} \qquad \int_{-\infty}^{+\infty} |\mathbf{h}(t)|^2 dt \leq \infty. \tag{2.57}$$

Therefore, it is possible to find the relation between the time domain model (2.56) and the frequency domain model (2.52) by means of the Fourier transform, provided that the transform

of $\ddot{\boldsymbol{\eta}}(t)$, $\dot{\boldsymbol{\eta}}(t)$ and $\zeta(t)$ exists; the existence of $\mathscr{F}\{\mathbf{K}(t)\}$ and $\mathscr{F}\{\mathbf{h}(t)\}$ is guaranteed by (2.57), where $\mathscr{F}\{f(t)\}$ indicates the Fourier transform of the function $f(t)$.

By comparing the right hand sides of (2.56) and (2.52), the excitation force coefficients vector $\mathbf{H}(\omega)$ is the Fourier transform of the excitation impulse response $\mathbf{h}(t)$, that is

$$\mathbf{H}(\omega) = \mathscr{F}\{\mathbf{h}(t)\}.$$

The relation between the time-domain (2.54) and the the frequency-domain (2.43) description of the radiation force can be found by applying the Fourier transform to (2.54):

$$\begin{aligned}\mathscr{F}\left\{\mathbf{f}_r(t)\right\} &= \left(-i\omega\,\boldsymbol{\mu} - \int_0^\infty \mathbf{K}(t)\,e^{i\omega t}\,dt\right)\boldsymbol{v}(\omega)\\ &= \left(-i\omega\,\boldsymbol{\mu} - \int_0^\infty \mathbf{K}(t)\,\cos\omega t\,dt - i\int_0^\infty \mathbf{K}(t)\,\sin\omega t\,dt\right)\boldsymbol{v}(\omega),\end{aligned} \tag{2.58}$$

where $\boldsymbol{\eta}(\omega) = \boldsymbol{v}(\omega)/i\omega$. By equating the real and imaginary parts of (2.58) with the frequency domain formulation of the radiation force in (2.43), it is possible to find the relations between the radiation damping, added mass and the impulse response:

$$\mathbf{R}(\omega) = \int_0^\infty \mathbf{K}(t)\,\cos\omega t\,dt, \tag{2.59}$$

$$\mathbf{m}(\omega) = \boldsymbol{\mu} - \frac{1}{\omega}\int_0^\infty \mathbf{K}(t)\,\sin\omega t\,dt. \tag{2.60}$$

Equations (2.59) and (2.60) are known as Ogilvie's relations [31]. Since the impulse response $\mathbf{K}(t)$ is square integrable, it follows that [31], [38]

$$\lim_{\omega\to\infty}\int_0^\infty \mathbf{K}(t)\,\cos\omega t\,dt = \lim_{\omega\to\infty}\int_0^\infty \mathbf{K}(t)\,\sin\omega t\,dt = \mathbf{0},$$

thus

$$\lim_{\omega\to\infty}\mathbf{R}(\omega) = \mathbf{0}, \tag{2.61}$$

$$\lim_{\omega\to\infty}\mathbf{m}(\omega) = \boldsymbol{\mu} = \mathbf{m}_\infty, \tag{2.62}$$

That is, the coefficient $\boldsymbol{\mu}$ is equal to the asymptotic value for $\omega\to\infty$ of the added mass, and it will be denoted by $\mathbf{m}_\infty$ for clarity.

Conversely to (2.59) and (2.60), the radiation impulse response can be calculated from both the radiation damping or the added mass as

$$\mathbf{K}(t) = \frac{2}{\pi}\int_0^\infty \mathbf{R}(\omega)\,\cos\omega t\,d\omega, \tag{2.63}$$

$$\mathbf{K}(t) = -\frac{2}{\pi}\int_0^\infty \omega\left(\mathbf{m}(\omega) - \mathbf{m}_\infty\right)\sin\omega t\, d\omega. \tag{2.64}$$

The integral in (2.63) converges considerably faster than (2.64), therefore (2.63) is generally used for computing the radiation impulse response when only frequency domain coefficients are available [38].

2.2.2.2 Properties of the radiation coefficients

The radiation impedance matrix $\mathbf{Z} = \mathbf{R} + i\omega\mathbf{m}$, the elements of which are defined in (2.42), is symmetric, and the asymptotic values for $\omega \to \infty$ of the radiation damping $\mathbf{R}$ and the added mass matrix $\mathbf{m}$ have been given in (2.61) and (2.62), respectively; furthermore, the matrix $\mathbf{m}_\infty$ is positive definite [39]. The asymptotic values for $\omega \to 0^+$ are [40]:

$$\lim_{\omega\to 0^+} \mathbf{R}(\omega) = \mathbf{0}, \tag{2.65}$$

$$\lim_{\omega\to 0^+} \mathbf{m}(\omega) - \mathbf{m}_\infty = -\int_0^\infty \mathbf{K}(t)\, dt \neq \pm\infty. \tag{2.66}$$

Radiation is a dissipative process [39], therefore the radiation mpedance matrix $\mathbf{Z}(\omega)$ is positive real, i.e. $\frac{1}{2}\left[\mathbf{Z}(\omega) + \mathbf{Z}^*(\omega)\right] \geq 0$, $\mathbf{R}(\omega) = \mathbf{R}^T(\omega) \geq 0$ and the diagonal elements of $\mathbf{R}(\omega)$ are positive for all frequencies, that is $\mathrm{R}_{ii}(\omega) \geq 0\ \forall\omega$.

From equation (2.63), and since $\mathbf{R}(\omega)$ is positive semi-definite, it follows that the asymptotic value of the impulse response for $t \to 0^+$ is

$$\lim_{t\to 0^+} \mathbf{K}(t) = \lim_{t\to 0^+} -\frac{2}{\pi}\int_0^\infty \mathbf{R}(\omega)\cos\omega t\, d\omega \neq \mathbf{0};$$

furthermore, since $\mathbf{K}(t)$ is of finite energy, it follows from (2.57) that

$$\lim_{t\to\infty} \mathbf{K}(t) = \mathbf{0}. \tag{2.67}$$

The asymptotic value of the impulse response in (2.67) can also be inferred from the fact that the radiation is dissipative; in fact, if a linear time-invariant system is dissipative then it is asymptotically stable therefore the impulse response satisfies (2.67).

The impulse response $\mathbf{K}(t)$ is real and causal, thus the real and imaginary part of its Fourier transform are related by means of the Kramers-Kronig relations

$$\mathbf{R}(\omega) = \frac{2\omega^2}{\pi}\int_0^\infty \frac{\mathbf{m}(\upsilon) - \mathbf{m}_\infty}{\omega^2 - \upsilon^2}\, d\upsilon,$$

$$\mathbf{m}(\omega) - \mathbf{m}_\infty = \frac{2}{\pi}\int_0^\infty \frac{-\mathbf{R}(\upsilon)}{\omega^2 - \upsilon^2}\, d\upsilon.$$

Furthermore, by introducing the Hilbert transform of the radiation resistance $\mathscr{H}\{\mathbf{R}(\omega)\}$, defined as

$$\mathscr{H}\{\mathbf{R}(\omega)\} = \frac{1}{\pi}\int_{-\infty}^{\infty} \frac{\mathbf{R}(\upsilon)}{\omega - \upsilon}\, d\upsilon, \tag{2.68}$$

the radiation impedance can be written in terms of the radiation resistance only:

$$\mathbf{Z}(\omega) = \mathbf{R}(\omega) + i\,\mathscr{H}\{\mathbf{R}(\omega)\}. \tag{2.69}$$

2.2.2.3 Equation of motion with additional terms

The behaviour of WECs is simulated with slightly modified versions of the models in (2.52) and (2.56), which were originally developed to describe the linear interaction between ships and water waves. The most significant difference between the linear models of WECs and ships is a term reflecting the specific purpose WECs, which are designed to absorb energy carried by water waves and to convert it into a usable form, such as electricity.

The energy absorption is performed by the PTO, which is a component capable of exerting forces on the device; the energy absorbed by the WEC can generally be considered, neglecting losses, as the mechanical work done by the force exerted by the PTO, denoted $\boldsymbol{F}_{pto}$.

Wave energy converters are generally connected to mooring lines which influence their behaviour. The effect of mooring lines on WECs can be described, to a first approximation, with a linear spring-damper model; thus, the generalized force vector $\boldsymbol{f}_m$ describing the forces and moments acting on the WEC due to moorings can be written as

$$\boldsymbol{f}_m(t) = -\mathbf{B}_m\,\dot{\boldsymbol{\eta}}(t) - \mathbf{S}_m\,\boldsymbol{\eta}(t).$$

The frequency- and time-domain models in (2.52) and (2.56) can be amended by adding the terms describing the PTO and other forces, including (linearised) moorings, as

$$\left(i\omega\,(\mathbf{M} + \mathbf{m}(\omega)) + \mathbf{B} + \mathbf{R}(\omega) + \frac{\mathbf{S}}{i\omega}\right)\boldsymbol{v}(\omega) = \mathbf{H}(\omega)\,\zeta(\omega) + \boldsymbol{F}_{pto}(\omega) \tag{2.70}$$

and

$$\tilde{\mathbf{M}}\,\ddot{\boldsymbol{\eta}}(t) + \int_{-\infty}^{t} \mathbf{K}(t-\tau)\,\dot{\boldsymbol{\eta}}(\tau)\,d\tau + \mathbf{B}\,\dot{\boldsymbol{\eta}}(t) + \mathbf{S}\,\boldsymbol{\eta}(t) = \int_{-\infty}^{+\infty} \mathbf{h}(t-\tau)\,\zeta(\tau)\,d\tau + \boldsymbol{f}_{pto}(t). \tag{2.71}$$

where $\boldsymbol{F}_{pto}(\omega) = \mathscr{F}\left\{\boldsymbol{f}_{pto}(t)\right\}$ and $\zeta(\omega) = \mathscr{F}\{\zeta(t)\}$; also, for convenience of notation, the matrix $\tilde{\mathbf{M}}$ has been defined as $\tilde{\mathbf{M}} = \mathbf{M} + \boldsymbol{\mu}$. Furthermore, the spring terms have been gathered into the term $\mathbf{S}$ as $\mathbf{S} = \mathbf{S}_h + \mathbf{S}_m$, and the damping terms into $\mathbf{B}$ as $\mathbf{B} = \mathbf{B}_m + \mathbf{B}_f$, where $\mathbf{B}_f$ can be used to describe additional linear dissipative effects, such as frictions between moving parts of the WEC and a linear approximation of the viscous forces.

2.2.2.4 Alternative descriptions of the time-domain equations of motion

The time-domain model in (2.56) is a vector Volterra integro-differential equation of convolution type [41] in the variable $\boldsymbol{\eta}(t)$. Time-domain simulations of WECs consist of the numerical integration of (2.56) for $t \in [t_0, t_f]$ for a given wave elevation $\zeta(t)$ and for certain initial conditions on the position and velocity, that is $\boldsymbol{\eta}(t_0) = \boldsymbol{\eta}_0$, $\dot{\boldsymbol{\eta}}(t_0) = \boldsymbol{v}_0$.

Although a variety of methods for the numerical integration of (2.56) are available [42] [43], the process could be computationally expensive due to the calculation of the convolution integral at each step. Since the excitation force is function of the wave elevation only, the convolution integral $\boldsymbol{f}_e(t) = \int_{-\infty}^{+\infty} \mathbf{h}(t-\tau)\,\zeta(\tau)\,d\tau$ can be computed before starting the simulation, and only the integral related to the radiation force is involved in the on-line computation.

The approximation of the radiation convolution kernels with a sum of exponentials has been proposed in [44]; in this case the elements of the matrix $\mathbf{K}(t)$ are described as

$$\mathrm{K}_{ij}(t) \approx \sum_{l=1}^{N_p} \alpha_l^{ij}\, e^{\beta_l^{ij} t}$$

and where the coefficients α_l^{ij} and β_l^{ij} can be calculated by using Prony's method. By defining the convolution integrals

$$I_l^{ij}(t) = \int_0^t \alpha_l^{ij}\, e^{\beta_l^{ij}(t-\tau)}\, \dot{\eta}_j(\tau)\, d\tau, \qquad i,j = 1,\dots,N_m \qquad l = 1,\dots,N_p \tag{2.72}$$

as the elements of the matrices $\mathbf{I}_l(t)$, where N_m is the number of modes, that is the size of the vector $\boldsymbol{\eta}$, the equation of motion (2.56) becomes a system of linear Ordinary Differential Equations (ODEs)

$$\begin{cases} \tilde{\mathbf{M}}\,\ddot{\boldsymbol{\eta}}(t) + \sum_{l=1}^{N_p} \mathbf{I}_l(t)\,\mathbf{1} + \mathbf{B}\,\dot{\boldsymbol{\eta}}(t) + \mathbf{S}\,\boldsymbol{\eta}(t) = \boldsymbol{f}_e(t) + \boldsymbol{f}_{pto}(t) \\ \dot{I}_l^{ij}(t) = \alpha_l^{ij}\,\dot{\eta}_j(t) + \beta_l^{ij}\, I_l^{ij}(t), \end{cases}$$

where $\mathbf{1}$ is the column vector with all elements equal to 1, and $\dot{I}_l^{ij}(t)$ is the derivative of (2.72). The computation of the convolution is avoided, but $N_m^2\, N_p$ variables have to be introduced ($I_l^{ij}(t)$) and the parameters α_l^{ij} and β_l^{ij} have to be calculated

In [35], the author proposes high-order ODEs for the description of the motion of floating bodies; high-order ODEs can be converted into a state representation, that is a system of first order ODEs. The first application of the state space representation to simulate WECs were described in [45] for an oscillating water column, and in [7] for a heaving body. The relation between a convolution integral and the state space description of a linear system is well known

in control theory; in fact, given the linear system

$$\begin{aligned} \dot{\boldsymbol{x}}_r(t) &= \mathbf{A}_r\, \boldsymbol{x}_r(t) + \mathbf{B}_r\, \dot{\boldsymbol{\eta}}(t) \\ \tilde{\boldsymbol{f}}_r(t) &= \mathbf{C}_r\, \boldsymbol{x}_r(t) + \mathbf{D}_r\, \dot{\boldsymbol{\eta}}(t) \end{aligned} \tag{2.73}$$

where $\dot{\boldsymbol{\eta}}(t)$ is the input and $\tilde{\boldsymbol{f}}_r(t)$ is the output, the input-output function $\boldsymbol{y}(t) = f\left(\boldsymbol{u}(.), \boldsymbol{x}_0\right)$, for the initial condition $\boldsymbol{x}_r(t_0) = \boldsymbol{x}_{r_0}$, can be written as

$$\tilde{\boldsymbol{f}}_r(t) = \mathbf{C}_r e^{\mathbf{A}_r(t-t_0)} \boldsymbol{x}_{r_0} + \int_{t_0}^{t} \mathbf{C}_r e^{\mathbf{A}_r(t-\tau)} \mathbf{B}_r\, \dot{\boldsymbol{\eta}}(\tau)\, d\tau + \mathbf{D}_r\, \boldsymbol{u}(t).$$

It is shown in [40] that, due to consideration of the physical system, the direct feed-through matrix $\mathbf{D}_r$ is zero when approximating the radiation force with a linear system ($\mathbf{D}_r = \mathbf{0}$).

By approximating the radiation force $\boldsymbol{f}_r$ with the output of the linear system (2.73), that is $\boldsymbol{f}_r(t) \approx \tilde{\boldsymbol{f}}_r(t)$, the time-domain equations of motion (2.56) becomes

$$\begin{aligned} &\tilde{\mathbf{M}}\, \ddot{\boldsymbol{\eta}}(t) + \mathbf{C}_r\, \boldsymbol{x}_r(t) + \mathbf{B}\, \dot{\boldsymbol{\eta}}(t) + \mathbf{S}\, \boldsymbol{\eta}(t) = \boldsymbol{f}_e(t) + \boldsymbol{f}_{pto}(t) \\ &\dot{\boldsymbol{x}}_r(t) = \mathbf{A}_r\, \boldsymbol{x}_r(t) + \mathbf{B}_r\, \dot{\boldsymbol{\eta}}(t), \end{aligned}$$

which, in turn, can be converted into the state space representation of a continuous time-invariant system as

$$\dot{\boldsymbol{x}}(t) = \mathbf{F}\, \boldsymbol{x}(t) + \mathbf{G}\, \boldsymbol{w}(t), \tag{2.74}$$

where the state vector $\boldsymbol{x}$, the input $\boldsymbol{w}$, the state transition matrix $\mathbf{F}$ and the input matrix $\mathbf{G}$ are defined as

$$\boldsymbol{x} = \begin{bmatrix} \boldsymbol{v} \\ \boldsymbol{\eta} \\ \boldsymbol{x}_r \end{bmatrix} \quad \boldsymbol{w} = \begin{bmatrix} \boldsymbol{f}_e \\ \boldsymbol{f}_{pto} \end{bmatrix} \quad \mathbf{F} = \begin{bmatrix} -\tilde{\mathbf{M}}^{-1}\mathbf{B} & -\tilde{\mathbf{M}}^{-1}\mathbf{S} & -\tilde{\mathbf{M}}^{-1}\mathbf{C}_r \\ \mathbf{I} & \mathbf{0} & \mathbf{0} \\ \mathbf{B}_r & \mathbf{0} & \mathbf{A}_r \end{bmatrix} \quad \mathbf{G} = \begin{bmatrix} \tilde{\mathbf{M}}^{-1} & \tilde{\mathbf{M}}^{-1} \\ \mathbf{0} & \mathbf{0} \\ \mathbf{0} & \mathbf{0} \end{bmatrix}.$$

The state space formulation of the equation of motion in (2.74) is particularly convenient for simulation and control because of the vast amount of literature and tools on linear control theory available for systems in state space form.

Procedures for calculating the matrices $\mathbf{A}_r$, $\mathbf{B}_r$ and $\mathbf{C}_r$ are based on system identification [6], which can be performed in the frequency-domain or in the time-domain [40]. The frequency-domain approach consists of applying system identification methods to obtain a transfer matrix $\Xi(\omega)$, the elements of which are transfer functions that approximate the elements of the radiation impedance matrix $\mathbf{Z}(\omega)$; the state space model is then the realization of the transfer matrix $\Xi(\omega)$. Time-domain identification techniques provide the matrices of the state space model directly from the impulse response matrix $\mathbf{K}(t)$. More details on system identification procedures

applied to the hydrodynamic radiation problem can be found in [6], [40], [8], [46], [47], [48] and [49]; a Matlab toolbox is also available for the frequency-domain identification [50].

The identification procedure for calculating the matrices $\mathbf{A}_r$, $\mathbf{B}_r$ and $\mathbf{C}_r$ of the state space representation (2.74) requires a certain degree of supervision. The work presented in this thesis has been partially motivated by this fact, and the method presented in chapter 4, which is the fundamental result, obviates the need for system identification to formulate the control problem for a WEC.

2.3 Energy absorption

The subject of the previous section (2.2) is a brief description of the interaction between a WEC and water from the point of view of the WEC motion. In this section, the interaction between water and a WEC is considered from the energy point of view. The energy transported by waves is considered first, while the description of the power flowing through the device is provided subsequently. The last part of the section describes the formulation of the theoretical optimal control law that provides the PTO force profile which yields the maximum amount of absorbed energy.

Only the special case of a single body WEC oscillating in heave is considered since the purpose of this section is to provide a reference for connecting the concepts of hydrodynamics, mechanics and control.

2.3.1 Energy transported by waves

The total stored-energy associated with water waves is the sum of the potential energy and the kinetic energy within the waves. The potential energy is due to the displacement of water in the vertical direction; it is calculated by multiplying the gravitational force acting on a vertical column of water by the vertical variation of its centre of gravity. Considering a unit horizontal area and a water depth of h, the gravitational force is $\rho g(h + \zeta)$ and the variation of the centre of gravity is $(h + \zeta)/2$. In the case of a harmonic, plane, progressive wave, the wave elevation is given by (2.23) and time-averaged potential energy is given by

$$E_p = \frac{\rho g}{4}|\zeta_a|^2.$$

The kinetic energy is associated with the motion of the fluid, the velocity of which is obtained by applying (2.5) to the velocity potential given in (2.21) [12]. The average kinetic energy

[12] Also in this case a harmonic, plane, progressive wave is considered

per unit volume is calculated as

$$\frac{1}{2}\rho\frac{1}{2}\,\mathrm{Re}\left\{|\hat{v}_x|^2+|\hat{v}_z|^2\right\}=\frac{\rho}{2}\omega^2|\zeta_a|^2e^{2kz},$$

where $\hat{v}_x$ and $\hat{v}_z$ are the horizontal and vertical components of the fluid velocity in (2.24) and in (2.25), respectively. The average kinetic energy per unit horizontal area in deep water is obtained by integrating on the interval $z\in(-\infty,0]$ and by approximating the dispersion relation in (2.22) with[13] $\omega^2=gk$; the result is

$$E_k=\frac{\rho g}{4}|\zeta_a|^2.$$

The time average, total stored-energy per unit horizontal area, for a plane, progressive, harmonic wave is then

$$E=E_p+E_k=\frac{\rho g}{2}|\zeta_a|^2. \tag{2.75}$$

The flow of the energy carried by water waves can be studied by looking at the propagation of power in the direction of the wave propagation. The time-average of the power propagating in the x direction, for a unit vertical area, is the intensity $I=1/2\,\mathrm{Re}\{\hat{p}\hat{v}_x^*\}$, where p is the water pressure given in (2.27), and $\hat{v}_x^*$ is given in (2.24). The wave-energy transport J, defined as the energy transported by water waves per unit width of the wave front, is then obtained by integrating I over the vertical direction, and the result is

$$J=\frac{\rho g^2 D(kh)}{4\omega}|\zeta_a|^2, \tag{2.76}$$

where $D(kh)$ is given by (2.30) .

The velocity at which the energy is transported can then be calculated as the ratio between the power transported by the waves per unit width (J) and the time-averaged total stored energy per unit horizontal area (E). By using (2.75) and (2.76), the result is:

$$\frac{J}{E}=\frac{g}{2\omega}D(kh)=v_g,$$

where v_g is the group velocity defined in (2.29). Thus, the energy propagates with the same velocity of the envelope modulating the amplitude of the wave, that is the group velocity v_g.

2.3.2 Energy absorbed by a wave energy converter

The absorption of wave-energy by an oscillating body can be studied as a destructive interference phenomenon. Energy absorption implies that the energy content of the incident wave is

[13] For deep water $kh >> 1$ thus $\tanh(kh)\approx 1$

reduced after the interaction with the oscillating body. Thus, the oscillating body must be able to radiate waves with appropriate amplitude and phase to destructively interfere with the incident wave. In other words, the energy content of the combination of the incident and radiated wave should be less than the energy content of the original incident wave.

For the simple case of a single body WEC subject to a harmonic wave, oscillating in one mode of motion only (the device in figure 2.2, for example), the absorbed power can be calculated by considering the balance of power flowing through the device, that is the difference between the power flowing into the device due to the excitation force, and the power being dissipated and radiated from the device. The time-average absorbed power, using (2.43), is then

$$P = \frac{1}{2}\,\mathrm{Re}\{\hat{F}_e\hat{v}^*\} - \frac{1}{2}\,\mathrm{Re}\{\hat{F}_r\hat{v}^*\} - \frac{1}{2}\,\mathrm{Re}\{\mathrm{B}\hat{v}\,\hat{v}^*\} = \frac{1}{2}|\hat{F}_e||\hat{v}|\cos(\gamma) - \frac{1}{2}\,(\mathrm{R}+\mathrm{B})\,|\hat{v}|^2, \quad (2.77)$$

where γ is the phase difference between phasors of the velocity $\hat{v}$ and the excitation force $\hat{F}_e$, and B is a linear dissipative term ($\mathrm{B} > 0$) approximating, for example, viscous losses (see Sec. 2.2.2.3). Equation (2.77) is a concave parabola ($\mathrm{R} > 0$) in the variable $|\hat{v}|$, which has its maximum when the amplitude of the velocity is

$$|\hat{v}|_{opt} = \frac{|\hat{F}_e|}{2\,(\mathrm{R}+\mathrm{B})}\cos(\gamma), \quad (2.78)$$

and the phase satisfies

$$\cos(\gamma) = 1 \qquad \Leftrightarrow \qquad \gamma = 0. \quad (2.79)$$

Thus, the maximum time-average absorbed power is

$$P_{MAX} = \frac{|\hat{F}_e|^2}{8\,(\mathrm{R}+\mathrm{B})}, \quad (2.80)$$

and is obtained when the velocity and the excitation force are in phase, and the velocity amplitude satisfies (2.78). The control strategy based on satisfying both the condition on the amplitude (2.78) and phase (2.79) of the velocity is known in the literature as *phase and amplitude control*, and it will be discussed in more detail in chapter 3.

The amount of energy absorbed by a WEC can also be related to the energy transported by waves. For an axisymmetric point absorber[14] oscillating in heave only and subject to harmonic waves, the radiation resistance R is related to the excitation force by means of the Haskind's relation (2.47) as

$$\mathrm{R} = \frac{2\omega k}{\rho g^2 D(kh)}|\mathrm{H}|^2, \quad (2.81)$$

[14] A point absorber is defined as an oscillating body, the horizontal dimensions of which are very small when compared to the wavelength

where H is the excitation force coefficient (2.45) , and $|\hat{F}_e|^2 = |\mathrm{H}|^2|\zeta_a|^2$. Therefore, by using (2.76) and neglecting the linear dissipative term B, the maximum absorbed power (2.80) is related to the wave energy transport J as

$$P_{MAX} = \frac{|\hat{F}_e|^2}{8\mathrm{R}} = \frac{1}{k}J. \tag{2.82}$$

The ratio $P_{MAX}/J = \lambda/(2\pi)$ is named *absorption width* [51, 52, 53], and it states that "the maximum energy which may be absorbed by a heaving axisymmetric body equals the wave energy transported by the incident wave front of width equal to the wavelength divided by 2π" [5]. Thus, a heaving point absorber is capable, at least in theory, of absorbing an amount of power flowing through a wavefront of width larger than the physical dimensions of the device.

In practice, however, when $\mathrm{B} \neq 0$, by using (2.80), (2.81) and (2.76), the upper bound for the maximum time-average absorbed power is

$$P_{MAX_B} = \frac{1}{\dfrac{k}{J} + \dfrac{8\mathrm{B}}{|\hat{F}_e|^2}}. \tag{2.83}$$

Both the upper bounds (2.82) and (2.83) increase as $\omega \to 0$; however, the corresponding optimal velocity (2.78) also increases, because the excitation force is bounded and the radiation resistance tends to zero (2.65) ($R \to 0$ as $\omega \to 0$). Consequently, the velocity magnitude may become so large that the device could oscillate with an amplitude larger than its own draft, that is it would fully emerge from the water. In this respect, and still under the assumption that the device is a point absorber, Budal and Falnes [54] have formulated an upper bound related to the volume V of the oscillating body, which is:

$$P_{MAX_V} = \frac{\rho g}{4} V \zeta_a \omega. \tag{2.84}$$

Figure 2.15 depicts the power bounds and the motion of a single oscillating body WEC referenced to the seabed (figure 2.2), composed of a vertical cylinder[15] of radius 5m and draught 6m, the hydrodynamic coefficients of which are shown in figure 2.14. In particular, the upper bounds in equations (2.82), (2.83) and (2.84) are plotted in figure 2.15a, together with the power absorbed by the WEC when the oscillation amplitude is constrained to be smaller than the draught ($|\hat{\eta}| \leq |\hat{\eta}_{max}|$=6m). That is:

$$P_{ABS} = \frac{1}{2}|\hat{F}_e||\hat{v}| - \frac{1}{2}(\mathrm{R}+\mathrm{B})|\hat{v}|^2, \qquad \text{with} \quad |\hat{v}| = \min\left\{\frac{|\hat{F}_e|}{2(\mathrm{R}+\mathrm{B})},\ \omega|\hat{\eta}_{max}|\right\},$$

and where the value of the linear damping term is $\mathrm{B} = 2\ 10^4$ Ns/m. The amplitude of the heave

[15] A vertical cylinder is a cylinder which has its axis of symmetry directed along the vertical direction

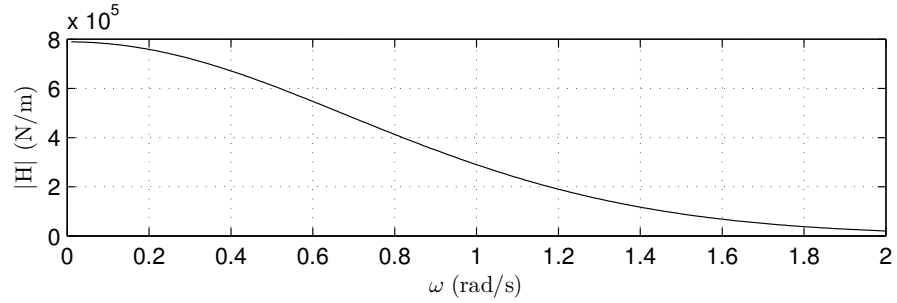

(a) Excitation force coefficient H(ω).

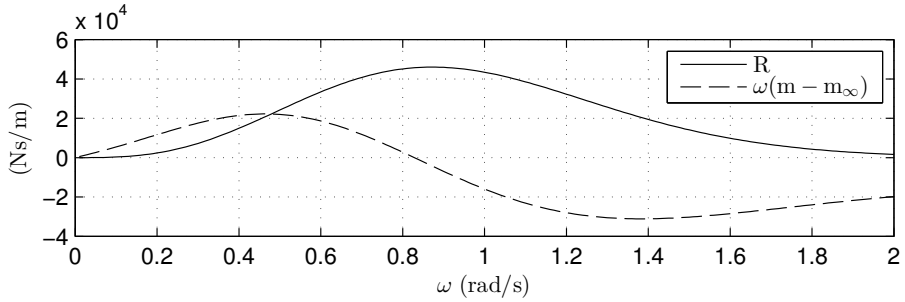

(b) Radiation resistance R(ω) and added mass m(ω), where m_∞=2.39 10^5kg.

Figure 2.14: Hydrodynamic coefficients of a vertical cylinder with radius=5m and draught=6m.

oscillation $|\hat{\eta}|$ and the corresponding velocity $|\hat{v}|$ are plotted in figure 2.15b.

The value in equation (2.80) is the maximum power that can be absorbed by an oscillating body under the excitation of a monochromatic wave. From the perspective of wave energy conversion, it may be more meaningful to consider the maximisation of the useful energy, which is the part of the absorbed energy that is extracted from the device and converted into a usable form, such as electricity, by means of the PTO. Considering again the simple case of the device depicted in figure 2.2, the useful energy may be defined as the mechanical work performed by the PTO force f_{pto}, which is applied between the oscillating body and a fixed reference, such as the sea bed. When the WEC is under the effect of a generic (polychromatic) sea profile, the mechanical work W_{pto} performed by f_{pto} is:

$$W_{pto} = -\int_{-\infty}^{+\infty} f_{pto}(t)\, v(t)\, dt.$$

If the conditions for the existence of the integral defining W_{pto} are verified, by means of the generalise Parseval's theorem[16] and by considering that $f_{pto}(t)$ and $v(t)$ are real, W_{pto} can be

[16] Also known as Plancharel's formula: $\int_{-\infty}^{\infty} f(t)g(t)\,dt = \frac{1}{2\pi}\int_{-\infty}^{\infty} F(\omega)G^*(\omega)\,d\omega$

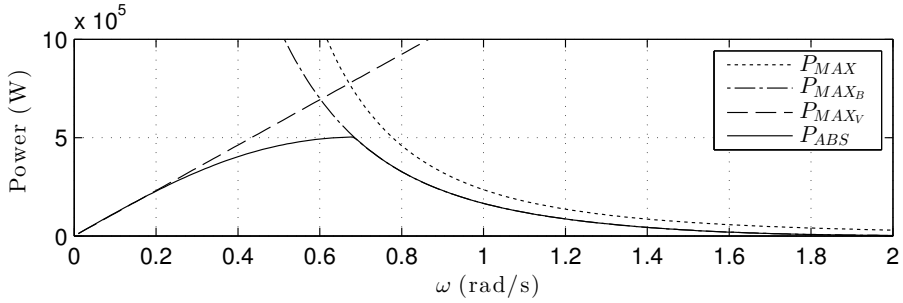

(a) Absorbed power (P_{ABS}) and upper bounds (P_{MAX},P_{MAX_B},P_{MAX_V})

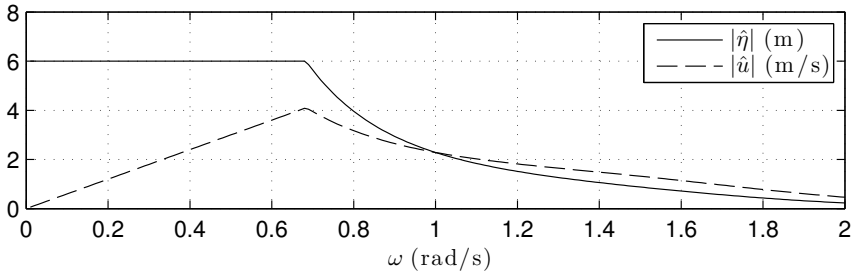

(b) Amplitudes of the oscillation in heave $|\hat{\eta}|$ and the velocity $|\hat{v}|$, when the oscillation amplitude is constrained to be smaller than the draught ($|\hat{\eta}| \leq |\hat{\eta}_{max}| = 6$m).

Figure 2.15: Maximum absorbed power and motion of a heaving vertical cylinder of radius 5m and draught 6m, for regular waves of frequency ω and amplitude ζ_a=1m.

written in terms of the frequency transforms of the velocity and the PTO force as

$$W_{pto} = -\frac{1}{2\pi}\int_0^\infty F_{pto}(\omega)v^*(\omega) + F^*_{pto}(\omega)v(\omega)\,d\omega.$$

By using the equation of motion in (2.70), and by defining the intrinsic impedance of the oscillating body $\mathbf{Z}_i(\omega)$ as

$$\mathrm{Z}_i(\omega) = i\omega\mathrm{M} + \mathrm{B} + \mathrm{Z}(\omega) + \frac{\mathrm{S}}{i\omega}, \tag{2.85}$$

it can be shown [5] that the maximum useful energy is

$$W_{pto,MAX} = \frac{1}{2\pi}\int_0^\infty \frac{|F_e(\omega)|^2}{2\mathrm{R}_i(\omega)}d\omega$$

when the PTO force satisfies

$$F_{pto}(\omega) = -\mathrm{Z}_i^*(\omega)\,v(\omega) \tag{2.86}$$

where R_i is the intrinsic resistance ($\mathrm{R}_i = \mathrm{Re}\{\mathrm{Z}_i\}$). The velocity of the oscillating body corresponding to the maximum useful energy is $v(\omega) = \mathrm{F_e}(\omega)/(2\mathrm{R_i}(\omega))$, which is similar to the expression of the optimal velocity for the maximum absorbed power in the harmonic case (2.78).

When a control system is applied to the WEC with the objective of controlling the PTO force according to (2.86), the control strategy is generally known in the literature as *complex conjugate*, *impedance-matching* or *reactive* control, and it will be discussed in more details in section 3.1. The names of these control strategies originate from the fact that if the PTO impedance $\mathrm{Z}_{pto}(\omega)$ is defined such that

$$F_{pto}(\omega) = -\mathrm{Z}_{pto}(\omega)\, v(\omega), \tag{2.87}$$

then maximum absorption is achieved when the PTO impedance is equal to the complex conjugate of the mechanical impedance Z_i ($\mathrm{Z}_{pto} = \mathrm{Z}_i^*$), or else when the reactance of the PTO (X_{pto}) cancels the mechanical reactance of the device (X_i), that is $\mathrm{X}_{pto} = -\mathrm{X}_i$, where $\mathrm{X}_{pto} = \mathrm{Im}\{\mathrm{Z}_{pto}\}$ and $\mathrm{X}_i = \mathrm{Im}\{\mathrm{Z}_i\}$. The term *impedance-matching* control originates from electrical engineering, where the condition for maximum power transfer between an electrical generator and complex load is analogous to eq.(2.86).

2.4 Summary

This chapter has presented a brief overview of oscillating body WECs. The first part (section 2.1) is dedicated to a general description of the most common type of oscillating body WECs, where the basic working principles of both the primary absorbers and the PTOs are considered.

The second part (sec. 2.2) presents a concise derivation of the mathematical model—which will be used throughout the rest of this thesis—that describes the motion of a floating body when subject to the force exerted by water waves. The derivation begins from the Navier-Stokes and the continuity equations, and ends at the linear model describing the wave-body interactions. An additional purpose of section 2.2 is to show the simplifications and assumptions that have been made in the derivation of the model, which restricts its validity.

The energy aspects of the wave-body interactions have been considered in section 2.3: transportation of energy by water waves has been described first, followed by a discussion on the absorption of energy by an oscillating body, the motion that permits the absorption to be maximised, and the relation between the maximum energy absorbed by a WEC and the energy transported by waves. Section 2.3.2 in particular provides a set of results, namely the phase and amplitude conditions in (2.79) and (2.78), and the impedance matching in (2.86), which are at the center of a number of control strategies that will be described in the review chapter of the control of WECs (chapter 3).

Chapter 3

Control of wave energy converters: Literature survey

The amount of energy absorbed by a WEC depends strongly on its motion, which can be controlled, for example, by means of the force exerted by the PTO, as described sec. 2.3.2. If a WEC is modelled by means of linear system (section 2.2), the energy absorption is maximised when the motion and the PTO force satisfy the conditions in equation (2.86), called reactive control or complex conjugate control.

This chapter provides an overview of the control methods that have been described in the literature for the control of WECs. At first, in section 3.1, the theory of reactive control is described with the addition of some illustrative examples which allow a better insight into the wave energy conversion process and, at the same time, highlight some of the drawbacks associated with reactive control. Section 3.1 also includes a brief description of different control strategies which share the common objective of the maximisation of the absorbed energy when no restriction is applied to the system.

Applications of linear PTO damping are described in section 3.2; this type of control is suboptimal, in the sense that it does not guarantee the maximum energy absorption, but it is widely studied in the literature and in practice because of its simple formulation. Latching control and related control strategies are described with illustrative examples in section 3.3; this type of control is more sophisticated than linear damping and requires more complex PTOs but allows significant performance improvement in terms of absorbed energy. Other control

strategies which don't fall in the previous categories are considered in section 3.4.

Wave energy converters are mechanical devices and the components with which they are built can operate safely and efficiently only within prescribed ranges. For example, an oscillating body WEC with an hydraulic PTO has a limited oscillation amplitude due to the length of the stroke of the hydraulic piston, and can only exerts a maximum force which is related to the maximum pressure for which the hydraulic circuit is rated. Consequently, the energy maximisation problem becomes a constrained optimal control problem, and section 3.5 presents the control techniques that have been implemented to address this problem.

When groups of WECs are deployed in an array, the control problem changes because of the hydrodynamic interaction; section 3.6 presents a brief description of the theory concerning the energy maximisation problem for a system of oscillating bodies, and some illustrative examples to highlight the main differences with the case of an isolated device.

The control system affects the amount power that a WEC absorbs and injects into the electrical grid; regulation concerning the characteristics of the power delivered by generators connected to the network is stringent and section 3.7 presents control strategies that address the issue of electrical network integration. The control system also affects the power rating of the PTO which, in turn, strongly affect the economic viability of a WEC, and section 3.7 also includes published works in which this problem has been addressed.

Several reviews and comparisons of control strategies are available in the literature and they are presented in section 3.8, while reviews of wave energy conversion in general terms are given in: [55], [52], [56], [57], [58], [59] and [2]. In [60] it is also presented an historical review of control for WECs, in which the author references the main publications that contributed to the development of the theory for optimality. A special issue of the Philosophical Transactions of the Royal Society on wave energy has also been also been published [26].

3.1 Linear unconstrained optimal control

3.1.1 Overview

A control strategy which is the result of some form of optimisation is generally known as optimal control. In the context wave energy conversion, the results presented in sec. 2.3.2 fall into the category of optimal control because they have been developed by pursuing the maximisation of the average power absorbed by WEC. In particular, the formulations presented therein, i.e. phase and amplitude control and reactive control (or impedance matching control), allow WECs to absorb the maximum amount of energy from waves when the systems (wave-body interaction) is linear (i.e. described by a linear model as illustrated in section 2.2).

All of the control strategies lead to the same results in terms of motion, forces and converted

power; however, they differ in the method by which they achieve the objective. In general, the maximisation of the energy absorbed by a WEC is pursued by acting on the PTO force to control the motion. In this respect, the main difference between reactive control and phase and amplitude control is that the latter requires knowledge of the excitation force to calculate the reference velocity [5] (see eq.(2.78) for the amplitude condition and eq.(2.79) for the phase condition). The PTO force resulting from reactive control is instead calculated directly from the velocity, as in eq.(2.86). This situation is illustrated by the block diagrams in figure 3.1: in particular, for the case of the phase and amplitude controller depicted in fig. 3.1a the controller, denoted by C_{PA}, is designed to provide the required PTO force which allows the WECs to oscillate with the reference optimal velocity, calculated from the excitation force as $v_{opt}(\omega) = F_e(\omega)/2\mathrm{R}_i(\omega)$, where R_i is the real part of the mechanical impedance Z_i defined in eq. (2.85). The control system denoted by C_{RC} in figure 3.1b is designed to produce a PTO force $F_{pto}(\omega) = -\mathrm{Z}_i^*(\omega)\, v(\omega)$, which depends only on the actual velocity of the WEC (u). That is, in the Laplace domain, if $P(s)$ is the transfer function of the PTO, ideally, the transfer function of the controller $C_{RC}(s)$ would be $C_{RC}(s) = -\mathrm{Z}_i^*(s)/P(s)$.

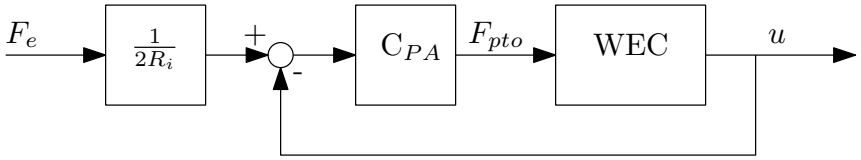

(a) phase and amplitude control

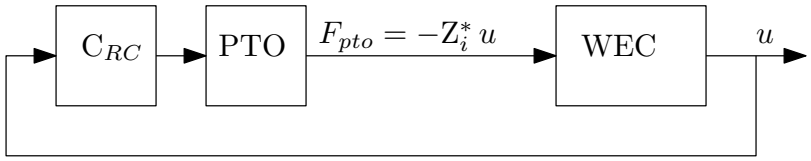

(b) Reactive control

Figure 3.1: Block diagrams of reactive control and phase and amplitude control

The maximisation of the absorbed energy by means of reactive control and phase and amplitude control is achieved at the cost of large motions, large forces and power fluctuations. Figures 3.2 and 3.3 depict the simulation results obtained by applying these control strategies to a heaving body WEC of the type depicted in fig. 2.2, for a monochromatic incident wave. More specifically, the oscillating body the same vertical cylinder described in section 2.3.2, and the wave period is T=8s for the results in figure 3.2, and T=5.9s for the results in fig. 3.3.

By implementing reactive control, as the name suggests, the PTO reactance X_{pto} is generally non-zero; in fact the PTO reactance is $\mathrm{X}_{pto} = \mathrm{X}_i$ (see eq. (2.86)). Consequently, when $\mathrm{X}_{pto} \neq 0$ the PTO absorbs power during some time intervals and returns power to the oscillating body during some other time intervals. This effect can be clearly observed in figure 3.2, where the

grey area denoted by R indicates that the PTO is working in "reactive mode", that is the power flows from the PTO to the oscillating body. Additionally, fig. 3.2 shows the large fluctuations of the total absorbed power $P(t) = -f_{pto}(t)\dot{z}(t)$ and, most importantly, the large ratio between the peak power and the average power $\bar{P}$.

When the period of the incident wave coincides with the natural period of the device, in this case T≈5.9s, the reactance of the PTO vanishes ($X_{pto} = 0$) because, by definition, the mechanical reactance of the device is zero at resonance [5]. Consequently, as it can be observed in fig. 3.3, no reactive power is present, thus the PTO is not required to return power to the oscillating body, and the ratio between the peak power and average power reaches its minimum[1], which is 2.

To achieve this behaviour, the PTO requires more expensive components, because the cost of the PTO increases with its power rating, that is the maximum power that it can manage; however, the revenue of a WEC is positively correlated (among many other factors) to the average power (or energy) delivered by the WEC to the electrical grid. Consequently, reactive control might reduce the economical convenience of the WEC because of the large ratio of peak power over average power.

Similar considerations arise by studying the system from the point of view of the PTO efficiency: in this respect it is useful to consider the plot in fig. 3.4, which shows the ratio of the average reactive power $\bar{P_R}$ over the average of the total absorbed power $\bar{P}$, as function of the wave period. As previously noted, the reactive power at resonance is zero ($\bar{P_r}|_{T=5.9s} = 0$); however, when the period of the incident wave is T=8s, the fraction of the power returned to the oscillating body by the PTO is $\bar{P_R}/\bar{P} = 0.38$, that is 38% of the energy absorbed by the PTO "oscillates" between the PTO and the kinetic and potential energy of the wave activated body. Further away from resonance, the ratio increases up to $\bar{P_R}/\bar{P} = 0.5$. In this situation, the total energy delivered to the electrical grid can be significantly reduced if the overall efficiency of the energy transformation processes is not high. Again, the increase in efficiency is associated with both higher cost of the the device but also with higher revenue (more electricity produced).

Figures 3.2 and 3.3 allows the observation of the characteristic relations between the motion and the forces. In particular, the phase condition in eq. (2.79) which establishes that, both in resonance and off-resonance, the velocity ($\dot{z}$) and the excitation force (f_e) are in phase. Addi-

[1] By considering both PTO force and velocity as sinusoidal functions with the same frequency ω and relative phase ϕ, that is $f_{pto} = A_f \cos(\omega t)$ and $\dot{z} = A_v \cos(\omega t + \phi)$, then the instantaneous power is

$$P = -A_f A_v \cos(\omega t)\cos(\omega t + \phi) = -A_f A_v \frac{1}{2}\left(\cos(\phi) + cos(2\omega t + \phi)\right)$$

By implementing reactive control $F_{pto} = -Z_i^* u$, thus $\tan(\phi) = X_i/R_i$; at resonance, $X_i = 0$ hence $\phi = \pi$ and the instantaneous power is $P_{res} = A_f A_v \frac{1}{2}[1 + \cos(2\omega t)]$. The average absorbed power is

$$\bar{P} = \frac{1}{T}\int_0^T P_{res}\, dt = \frac{1}{T}\int_0^T A_f A_v \cos^2(\omega t)\, dt = \frac{1}{2} A_f A_v, \qquad \text{with } T = \frac{2\pi}{\omega}$$

and the ratio $\frac{\max|P_{res}|}{\bar{P}} = 2$.

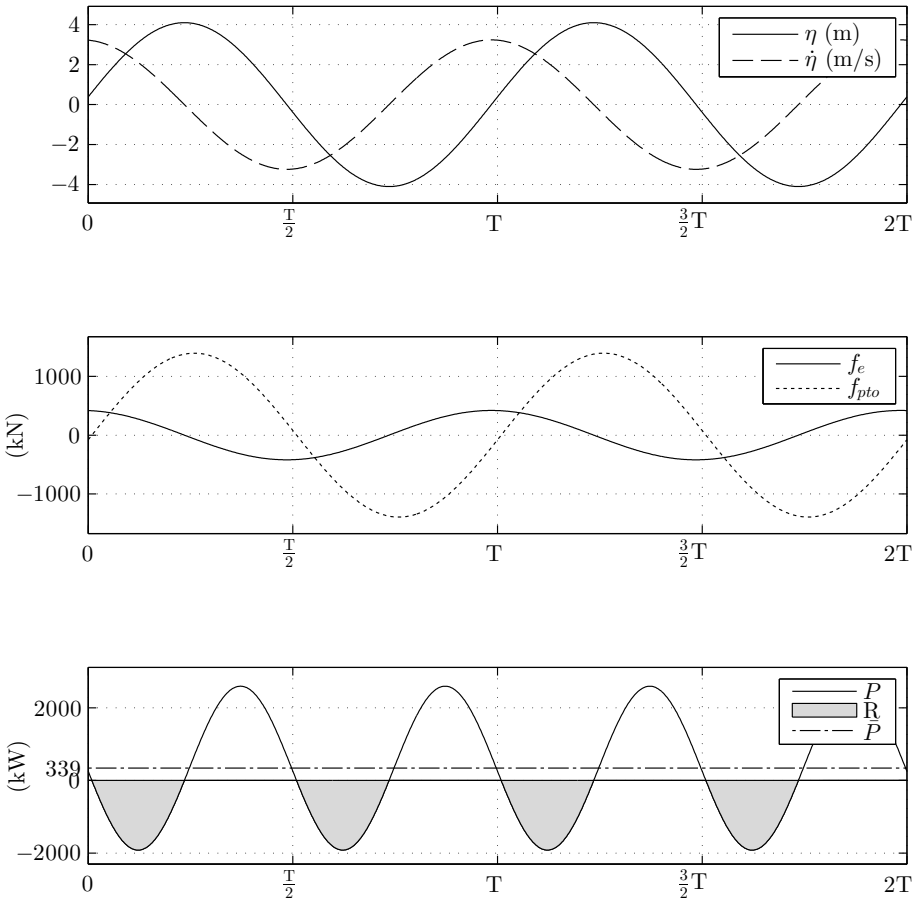

Figure 3.2: Position (η), velocity ($\dot{\eta}$), excitation force (f_e), PTO force (f_{pto}), total absorbed power (P), average absorbed power ($\bar{P}$), on a vertical cylinder, controlled using reactive control, for monochromatic wave with period T=8s. The grey area (R) indicates the PTO working in reactive mode.

tionally, when the device is oscillating at its resonance period (figure 3.3), the phase of the PTO force is opposite to the phase of both the excitation force and the velocity; in fact, at resonance the imaginary part of the PTO impedance is zero because $\mathrm{X}_i = 0$, thus $F_{pto} = -\mathrm{R}_i v$, with $\mathrm{R}_i > 0$ (see sec. 2.2.2.2).

A brief discussion on the causality of the control strategies presented in this chapter is also of particular interest. The impulse response $\mathrm{h}_i(t)$ associated with the mechanical impedance Z_i is non-causal, because the inverse Fourier transform of Z_i, defined in (2.85), is

$$\mathrm{h}_i(t) = \mathrm{K}(t) + \mathrm{B}\sqrt{2\pi}\delta(t) - \mathrm{M}\sqrt{2\pi}\dot{\delta}(t) - \sqrt{\frac{\pi}{2}}S\,\mathrm{sgn}(t),$$

where $\mathrm{K}(t)$ is the causal impulse response of the radiation impedance (see section 2.2.2), $\dot{\delta}(t)$

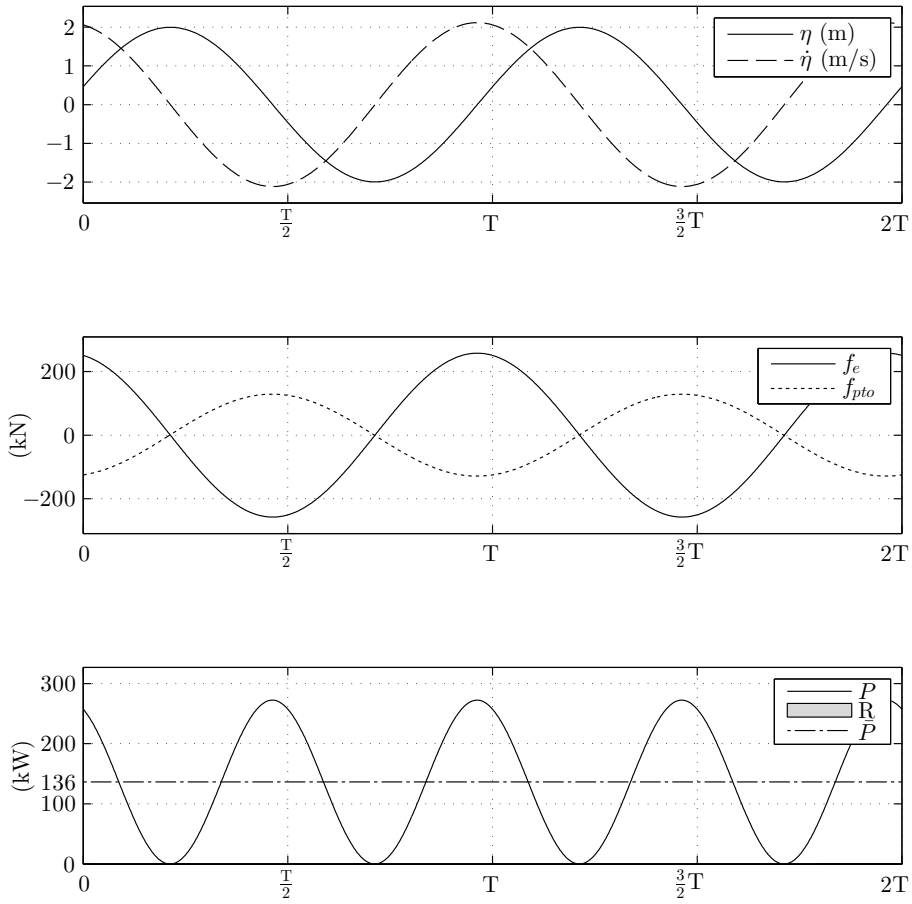

Figure 3.3: Position (η), velocity ($\dot{\eta}$), excitation force (f_e), PTO force (f_{pto}), total absorbed power (P), average absorbed power ($\bar{P}$), on a vertical cylinder, controlled using reactive control, for monochromatic wave at resonance (T=5.9s).

is the first derivative of the Dirac delta function and sgn(t) is the sign function. The impulse response $\mathrm{h}_i(t)$ is non-zero for for $t < 0$, that is $\mathrm{h}_i(t) = \sqrt{\pi/2}\,\mathrm{S} \neq 0$, for $t < 0$, if $\mathrm{S} \neq 0$. However, the impedance Z_i can be modified by adding the term $-\mathrm{S}\pi\delta(\omega)$, resulting in

$$\widetilde{\mathrm{Z}}_i(\omega) = \mathrm{Z}(\omega) + \mathrm{B} + i\omega\mathrm{M} + \frac{\mathrm{S}}{i\omega} - \mathrm{S}\pi\delta(\omega),$$

in which case the corresponding impulse response is causal ($\tilde{\mathrm{h}}_i(t) = 0$ for $t < 0$). The impedance Z_i differ from the impedance $\widetilde{\mathrm{Z}}_i$ only for $\omega = 0$; this difference is not relevant in practice because the mean velocity of oscillating-body WECs is generally zero (no drift), that is $v(\omega)|_{\omega=0} = 0$.

From the causality of $\widetilde{\mathrm{Z}}_i$, it follows that reactive control, the transfer function of which is $-\mathrm{Z}_i^*$, is non-causal; in fact, if the impulse response of $\widetilde{\mathrm{Z}}_i$ is causal, then the impulse response of its complex-conjugate is non-causal. The non-causality of $\widetilde{\mathrm{Z}}_i^*$ can be determined by considering

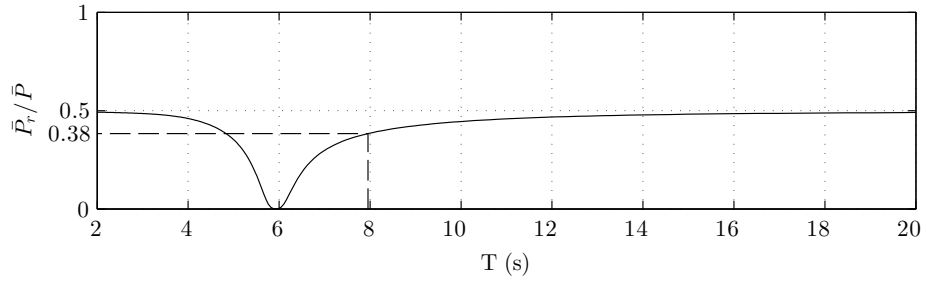

Figure 3.4: Ratio of the total energy flowing through the PTO (W_{pto}) and the energy returned to the device (R).

that the real and imaginary parts of the Fourier transform of a causal and real impulse response are related by the Hilbert transform as in eq.(2.69). In more detail, $\tilde{h}_i(t)$ is causal if and only if its Fourier transform satisfies [61]

$$\widetilde{Z}_i = \widetilde{R}_i + i\mathscr{H}\{\widetilde{R}_i\};$$

consequently, the impulse response associated with $\widetilde{Z}_i^*$ is non-causal because

$$\widetilde{Z}_i^* = \widetilde{R}_i - i\mathscr{H}\{\widetilde{R}_i\}.$$

In particular, the impulse response associated with reactive control ($-Z_i^*$) is anticausal, which means that is it zero for $t > 0$. This fact can be easily verified by considering that a generic impulse response $h(t) \in \mathscr{R}$ can be decomposed as the sum of an even and an odd part, that is $h(t) = h_e(t) + h_o(t)$, the Fourier transform of which is

$$\mathscr{F}\{h(t)\} = \int_{-\infty}^{+\infty} h_e(t)\cos(\omega t)\,dt - i\int_{-\infty}^{+\infty} h_o(t)\sin(\omega t)\,dt.$$

If $h(t)$ is causal, $h_e(t)$ and $h_o(t)$ can be defined as:

$$h_e(t) = \begin{cases} r(t) & \text{if } t > 0, \\ r(-t) & \text{if } t \leq 0 \end{cases}$$

$$h_o(t) = \begin{cases} r(t) & \text{if } t > 0, \\ 0 & \text{if } t = 0, \\ -r(-t) & \text{if } t < 0 \end{cases}$$

where $r(t) = h(t)/2$. Therefore, complex conjugation of the Fourier transform of a causal impulse response corresponds to change of sign of the odd part of the impulse response, which

results in the anticausal impulse response

$$\mathrm{h}_e(t) - \mathrm{h}_o(t) = \begin{cases} 0 & \text{if } t > 0, \\ 2\mathrm{r}(-t) & \text{if } t \leq 0. \end{cases}$$

Phase and amplitude control is also non-causal, because the radiation resistance is real and even, therefore $\mathscr{F}^{-1}\{1/2\mathrm{R}_i(\omega)\}$ is an even function of time, and the associated impulse response is non-zero for $t < 0$.

The non-causality of the reactive control ($F_{pto} = -\mathrm{Z}_i^* v$) implies that the calculation of the PTO force at any time requires future knowledge of the velocity, whereas non-causality of the phase and amplitude control ($u_{opt} = F_e/2\mathrm{R}_i$) implies that the calculation of the optimal velocity reference requires future knowledge of the excitation force. Future knowledge of the excitation force may be obviated by wave forecasting or by measuring the wave elevation at a certain distance from the WEC. However, in doing so, it has to be taken into account that the wave elevation to excitation force transfer function is also non-causal, as discussed in sec. 2.2.2.

3.1.2 Literature review

The analytical formulation of the maximum power absorbed by an system of oscillating devices has been originally derived, independently, by Evans [62] and Falnes [63], while overviews of the optimal control theory for heaving body wave energy converters are provided in [60], [64] and [65]. The book by Falnes [5] gives a comprehensive description and discussion about the theory of maximum power absorption. Korde in [66] also provides an overview of the theory of WEC optimal control; in addition, the author presents a time domain formulation of the optimality problem and a solution for a motion-compensated platform on a floating body in an irregular sea.

One of the first applications of reactive control is described in [67] and applied to the Salter duck, which is a WEC capable of oscillating in heave and pitch. Complex-conjugate control applied to the Salter duck is also described in [68]; the paper includes both simulation and experimental results, in which the author shows that the device "can absorb 100 % of the incident power in its own width for linear monochromatic waves" in a certain frequency band. Hals [69] implements reactive (complex-conjugate) control applied to a semi-submerged sphere oscillating in heave.

Numerical modelling and simulation for a single DoF heaving body type WEC is presented in [70] and [71]; the buoy is directly coupled with a linear generator capable of generating a reaction force. Both the body and the linear generator have been modelled by means of an analogous electrical circuit and then simulated using Matlab/Simulink environment, applying optimal phase and amplitude control.

A two-body coupled oscillator WEC is considered in [72] and [73]; the author presents a frequency domain model for the two DoF systems, and describes the calculation of the optimal complex load that maximizes the converted energy. A study of optimal control applied to a two-body point absorber oscillating in heave is also described in [74].

Simulation of the AWS first prototype is presented in [75], [76], [77] and [78]. Detailed descriptions of reactive control and phase and amplitude control implementation are provided, together with mathematical models and discussions regarding issues on the practical implementation of such techniques. Optimal control of the AWS is presented in [79] from an electrical point of view; in particular, the PTO is composed of a linear generator, and the authors describe a method to optimise the stiffness and damping of the linear generator.

The effect of irregular waves (polychromatic waves) on complex-conjugate control is analysed in [80] and [81] while, in [82], signal processing techniques are applied to irregular wave measurements to mitigate the effect of the anti-causality and improve power absorption when implementing reactive control. The implementation of the complex-conjugate control law in (2.86) requires future knowledge of the excitation force or of the incoming waves, which can be obtained by prediction or by measurements at an appropriate distance. In [83], [84], [85] and [86], the authors provide an analysis of the prediction requirements and of the effect of prediction errors in the control of heaving buoy WECs and in the absorbed energy, and in [87] wave elevation predictions have been used to implement a suboptimal control algorithm based on complex conjugate control.

In [88] and [89], reactive control of WEC with a linear generator is implemented by tuning the PTO at the peak frequency of the spectrum, that is, the PTO force is provided by the equation in (2.86), for $Z_i(\omega_p)$, where ω_p is the peak frequency of the spectrum. The result is that the PTO force is described by the equation of a second order oscillator with frequency independent coefficients, where the damping term is the radiation resistance at ω_p and the mass is the sum of the added mass at ω_p and the mass of the WEC. A similar approach has been described in [90], where the complex-conjugate control has been implemented by tuning the device to the peak frequency of the current sea-state.

Implementation of causal control for the Wavestar device is described in [91]. The Wavestar prototype considered in the paper is a WEC composed of two hemispherical absorbers of 5m radius which are independently controlled. Each of the absorbers is attached to a hinged arm and has one DoF, and the resulting oscillating motion is a combination of heave and pitch. The device is equipped with an hydraulic PTO capable of returning energy to the floater. The PTO has been modelled as a mass-spring-damper, the coefficients of which are calculated by a causal reactive control algorithm, named the Wave Power Extraction Algorithm, based on wave elevation measurements in the proximity of the device. The wave elevation measurements are then averaged on a 10 minutes period in order to estimated the mean wave period and significant

wave height. The effect of PTO force restrictions on the absorbed energy has also been studied.

In [92], the authors approximate the model of a single-body heaving WEC with a second order oscillator, and the non-causal transfer function between the optimal velocity and the excitation force is approximated by a constant. The authors show that, "from theoretical considerations and numerical simulations over a range of heaving WECs in different sea conditions", "such suboptimal and causal approximation, while significantly reducing the complexity and improving the robustness of reactive control, allows the achievement of values of energy capture very close to the ideal optimum."

A different approach is presented by Scruggs and Lattanzio in [93] [94], where the authors developed an optimal causal control system for a three DoF (surge, pitch and heave) WEC based on a Linear Quadratic Gaussian regulator which obviates the causality issue. The causal control law requires only the knowledge of past measurements and of the spectral characteristics of the sea. The authors also provide a discussion on the power factor (reactive power) for both reactive control and causal control, in addition to the sensitivity analysis of the produced power with respect to the variation of the spectral characteristic of the sea.

Causal stochastic optimal control has been implemented in [17] on a heaving point absorber with nonlinear hydrostatic. The optimal non-causal feedback control law for the nonlinear model has been derived by means of PMP. The causal controller, derived by approximating the non-causal control law, is expressed as the difference between a term proportional to the body velocity and the radiation force, the proportionality coefficient of which is frequency independent. However, the algorithm devised to calculate the proportionality coefficient depends on the spectral characteristics of the wave elevation.

3.2 Linear power take off damping

Maximum energy absorption using reactive control requires real time feedback control of the instantaneous PTO force, and sophisticated machinery for the construction of the PTO capable of exerting the required optimal force. A widely studied approach to avoid the difficulties in the implementation of feedback control of WECs is known in the literature as *linear PTO damping*, where the instantaneous value of the PTO force is linearly proportional to the velocity of the oscillating body, that is

$$f_{pto}(t) = -\mathrm{B}_{pto} v(t),$$

where B_{pto} is the PTO the damping coefficient and $\mathrm{B}_{pto} > 0$. In theory, this approach is simpler to implement than reactive control, because no prediction of the excitation force is required, but only the instantaneous value of the body velocity, for which measurements off the shelf instrumentation is commonly available.

Linear damping provides some advantages over reactive control from the mechanical point of view, in that the PTO is not required to return energy to the oscillating body, requiring less sophisticated components and alleviating the issue regarding the overall mechanical efficiency of the conversion machinery. In fact, the instantaneous power absorbed by the PTO, which is

$$P(t) = -f_{pto}(t)\, v(t) = \mathrm{B}_{pto} v(t)^2, \tag{3.1}$$

is always positive, because $\mathrm{B}_{pto} > 0$.

Linear damping, however, gives a much smaller amount of absorbed power when compared to reactive control, and the linear relation between velocity and PTO force, even if it is simple from the theoretical point of view, it may not be straightforward to implement with mechanical components only, without using any feedback control. Additionally, the optimal value of the PTO damping, that is the value of B_{pto} which maximises the instantaneous absorbed power in (3.1), can be easily calculated for a monochromatic incident wave [5]. However, in practice, where the incident wave is polychromatic, B_{pto} is more difficult to calculate, also because the sea state changes over time, that is the spectral components of the incident wave are not constant over time.

Damping optimisation and shape optimisation are carried out in [95] for a vertical cylinder heaving WEC, for both regular and irregular seas; damping optimisation has been studied also for a similar device subject to constraints in [96]. Restriction on the excursion of the stroke and on the PTO applied forces are considered in order to satisfy design constraints; besides, minimisation of the probability of slamming is considered to improve the longevity.

In [97], several passive tuning strategies for irregular sea are compared; the tuning is performed by setting the natural frequency of the device to the peak frequency, to the "energy frequency" (that is an energy averaged frequency) or to the weighted average frequency of a JONSWAP spectrum. Passive tuning is also compared with active tuning, in which the natural frequency is continuously adjusted based on the current power spectrum provided by FFT computation of the wave-elevation data. Damping optimisation is also reported in [98], where the device considered is a cylinder of 10m diameter and 2m draught, which is not designed to work in resonance, but to behave as a wave follower, and it is allowed to move in all the six DoF. The authors observed that by tuning the damping every hour rather than on a yearly basis, the gain in absorbed energy in only 3%. A two-body heaving WEC has been considered in [99]; in this paper, the authors optimise the damping coefficients for several wave climates with the objective of maximising the energy production.

Experimental results from sea trials for a WEC with resistive load are provided in [100], while in [101] the experimental results of the same device are compared with the simulation of its model. The device is equipped with a PTO load that is a nonlinear function of the velocity,

and the dependence of the absorbed power on the applied load is studied. In [102], the same device has been modified by adding a submerged mass to change the resonance characteristics. The study is extended in [103] and [104] where the influence of damping on absorbed power is considered for different sea states.

Nonlinear damping control applied to the Wavebob device is considered in [105], where the performance of two different type of hydraulic circuit are compared. The damping is set to be proportional to the velocity when the velocity is smaller than a given threshold, while it is constant when the velocity is larger than the threshold. A WEC with an hydraulic PTO is also considered in [106] and [107], where the authors optimize the PTO damping in regular and irregular seas and the control of the damping is attained by controlling the displacement of the hydraulic motor.

3.3 Latching and unlatching control

Phase and amplitude control states that the maximum absorbed power is achieved when the velocity of oscillating body is in phase with the excitation force and the amplitude of the velocity is proportional to the excitation force, with $1/2R_i$ being the constant of proportionality. In this case, the PTO is required to provide reactive power to satisfy the conditions for optimal absorption when the period of the incident wave is different from the resonant period of the WEC.

In the late 70's, several researchers (Budal and Falnes [51], Guenther *et al.* [108], French [109]) independently proposed a suboptimal control strategy named *latching* which aims at satisfying the phase condition only [60], and for this reason latching fits into the category of phase control. The excitation force and the velocity are kept in phase by locking (latching) the motion of the device for an appropriate time interval; that is, during the oscillation, when the velocity vanishes, the body is held still for a period of time which satisfies the phase condition (or some other prescribed conditions). Although this approach may seem to be suitable only for incident waves which have period larger than the resonant period of the oscillating body, it has been shown in [110] that latching improves energy absorption, when compared to a linear PTO damping, also when the period of the incident wave is shorter than resonance period of the device.

Essentially, latching control does not require a PTO capable of reactive power, similarly to a linearly damped PTO; although the absorbed energy is considerably improved when compared to the latter. The price to pay in term of complexity is due to the calculation of the latching period, which requires prediction of the excitation force and to find a solution of an optimisation problem, which can be quite difficult to solve in real-time when the incident wave is polychromatic.

Additionally, when the incident wave contains more than one frequency component, the concept of phase between excitation force and velocity is not well defined, in which case the objective of optimisation of the latching interval is not unique [110]. In this case, the latching time can be optimised to synchronise the peak of the velocity with the peak of the excitation force [69], or to maximise the absorbed power [111].

Figure 3.5 depicts the simulation results of an illustrative example of latching control applied to a heaving cylinder. The device is latched at time t_0, when the control signal (fig. 3.5b) switches from A (Absorbing mode) to L (Latched mode), which is triggered by the body reaching zero velocity (fig. 3.5a). The device is released at time t_1, and the latching period is $t_1 - t_0$, during which time the PTO exerts a force (fig. 3.5c) which compensates for the external forces resulting in a zero velocity. In practice, this is implemented by mechanical brakes, or by using valves if the PTO is built using hydraulic components. When the device is working in absorbing mode, the PTO behaves as a linear damper, that is $f_{pto} = \mathrm{B}\dot{z}$.

If the WEC is equipped with a constant pressure hydraulic PTO such as those in figs. 2.9 and 2.10, the PTO force exhibits a Coulomb damping characteristic (figure 2.11), as discussed in section 2.1.2, that is, the PTO is only capable of exerting either zero force or a constant force $f_{pto_0} = \mathrm{A}_p\, p_h$, which is proportional to the oil pressure in the hydraulic circuit (p_h), by means of the area of the hydraulic piston A_p. In this case, the pressure in the hydraulic circuit prevents the body from moving until the external forces are greater than the force exerted by the PTO, resulting in a similar behaviour to latching. However, there is limited control on the unlatching instant t_1, because it depends on the external forces and on the pressure of the hydraulic circuit.

The effects of the Coulomb damping could be reduced by implementing the unlatching (or de-clutching), which sets the PTO force to zero for a given time interval, to allow the oscillating body to acquire velocity. Latching and unlatching can be also combined, in which case the conversion performance increases considerably, when compared to both latching and unlatching individually implemented [112]. Figure 3.6 illustrates the working principle for the combination of latching and unlatching, when the PTO is composed of a constant pressure hydraulic system. The main difference from latching only control is in the interval $[t_1, t_2]$, during which the PTO force is set to zero (fig. 3.6c), and the body is allowed to experience a greater acceleration under the effect of external forces (excitation and hydrostatic restoring forces). The drawback is that, when implementing latching-unlatching using a constant pressure hydraulic PTO, the absorbed power is not as smooth as in the case of latching only (compare fig. 3.5d with fig. 3.6d). This effect is due to the fact that, at t_2, the PTO force switches from zero to f_{pto_0}, potentially causing a large mechanical stress in the device.

The fundamentals underpinning latching control are presented by Falnes in [64], further in depth in his book [5], and in his recent review of wave energy conversion [2]. Cretel *et al.* have extensively analysed latching and some of its variants from both the theoretical and

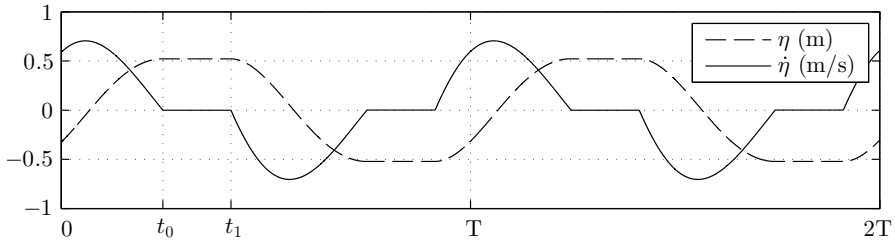

(a) Position and velocity

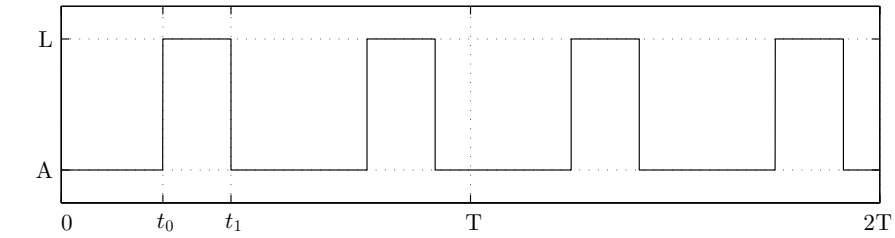

(b) Control signal: L=device latched; A=device absorbing energy

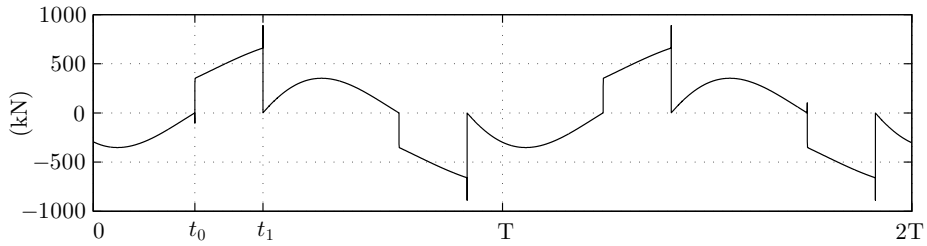

(c) PTO force

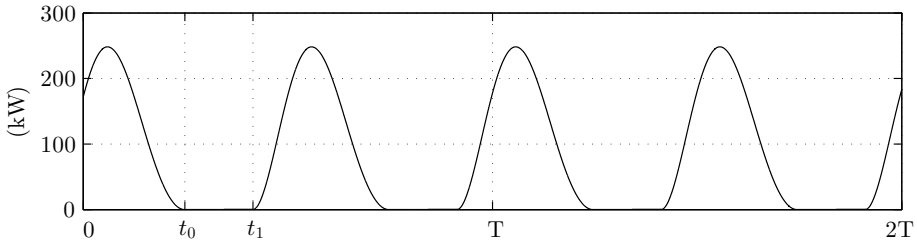

(d) Absorbed power

Figure 3.5: Simulation results for a heaving cylinder WEC controlled using latching, for monochromatic incident wave of period T=7s.

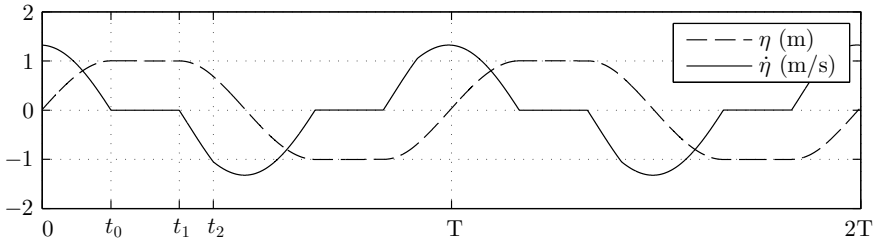

(a) Position and velocity

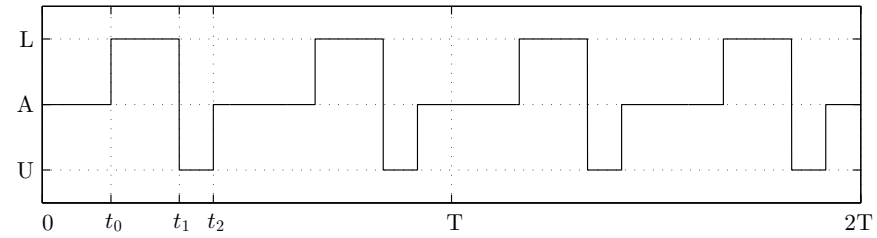

(b) Control signal: L=device latched; A=device absorbing energy; U=device unlatched

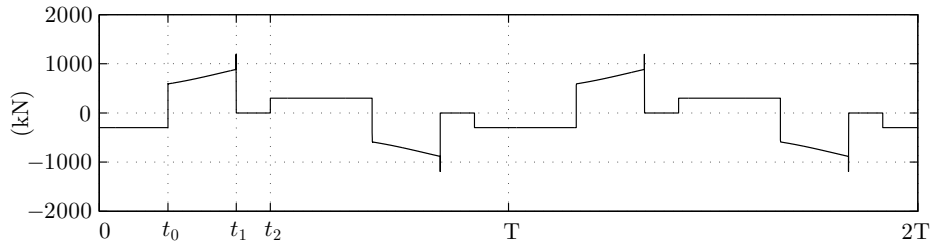

(c) PTO force

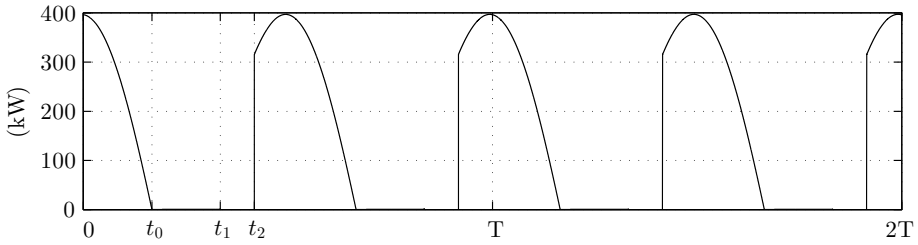

(d) Absorbed power

Figure 3.6: Simulation results for a heaving cylinder WEC controlled using latching-unlatching, for monochromatic incident wave of period T=7s.

practical point of view, in [113]. Greenhow and White [114] produced detailed modelling and comprehensive simulation results from the application of latching control to a heaving hemisphere and to a two-vertical-cylinder WEC.

In [115], latching control is implemented using neural networks while, in [116], effects on the grid of the power produce by a WEC controlled with latching are studied. Latching control applied to a heaving hemisphere has been studied in [117].

In [28], Falcao designed a control algorithm that exploits the Coulomb damping characteristic of an hydraulic PTO to implement latching. In particular, using an hydraulic PTO, the device is locked as long as the hydrodynamic forces are smaller than the damping force, that depends on the hydraulic pressure; the author developed a control algorithm that regulates the hydraulic pressure, based on the sea state, in order to obtain the damping force that latches the device for the time required to satisfy the phase condition. The same approach has been taken by Falcao *et al.* with a two-body device in [118] where it is shown that the improvement in converted energy provided by latching is not as consistent as in the case of a single-body device. Cândido and Justino, in [119], also tested latching control on a two-body device with an hydraulic PTO and reached similar conclusions. However, newer studies in [120] and [121] found that latching control applied to a two-body device can increase the annual average power output up to five times.

Simulation of latching control applied to multi-body WECs is provided in [122], where a two-body WEC is compared with a similar device composed of an additional reacting mass. The same author, in [123], compares the absorbed power of a two-body WEC with the absorbed power of an equivalent single-body system connected to the seabed. Simulation of a two-body force-compensated WEC, subject to latching control, is provided in [124]; force compensation allows the system to exploit the large but opposite excitation forces applied to a floating column and on an attached submerged structure. In [105], latching control is applied to the Wavebob device with an hydraulic PTO.

Experimental application of latching on prototypes have been reported by Bjarte-Larsson and Falnes in [125], [126] and [127]; a mathematical model of a vertical cylinder with an hemispherical bottom is simulated, and the results are compared with experimental data obtained with wave-tank testing. Experimental results are also reported in [128]; in this paper, the author tests three different heaving buoys with a pneumatic PTO, and applies three different versions of latching control. The device considered has resonant periods smaller than the wave periods. The first method consists of latching the device during two intervals of the oscillation cycle and the target of unlatching is to obtain the maximum oscillation velocity at the instant of maximum excitation force. The second method consists of latching the device only when it reaches zero velocity at the lowest value of the heave position, and unlatch the device with the objective of achieving the highest heave position. The third method consists of keeping the device con-

tinuously latched; this method is used in case of extreme weather conditions, and the device functions as an oscillating water column, due to the pneumatic PTO. Latching control has been tested also on experimental prototypes, such as on the Buldra [129], on the first prototype of the AWS [130], [77], [131] and on the SEAREV [132], [111], [27], [133].

The time interval for which the device needs to be locked, called *latching time* or *duration*, is a critical variable which affects the conversion efficiency. Analytical computation of optimal latching duration for monochromatic sea is reported in [134], while numerical optimisation is used to derive the optimal latching duration in [122] and [123] for random and non random sea. Babarit *et al.* [110] compared several latching control strategies in regular and random seas; the authors studied semi-analytical solution for regular seas, and numerical solution for random seas. Three control strategies for the computation of the latching duration are compared for random seas: maximisation of the estimated energy absorption, maximisation of the oscillation amplitude and minimisation of the phase difference between the peak of velocity and the peak of the excitation force. A similar approach is taken in [111] where investigation of optimal latching time for regular and random seas is considered. A semi-analytical approach is taken for regular sea optimisation, while a numerical algorithm is used for the random sea case, where the optimisation method used is based on a Hamiltonian formulation and the PMP. A sensitivity analysis of the power converted using latching control for the SEAREV is described in [135]; the conversion efficiency is analysed with respect to the actuators time constants considering both regular and random seas.

Eidsmoen in [136], [137] and [138] describes the phase control of a heaving buoy WEC subject to amplitude constraints; the phase control applied produces results similar to latching, and it aims to keep the velocity in phase with the excitation force. It is assumed that a four second prediction of the excitation force is available; the control algorithm searches for its extremum and computes the time for opening a control valve used to control the damping exerted by the hydraulic PTO.

An extension of latching, named de-clutching (unlatching), is developed by Babarit *et al.* in [29, 139] and applied to the SEAREV device to obviate a characteristic effect of hydraulic PTOs called Coulomb damping. The combination of latching and de-clutching has been studied in [112], where a substantial increase in energy absorption is shown when compared to latching or de-clutching implemented independently.

Folley and Whittaker in [140] have described, implemented and simulated active bipolar damping control, which is the combination of latching and unlatching with a PTO force that is constant during the absorbing interval, as shown in the example in figure 3.6. The force/torque applied by the bipolar damping system is set equal to the maximum applied force/torque required for maximum power capture in the linear damping system.

Validation of latching control by means of evolutionary algorithms is described in [141].

The authors assumes that the PTO force is a static function of the excitation force and its first derivative; this function is described by a neural network, the parameters of which are optimised by means of an evolutionary algorithm. The authors found that the resulting profile of the time varying PTO damping resembles the PTO damping obtained by using latching–de-clutching.

3.4 Other control strategies

The problem of energy absorption maximisation for WECs has been studied also as function of a time-varying damping coefficient; in particular, Nolan *et al.* [142] carried out a numerical optimisation in order to obtain the damping profile that provides maximum converted energy. The authors parametrised the damping profile with a general sigmoid function; optimisation performed by means of a genetic algorithm then provided the parameters that maximized the converted energy. The work was extended in [143] and similar approach have also been considered in [129].

Beirao *et al.* applied feedback linearisation control and internal model control with both linear and neural networks models to the AWS [144], [75]. The work was extended in [145] to include a switching controller that selects the appropriate control strategy based on the sea state. Falcao implemented an instantaneous control algorithm for a two-body WEC with an hydraulic PTO . The algorithm in [146] consists of a linear relationship between the hydraulic motor flow and the pressure applied on the piston; the constant of proportionality is obtained graphically, plotting curves of absorbed power for several sea states and for different values of the control constant. Although no phase control has been attempted, it was found that this highly non-linear power take-off mechanism can attain nearly the same level of wave energy extraction as an optimally controlled fully linear PTO.

A parameter optimisation for a generic WEC, with respect to wave climate, is described in [147]. The WEC considered is a vertical cylinder with a limited range of motion and a linear damper. The influence of damping and stiffness on the device efficiency is studied for sea state statistics of several test sites. It is shown that an uncontrolled device with optimized parameters generally performs better than a controlled device, where the parameters are not optimized for that specific site.

Fuzzy logic control has also been used for the control of WECs: in [148], a control action based on fuzzy logic adjusts PTO damping and stiffness based on sea state and instantaneous wave profile. Optimal values of damping and stiffness are calculated using historical data; damping and stiffness are then corrected using real-time wave elevation using fuzzy logic. The fuzzy logic controller action is based on a prediction of the future incoming irregular wave. The work was extended in [149] and [150], where the control system is designed by combining fuzzy logic, genetic algorithms and robust control. The fuzzy logic controller tunes the PTO damping

in response to the short-term variation of the wave elevation, while genetic algorithms have been used to optimise the PTO parameters with respect to the long term trends of the sea state, and a robust controller used to compensate for inaccuracies in the model. Genetic algorithms have also been used, in conjunction with neural control, also for the design of a causal latching control strategy, as described in [151]. In particular, real-time control is performed by the neural network, which has been optimised using genetic algorithms.

A WEC equipped with an hydraulic PTO has been considered in [152], where the fuzzy controller has been designed to adjust the hydraulic pump displacement, with the objective of regulating the speed of the electric generator shaft to the set-point which maximises the conversion efficiency or the overall power absorption. An additional example of fuzzy logic applied to the control of WEC can be found in [153], while the work in [154] describes a control strategy based on a Multi Objective Particle Swarm optimisation technique.

A stochastic approach for the optimisation of the PTO damping and spring coefficients for a self reacting heaving WEC are described in [155] and [156]. The authors have developed a linear frequency domain stochastic model of the WEC and they have calculated the optimal values of the damping and spring coefficients be means of PMP. A WEC with a nonlinear hydraulic PTO has been simulated, and the results have been compared with the ones obtained using the frequency domain stochastic model.

The control system presented in [157] is composed of high level and low level controllers. The high level controller generates a PTO damping reference, while the low level controller is the Proportional Integral Plus (PIP), which has been implemented in two modified versions: feed-forward PIP and state-dependent PIP [158]. The high level optimisation of the captured energy is based on evolutionary algorithms [159].

Losses of the hydraulic PTO have been considered in [160] and [161] for a point absorber WEC. The authors also consider an alternative configuration of the hydraulic PTO which includes an additional accumulator (control accumulator) that is capable of returning energy to the oscillating body and allows the device to attain a higher velocity and increases the absorbed power. The accumulator is connected by means of a control valve, the optimal switching time of which has been optimised. Efficiency of the hydraulic PTO has also been studied [30]; in particular, the authors optimise a passive damping for the Wavebob device which maximises the absorbed energy, when losses of the PTO are included.

In [162], the authors describe the Maximum Power Point Tracking algorithm for the control of a point absorber WEC equipped with a linear electrical generator. The control algorithm compares the average power absorbed during a certain wave-cycle with the power absorbed in the previous cycle, and modifies the duty cycle of the electrical power converter according to the power variation. The paper presents experimental results for both laboratory and ocean.

Control of WECs has been studied also by adjusting the inertia of the system, as described

in [163], where mechanical amplification of oscillations are pursued by means of mass modulation, which is implemented by using water as ballast. The mass modulation is performed within the oscillation cycle, more precisely twice per cycle; the result is a near square wave mass modulation. Power production and bounded-input-bounded-output stability are studied with respect to the mass modulation and PTO damping. A different approach for the control of the inertia of the absorbing system has been described in [164], where the natural frequency of the WEC is adjusted by repositioning an internal mass. The sliding mass position is controlled with the objective of matching the resonant frequency of the device with the current sea conditions.

The reduction of parametric resonance for a heaving buoy WEC has been investigated in [165]. The authors have implemented "Pitch Stability Control", in which they use the PTO to reduce parametric resonance, that results in oscillations in pitch caused by coupling between pitch and heave. The paper describes experimental results in a wave basin to validate the approach.

Filter design principles have been used to implement the wide bandwidth controller described in [166], which aims at improving the independence of WEC absorption performance from the sites in which they are deployed. The authors claim that the wide-band response of the controller could allow for the capture of a wider frequency range of ocean energy and that it could be possible to design a controller which does not require real-time tuning.

When the conditions of the sea become too severe, the control systems are generally programmed to shut down the device, in order to protect the WEC. In [167, 168], the author presents a control strategy called quiescent period predictive control which, the author claims, allows an increase in the average annual power production by preventing the control system deactivating the device when it is not necessary.

3.5 Control of constrained wave energy converters

Wave energy converters are built using mechanical components which have limited operating ranges. For example, in the case of an hydraulic PTO, the safe and efficient operation of energy conversion is achieved only if the oil pressure varies within a prescribed range. Also, if the PTO exerts its force on the floating body by means of an hydraulic ram, the length of the stroke imposes an upper bound on the maximum oscillation amplitude of the device. It has been briefly discussed in sec. 3.1 that reactive control is associated with large excursions, large forces and large peak power; therefore, it may not be possible to implement such a control strategy in every WEC. For this reason, several researchers have studied the problem of maximising the absorbed energy under the effect of constraints on the motion of the oscillating body, or on the maximum PTO forces.

Newman, in [169], has studied the power absorption capabilities of a slender body with motion restrictions. A few years later, in [170], Evans presented a theory for the maximisation of wave-power absorption of a system of oscillating bodies in the frequency domain subject to oscillation amplitude restrictions. The author provides examples for a sphere and a vertical cylinder in which absorbed power is related to amplitude restrictions. A more general formulation was provided by Pizer, in [171], where the author removes the limitation of having the same amplitude restriction on all the DoF. In [163], the oscillation amplitude constraints are enforced by increasing the PTO damping. The authors provide an expression for the minimum value of the damping for a given excitation force and given amplitude constraint. In all the previous cases, however, the methods are only applicable for monochromatic waves.

Korde, in [172], formulated an optimisation problem in the frequency domain considering a WEC where energy is absorbed by means of the relative oscillation between a floating body and an on-board, actively controlled motion-compensated platform. The constraint on the amplitude of the relative oscillation is introduced as a penalty term in the cost function which describes the balance between absorbed energy and oscillation amplitude. In fact, the cost function is the weighted sum of two terms describing the absorbed power and oscillation amplitude. The approach presented is also valid for polychromatic waves.

The maximisation of the absorbed energy ,with motion and force restrictions, has also been considered from the probabilistic standpoint. In [96], the authors have developed a linear frequency domain model to simulate the behaviour of a heaving point absorber moving with respect to a floating reference. The buoy is subject to restrictions on the relative oscillation amplitude due to the finite length of the stroke and to avoid slamming, that is prevent the device from fully emerging from water. Restrictions on the maximum PTO force have also been studied. The authors carry out a sensitivity analysis to study the effect of motion and force restrictions on the absorbed energy. The work has been extended in [173] where the same analysis has been carried out for a small array of WECs.

Scruggs, in [174], implemented linear quadratic Gaussian control on a three DoF WEC, with constraints on the PTO force, displacement, and voltage and current of the electrical generator. The constraints have been formulated in terms of variance; more specifically, the cost function includes a penalty term related to the variance of the constraint violation. The resulting optimisation problem is a linear matrix inequality, and the control law is causal.

A time-domain formulation for maximisation of the energy absorbed when the device is subject to amplitude constraints was described by Eidsmoen in [21], where the WEC considered is a heaving cylinder in both regular and irregular (polychromatic) weaves. The control force is obtained from the numerical solution of a maximisation problem, formulated using Lagrange multipliers in which the useful energy is maximized. It is found that the mean output power is reduced when the excursion is constrained compared to the unconstrained case, but the ratio

between the output energy and the total energy passing through the system is increased, meaning that the conversion efficiency of the machine is less critical. The method presented in the paper, however, requires prediction of the incident wave.

A powerful tool for the real-time optimal control of contained systems is Model Predictive Control (MPC), which has been used in the context of wave energy conversion in [175], [176], [177] and [19]. In [175], the authors have considered a semi-submerged heaving sphere as an example, and they have shown how amplitude and force constraints affect the amount of absorbed energy, with the assumption of perfect knowledge of future excitation force. Is is also shown that MPC allows the WEC to perform closely to the power absorption upper bounds (Budal diagrams) discussed in section 2.3.2. The authors have also studied the influence of the excitation force prediction horizon on the absorbed energy. Cretel *et al.*, in [176], have described an improved formulation of MPC compared to [175], which provide similar results in terms of absorption and motion of the device; however, the new formulation is characterised by more favourable structural properties of the optimisation problem which facilitates the online implementation. Brekken, in [177], has implemented MPC on a simple point absorber, with constraints on velocity, position and generator force; the prediction of the excitation force was calculated using of a Kalman filter. Nonlinear MPC has been implemented in [18] on a generic WEC and, in [19], on a two-body heaving point-absorber, where the hydrodynamic model of the device is linear, and the nonlinearities are due to mooring forces.

3.6 Control of arrays of wave energy converters

The analytical formulation of the maximum power absorbed by an array of oscillating devices has been derived in independently by Evans [62] and Falnes [63]. The authors obtained a result which is the general case of reactive control (and phase and amplitude control) for a single device, which was described in section 3.1.

When considering multiple devices, or multiple oscillating modes, the motion of the system is described, in the frequency domain, by the equation (2.70), from which the intrinsic mechanical impedance of the WEC can be defined as

$$\mathbf{Z}_i(\omega) = \mathbf{B} + \mathbf{R}(\omega) + i\omega\left(\mathbf{M} + \mathbf{m}(\omega)\right) + \frac{\mathbf{S}}{i\omega},$$

where the quantities $\mathbf{B}$, $\mathbf{S}$, $\mathbf{M}$ and $\mathbf{Z} = \mathbf{R} + \mathbf{m}$ are now $N_m \times N_m$ matrices, with N_m the number of modes. The formulation of reactive control which maximises the combined average power absorbed by a system of oscillators is given by the matrix equation

$$\hat{\boldsymbol{F}}_{pto} = -\mathbf{Z}_i^* \, \hat{\boldsymbol{v}}, \tag{3.2}$$

where $\hat{\boldsymbol{F}}_{pto}$ and $\hat{\boldsymbol{v}}$ are, respectively, the vectors of complex amplitudes of the optimal PTO forces and velocities, as defined in section 2.2.2.3. The corresponding optimal velocity is

$$\hat{\boldsymbol{v}}_{opt} = \frac{1}{2}\mathbf{R}_i^{-1}\hat{\boldsymbol{F}}_e,$$

where $\hat{\boldsymbol{F}}_e$ is the vector of the excitation forces, and the combined, time-averaged maximum absorbed power is

$$P_{MAX} = \frac{1}{8}\hat{\boldsymbol{F}}_e^T\mathbf{R}_i^{-1}\hat{\boldsymbol{F}}_e^*.$$

The radiation resistance matrix $\mathbf{R}$ can be singular in some cases [5], for example at low frequencies [178]; however, the singularity of the intrinsic mechanical resistance $\mathbf{R}_i$ can be obviated by the presence of a friction term $\mathbf{B}$, which is diagonal with positive values.

The simulation results for an illustrative example of an array composed of three identical heaving vertical cylinders, the layout of which is depicted in figure 3.7, are provided in figure 3.8. The geometry of the WEC is the same as used for the example presented in sec. 3.1. The period of the incident wave for which the array has been simulated is T=5.9s, which is the resonant period in heave for the single device. In contrast to the single device case depicted in fig 3.3, the heave velocities of the bodies (fig. 3.8a) are not in phase with the excitation forces (fig. 3.8c), because the matrix $\mathbf{R}_i$ is not diagonal.

Also, it is worthy of note that the three WECs return a small portion of reactive power to the sea, especially WEC 3, which is the front-most device. However, at different wave periods, the amount of reactive power increases considerably, as shown in figure 3.9 as in the case of single body (fig. 3.4).

A positive effect of the array of WECs, when compared to the single device is that, in some configurations, the total power generated by the array can exhibits smaller fluctuations within a wave period (compare P on fig. 3.3d with $\bar{P}$ on fig. 3.8d).

A system of optimally controlled WECs has been described by Evans in [170], where that author has also studied the effect of motion constraints on maximum power absorption. Falnes and Budal, in [179], also reported a study on linear arrays of heaving buoys, where they have

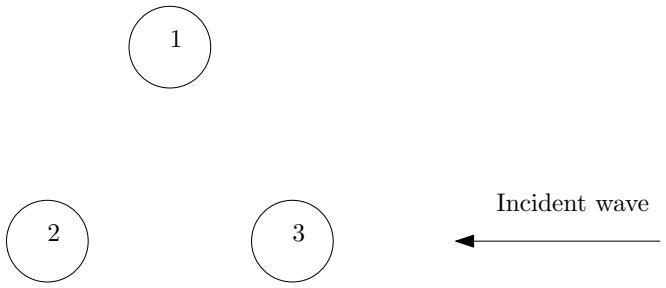

Figure 3.7: Top view of the array layout

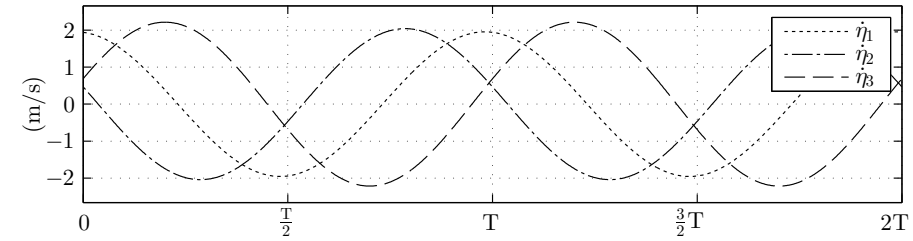

(a) Heave velocities

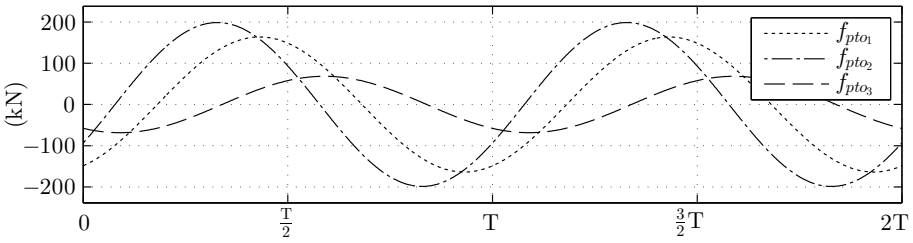

(b) PTO forces

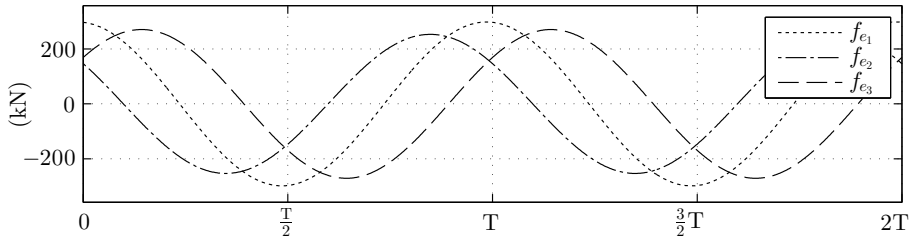

(c) Excitation forces

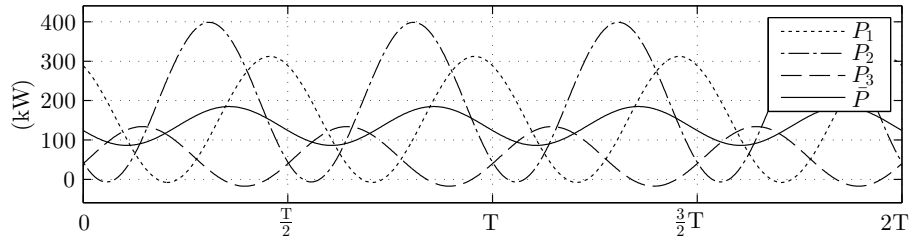

(d) Power absorbed by each device (P_1, P_2, P_3) and instantaneous average power ($\bar{P}$)

Figure 3.8: Motion, forces and power on an array of three vertical cylinders, controlled using reactive control, for a monochromatic wave of period T=5.9s.

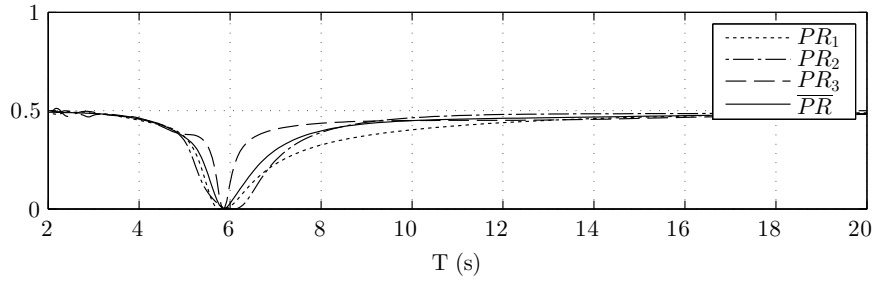

Figure 3.9: Total power vs reactive power for an array of three vertical cylinders

considered unconstrained motion as well as constrained motion. Falnes extended his previous work in [180], where he has considered an infinite linear array of evenly spaced oscillating bodies. The author also discussed the theory of the general case of wave power absorption by an array of equidistant equal groups of oscillating bodies. Constraints on oscillation amplitude have also been considered by Fitzgerald and Thomas in [181], where the authors have observed that by limiting the oscillation amplitude to two or three times the incoming wave amplitude, the positive interference has been reduced and the negative interference has not been significantly affected.

The implementation of the optimal control law in (3.2) for an array requires communication between devices. In fact, the optimal force that the PTO on each device has to exert depends on the velocities of all the oscillating modes, because the matrix $\mathbf{Z}_i$ is non diagonal; thus, the PTO force on each device is calculated as a linear combination of all the velocities contained in the vector $\boldsymbol{v}$. Justino and Clement, in [182], have presented a suboptimal method for the control of an array of WECs to obviate the issue associated with knowledge of the velocities of all devices, when calculating the optimal force for each device. The authors have considered two types of arrays: a linear array (in attenuator and in terminator configurations) and a cross array, both oscillating in three modes of motion simultaneously (heave surge and sway). The hydrodynamic coefficients were obtained with Boundary Element Methods (WAMIT, AQUADYN), from which the authors have calculated the optimal impedance matrix for the power take off. The sub-optimal control strategy that the authors proposed consists of taking only the diagonal of the optimal PTO matrix; in practice, this results in controlling each device independently, because each PTO force depends only on the velocity of the corresponding WEC. The authors have demonstrated that if $\mathbf{Z}^*_{pto}$ is the optimal PTO impedance for an array and if the PTO impedance matrix $\mathbf{Z}_{pto}$ and is expressed as $\mathbf{Z}_{pto} = C\text{diag}(\mathbf{Z}^*_{pto})$, where C is a real number, then the maximum absorbed power for the array is obtained for $C = 1$. A comparison between reactive control and sub-optimal control has been reported in [183], where the sub-optimal control has been implemented by taking the diagonal of the real part only of the optimal PTO impedance

matrix, resulting in the linear damping terms only.

Several suboptimal control strategies have been studied by Ricci *et al.* in [184], where two array configurations have been considered, both of which are composed of five bodies: a linear and a cross array. The PTOs are linear dampers, and their damping coefficients have been calculated in two different ways, both where the damping matrix is diagonal, that is each device is independently controlled. In the first case, each element of the damping matrix is optimised independently, whereas in the second case, called scalar optimisation, the damping matrix is the identity matrix multiplied by a constant, that is all the PTOs have the same damping. The authors have reported that the simulation results show a negligible difference between the two methods. A similar approach has been presented also in [185, 186] for an array of vertical cylinder, they layout of which is a square[2]. As in [184], the damping has been optimised in two manners: independently for each device and by imposing the same value for all the devices. In the paper, the authors support the idea of the minimisation of destructive interference as a design objective; they have also considered the sensitivity of the produced power to device tuning for several sea-states. In [187], the damping optimisation for an array of four heaving hemispheres was carried out for each frequency, resulting in a frequency dependent damping coefficient.

Child and Venugopal, in [188] and [189], considered arrays of WECs where PTOs have both damping and spring terms. The PTO tuning is the same for each device in the array, and it corresponds to the optimal tuning for an isolated WEC; in particular, the device has been tuned to the peak frequency of a JONSWAP spectrum and for the heading angle equal to zero. The PTO damping of all the WECs has been set to be equal to the optimal damping of an isolated device also in [190] and [191]. However, in [191] the PTO damping has been calculated by means of an optimisation problem, the objective of which is the maximisation of the yearly energy production. In this case, the spring coefficient has been selected with the objective of adjusting the resonance period of the oscillating bodies to 7.3s.

Independently optimised damping for each device has been implemented in [192], where the array is composed of five aligned heaving hemispheres. The PTO damping has been optimised by means of a Gauss-Newton iterative procedure, and the results show that this method provides better results in terms of absorbed energy than using both the real part of the diagonal of optimal PTO matrix in (3.2), and setting all the PTO damping coefficients equal to the optimal damping of an isolated device. The authors have also formulated an optimisation problem with the objective of calculating the damping coefficients of each WEC in the array which allows a uniform mean power absorption across all the devices.

Constrained control of an array of twelve closely spaced heaving point absorbers has been studied in [193, 194], where the inter-body distance is 1.3 times the diameter of the WEC. Con-

[2]The devices are located at the vertices of a square.

straints have been introduced for oscillation amplitude, anti-slamming and PTO force in a probabilistic framework. The authors optimise the control parameters, which are the damping coefficients and and a supplementary mass, using three different strategies:

1. Optimal control parameters for the single body case, where the control coefficients are the same for all the devices, and are obtained by optimising the PTO force of a single isolated device.

2. Diagonal optimisation, where all the devices have the same coefficients, but optimised for the array using simplex search for the unconstrained case and sequential quadratic programming for the constrained case, as in [184].

3. Individual optimisation using sequential quadratic programming using the result of diagonal optimisation as initial conditions.

The authors have observed that that the power production benefits from individual PTO coefficient optimisation because of the large number of bodies and the close distance; in particular, the bodies in the back rows benefit the most from individual tuning. The authors have noted that when introducing constraints, the devices in the front row absorb less power while the devices in back rows absorb more power, and that an isolated device loses about 25% of power due to constraints while an array loses about half as much (12% to 14%). Additionally, the power absorption is more equally distributed among floaters when introducing constraints compared to the unconstrained case. The paper also includes a sensitivity analysis on the effects of the PTO miss-tuning. A similar analysis has been carried out in [195], where the authors studied the effect on power absorption of a mismatch in the control force amplitude, when using both reactive control and linear damping.

An array of two heaving cylinders with nonlinear PTOs was considered in [196]. The WECs are equipped with hydraulic PTOs; several values of the hydraulic pre-charge pressure were compared in order to find a relation between the PTO pre-charge pressure and the incident wave period. The authors observed that high pre-charge pressure produces more energy at longer periods but none at low periods, while low pressure gives a large motion and a broader band.

3.7 Grid compliance and power ratings of the power take off

The control system of a WEC has a strong influence on the time profile of the instantaneous power produced by the device, as can be observed by comparing figs. 3.2, 3.3, 3.5d and 3.6d. If a WEC is designed to be connected to an electrical grid, the electricity it delivers must satisfy certain properties regarding, for example, the power quality, the frequency and the ability to withstand small faults in the line without being damaged. Some of these issues have been described in [197], in relation to the manner in which they are affected by the control system.

Due to the oscillatory nature of waves, the output power of WECs also tends to be oscillatory. When WECs are deployed in arrays, the output power variability can be mitigated, (section 3.5), but not completely eliminated. Energy storage can be very effective for separating the WEC from the grid, and produces power with a higher quality, but energy storage can also be quite costly. In [116], the authors present a brief discussion on the energy conversion stages, from ocean waves to the grid, and discussion about the effect of arrays on power quality, with particular focus on the role of arrays for reducing the need for energy storage. The control strategies considered are passive loading and latching. Three types of PTOs are considered, with different grades of flexibility/controllability, in terms of force exerted and active/reactive power. The paper presents a set of control strategies (linear damping and latching) and several PTO configurations with different grades of flexibility/controllability, in terms of force exerted and active/reactive power. For each combination of control-PTO, the authors discuss the implications in terms of absorbed energy, PTO capability and effects on the grid (power quality).

In [198], a control system was designed for the first AWS prototype to decouple the WEC from the grid; in particular the control system was divided into a grid side converter and a generator side converter. The generator side controller was designed to absorb the maximum amount of power from the seas, whereas the grid side controller was designed to regulate the terminal voltage and the active power delivered to the grid at constant values.

The ratio between the peak power and average absorbed power is an important factor for the economic viability of WECs because the average absorbed energy is related to the revenue generate by selling electricity, while the peak power is related to the power rating of the PTO, which has a strong impact on the cost of the device. It has been shown, in sec. 3.1, that reactive control can produce large ratios of the peak to average power, thus several researchers have studied different control strategies to mitigate this issue. A comparison of control strategies considering the PTO rating was carried out in [199]. In [200] it is presented a study regarding the power rating of an electric PTO controlled by applying reactive control and passive loading; in the same paper it is described also a method to reduce the power rating with the drawback, however, of a reduction in average extracted power. Santos *et al.*, in [201], developed two control strategies with the objective of improving the energy absorption of both the single device and a whole array, without increasing the power rating of the PTO, and to improve the power quality when the devices are deployed in arrays. The control methods, called saturation control, are based on the idea of reducing the PTO damping when the instantaneous power is approaching the PTO power limit. The work was extended in [202] by implementing a multilevel, or hierarchical, control scheme composed of three levels: control of the single WEC, control of the farm, and system operator. The system operator imposes frequency and voltage on the electrical line, while the WEC control is implemented as a linear damping with power saturation (the damping coefficient is reduced when the instantaneous power reaches a maximum allowed value). For

the control at the farm level, the authors have considered two strategies: decentralised control, where each WEC has its own constant damping coefficient, and centralised control, where the control parameters are adjusted to control the active and reactive power.

A similar approach was described in [203], where a real test case (the Biscay Marine Energy Platform) has been used to simulated the grid connection of a WEC. The authors describe a wave-to-wire model of a 20MW farm of point absorbers, and evaluate several PTO configurations and control strategies in terms of total power absorbed and power quality on the grid. Several strategies are described for both the WEC side controller and the grid side controller, for three types of PTOs. The authors note that if the WECs are equipped with a fully controlled bi-directional converter, both the WECs control and the grid side control can be performed independently. The control strategies that have been applied are linear PTO damping, linear PTO damping with saturation control (to limit the peak power) and a third control strategy which is capable of regulating the reactive power. The author also notes that the output power variability can be mitigated by suitable control strategies and suitable energy storage, and that reactive control components on the WEC side can increase the average power absorbed with a potential reduction in the PTO power rating. Saturation control has been implemented also in [204] for a two-body WEC.

A study on the impact of control strategies on the peak to average power ratio is documented in [205], where the authors consider "the two extreme cases of linear PTO damping and reactive control", and they theoretically prove that "the ratio between peak and average extracted power is entirely dependant on the load power factor", which is the phase of the load impedance (i.e. the PTO impedance). The work has been extended in [206], where an adaptive control system has been developed to increases the peak to average power ratio. The control system tunes the parameters of the PTO, which is capable of reactive power, in response to the measured wave amplitude, in order to maximise the absorbed power under constraint on the PTO power rating. The control system has been simulated for both monochromatic and polychromatic waves.

3.8 Comparison of control strategies

Several publications compare different control strategies. Theory shows that latching is a sub-optimal control strategy, thus it always performs worse than optimal control. However, latching generally provides significant improvements with respect to passive control, as shown for example in [116] and [124]. More detailed comparisons between optimal control, latching and passive control are reported by Falnes and Bjarte-Larsson in [125], [126] and [127], in which model simulations as well as wave tank tests are performed.

Falcao [118] performed a comparison between latching and reactive control for a two-body device. It is shown that reactive control provides a significant improvement in the converted

energy, while latching does not provide substantial improvements with respect to passive linear damper, compared to the single body WEC. The explanation provided by the author is that, in case of a two-body WEC, latching is not capable of producing the effect for which it is intended: "to keep the floater unmoving during part of the wave cycle and in this way (approximately) bringing the floater velocity into phase with the diffraction (or excitation) force".

Several control techniques are applied to the first AWS prototype and the simulation results as well as performance comparison are reported in [75], [77] and [207]. The control algorithms implemented are reactive control, phase and amplitude control, latching, internal model control and feedback linearisation; it is shown that feedback linearisation and latching provide the maximum converted energy over the year, more than phase and amplitude and reactive control. The authors motivated these results with the fact that the two optimal control strategies are non-causal, and for practical implementation they require approximation, decreasing their effectiveness.

A number of control methods have been reviewed by Hals *et al.* in [208], applied to a heaving point absorber. The control techniques considered are: velocity-proportional control (linear damping), approximate complex conjugate control, approximate optimal velocity tracking, phase control by latching and clutching, model-predictive control, gain scheduling and extremum seeking. The comparisons were carried out with respect to absorbed power, reactive power flow, peak-to-average power ratios, and implementation complexity, based on simulation results. The authors also discussed the strengths and weaknesses of each method, and they provide suggestions on how to implement the controllers, including how to tune control parameters and handle amplitude constraints.

Control strategies have also been compared with respect to the mechanical fatigue that they impose on the machines where they have been implemented. In [209], a fatigue analysis was carried out based on the *accumulated fatigue damage* metric for the Wavestar device, where the PTO was modelled with a mass-spring-damper. The simulation results show that by tuning the device to the current sea-state, rather than keeping constant values optimised over a long period, the power production increases, but the accumulated fatigue damage increases by a much larger factor.

Chapter 4

Optimal control of wave energy converters

The focus of this thesis is the control of wave energy converters. The previous chapters have introduced the wave energy conversion problem; in particular, chapter 2 has provided the theoretical background for the development of mathematical models, describing the interaction between WECs and water, while chapter 3 is a review of the strategies that have been applied for the control of WECs.

This chapter provides the main contribution of the thesis, which is the formulation of the optimal control problem of WECs in the framework of the direct transcription methods known as spectral and pseudospectral optimal control. It is shown that the application of these methods obviates the necessity of converting the convolution integral describing the radiation force into a linear state space model, and that they also permit an approximate solution to the nonlinear optimal control problems for WECs.

This chapter is divided into three main parts: the first part (sec. 4.1) is an introduction to numerical optimal control, beginning from a generic continuous time optimal control problem, and gives an overview of the classical approaches for solving the problem, namely dynamic programming and Pontryagin's Minimum Principle (PMP). Section 4.1.2 covers indirect and direct transcription methods, which allow the approximation of the optimal control problem with a NLP problem, while sec. 4.1.3 provides the main results in the area of nonlinear programming.

The second part of this chapter (sec. 4.2) focuses on the direct transcription of the opti-

mal control problem of WECs described by linear models. In particular, sec. 4.2.1 covers the application of the discretisation method for a generic system of WECs, while sec. 4.2.2 focuses on a specific device (heaving point absorber) and a specific choice of discretisation method, namely the Galerkin method with the Fourier series aproximation of the state and control variables. Simulation results are provided in sec.4.2.2.3, while sec. 4.2.3 shows how spectral and pseudospectral methods allow the simplification of the convolution integral.

The third part of this chapter is concerned with the nonlinear optimal control of a WEC using the pseudospectral method. In particular, the device considered is a flap-type WEC described by a model which includes nonlinear viscous effects. Simulation results show significant differences in the optimal behaviour of the device from the linear case, and also the computational efficiency resulting from the application of this method.

4.1 Numerical optimal control: Background

4.1.1 Continuous time optimal control

Optimal control is the area of control theory where the objective is to govern the state of a dynamical system by means of the control input in order to minimise (or maximise) a cost (or performance) criterion. A more precise description can be stated by first considering the dynamics of the system, to be described by the (nonlinear) differential equation as

$$\dot{\boldsymbol{x}} = \boldsymbol{f}(\boldsymbol{x}, \boldsymbol{u}, t), \qquad \boldsymbol{x}_0 = \boldsymbol{x}(t_0), \tag{4.1}$$

with $\boldsymbol{f} : \mathbb{R}^n \times \mathbb{R}^m \times \mathbb{R} \to \mathbb{R}^n$, where $\boldsymbol{x} \in \mathbb{R}^n$ denotes the state variable and $\boldsymbol{u} \in \mathbb{R}^m$ denotes the control input, and by considering the functional

$$J(\boldsymbol{u}) = \Phi\left(\boldsymbol{x}(t_f), t_f\right) + \int_{t_0}^{t_f} L\left(\boldsymbol{x}(t), \boldsymbol{u}(t), t\right)\, dt, \tag{4.2}$$

where $L : \mathbb{R}^n \times \mathbb{R}^m \times \mathbb{R} \to \mathbb{R}$ is known as Lagrangian (or *running cost*), and $\Phi : \mathbb{R}^n \times \mathbb{R} \to \mathbb{R}$ is the penalty function on the terminal state (*terminal cost*).

The objective of a generic optimal control problem is to seek the control input $\boldsymbol{u}(t)$, defined in the time interval $t \in [t_0, t_f]$, which maximises (or minimises) the functional J in (4.2), subject to the dynamic of the system in (4.1), that is:

$$\begin{aligned} &\min_{\boldsymbol{u}} J(\boldsymbol{u}) \\ &\text{subject to:} \\ &\qquad \dot{\boldsymbol{x}} = \boldsymbol{f}(\boldsymbol{x}, \boldsymbol{u}, t), \qquad \boldsymbol{x}(t_0) = \boldsymbol{x}_0. \end{aligned} \tag{4.3}$$

If the objective is to maximise J, then the problem can be reformulated to an equivalent minimisation problem by changing the sign to the performance function, that is $\min_{\boldsymbol{u}} -J$, thus only the minimisation problem is generally considered in the literature. When the functional J is composed of both the Lagrangian and the penalty on the terminal state as in (4.2), the optimal control problem is said to be in the *Bolza* form. It is often the case that one of the two terms are not present. If J is composed of the terminal penalty only, then the problem is in the *Mayer* form, whereas if the cost function contains the integral part only, then the problem is in the *Lagrange* form. The three forms are equivalent and it is always possible to transform the problem from one form to any other [210].

In the context of wave energy conversion, the problem of maximising the energy absorbed by a WEC can be immediately formulated as an optimal control problem by using the time domain model of the WEC in (2.71) as the system dynamic (4.1), and by defining the Lagrangian L in the cost function (4.2) as the instantaneous power absorbed by the PTO.

Optimal control traces its roots to the calculus of variations, a discipline that is considered to have begun in 1696 when Bernoulli raised the Brachistochrone problem, which reads:

> *Given two points A and B in a vertical plane, what is the curve traced out by a point acted on only by gravity, which starts at A and reaches B in the shortest time?*

Some authors [211] consider the same date to be the beginning also of optimal control, although two of the most important results have been formulated independently in the early 1950s by Richard Bellman and Rudolph Kalman in the United States, and by Lev Pontryagin in the Soviet Union. Bellman developed the theory of *dynamic programming*, while a few years later Kalman derived the sufficient condition for optimal control, and established the connection between dynamic programming and the previous results in the calculus of variations. Besides providing a sufficient condition for optimality, dynamic programming may also allow (if it exists) a feedback law to be derived. However, the calculation of the solution is computationally expensive and it demands a large amount storage; Bellman termed this nuance the *curse of dimensionality*. Thus, dynamic programming, in practice, can only be applied to small problems[1], or for problems with a particular structure, such as linear systems with a quadratic cost, for which an analytical solution exists ([210]). Pontryagin's approach, known as PMP[2], on the other hand, provides a necessary condition for optimality only, but can be applied to a wider range of problems.

[1] Small dimension of the state space and interval $[t_0, t_f]$.

[2] It is also widely known as Pontryagin Maximum Principle.

4.1.1.1 Dynamic programming

Bellman's objective when he developed dynamic programming was [212]: "In place of determining the optimal sequence of decisions for the *fixed* state of the system, we wish to determine the optimal decision to be made at *any* state of the system". Thus, instead of attempting to solve to original optimal control problem (4.3), where the cost function is specific for the given initial conditions $\boldsymbol{x}_0$ and t_0, that is $J(\boldsymbol{u}) = J(\boldsymbol{x}_0, \boldsymbol{u}, t_0)$, the idea of dynamic programming is to consider the family of minimisation problems associated with the cost functionals

$$J(\boldsymbol{x}, \boldsymbol{u}, t) = \Phi\left(\boldsymbol{x}(t_f), t_f\right) + \int_t^{t_f} L\left(\boldsymbol{x}(\tau), \boldsymbol{u}(\tau), \tau\right)\, d\tau,$$

where $t \in [t_0, t_f]$ and $\boldsymbol{x} \in \mathbb{R}^n$, and to solve them all at the same time. The first step is to introduce the value function

$$V(\boldsymbol{x}, t) = \min_{\boldsymbol{u}} J(\boldsymbol{x}, \boldsymbol{u}, t),$$

which describes the optimal *cost-to-go* from the configuration $(\boldsymbol{x}, t)$ to $(\boldsymbol{x}(t_f), t_f)$, and satisfies the boundary condition

$$V(\boldsymbol{x}, t_f) = \Phi\left(\boldsymbol{x}, t_f\right) \qquad \forall \boldsymbol{x} \in \mathbb{R}^n. \tag{4.4}$$

An additional important contribution of dynamic programming is the *principle of optimality*, which is stated as [210]:

> *An optimal policy has the property that whatever the initial state and initial decision are, the remaining decisions must constitute an optimal policy with regard to the state resulting from the first decision,*

and can be described by the equation

$$V(\boldsymbol{x}, t) = \min_{\boldsymbol{u}} \left\{ \int_t^{t+\Delta t} L\left(\boldsymbol{x}(\tau), \boldsymbol{u}(\tau), \tau\right)\, d\tau + V(t + \Delta t, \boldsymbol{x}(t + \Delta t)) \right\}. \tag{4.5}$$

The meaning of (4.5) is that the optimal problem for the interval $[t, t_f]$ is split into two and, since the value function appears on both sides with different arguments, this equation provides a dynamic relation between the optimal cost for different values of the state $\boldsymbol{x}$ and time t. Equation (4.5) can be expressed in infinitesimal form as the partial differential equation known as the *Hamilton-Jacobi-Bellman* equation:

$$-\frac{\partial}{\partial t} V(\boldsymbol{x}, t) = \min_{\boldsymbol{u}} \left\{ L(\boldsymbol{x}, \boldsymbol{u}, t) + \frac{\partial}{\partial \boldsymbol{x}} V(\boldsymbol{x}, t)^T \boldsymbol{f}(\boldsymbol{x}, \boldsymbol{u}, t) \right\}, \tag{4.6}$$

which must hold for all $t \in [t_0, t_f]$ and $\boldsymbol{x} \in \mathbb{R}^n$. The boundary condition in (4.4) is defined for the final time t_f, thus the Hamilton-Jacobi-Bellman equation describes the evolution of the value function backwards in time from the final time. Once equation (4.6) has been solved, the

optimal control $\boldsymbol{u}^*$, if it exists, is given by

$$\boldsymbol{u}^*(\boldsymbol{x}, t) = \arg\min_{\boldsymbol{u}} L(\boldsymbol{x}, \boldsymbol{u}, t) + \frac{\partial}{\partial \boldsymbol{x}} V(\boldsymbol{x}, t)^T \boldsymbol{f}(\boldsymbol{x}, \boldsymbol{u}, t), \tag{4.7}$$

where $\boldsymbol{u}^*(\boldsymbol{x}, t)$ is an optimal feedback control, because it depends only on the current value of the state vector $\boldsymbol{x}(t)$ and the time t. Equation (4.7) shows where the curse of dimensionality comes into play; in fact, the computation of the optimal control $\boldsymbol{u}^*(\boldsymbol{x}, t)$ requires knowledge of the value function $V(\boldsymbol{x}, t)$ for all the states $\boldsymbol{x} \in \mathbb{R}^n$ and the times $t \in [t_0, t_f]$, which can only be performed for problems where the dimension n of the state vector and the interval $[t_0, t_f]$ are small, unless an analytical solution exists, as for linear systems with quadratic cost.

The optimal control and equation (4.6) can be written in a more compact form by introducing the adjoint vector

$$\lambda = \frac{\partial}{\partial \boldsymbol{x}} V(\boldsymbol{x}, t)$$

and the Hamiltonian

$$H(\boldsymbol{x}, \lambda, \boldsymbol{u}) = L(\boldsymbol{x}, \boldsymbol{u}, t) + \lambda^T \boldsymbol{f}(\boldsymbol{x}, \boldsymbol{u}, t), \tag{4.8}$$

resulting in

$$\begin{aligned} \boldsymbol{u}^* &= \arg\min_{\boldsymbol{u}} H(\boldsymbol{x}, \lambda, \boldsymbol{u}), \\ -\frac{\partial}{\partial t} V(\boldsymbol{x}, t) &= H^* \left(\boldsymbol{x}, \frac{\partial}{\partial \boldsymbol{x}} V(\boldsymbol{x}, t) \right), \end{aligned} \tag{4.9}$$

where the *lower Hamiltonian* H^* is defined as:

$$H^*(\boldsymbol{x}, \lambda) = \min_{\boldsymbol{u}} H(\boldsymbol{x}, \lambda, \boldsymbol{u}).$$

The definition of the Hamiltonian (4.8) and the adjoint vector, in addition to giving a more compact notation for the results of dynamic programming, also allow the connection between the main results of the dynamic programming and the results given by PMP, which will be described in the following section.

4.1.1.2 Calculus of variations and Pontryagin's Minimum Principle

Before introducing Pontryagin's Minimum Principle, it can be useful to summarise the main results provided by applying the calculus of variations; in this way, it will be possible to illustrate some of the reasons why Pontryagin was led to extend the calculus of variations to allow the solution of a wider range of optimal control problems.

Calculus of variations, as PMP, provides only necessary conditions for the optimality, meaning that if $\boldsymbol{u}^*$ is an optimal control, then it must satisfy these conditions. However, there may

exist some candidate solutions calculated in some manner which satisfy the necessary conditions but they are not optimal because they do not minimise the cost $J(\boldsymbol{u})$.

If $\boldsymbol{u}^*$ is an optimal control, then it provides a global minimum for the cost, that is

$$J(\boldsymbol{u}^*) \leq J(\boldsymbol{u})$$

for all the piecewise continuous controls. Let $\boldsymbol{x}^*$ be an optimal state trajectory, that is a trajectory obtained by the dynamic equation (4.1) when the input is the optimal control $\boldsymbol{u}^*$. The necessary conditions for optimality are derived by formulating the optimal control problem using Lagrange multipliers to include the dynamic equation (4.1) as a constraint in the cost functional (4.2), leading to the augmented cost

$$\bar{J} = \Phi\left(\boldsymbol{x}(t_f), t_f\right) + \int_{t_0}^{t_f} L\left(\boldsymbol{x}, \boldsymbol{u}, t\right) + \boldsymbol{\lambda}^T\left(\boldsymbol{f}(\boldsymbol{x}, \boldsymbol{u}, t) - \dot{\boldsymbol{x}}\right) dt,$$

which can be written, using the definition of the Hamiltonian in (4.8), as

$$\bar{J} = \Phi\left(\boldsymbol{x}(t_f), t_f\right) + \int_{t_0}^{t_f} H\left(\boldsymbol{x}, \boldsymbol{\lambda}, \boldsymbol{u}, t\right) - \boldsymbol{\lambda}^T \dot{\boldsymbol{x}}\, dt,$$

The first-order necessary condition for optimality states that the first variation of the augmented cost $\bar{J}$ is zero throughout the time interval, that is:

$$\delta \bar{J}\big|_{\boldsymbol{u}^*} = 0,$$

which results in the Euler-Lagrange equation

$$\dot{\boldsymbol{\lambda}}^T = -\frac{\partial}{\partial \boldsymbol{x}} H\left(\boldsymbol{x}^*, \boldsymbol{\lambda}, \boldsymbol{u}^*, t\right) \tag{4.10}$$

with boundary condition

$$\boldsymbol{\lambda}^T(t_f) = \frac{\partial}{\partial \boldsymbol{x}} \Phi(\boldsymbol{x}(t_f)), \tag{4.11}$$

and the equation

$$\frac{\partial}{\partial \boldsymbol{u}} H\left(\boldsymbol{x}^*, \boldsymbol{\lambda}, \boldsymbol{u}^*, t\right) = 0 \qquad \forall t \in [t_0, t_f], \tag{4.12}$$

which states that the Hamiltonian has a stationary point as a function of the control, along the optimal trajectory. This last result is in accordance with dynamic programming, where it has been shown that the optimal control $\boldsymbol{u}^*$ is the control that minimises the Hamiltonian.

By using the Hamiltonian in (4.8), the dynamic equation (4.1) can be written as $\dot{\boldsymbol{x}}^T = \frac{\partial H}{\partial \boldsymbol{\lambda}}$, thus the evolution of the state in (4.1) and the adjoint state in (4.10) are described by Hamilton's

canonical equations

$$\dot{\boldsymbol{x}}^T = \frac{\partial H}{\partial \boldsymbol{\lambda}}, \tag{4.13}$$

$$\dot{\boldsymbol{\lambda}}^T = -\frac{\partial H}{\partial \boldsymbol{x}}, \tag{4.14}$$

with boundary conditions in (4.11) and $\boldsymbol{x}(t_0) = \boldsymbol{x}_0$. This is a two-point boundary value problem, because the boundary conditions for the state are defined at the initial time and the boundary conditions on the adjoint vector are defined at the final time.

Pontryagin's Minimum Principle Up to this point, it has been assumed that there are no path constraints (restrictions on the state trajectory), nor control constraints. If, for example, the control is restricted by the inequalities $\mathbf{h}^L \leq \boldsymbol{h}(\boldsymbol{u}) \leq \mathbf{h}^U$, then the results provided by calculus of variations are not valid any more. In fact, if the minimum of the Hamiltonian is obtained on the boundary of the admissible control set, that is when $\mathbf{h}^L = \boldsymbol{h}(\boldsymbol{u})$ or when $\mathbf{h}^U = \boldsymbol{h}(\boldsymbol{u})$, then the condition in (4.12) concerning the stationarity of the Hamiltonian with respect to the control $\boldsymbol{u}$ does not apply.

Pontryagin's principle extends calculus of variations by stating (informally) that the optimal control $\boldsymbol{u}^*$ minimises the Hamiltonian on the optimal trajectory, that is

$$H\left(\boldsymbol{x}^*, \boldsymbol{\lambda}^*, \boldsymbol{u}^*, t\right) \leq H\left(\boldsymbol{x}^*, \boldsymbol{\lambda}^*, \boldsymbol{u}, t\right)$$

for $\boldsymbol{u} \in U$, where U is the set of admissible controls. The connection with dynamic programming is evident by looking at the optimal feedback control in (4.9): in both approaches, the optimal control $\boldsymbol{u}^*$ is a minimiser for the Hamiltonian.

Pontryagin's principle is more general than the necessary conditions provided by calculus of variations in (4.10)–(4.12). In fact, let us consider the illustrative example where the set U is $U = \left\{\boldsymbol{u} \in \mathbb{R}^m : \mathbf{h}^L \leq \boldsymbol{h}(\boldsymbol{u}) \leq \mathbf{h}^U\right\}$, then the Hamiltonian minimisation can be stated as [213]:

$$\begin{aligned} &\min_{\boldsymbol{u}} H\left(\boldsymbol{x}^*, \boldsymbol{\lambda}^*, \boldsymbol{u}, t\right) \\ &\text{subject to:} \quad \mathbf{h}^L \leq \boldsymbol{h}(\boldsymbol{u}) \leq \mathbf{h}^U, \end{aligned}$$

for each time $t \in [t_0, t_f]$. This problem can be solved by using Lagrange multipliers and by defining the Lagrangian of the Hamiltonian as

$$\bar{H}\left(\boldsymbol{x}^*, \boldsymbol{\lambda}^*, \boldsymbol{u}, t, \boldsymbol{\mu}\right) = H\left(\boldsymbol{x}^*, \boldsymbol{\lambda}^*, \boldsymbol{u}, t\right) + \boldsymbol{\mu}^T \boldsymbol{h}(\boldsymbol{u}),$$

where $\boldsymbol{\mu}$ is a time-dependent multiplier. The resulting necessary conditions for optimality are

that $\bar{H}$ must be stationary with respect to the control $\boldsymbol{u}$ as

$$\frac{\partial \bar{H}}{\partial \boldsymbol{u}} = \frac{\partial H}{\partial \boldsymbol{u}} + \left(\frac{\partial \boldsymbol{h}}{\partial \boldsymbol{u}}\right)^T \boldsymbol{\mu} = 0,$$

and that, at each instant in time t, the multiplier and the constraint must satisfy the *complementarity conditions*

$$\mu_i \begin{cases} \leq 0 & h_i(\boldsymbol{u}) = \mathrm{h}_i^L \\ = 0 & \mathrm{h}_i^L < h_i(\boldsymbol{u}) < \mathrm{h}_i^U \\ \geq 0 & h_i(\boldsymbol{u}) = \mathrm{h}_i^U \\ \text{unrestricted} & \mathrm{h}_i^L = \mathrm{h}_i^U \end{cases} \tag{4.15}$$

where μ_i is the i-th element of the multiplier $\boldsymbol{\mu}$.

4.1.2 Approximation of optimal control problems

Optimal control problems, as shown in previous section, are optimisation problems in (infinite-dimensional) functional spaces, meaning that the solution, i.e. the optimal control $\boldsymbol{u}^*$, is a function defined in the interval $t \in [t_0, t_f]$. The necessary conditions for optimality in (4.13) and (4.14) reduce the optimal control problem to a two-point boundary value problem which is difficult, if not often impossible, to solve analytically. Thus, the solution to the optimal control problem is then approximated using numerical techniques, which are generally categorised into *Direct methods* and *Indirect methods*. Indirect methods attempt to numerically solve the necessary conditions for optimality, whereas the direct methods attempt the minimisation of the cost function $\boldsymbol{J}$.

The advantages of indirect methods are the high accuracy and the assurance that they satisfy the necessary conditions for optimality. However, they suffer from significant drawbacks, as the necessary conditions are problem specific [20], and they must be derived analytically for *each* problem, a task that may not be trivial. Also, the method is not robust because the radius of convergence is generally small, requiring a good guess for the initial value of the adjoint vector, which may be difficult to achieve because, in contrast to the state variable $\boldsymbol{x}$, $\boldsymbol{\lambda}$ does not carry any physical meaning. Additionally, if the control problem includes control or path inequalities[3], it is difficult to estimate the switching time between the complementarity conditions in (4.15); in other words, it is difficult to decide which one of the four conditions in (4.15) is true at each time $t \in [t_0, t_f]$.

[3] i.e. restrictions on the control set or on the admissible state set

4.1.2.1 Direct transcription methods

Direct methods transcribe the optimal control problem into a NLP problem. The solution that they provide is not as accurate as the one provided by the indirect methods; also, the adjoint vector which provides information about the optimality and sensitivity of the cost functional is not obtained directly [214],[215]. However, the optimisation problem is less sensitive to the initial guess on the state and there is no need for an initial guess for the adjoint vector.

The two main approaches for the direct transcription of optimal control problems are the direct shooting methods and the family of methods based on the discretisation scheme known as mean weighted residuals [216], which includes Galerkin and pseudospectral methods, among others.

Direct shooting methods The direct shooting approach [217, 218, 219] consists of parametrising the control function by polynomials, piecewise constant functions or piecewise polynomials, and by considering the state as the dependent variable, which is calculated by numerical forward integration of the system dynamic equation. The solution to the resulting optimisation problem is the vector of parameters describing the control input which minimises the cost functional J. Direct shooting methods are divided into two main branches: single shooting [217, 218] and multiple shooting [219] methods. In the single shooting approach, the integration of the dynamic equation is carried out over the entire time interval $[t_0, t_f]$, whereas the multiple shooting approach divides the time interval into subintervals, and the dynamic equation is integrated separately in each subinterval. Direct multiple shooting results in a larger NLP problem because additional constraints on the continuity of the state trajectory have to be introduced. However, the optimisation problem is sparse and it is characterised by better numerical properties compared to the problem generated by the single shooting method, which could be very sensitive to the initial guess, if the problem is not very small ([20]).

Mean weighted residuals discretisation The approach used by the family of discretisation methods based on the mean weighted residuals is to parametrise both the state and the control variables. This class of methods includes spectral and pseudospectral (collocation) methods, which are extensively used in fluid dynamics, and are characterised by a fast convergence rate [216, 220, 221], meaning that the approximation error decreases quickly as the number of parameters increases.

The basic idea of the mean weighted residual methods [216] is to assume that the state and the control can be approximated by a linear combination of basis functions $\phi_k^x(t)$ and $\phi_k^u(t)$,

respectively, as

$$x_i(t) \approx x_i^{N_x}(t) := \sum_{k=1}^{N_x} \hat{x}_{ik}\phi_k^x(t), \tag{4.16}$$

$$u_i(t) \approx u_i^{N_u}(t) := \sum_{k=1}^{N_u} \hat{u}_{ik}\phi_k^u(t). \tag{4.17}$$

where x_i, u_i, $x_i^{N_x}$ and $u_i^{N_u}$ denote, respectively, the i-th components of the vectors $\boldsymbol{x}$, $\boldsymbol{u}$, $\boldsymbol{x}^{N_x}$ and $\boldsymbol{u}^{N_u}$. When the series are substituted into the dynamic equation (4.1), the resulting residual function is defined as

$$\boldsymbol{R}(\boldsymbol{X}, \boldsymbol{U}, t) = \dot{\boldsymbol{x}}^{N_x} - \boldsymbol{f}(\boldsymbol{X}, \boldsymbol{U}, t), \tag{4.18}$$

where the i-th component of the time-derivative of the state $\dot{\boldsymbol{x}}^{N_x}$ is

$$\dot{x}_i^{N_x}(t) = \sum_{k=1}^{N_x} \hat{x}_{ik}\dot{\phi}_k^x(t)$$

and the vectors $\boldsymbol{X}$ and $\boldsymbol{U}$ contain, respectively, the coefficients $\hat{x}_{ik}$ and $\hat{u}_{ik}$ (more precise details will be provided in section 4.2.2). The important fact about equation (4.18) is that the residual $\boldsymbol{R}$ is a function of a finite number ($N_x + N_u$) of coefficients, as well as the time t.

For any given values of the control vector $\boldsymbol{U}$, the corresponding vector $\boldsymbol{X}$ which satisfies the dynamic equation is calculated by solving the system of equations

$$\langle R_i(\boldsymbol{X}, \boldsymbol{U}, t), \psi_j(t)\rangle = 0 \qquad \text{for } i, j = 1, \dots, N_x, \tag{4.19}$$

where the inner product is defined as $\langle f, g\rangle = \int_\Gamma f(t)g(t)\,dt$, and where the test (or weight) functions $\psi_j(t)$ are linearly independent ($\langle \psi_j, \psi_i\rangle = 0$ for $j \neq i$). The meaning of equation (4.19) is that, for any given values of $\boldsymbol{U}$, the corresponding vector $\boldsymbol{X}$ is obtained by imposing the residual being orthogonal to all the element of the basis with elements $\psi_j(t)$. Thus, the residual is imposed to be equal to the zero element of the vector space for which $\{\psi_j(t)\}_{j=1}^{N_x}$ form a basis. In practice, the control input $\boldsymbol{u}$ is specified by the vector $\boldsymbol{U}$ by means of equation (4.17), and the approximated state trajectory $\boldsymbol{x}^{N_x}$ is fully described by the elements of the vector $\boldsymbol{X}$ by means of (4.16). Thus, for any choice of the control vector $\boldsymbol{U}$, equation (4.19) allows, under appropriate conditions, the calculation of the state vector $\boldsymbol{X}$, which satisfies the dynamic equation(4.1).

If the test functions $\phi_j(t)$ are elements of the same set as the basis functions approximating the state, that is $\phi_j(t) = \phi_k^x(t)$, then the method is known as *Galerkin method*. If, on the other hand, the test functions are translated Dirac-deltas $\delta(t - t_j)$, then the method takes the name of *pseudospectral* or collocation method, and the points t_j are called collocation points.

By applying the mean weighted residual discretisation, the optimal control problem is approximated with a NLP problem, where the dynamic equation corresponds to the set of (nonlinear) equality constraints (4.19), and the cost functional $\boldsymbol{J}$ is approximated by an appropriate quadrature formula, with weights w_j, as

$$J(\boldsymbol{X},\boldsymbol{U}) = \Phi(\boldsymbol{X}) + \int_{t_0}^{t_f} L(\boldsymbol{X},\boldsymbol{U},t)\,dt \approx J^{N_{xu}}(\boldsymbol{X},\boldsymbol{U}) = \sum_{j=0}^{Nq} L(\boldsymbol{X},\boldsymbol{U},t_j)w_j, \tag{4.20}$$

where the function $\boldsymbol{J}^{N_{xu}} : \mathbb{R}^{N_x+N_u} \to \mathbb{R}$. The objective of this section is to provide a general overview of the connection between the several discretisation techniques, and more details are provided in section 4.2.2 with regard to the Galerkin method applied to a linear WEC, while the application of a pseudospectral method to a non linear WEC is described in section 4.3.

It should be noted that the terminology regarding mean weighted residual methods is not standardised. According to Boyd ([216]), "pseudospectral" and "collocation" are generally considered synonyms, while some authors call "Galerkin" the general "mean weighted residual" approach, and "Rayleigh-Ritz" the "Galerkin" method. It is also common to use the label "Petrov-Galerkin" when the basis functions differ from the test functions. Additionally, some other authors [214, 220] discern between "tau-method" and "Galerkin" based on whether the basis function individually satisfy the boundary conditions or not.

4.1.3 Nonlinear programming

The approximation of optimal control problems leads to NLP problems. In particular, when using mean weighted residuals, the finite dimensional optimisation problem is carried out over the N_x+N_u coefficients describing the state and the control (the vectors $\boldsymbol{X}$ and $\boldsymbol{U}$). In this case, the cost function is $\boldsymbol{J}(\boldsymbol{X},\boldsymbol{U})$ in (4.20) and the system dynamic equation (4.1) becomes a set of equality constraints, as in (4.19). This section covers the basic results in finite dimensional optimisation, describing the necessary and sufficient conditions for optimality in the case of both unconstrained and constrained problems [222, 223].

At first, it is useful to provide some background, starting from the definition of a convex set, that is a set $\Omega \subset \mathbb{R}^N$ for which all the connecting lines between any two points ($\boldsymbol{x}$ and $\boldsymbol{y}$) belonging to the set lie inside the same set; more formally,

$$\forall\ \boldsymbol{x},\boldsymbol{y} \in \Omega \subset \mathbb{R}^N, t \in [0,1]\ :\ \boldsymbol{x} + t(\boldsymbol{y}-\boldsymbol{x}) \in \Omega.$$

Additionally, a function $\boldsymbol{J} : \Omega \to \mathbb{R}$ is convex if Ω is convex and

$$\forall \boldsymbol{x},\boldsymbol{y} \in \Omega, t \in [0,1]\ :\quad \boldsymbol{J}(\boldsymbol{x} + t(\boldsymbol{y}-\boldsymbol{x})) \leq \boldsymbol{J}(\boldsymbol{x}) + t\left(f(\boldsymbol{y}) - f(\boldsymbol{x})\right),$$

that is, the value of the function on the line segment connecting any two elements of Ω lies below the line segment connecting the value of the function at the same two points.

A general unconstrained NLP problem is given by

$$\min_{\boldsymbol{q}} \; J(\boldsymbol{q}) \tag{4.21}$$

where $J : \mathbb{R}^N \to \mathbb{R}$ is assumed to be continuously differentiable and $\boldsymbol{q} \in \mathbb{R}^N$. A point $\boldsymbol{q}^*$ is a global minimiser if and only if $\boldsymbol{q}^* \in \Omega$ and $J(\boldsymbol{q}^*) \leq J(\boldsymbol{q}) \; \forall \boldsymbol{q} \in \Omega$; that is, if the value of the function at $\boldsymbol{q}^*$ is smaller than the value of the function at any other point in Ω. A local minimiser is a point $\boldsymbol{q}^*$ for which the value of the function at that point is smaller than the value of the function only in a neighbourhood[4] $\mathcal{N}$ of $\boldsymbol{q}^*$; more concisely, $\boldsymbol{q}^*$ is a local minimiser if and only if $\boldsymbol{q}^* \in \Omega$ and there exists a neighbourhood $\mathcal{N}$ of $\boldsymbol{q}$, such that $J(\boldsymbol{q}^*) \leq J(\boldsymbol{q}) \; \forall \boldsymbol{q} \in \Omega \cap \mathcal{N}$.

An important property of convex functions is that every local minimiser is also a global minimiser. Convexity of a function can be detected by means of the Hessian matrix, thus if the function J is twice continuously differentiable and Ω is a convex set, J is convex if and only if the Hessian is positive semi-definite:

$$\nabla^2 J(\boldsymbol{q}) \geq 0, \; \forall \boldsymbol{q} \in \Omega.$$

For the particular case of a quadratic cost function

$$J(\boldsymbol{q}) = \frac{1}{2} \boldsymbol{q}^T G \, \boldsymbol{q} + c^T \boldsymbol{q},$$

the Hessian is the matrix G ($\nabla^2 J(\boldsymbol{q}) = G$), thus J is convex if and only if G is positive semi-definite.

Minimisers can be detected by seeking the stationary points of the function J; if J is differentiable, the first-order necessary condition for optimality is obtained when the gradient of J vanishes, which corresponds to

$$\nabla J(\boldsymbol{q}) = 0,$$

Stationary points $\bar{\boldsymbol{q}}$ satisfying the first-order necessary conditions can be local minima, maxima, or saddle points. If the function is also convex, then stationary points are global minimisers.

In practical applications, the set of values $\boldsymbol{q}$ over which the optimisation is carried out is restricted by means of equality or inequality constraints. For example, the approximated optimal control problem obtained by applying the discretisation method described in sec. 4.1.2.1 includes equality constraints due to the dynamic equation of the system in (4.19). Additional path and control restriction are also common, and they result in a constrained Non Linear Pro-

[4] A neighbourhood can be, for example, an open ball $B_r(\boldsymbol{q})$ or radius $r \in \mathbb{R}$ defined as $B_r(\boldsymbol{q}) = \{p \in \Omega | \|p - q\| \leq r\}$, where $\| \; \|$ is a norm on Ω.

gramming (NLP) problem, with equality and inequality constraints as:

$$\begin{aligned} \min_{\boldsymbol{q}} \quad & \boldsymbol{J}(\boldsymbol{q}) \\ \text{subject to} \quad & \boldsymbol{g}(\boldsymbol{q}) = 0, \\ & \boldsymbol{h}(\boldsymbol{q}) \leq 0, \end{aligned} \tag{4.22}$$

where $\boldsymbol{J} : \mathbb{R}^N \to \mathbb{R}$, $g : \mathbb{R}^N \to \mathbb{R}^{N_g}$, and $h : \mathbb{R}^N \to \mathbb{R}^{N_h}$, are assumed to be continuously differentiable. The feasible set Ω is defined as $\Omega = \{\boldsymbol{q} \in \mathbb{R}^N | \boldsymbol{g}(\boldsymbol{q}) = 0, \boldsymbol{h}(\boldsymbol{q}) \leq 0\}$. An inequality constraint is called active at $\boldsymbol{q}^*$ if $\boldsymbol{h}(\boldsymbol{q}^*) = 0$, otherwise it is called inactive, and the active set $\mathscr{A}(\boldsymbol{q}^*)$ is the set of the indices of the active constraints: $\mathscr{A}(\boldsymbol{q}^*) = \{i | h_i(\boldsymbol{q}^*) = 0\}$.

Before stating the first-order necessary condition for optimality, an additional definition must be provided, which is the "linear independent constraint qualification". The linear independent constraint qualification holds at a given point $\boldsymbol{q}^*$ if all the gradients $\nabla g_i(\boldsymbol{q}^*)$ for $i \in \{1, \dots, N_g\}$ and $\nabla h_i(\boldsymbol{q}^*)$ for $i \in \mathscr{A}(\boldsymbol{q}^*)$ are linearly independent.

The first-order necessary condition for optimality, known as Karush-Kuhn-Tucker conditions [222] can be stated as: If $\boldsymbol{q}^*$ is a local minimiser for the NLP problem in (4.22) and the linear independent constraint qualification holds at $\boldsymbol{q}^*$, then there exist multiplier vectors $\boldsymbol{\lambda}^* \in \mathbb{R}^{N_g}$ and $\boldsymbol{\mu}^* \in \mathbb{R}^{N_g}$ with

$$\begin{aligned} \nabla \boldsymbol{J}(\boldsymbol{q}^*) + \nabla \boldsymbol{g}(\boldsymbol{q}^*)\boldsymbol{\lambda}^* + \nabla \boldsymbol{h}(\boldsymbol{q}^*)\boldsymbol{\mu}^* &= 0 \\ \boldsymbol{g}(\boldsymbol{q}^*) &= 0 \\ \boldsymbol{h}(\boldsymbol{q}^*) &\leq 0 \\ \boldsymbol{\mu}^* &\geq 0 \\ \mu_i^* h_i(\boldsymbol{x})^* &= 0, \qquad i = 1, \dots, N_h. \end{aligned}$$

where $\nabla \boldsymbol{g}(\boldsymbol{q}^*)$ and $\nabla \boldsymbol{h}(\boldsymbol{q}^*)$ are the transposes of, respectively, the Jacobians of $\boldsymbol{g}(\boldsymbol{q}^*)$ and $\boldsymbol{h}(\boldsymbol{q}^*)$, and $\nabla \boldsymbol{J}(\boldsymbol{q}^*)$ is the gradient of $\boldsymbol{J}$. If the feasible set Ω is convex and the objective function $\boldsymbol{J}$ is convex, then the Karush-Kuhn-Tucker conditions are also sufficient, and the point $\boldsymbol{q}^*$ is a global minimum.

A recent result in the area of numerical optimal control is the *covector mapping principle* [224]; it establishes a connection between the Karush-Kuhn-Tucker conditions of a NLP problem obtained by direct transcription of an optimal control problem using pseudospectral methods, and the discretisation of the two-point boundary value problem describing the necessary conditions for optimality provided by PMP (sec. 4.1.1.2).

4.2 Linear optimal control of wave energy converters

This section describes the application of a direct transcription method to the optimal control of WECs. The optimal control problem is the maximisation of the total energy absorbed by a system of WECs, which are described by the linear model presented in sec. 2.2.2.3. The transcription method used for the discretisation of the control problem is the mean weighted residuals which has been described detailed in sec. 4.1.2.1.

Initially, the discretisation is carried out for a generic configuration of WECs and for generic sets of basis and test functions; detailed derivations of the quadratic program resulting from the direct transcription are also included here. As an illustrative example, sec. 4.2.2 describes the application of the Galerkin method to a single body WEC, where the basis functions are truncated Fourier series. Derivations of the matrices composing the quadratic program, and a discussion about some of their properties are also illustrated (e.g. convexity).

Simulation results are presented in sec. 4.2.2.3 for both regular and irregular incident waves, including restrictions on both PTO force and oscillation amplitude. Section 4.3 provides a discussion regarding the simplification of the convolution integral associated with the radiation force when the velocity is approximated with a generic expansion. It is shown that, because of linearity, the computations involving the numerical integration of the convolution integral can be carried out offline, thus significantly reducing the computational load when solving the NLP problem.

4.2.1 General case: mean weighted residual formulation of a system of WECs

The objective of this section is to describe the steps for the direct transcription of the optimal control problem of a generic system WECs, the model of which has been described in sec.2.2.2.3 and given in equation (2.71), that is:

$$\mathbf{M}\,\ddot{\boldsymbol{\eta}}(t) + \mathbf{B}\,\dot{\boldsymbol{\eta}}(t) + \int_0^t \mathbf{K}(t-\tau)\dot{\boldsymbol{\eta}}(\tau)\,d\tau + \mathbf{S}\,\boldsymbol{\eta}(t) = \tilde{\boldsymbol{f}}_p(t) + \boldsymbol{f}_e(t), \tag{4.23}$$

where $\boldsymbol{\eta}(t) \in \mathbb{R}^n$ is the position vector of the WEC and n is the number of degrees of freedom of the system. The matrix $\mathbf{M} \in \mathbb{R}^{n\times n}$ is the sum of the generalized mass matrix and the added mass at infinite frequency; $\mathbf{B}$ and $\mathbf{S}$ are positive constant $n \times n$ diagonal matrices describing the linear damping and the stiffness respectively. The elements of the $n \times n$ matrix of radiation impulse responses $\mathbf{K}(t)$ are continuous functions in $[0, \alpha)$ and zero for $t < 0$, where $\alpha \leq \infty$. In this section, it is assumed that the velocity is zero for $t < 0$, thus the interval of integration of the convolution integral is $[0, t]$; the case where $\dot{\boldsymbol{\eta}}(t) \neq 0$ for $t < 0$ requires little modification and is addressed in sec. 4.2.1.1.

The vector of excitation forces $\boldsymbol{f}_e(t) \colon [0, t] \to \mathbb{R}^n$ is assumed to be continuous, and the

vector of the PTO forces is considered to be $\tilde{\boldsymbol{f}}_p(t) = \mathbf{F}_P \boldsymbol{f}_{pto}$, where $\mathbf{F}_P$ is an $n \times m$ constant matrix. The role of the matrix $\mathbf{F}_P$ is to allow a general combinations of PTOs, in particular where the number of PTO forces (m) are different from the number of modes of oscillation of the system (n), and in general there are less PTO forces than modes of oscillations ($m \leq n$). Considering for example the two-body self-reacting point absorber in fig. 2.4, if the two bodies are restricted to oscillate in heave only, then there are two modes of oscillation ($n = 2$) and only one PTO ($m = 1$), which applies the same force with opposite direction on each of the bodies. A more detailed explanation regarding the matrix $\mathbf{F}_P$, and some more examples, will be provided in section 4.2.1.2.

The matrix $\mathbf{F}_P$ also takes part in the definition of the total absorbed energy over the time interval $[0, T]$, which is defined as the sum of the mechanical work done by all the PTO forces:

$$J = -\int_0^T \dot{\boldsymbol{\eta}}(t)^T \mathbf{F}_p \boldsymbol{f}_{pto}(t)\, dt. \tag{4.24}$$

In practice, $\mathbf{F}_P$ specifies how the PTO forces and the velocities are combined to produce the usable power.

The optimal control problem is to find the PTO force vector $\boldsymbol{f}_{pto}$ that maximizes the total absorbed energy J, subject to the equation of motion (4.23) and, eventually, to additional control and path constraints described as:

$$\boldsymbol{h}(\boldsymbol{\eta}, \dot{\boldsymbol{\eta}}, \boldsymbol{f}_{pto}, t) = 0 \tag{4.25}$$

$$\boldsymbol{g}(\boldsymbol{\eta}, \dot{\boldsymbol{\eta}}, \boldsymbol{f}_{pto}, t) \leq 0. \tag{4.26}$$

Before proceeding with the discretisation of the optimal control problem, the equation of motion (4.23) has to be rewritten as a system of first order integro-differential equations. This is achieved, as usual, by introducing an additional state variable describing the velocity ($\boldsymbol{v}$), and the resulting system dynamic is

$$\dot{\boldsymbol{\eta}} = \boldsymbol{v} \tag{4.27}$$

$$\mathbf{M}\,\dot{\boldsymbol{v}} = -\mathbf{B}\,\boldsymbol{v} - \int_0^t \mathbf{K}(t-\tau)\boldsymbol{v}(\tau)\, d\tau - \mathbf{S}\,\boldsymbol{\eta} + \mathbf{F}_P \boldsymbol{f}_{pto} + \boldsymbol{f}_e. \tag{4.28}$$

The discretisation of the control problem is performed by approximating the position ($\boldsymbol{\eta}$) and the velocity ($\boldsymbol{v}$) vectors with a linear combination of the basis functions $\phi_k(t)$, and the PTO force ($\boldsymbol{f}_{pto}$) vector with a linear combination of the functions $\phi_k^P(t)$; the i-th components of these vectors are:

$$\eta_i(t) \approx \eta_i^N(t) = \sum_{k=1}^{N} x_{ik}^{\eta}\, \phi_k(t) = \Phi(t)\hat{\boldsymbol{x}}_i^{\eta} \qquad i = 1, \ldots, n \tag{4.29}$$

$$v_i(t) \approx v_i^N(t) = \sum_{k=1}^{N} x_{ik}^{v}\, \phi_k(t) = \Phi(t)\hat{\boldsymbol{x}}_i^{v} \qquad i = 1, \dots, n \tag{4.30}$$

$$f_{pto_i}(t) \approx f_{pto_i}^{N^P}(t) = \sum_{k=1}^{N^P} u_{ik}\, \phi_k^P(t) = \Phi^P(t)\hat{\boldsymbol{u}}_i \qquad i = 1, \dots, m, \tag{4.31}$$

where

$$\hat{\boldsymbol{x}}_i^{\eta} = \left[\hat{x}_{i1}^{\eta}, \hat{x}_{i2}^{\eta}, \dots, \hat{x}_{iN}^{\eta}\right]^T, \qquad \hat{\boldsymbol{x}}_i^{v} = \left[\hat{x}_{i1}^{v}, \hat{x}_{i2}^{v}, \dots, \hat{x}_{iN}^{v}\right]^T,$$
$$\hat{\boldsymbol{u}}_i = \left[\hat{u}_{i1}, \hat{u}_{i2}, \dots, \hat{u}_{iN_P}\right]^T,$$

and

$$\Phi(t) = \left[\phi_1(t), \phi_2(t), \dots, \phi_N(t)\right],$$
$$\Phi^P(t) = \left[\phi_1^P(t), \phi_2^P(t), \dots, \phi_{N_P}^P(t)\right].$$

Using the approximated velocity and PTO force, the total absorbed energy $\boldsymbol{J}^N$ is

$$\boldsymbol{J}^N = -\int_0^T \Phi(t)\boldsymbol{X}^{v}\mathbf{F}_p\boldsymbol{U}^T\Phi^{P^T}(t)\,dt = \sum_{i=1}^{N^P}\sum_{j=1}^{N} w_{ij}\Gamma_{ij}, \tag{4.32}$$

where w_{ij} are the elements of the matrix $\boldsymbol{W} = \boldsymbol{X}^{v}\mathbf{F}_p\boldsymbol{U}^T$, which depends on the coefficients of the velocity ($\boldsymbol{X}^{v}$) and the PTO force ($\boldsymbol{U}$), whereas Γ_{ij} are the elements of the constant matrix Γ which depends on the bases Φ and Φ^P as

$$\Gamma = \int_0^T \Phi^T(t)\,\Phi^P(t)\,dt. \tag{4.33}$$

The matrices $\boldsymbol{X}^{\eta}$, $\boldsymbol{X}^{v}$ and $\boldsymbol{U}$ are defined as

$$\boldsymbol{X}^{\eta} = [\hat{\boldsymbol{x}}_1^{\eta}, \dots, \hat{\boldsymbol{x}}_N^{\eta}] \qquad \boldsymbol{X}^{v} = [\hat{\boldsymbol{x}}_1^{v}, \dots, \hat{\boldsymbol{x}}_N^{v}] \qquad \boldsymbol{U} = [\hat{\boldsymbol{u}}_1, \dots, \hat{\boldsymbol{u}}_{N_P}].$$

The derivatives of the approximated state variables (positions and velocities) are

$$\dot{\eta}_i^N(t) = \sum_{k=1}^{N} x_{ik}^{\eta}\,\dot{\phi}_k(t) = \dot{\Phi}(t)\hat{\boldsymbol{x}}_i^{\eta} \qquad i = 1, \dots, n \tag{4.34}$$

$$\dot{v}_i^N(t) = \sum_{k=1}^{N} x_{ik}^{v}\,\dot{\phi}_k(t) = \dot{\Phi}(t)\hat{\boldsymbol{x}}_i^{v} \qquad i = 1, \dots, n \tag{4.35}$$

because the vectors $\hat{\boldsymbol{x}}_i^{\eta}$ and $\hat{\boldsymbol{x}}_i^{v}$ are independent of time. Substituting the approximated states

(4.29) (4.30), their derivatives (4.34), (4.35) and the PTO forces (4.31) into the dynamic equations (4.27) yields, in residual form

$$r_i^\eta = \dot{\eta}_i^N - v_i^N \tag{4.36}$$

$$r_i^v = \sum_{j=1}^{n} m_{ij}\dot{v}_j^N + \mathrm{B}_{ii}v_i^N + \sum_{j=1}^{n}\int_0^t \mathrm{K}_{ij}(t-\tau)v_j^N(\tau)\,d\tau + \mathrm{S}_{ii}\eta_i^N(t) + \sum_{j=1}^{m} f_{p_{ij}} f_{pto_j}^{N^P} + f_{e_i}, \tag{4.37}$$

where m_{ij} are the elements of the matrix $\mathbf{M}$; B_{ii} and S_{ii} the diagonal elements of the diagonal matrices $\mathbf{B}$ and $\mathbf{S}$, respectively; $f_{p_{ij}}$ are the elements of $\mathbf{F}_P$ and K_{ij} the elements of $\mathbf{K}$.

By applying the mean weighted residual method, for any given values of the PTO force described by the coefficients $\boldsymbol{U}$, the coefficients of the velocity and position satisfying the equation of motion are calculated by solving the linear system of equations

$$\langle r_i^\eta, \psi_j \rangle = 0 \tag{4.38}$$

$$\langle r_i^v, \psi_j \rangle = 0 \qquad \text{for } i = 1, \dots, n \text{ and } j = 1, \dots, N \tag{4.39}$$

where ψ_j are linearly independent test functions. The system of equations (4.38)–(4.39) is linear because the dynamic equation is linear, and they form a system of $2nN$ equations in $2nN$ variables $(\boldsymbol{X}^\eta, \boldsymbol{X}^v)$.

The result of the discretisation is the finite dimensional nonlinear program described by the quadratic cost function $\boldsymbol{J}^N$ in (4.32), the linear equality constraints due to dynamic equation in (4.38) and (4.39), and, eventually by the additional equality and inequality path and control constraints in (4.25) and (4.26) which are now functions of the vectors $\boldsymbol{X}^\eta, \boldsymbol{X}^v, \boldsymbol{U}$ and time, as:

$$\boldsymbol{h}(\boldsymbol{X}^\eta, \boldsymbol{X}^v, \boldsymbol{U}, t) = 0, \tag{4.40}$$

$$\boldsymbol{g}(\boldsymbol{X}^\eta, \boldsymbol{X}^v, \boldsymbol{U}, t) \leq 0. \tag{4.41}$$

4.2.1.1 Non-zero past velocity

If the velocity is non-zero for $t < 0$, the lower limit of the convolution integral in (4.23) is σ, with $\sigma < 0$, and the convolution integral can be split as

$$\int_\sigma^t \mathbf{K}(t-\tau)\dot{\boldsymbol{\eta}}(\tau)\,d\tau = \int_\sigma^0 \mathbf{K}(t-\tau)\dot{\boldsymbol{\eta}}(\tau)\,d\tau + \int_0^t \mathbf{K}(t-\tau)\dot{\boldsymbol{\eta}}(\tau)\,d\tau. \tag{4.42}$$

The first term on the right hand side of (4.42) describes the past evolution of the system and it results in a force which may not be zero for $t \geq 0$. However, since the past velocity cannot be optimised, the fraction of the radiation force corresponding to the velocity $\dot{\boldsymbol{\eta}}(t) : t < 0$ can be

considered as an "external" force, and it can be added to the excitation as

$$\hat{\boldsymbol{f}}_e(t) = \boldsymbol{f}_e(t) - \int_{\sigma}^{t_0} \mathbf{K}(t-\tau)\,\dot{\boldsymbol{\eta}}(\tau)\,d\tau. \tag{4.43}$$

Thus, the situation where $\dot{\boldsymbol{\eta}}(t) \neq 0$ for $t < 0$ can be reformulated as the original problem described by the model in (4.23), by replacing the excitation force $\hat{\boldsymbol{f}}_e(t)$, given by (4.43), in place of $\boldsymbol{f}_e(t)$.

4.2.1.2 Definition of the PTO configuration matrix for a number of examples

The role of the matrix $\mathbf{F}_P$ in (4.28) and (4.24) is to combine the PTO forces and the velocities of the oscillating modes for which energy is absorbed, and this section illustrates how to build the matrix for some common configurations of WECs.

In the case of a single body device referenced to the seabed, such as the heaving buoy in fig. 2.2 or the pitching flap in 2.3, the system has one degree of freedom and there is only one velocity and one PTO force. The absorbed energy is

$$J = \int_0^T v(t)\, f_{pto}(t)\, dt,$$

with $\mathbf{F}_P = 1$.

A self-reacting WEC composed of two heaving bodies, which are restricted to oscillate in heave only (fig. 2.4), has two DoF. In this configuration, there is only one PTO force, and it acts on each of the bodies with the same magnitude but with opposite direction; if the system coordinates are the absolute vertical positions of the two bodies, then the absorbed energy is

$$J = \int_0^T \left(v^B(t) - v^A(t)\right)\, f_{pto}(t)\, dt = \int_0^T [v^B(t)\, v^A(t)]\, \mathbf{F}_P\, f_{pto}(t)\, dt,$$

where $v^A(t)$ and $v^B(t)$ are the absolute vertical velocities of bodies A and B, respectively, thus

$$\mathbf{F}_P = \begin{bmatrix} -1 \\ 1 \end{bmatrix}.$$

When considering multiple devices of this type (two-body self reacting WECs), for example an array of three WECs, the velocity vector can be arranged as

$$\boldsymbol{v} = \left[v_1^A,\, v_1^B,\, v_2^A,\, v_2^B,\, v_3^A,\, v_3^B\right]^T$$

and the PTO force vector as

$$\boldsymbol{f}_{pto} = \left[f_{pto_1},\, f_{pto_2},\, f_{pto_3}\right]^T,$$

where the subscript indicates the device number (1,2,3) and the superscript indicates the body component number of each device (A,B). The total absorbed energy is then

$$\begin{aligned} J &= \int_0^T \left(v_1^B(t) - v_1^A(t)\right)\, f_{pto_1}(t) + \left(v_2^B(t) - v_2^A(t)\right)\, f_{pto_2}(t) + \left(v_3^B(t) - v_3^A(t)\right)\, f_{pto_3}(t)\, dt \\ &= \int_0^T \boldsymbol{v}(t)^T\, \mathbf{F}_P\, \boldsymbol{f}_{pto}(t)\, dt, \end{aligned}$$

and the PTO configuration matrix is

$$\mathbf{F}_P = \begin{bmatrix} -1 & 0 & 0 \\ 1 & 0 & 0 \\ 0 & -1 & 0 \\ 0 & 1 & 0 \\ 0 & 0 & -1 \\ 0 & 0 & 1 \end{bmatrix}.$$

A different example is given by the three-body attenuator in fig. 2.6. If the motion of the WEC is restricted to the vertical plane, the total number of coordinates describing the configuration of the system is nine[5]; however, the floating bodies are constrained by the hinges, and the number of DoF are reduced to five. In fact, the configuration of the WEC can be fully described, for example, by the surge, heave and pitch of body A, and the pitch angles of bodies B and C, although this choice is not unique. The purpose of this section is to give examples on how to build the matrix $\mathbf{F}_P$, thus it is only important to note that the dynamic of the WEC is described by a system of 9 differential equations, in addition to the equations describing the cylindrical constraints introduced by the hinges, each of which eliminates two translating modes.

In this case there are two PTOs, one on each hinge, and they exert a moment between two adjacent bodies. If the linear velocities (v_x^A,v_z^A,v_x^B,v_z^B,v_x^C,v_z^C) angular velocities ($\dot{\theta}^A, \dot{\theta}^B, \dot{\theta}^C$) and PTO moments ($\gamma_{pto}^{BA}, \gamma_{pto}^{CB}$) are arranged as

$$\begin{aligned} \boldsymbol{v} &= \left[v_x^A,\ v_z^A,\ \dot{\theta}^A,\ v_x^B,\ v_z^B,\ \dot{\theta}^B,\ v_x^C,\ v_z^C,\ \dot{\theta}^C\right], \\ \boldsymbol{f}_{pto} &= \left[\gamma_{pto}^{BA},\ \gamma_{pto}^{CB}\right], \end{aligned}$$

then the total absorbed energy is

$$\begin{aligned} J &= \int_0^T \left(\dot{\theta}^B(t) - \dot{\theta}^A(t)\right)\, \gamma_{pto}^{BA}(t) + \left(\dot{\theta}^B(t) - \dot{\theta}^A(t)\right)\, \gamma_{pto}^{BA}(t) \\ &= \int_0^T \boldsymbol{v}(t)^T\, \mathbf{F}_P\, \boldsymbol{f}_{pto}(t)\, dt, \end{aligned}$$

[5]Heave, surge and pitch of each body.

and the PTO configuration matrix is

$$\mathbf{F}_P = \begin{bmatrix} 0 & 0 \\ 0 & 0 \\ -1 & 0 \\ 0 & 0 \\ 0 & 0 \\ 1 & -1 \\ 0 & 0 \\ 0 & 0 \\ 0 & 1 \end{bmatrix}.$$

In the general case of an array of n_a devices, by building the velocity and PTO vectors as

$$\boldsymbol{V}_a = \begin{bmatrix} \boldsymbol{v}_1 \\ \vdots \\ \boldsymbol{v}_{n_a} \end{bmatrix} \qquad \boldsymbol{F}_{pto} = \begin{bmatrix} \boldsymbol{f}_{pto_1} \\ \vdots \\ \boldsymbol{f}_{pto_{n_a}} \end{bmatrix},$$

the PTO configuration matrix for the array is block diagonal, and each block is the matrix $\mathbf{F}_P$ corresponding to each single device, that is:

$$\mathbf{F}_{P_{n_a}} = \begin{bmatrix} \mathbf{F}_P & 0 & \dots & 0 \\ 0 & \mathbf{F}_P & \dots & 0 \\ \vdots & \vdots & \ddots & \vdots \\ 0 & 0 & \dots & \mathbf{F}_P \end{bmatrix}.$$

4.2.2 Fourier-Galerkin direct transcription

As an illustrative example, a single DoF system describing the point absorber wave energy converter depicted in fig. 4.1 is considered [51], the motion of which is restricted to heave only; that is, the general WEC position vector $\boldsymbol{\eta}$ is now the (scalar) heave position z. The Galerkin method is used in conjunction with trigonometric polynomials as approximating functions because the trigonometric polynomials, or truncated Fourier series, seem a natural choice for the oscillating system. In this case, the time-domain model of the wave energy converter in (4.23) reduces to the scalar equation

$$\mathrm{M_t}\, \ddot{z}(t) + \mathrm{B}\, \dot{z}(t) + \int_{-\infty}^{t} \mathrm{K}(t-\tau)\dot{z}(\tau)\, d\tau + \mathrm{S}\, z(t) = f_e(t) + f_{pto}(t), \tag{4.44}$$

with $\mathrm{M_t} = m + m_\infty$ and where m is the mass of the oscillating body and m_∞ is the added mass at infinite frequency for the heave mode. Since the PTO force is applied between the body and a

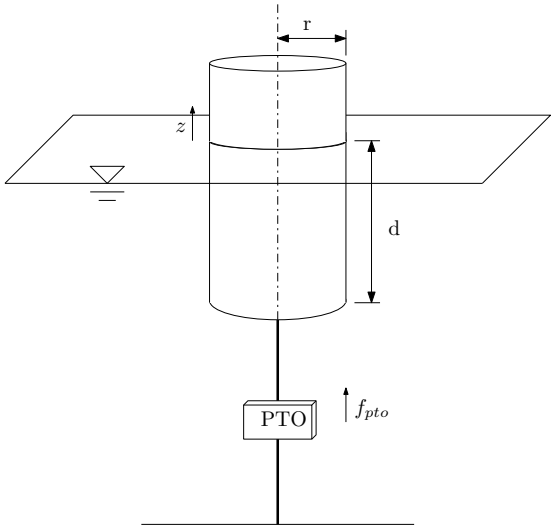

Figure 4.1: Heaving WEC

fixed reference, the PTO configuration matrix is $\mathbf{F}_P = 1$, and the absorbed energy is now defined as

$$J = -\int_0^T \dot{z}(t)\, f_{pto}(t)\, dt. \tag{4.45}$$

For convenience of notation, the state variables are renamed as $z = x_1$ and $v = x_2$, and the PTO force, which is the control input, as $f_{pto} = u$; the resulting dynamic model is

$$\dot{x}_1 = x_2 \tag{4.46}$$

$$I_t \dot{x}_2 = -Bx_2 - \int_{-\infty}^{t} \mathrm{K}(t-\tau)x_2(\tau)\, d\tau - Sx_1 + u + f_e \tag{4.47}$$

The heave positions and velocities in (4.29) and (4.30), respectively, and the PTO force in (4.31) are all approximated by zero-mean truncated Fourier series with N terms with $N{=}N^P$ for this case, that is:

$$x_i(t) \approx \sum_{k=1}^{N/2} x_{ik}^c \cos(k\omega_0 t) + x_{ik}^s \sin(k\omega_0 t) = \Phi(t)\hat{\boldsymbol{x}}_i \quad i = 1, 2 \tag{4.48}$$

$$u(t) \approx \sum_{k=1}^{N/2} u_k^c \cos(k\omega_0 t) + u_k^s \sin(k\omega_0 t) = \Phi(t)\hat{\boldsymbol{u}} \tag{4.49}$$

where

$$\hat{\boldsymbol{x}}_i = \left[x_{i1}^c, x_{i1}^s, \ldots, x_{i\frac{N}{2}}^c + x_{i\frac{N}{2}}^s \right]^T$$

$$\hat{\boldsymbol{u}} = \left[u_1^c, u_1^s, \ldots, u_{\frac{N}{2}}^c + u_{\frac{N}{2}}^s \right]^T$$

and

$$\Phi(t) = \left[\cos(\omega_0 t), \sin(\omega_0 t), \dots, \cos\left(\frac{N}{2}\omega_0 t\right), \sin\left(\frac{N}{2}\omega_0 t\right)\right], \tag{4.50}$$

and the fundamental frequency is $\omega_0 = 2\pi/T$. The constant terms of the bases ($k = 0$) have been discarded because the exciting force is assumed to be zero-mean; therefore also the resulting (optimal) oscillation is expected to be zero-mean.

By substituting the approximations (4.48) and (4.49) into the expression for the total absorbed energy in (4.45), and by using equation (4.32), the approximated absorbed energy $\boldsymbol{J}^N$ is

$$\boldsymbol{J}^N = -\int_0^T \hat{\boldsymbol{u}}^T \Phi^T(t)\,\Phi(t)\hat{\boldsymbol{x}}_2\,dt = -\hat{\boldsymbol{u}}^T \int_0^T \Phi^T(t)\,\Phi(t)\,dt\;\hat{\boldsymbol{x}}_2 = -\frac{T}{2}\hat{\boldsymbol{u}}^T\hat{\boldsymbol{x}}_2, \tag{4.51}$$

In fact, the matrix Γ in (4.33) is

$$\Gamma = \int_0^T \Phi^T(t)\,\Phi(t)\,dt = \frac{T}{2}\boldsymbol{I}_N \tag{4.52}$$

where $\boldsymbol{I}_N$ is the identity matrix of size N, because the basis is orthogonal, that is

$$\langle \phi_i, \phi_j \rangle = \int_0^T \phi_i(t)\phi_j(t)\,dt = \frac{T}{2}\delta_{ij},$$

where δ_{ij} is the Kronecker delta.

The next step of the discretisation process is the construction of the linear system resulting from the minimization of the residual r^N in (4.39) by applying the Galerkin method, as described in sec. 4.1.2.1. When using the Fourier series to approximated the states, the differentiation of the approximated states can be conveniently written as

$$\dot{x}_i^N = \dot{\Phi}(t)\hat{\boldsymbol{x}}_i = \Phi(t)\,\mathrm{D}_\phi\,\hat{\boldsymbol{x}}_i$$

where the differentiation matrix $\mathrm{D}_\phi \in \mathbb{R}^{N\times N}$ is block diagonal. Each block D_ϕ^k, for $k = 1, \dots, N/2$ is

$$\mathrm{D}_\phi^k = \begin{bmatrix} 0 & k\,\omega_0 \\ -k\,\omega_0 & 0 \end{bmatrix},$$

In fact, the derivative of a zero-mean Fourier series is still a Fourier series where the terms are reordered and scaled, because

$$\frac{d}{dt}\sin(k\omega_0 t) = k\omega_0\cos(k\omega_0 t) \qquad \text{and} \qquad \frac{d}{dt}\cos(k\omega_0 t) = -k\omega_0\sin(k\omega_0 t),$$

Consequently, the approximated state equations in (4.46) and (4.47) become

$$\Phi(t)\,\mathrm{D}_\phi\,\hat{\boldsymbol{x}}_1 = \Phi(t)\hat{\boldsymbol{x}}_2 \tag{4.53}$$

$$\mathrm{M_t}\,\Phi(t)\,\mathrm{D}_\phi\,\hat{\boldsymbol{x}}_2 = -B\Phi(t)\hat{\boldsymbol{x}}_2 - \int_{-\infty}^{t} \mathrm{K}(t-\tau)\Phi(t)\hat{\boldsymbol{x}}_2(\tau)\,d\tau - S\Phi(t)\hat{\boldsymbol{x}}_1 + \Phi(t)\hat{\boldsymbol{u}} + f_e. \quad (4.54)$$

The Galerkin method, as described in section 4.1.2.1, consists of writing the dynamic equations in residual form, and then minimising the residual by imposing its orthogonality to all the element of the basis. However, with regard to the first state equation (4.53), it is possible to note immediately that

$$\Phi(t)\,\mathrm{D}_\phi\,\hat{\boldsymbol{x}}_1 - \Phi(t)\,\hat{\boldsymbol{x}}_2 = 0 \quad \Leftrightarrow \quad \mathrm{D}_\phi\,\hat{\boldsymbol{x}}_1 - \hat{\boldsymbol{x}}_2 = 0 \quad (4.55)$$

because two Fourier series are equal if and only if all the corresponding coefficients are equal.

The residual form of the second dynamic equation (4.54) is

$$r_2^N = \mathrm{M_t}\,\Phi(t)\,\mathrm{D}_\phi\,\hat{\boldsymbol{x}}_2 + \mathrm{B}\Phi(t)\hat{\boldsymbol{x}}_2 + \int_{-\infty}^{t} \mathrm{K}(t-\tau)\Phi(t)\hat{\boldsymbol{x}}_2\,d\tau + \mathrm{S}\Phi(t)\hat{\boldsymbol{x}}_1 - \Phi(t)\hat{\boldsymbol{u}} - f_e \quad (4.56)$$

and is minimised by solving

$$\langle r_2^N, \phi_i \rangle = 0 \qquad\qquad i = 1, \ldots, N,$$

which can be written, since the inner product is commutative, in a more concise form as

$$\langle \Phi^T, r_2^N \rangle = \mathbf{0}, \quad (4.57)$$

where $\mathbf{0} \in \mathbb{R}^N$ is the zero vector, which has all its elements equal to zero. Because of linearity, the inner product between ϕ_i and each term on the right hand side of (4.56) can be considered separately; thus for the first term, the results is:

$$\langle \Phi^T, \mathrm{M_t}\,\Phi\,\mathrm{D}_\phi\,\hat{\boldsymbol{x}}_2 \rangle = \mathrm{M_t} \int_0^T \Phi^T(t)\,\Phi(t)\,dt\,\mathrm{D}_\phi\,\hat{\boldsymbol{x}}_2 = \mathrm{M_t}\,\Gamma\,\mathrm{D}_\phi\,\hat{\boldsymbol{x}}_2 = \frac{T}{2}\mathrm{M_t}\,\mathrm{D}_\phi\,\hat{\boldsymbol{x}}_2,$$

where the matrix Γ is defined in (4.52). Similarly, the remaining terms of the residual in (4.56) become:

$$\begin{aligned}
\langle \Phi^T, \mathrm{B}\,\Phi\,\hat{\boldsymbol{x}}_2 \rangle &= \frac{T}{2}\mathrm{B}I_N\hat{\boldsymbol{x}}_2 \\
\langle \Phi^T, \mathrm{S}\Phi\hat{\boldsymbol{x}}_1 \rangle &= \frac{T}{2}\mathrm{S}I_N\hat{\boldsymbol{x}}_1 \\
\langle \Phi^T, \Phi\hat{\boldsymbol{u}} \rangle &= \frac{T}{2}I_N\hat{\boldsymbol{u}} \\
\langle \Phi^T, f_e \rangle &= \frac{T}{2}I_N\hat{\boldsymbol{e}}
\end{aligned}$$

where $\hat{\boldsymbol{e}}$ is the vector of Fourier coefficients of the excitation force. The product corresponding

to the convolution term requires some manipulations in order to be expressed in matrix form. Because of the linearity of the convolution integral, and of the orthogonality of the basis, the derivations can be carried out one frequency at the time; thus it is convenient to consider Φ and $\hat{\boldsymbol{x}}$ as composed of two elements only, such as

$$\Phi^k = [\cos(k\omega_0 t),\ \sin(k\omega_0 t)] \qquad \hat{\boldsymbol{x}}_2^k = [x_{2k}^c,\ x_{2k}^s]^T.$$

In this case, by the commutativity property of the convolution, the result is

$$\int_{-\infty}^{t} \mathrm{K}(t-\tau)\Phi^k(t)\hat{\boldsymbol{x}}_2^k\, d\tau = \int_0^{+\infty} \mathrm{K}(\tau)\Phi^k(t-\tau)\hat{\boldsymbol{x}}_2^k\, d\tau. \tag{4.58}$$

By developing the product terms,

$$\begin{aligned}
\int_0^{+\infty} \mathrm{K}(\tau)\Phi^k(t-\tau)\hat{\boldsymbol{x}}_2^k\, d\tau &= \int_0^{+\infty} \mathrm{K}(\tau)\left(x_{2k}^c\cos(k\omega_0(t-\tau)) + x_{2k}^s\sin(k\omega_0(t-\tau))\right)\, d\tau \\
&= \quad x_{2k}^s\sin(k\omega_0 t)\int_0^{+\infty}\mathrm{K}(\tau)\cos(k\omega_0(\tau))\,d\tau \\
&\quad - x_{2k}^s\cos(k\omega_0 t)\int_0^{+\infty}\mathrm{K}(\tau)\sin(k\omega_0(\tau))\,d\tau \\
&\quad + x_{2k}^c\cos(k\omega_0 t)\int_0^{+\infty}\mathrm{K}(\tau)\cos(k\omega_0(\tau))\,d\tau \\
&\quad + x_{2k}^c\sin(k\omega_0 t)\int_0^{+\infty}\mathrm{K}(\tau)\sin(k\omega_0(\tau))\,d\tau
\end{aligned}$$

By applying Ogilvie's relations in (2.60) [31], which are

$$\begin{aligned}
-\omega(\mathrm{m}(\omega) - \mathrm{m}_\infty) &= \int_0^\infty \mathrm{K}(t)\,\sin(\omega t)\,dt, \\
\mathrm{R}(\omega) &= \int_0^\infty \mathrm{K}(t)\,\cos(\omega t)\,dt, \\
\mathrm{m}_\infty &= \lim_{\omega\to\infty}\mathrm{m}(\omega),
\end{aligned}$$

where $\mathrm{m}(\omega)$ and $\mathrm{R}(\omega)$ are the added mass and radiation resistance, respectively (see section 2.2.2), the convolution integral becomes

$$\begin{aligned}
\int_0^{+\infty} \mathrm{K}(\tau)\Phi^k(t-\tau)\hat{\boldsymbol{x}}_2^k\, d\tau = \quad & x_{2k}^s\sin(k\omega_0 t)\mathrm{R}(k\omega_0) - x_{2k}^s\cos(k\omega_0 t)\left(-k\omega_0(m(k\omega_0) - m_\infty)\right) \\
& + x_{2k}^c\cos(k\omega_0 t)\mathrm{R}(k\omega_0) + x_{2k}^c\sin(k\omega_0 t)\left(-k\omega_0(m(k\omega_0) - m_\infty)\right) \\
= \Phi^k & \begin{bmatrix} \mathrm{R}(k\omega_0) & k\omega_0 m(k\omega_0) \\ -k\omega_0 m(k\omega_0) & \mathrm{R}(k\omega_0) \end{bmatrix} \hat{\boldsymbol{x}}_2^k - m_\infty\Phi^k\mathrm{D}_\phi^k\hat{\boldsymbol{x}}_2^k.
\end{aligned} \tag{4.59}$$

Before combining all the terms, it is convenient to carry out an additional substitution: by

noting that the matrix D_ϕ is invertible, and its inverse is still block diagonal with blocks

$$\mathrm{D}_\phi^{k^{-1}} = \begin{bmatrix} 0 & \frac{1}{k\,\omega_0} \\ -\frac{1}{k\,\omega_0} & 0 \end{bmatrix},$$

and by using (4.55), the variable $\hat{\boldsymbol{x}}_1$ in the residual (4.56) can be substituted with

$$\hat{\boldsymbol{x}}_1 = \mathrm{D}_\phi^{-1}\hat{\boldsymbol{x}}_2. \tag{4.60}$$

Thus the inner product relating to the restoring force term becomes

$$\langle \mathrm{S}\Phi\mathrm{D}_\phi^{-1}\hat{\boldsymbol{x}}_2, \phi_i\rangle \quad \Rightarrow \quad \frac{T}{2}\mathrm{S}I_N\mathrm{D}_\phi^{-1}\hat{\boldsymbol{x}}_2.$$

By combining all the terms of the inner product in (4.57), the discretised equation of motion becomes the linear system

$$\mathbf{G}\,\hat{\boldsymbol{x}}_2 = \hat{\boldsymbol{u}} + \hat{\boldsymbol{e}}, \tag{4.61}$$

where the matrix $\mathbf{G}$ is block diagonal, with 2×2 blocks as

$$\mathbf{G} = \begin{bmatrix} \mathrm{D}_1 & \mathrm{M}_1 & 0 & \cdots & 0 & 0 \\ -\mathrm{M}_1 & \mathrm{D}_1 & 0 & \cdots & 0 & 0 \\ 0 & 0 & \ddots & & \vdots & \vdots \\ \vdots & \vdots & & \ddots & 0 & 0 \\ 0 & 0 & \cdots & 0 & \mathrm{D}_{N/2} & \mathrm{M}_{N/2} \\ 0 & 0 & \cdots & 0 & -\mathrm{M}_{N/2} & \mathrm{D}_{N/2} \end{bmatrix}, \tag{4.62}$$

and where

$$\begin{aligned} \mathrm{D}_k &= \mathrm{R}(k\omega_0) + \mathrm{B}, \\ \mathrm{M}_k &= n\omega_0\left(m + m(k\omega_0)\right) - \mathrm{S}/(k\omega_0), \end{aligned}$$

for $k = 1 \ldots N/2$. The matrix $\mathbf{G}$ is non-singular, since $\mathrm{B} > 0$, thus

$$\det \mathbf{G} = \prod_{n=1}^{N/2} \mathrm{D}_n^2 + \mathrm{M}_n^2 > 0.$$

The equation of motion (4.61) can then be solved with respect to $\hat{\boldsymbol{x}}_2$ as

$$\hat{\boldsymbol{x}}_2 = \mathbf{G}^{-1}\hat{\boldsymbol{u}} + \mathbf{G}^{-1}\hat{\boldsymbol{e}}, \tag{4.63}$$

and, by substituting $\hat{\boldsymbol{x}}_2$ into the approximated absorbed energy J^N in (4.51), get

$$J^N = -\frac{T}{2}\hat{\boldsymbol{u}}^T\mathbf{G}^{-1}\hat{\boldsymbol{u}} - \frac{T}{2}\hat{\boldsymbol{u}}^T\mathbf{G}^{-1}\hat{\boldsymbol{e}}, \tag{4.64}$$

which is a quadratic function of the variable $\hat{\boldsymbol{u}}$ solely. In essence, the state variables have been eliminated by substitution, and the optimisation is carried out over the control variable $\hat{\boldsymbol{u}}$ only. More importantly, the constrained optimisation problem given by the cost function describing the total absorbed energy J^N in (4.51) and the linear equality constraints describing the system dynamics in (4.61), has been transformed into an unconstrained quadratic program.

Additionally, since radiation is a dissipative process [39], the radiation resistance is positive, that is $\mathrm{R}(\omega) > 0$, and all the diagonal elements of the matrix $\mathbf{G}$ are positive; thus, the symmetric part of $\mathbf{G}$, $(\mathbf{G} + \mathbf{G}^T)/2$, is positive definite and the absorbed energy function (4.64) is concave. Therefore, the optimal solution $\hat{\boldsymbol{u}}^*$ for the unconstrained problem is then:

$$\hat{\boldsymbol{u}}^* = \left(\mathbf{G}^{-1} + \mathbf{G}^{-T}\right)^{-1}\mathbf{G}^{-1}\hat{\boldsymbol{e}}.$$

4.2.2.1 Initial conditions on position and velocity

Initial conditions on position and velocity may be required, for example, when optimal control is implemented in a receding horizon fashion as in [225], to enforce continuity of the motion. The initial condition on the velocity is expressed as $v(t_0) = v_0$, and it is enforced on the approximated state $\hat{\boldsymbol{x}}_2$ with

$$v_0 = \Phi_0\,\hat{\boldsymbol{x}}_2,$$

where $\Phi_0 = \Phi(t_0)$. By using (4.63), the initial condition can be expressed in terms of the control vector $\hat{\boldsymbol{u}}$ as

$$\Phi_0\,\mathbf{G}^{-1}\hat{\boldsymbol{u}} = v_0 - \Phi_0\mathbf{G}^{-1}\hat{\boldsymbol{e}} \tag{4.65}$$

which is a linear equality constraint. Similarly, the initial condition on the position is $z(t_0) = z_0$, which is enforced on the variable $\hat{\boldsymbol{x}}_1$ as

$$z_0 = \Phi_0\,\hat{\boldsymbol{x}}_1,$$

and, by using (4.60) and (4.63), it can be expressed in terms of the control vector as

$$\Phi_0\mathrm{D}_\phi^{-1}\mathbf{G}^{-1}\hat{\boldsymbol{u}} = z_0 - \Phi_0\mathrm{D}_\phi^{-1}\mathbf{G}^{-1}\hat{\boldsymbol{e}}, \tag{4.66}$$

which is a further linear equality constraint, similar to the initial condition on the velocity. When including initial conditions, the optimisation problem is the convex quadratic program composed of the cost function (4.64) and the linear equality constraints of (4.65) and (4.66).

4.2.2.2 Force and oscillation amplitude constraints

Constraints on the PTO force and on the oscillation amplitude are often introduced to prevent the device from working beyond the physical limitations of its components. In this section, we consider inequality constraints describing the maximum allowed force and maximum allowed oscillation amplitude, described as

$$|f_{pto}(t)| \leq \mathrm{F}_{max}, \tag{4.67}$$

$$|z(t)| \leq \mathrm{Z}_{max}, \tag{4.68}$$

which correspond, for the approximated problem, to

$$|\Phi(t)\hat{\boldsymbol{u}}| \leq \mathrm{F}_{max}, \tag{4.69}$$

$$|\Phi(t)\hat{\boldsymbol{x}}_1| \leq \mathrm{Z}_{max}. \tag{4.70}$$

It is a difficult problem to find the extrema of a Fourier series, thus one possible approach to deal with the constraints in (4.69) and (4.70) is to consider their 2-norm approximation, as described in [225] and in chapter 6. An alternative approach is to enforce the constraint only at a set of specified time instants $\{t_k\}_{k=0}^{N_c}$, that is

$$\Phi(t_k)\hat{\boldsymbol{u}} \leq \mathrm{F}_{max}, \qquad -\Phi(t_k)\hat{\boldsymbol{u}} \leq \mathrm{F}_{max}, \tag{4.71}$$

$$\Phi(t_k)\hat{\boldsymbol{x}}_1 \leq \mathrm{Z}_{max}, \qquad -\Phi(t_k)\hat{\boldsymbol{x}}_1 \leq \mathrm{Z}_{max}. \tag{4.72}$$

for $k = 0, \ldots, N_c$.

By defining the vector $\boldsymbol{\Theta}$ as

$$\boldsymbol{\Theta} = \begin{bmatrix} \Phi_0 \\ \Phi_1 \\ \vdots \\ \Phi_{N_c} \end{bmatrix}$$

the constraints in (4.71) and (4.72) can be approximated by the linear inequalities

$$\begin{bmatrix} \boldsymbol{\Theta} \\ -\boldsymbol{\Theta} \end{bmatrix} \hat{\boldsymbol{u}} \leq \mathbf{1}_{2(N_c+1)\times 1}\, \mathrm{F}_{max}, \tag{4.73}$$

$$\begin{bmatrix} \boldsymbol{\Theta} \\ -\boldsymbol{\Theta} \end{bmatrix} \hat{\boldsymbol{x}}_1 \leq \mathbf{1}_{2(N_c+1)\times 1}\, \mathrm{Z}_{max}, \tag{4.74}$$

where $\mathbf{1}_{2(N_c+1)\times 1}$ is the vector of all ones of size $2(N_c + 1)$. The inequality constraint relative

to the position in (4.72) can be expressed as a function of $\hat{\boldsymbol{u}}$ by using (4.60) and (4.63), as

$$\begin{bmatrix} \boldsymbol{\Theta} \\ -\boldsymbol{\Theta} \end{bmatrix} \mathrm{D}_{\phi}^{-1}\mathbf{G}^{-1}\hat{\boldsymbol{u}} \leq \mathbf{1}_{2(N_k\times 1)}\mathrm{Z}_{max} - \begin{bmatrix} \boldsymbol{\Theta} \\ -\boldsymbol{\Theta} \end{bmatrix} \mathrm{D}_{\phi}^{-1}\mathbf{G}^{-1}\hat{\boldsymbol{e}}. \tag{4.75}$$

In summary, the resulting constrained optimal control problem is the convex quadratic program defined by the cost function $\boldsymbol{J}^N$ in (4.64), subject to the linear equality constraints due to the initial conditions in (4.65) and (4.66), and the linear inequality constraints on the PTO force in (4.73) and on the oscillation amplitude in (4.75).

4.2.2.3 Simulation results

This section presents simulation results for the heaving-body point absorber WEC depicted in fig. 4.1, which is a vertical cylinder of radius $r = 4m$ and draught $d = 10m$. Simulations have been carried out for both regular and irregular incident waves, and considering both PTO force and oscillation amplitude constraints. Figures 4.2–4.4 depict simulation results for a monochromatic incident wave with period $T_r = 10s$ and amplitude $A = 5m$. The expansions for the approximation of the state in (4.48) and the control in (4.49) are composed of 40 frequency components, corresponding to $N = 80$. The oscillation amplitude constraint has been set to $\mathrm{Z}_{max} = 2.5m$, while several values of the PTO force constraints have been considered, that is $\mathrm{F}_{max} = \{1, 1.25, 1.5, 2\} \cdot 10^6 N$.

Each plot in figs. 4.2–4.4 depicts two sets curves: the curves associated with the variables with subscript "c" (i.e. x_{1_c}, x_{2_c}, u_c) denote the simulation results when the PTO force is constrained with the most stringent value ($\mathrm{F}_{max} = 1\,10^6 N$), whereas the curves associated with the variables with subscript "u" (i.e. x_{1_u}, x_{2_u}, u_u) denote the simulation results when the PTO force in unconstrained. The "dot" marks superimposed on the plots of the positions (x_{1_c}, x_{1_u}) in fig. 4.2 and the PTO forces in fig. 4.4 denote the time points t_k at which the constraints are being enforced, as in eq. (4.73) and (4.75) for the PTO force and device position, respectively.

It is interesting to note that both the optimal motion of the device and the optimal time profile of the PTO force are smoother when the PTO force is strongly constrained, thus the device is subject to smaller mechanical stress. Figure 4.5 shows the frequency components of the optimal PTO force for the situation where the PTO force is unconstrained ($*$ mark) and when the most stringent constraint is active ($\circ$ mark), confirming the previous observation. In fact, the unconstrained PTO force is characterised by large values of higher frequency components up to the 7-th harmonic, while the harmonic content of the constrained PTO force is considerably smaller.

Figure 4.5 also shows that the optimal profiles of both the constrained and unconstrained PTO forces only contain odd harmonics, when the position constraints are active. For the real-

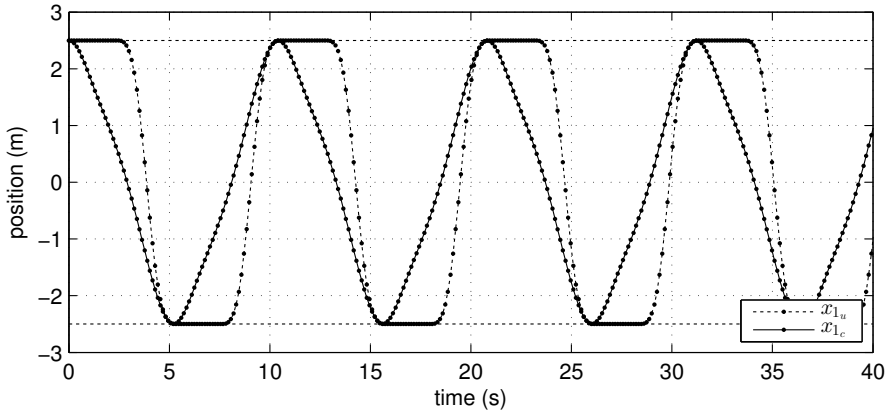

Figure 4.2: Vertical position for an incident regular wave of period $T_w = 10s$ and amplitude $A = 5m$: x_{1_u} is the vertical position when the PTO force is not constrained; x_{1_c} is the vertical position when the PTO force is constrained.

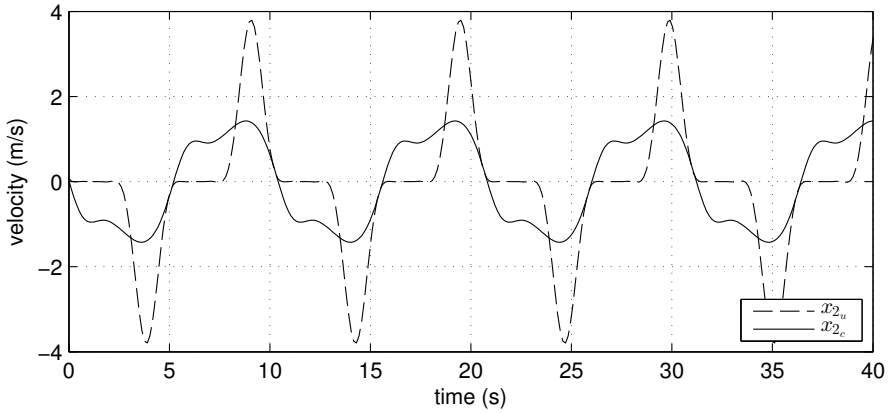

Figure 4.3: Vertical velocity for an incident regular wave of period $T_w = 10s$ and amplitude $A = 5m$: x_{2_u} is the vertical velocity when the PTO force is not constrained; x_{2_c} is the vertical velocity when the PTO force is constrained.

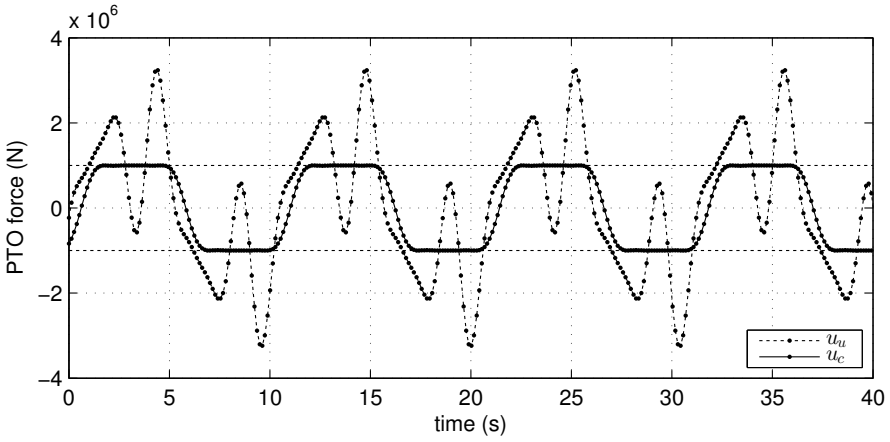

Figure 4.4: Unconstrained PTO force u_u and constrained PTO force u_c for an incident regular wave of period $T_w = 10s$ and amplitude $A = 5m$.

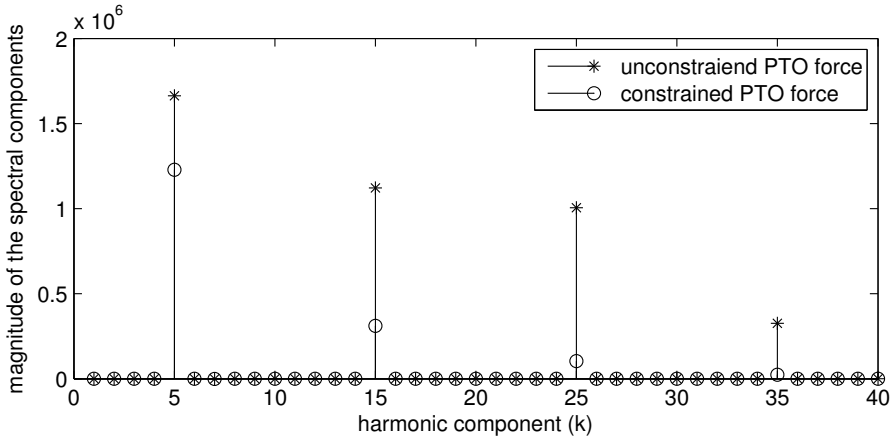

Figure 4.5: Spectral components of the PTO force

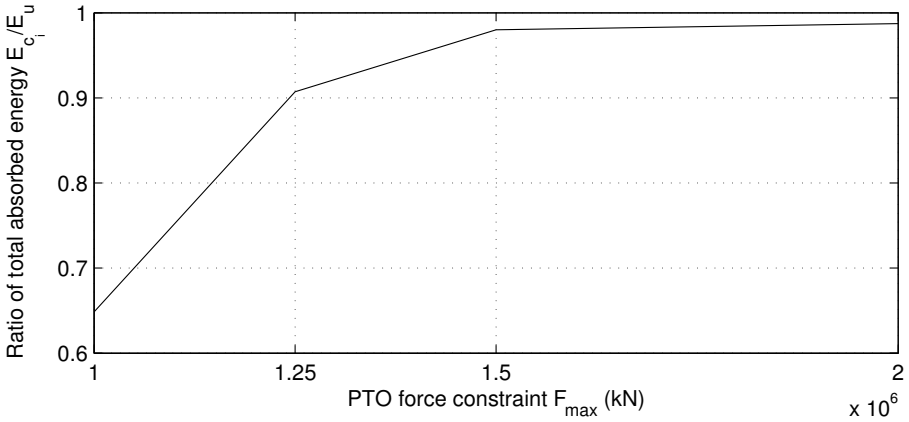

Figure 4.6: Total absorbed energy as function of the force constraint

time implementation, it could be beneficial to reduce the dimension of the NLP problem by eliminating all the frequencies for which the energy is zero or negligible. Due to the orthogonality of the Fourier series, this could be achieved by looking at the vector of Fourier coefficients of the excitation force ($\hat{\boldsymbol{e}}$), and by solving the optimisation problem considering only the frequencies which contain "most" of the energy and their harmonics. The reduced problem will consist of the quadratic program with the cost function

$$J^N = -\frac{T}{2}\tilde{\boldsymbol{u}}^T\widetilde{\mathbf{G}}^{-1}\tilde{\boldsymbol{u}} - \frac{T}{2}\tilde{\boldsymbol{u}}^T\widetilde{\mathbf{G}}^{-1}\tilde{\boldsymbol{e}},$$

in place of (4.64), where $\tilde{\boldsymbol{u}}$ and $\tilde{\boldsymbol{e}}$ are the "reduced" vectors of Fourier coefficients of the control signal and excitation force, respectively, which are built by extracting the elements of $\hat{\boldsymbol{u}}$ and $\hat{\boldsymbol{e}}$ for which the energy is non zero, and their harmonics.

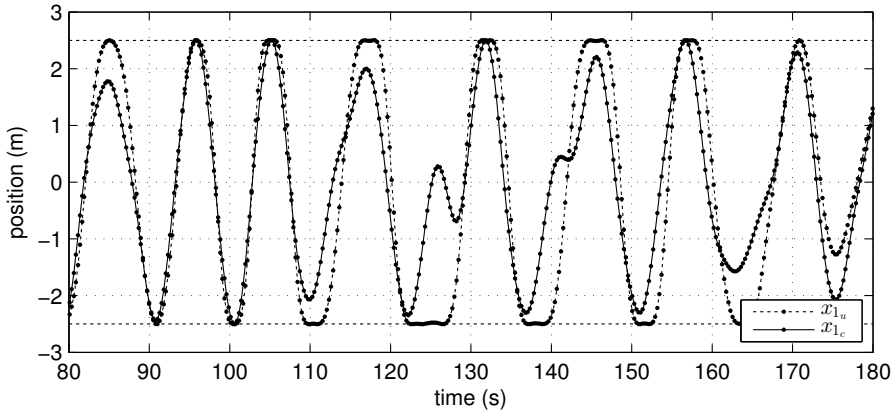

Figure 4.7: Vertical position for a Bretschneider sea state of $T_p = 10s$ and $H_s = 1m$: x_{1_u} is the vertical position when the PTO force is not constrained; x_{1_c} is the vertical position when the PTO force is constrained.

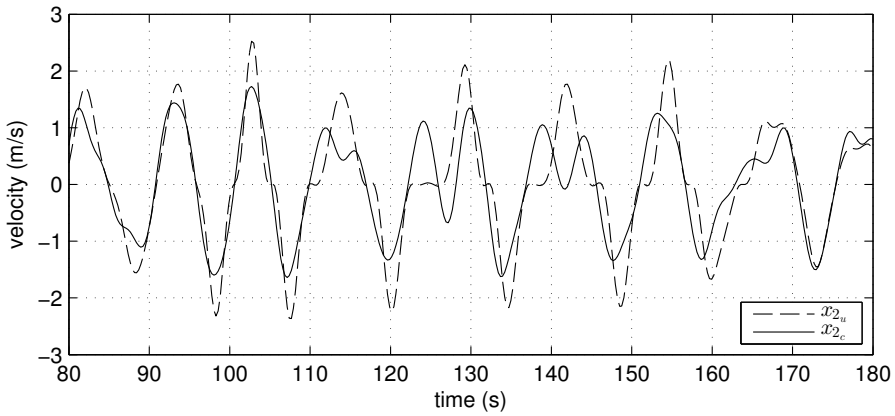

Figure 4.8: Vertical velocity for a Bretschneider sea state of $T_p = 10s$ and $H_s = 1m$: x_{2_u} is the vertical velocity when the PTO force is not constrained; x_{2_c} is the vertical velocity when the PTO force is constrained.

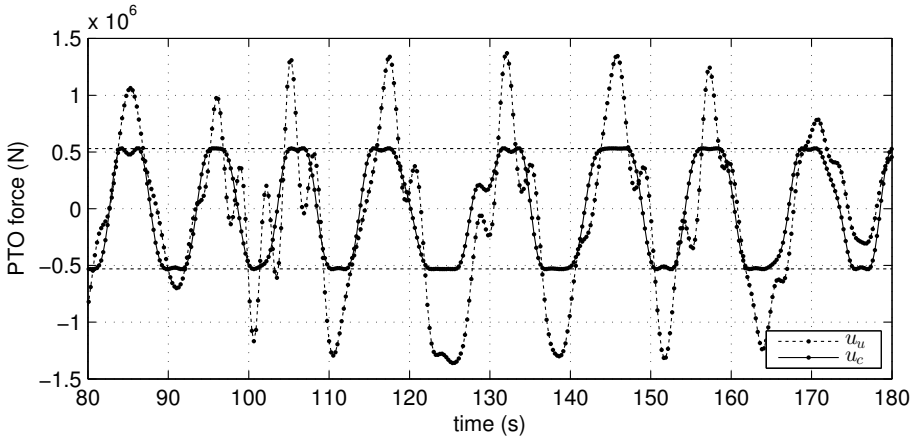

Figure 4.9: Unconstrained PTO force u_u and constrained PTO force u_c for a Bretschneider sea state of $T_p = 10s$ and $H_s = 1m$.

The matrix $\widetilde{\mathbf{G}}$ is derived from the matrix $\mathbf{G}$ in a similar manner by extracting the rows and columns corresponding to the frequencies which contain most of the energy, and their harmonics.

Figure 4.6 depicts the ratio of the total absorbed energy for several values of the PTO force constraints and the energy absorbed in the unconstrained case, that is E_c/E_u, where E_c is the absorbed energy in the constrained case and E_u is the absorbed energy in the unconstrained case. With a force constraint of $1.25\,10^6\,N$, which is 30% of the maximum value of the PTO force in the unconstrained case (see fig. 4.4), it is still possible to absorb around 90% of the energy that is absorbed when the PTO force is not constrained. This analysis plays an important role in the techno-economical optimisation of WECs, because absorbed energy is related to the revenue generated by the device and the power rating is related to the cost of the device. Chapter 6 describes a procedure for the analysis of force and position constraints based on the discretisation method presented in this chapter, in addition to a more detailed discussion about the sensitivity of the absorbed energy with respect to the constraints.

Simulation results for a Bretschneider spectrum of peak period $T_p = 10s$ and significant wave height $H_s = 1m$ are depicted in figs. 4.7–4.9. In this case, the approximations of the state and control in (4.48) and (4.49) are composed of 80 frequencies ($N = 160$), the oscillation amplitude has been restricted to $\mathrm{Z}_{max} = 1m$ and the PTO force to $\mathrm{Z}_{max} = 5.3\,10^6 N$.

With regard to the effect of constraints on the motion of the device (figs. 4.2 and 4.3) and PTO force, the observations described for the regular incident wave still apply; in particular, a more stringent PTO force constraint results in a smoother motion and PTO force profile. Additionally, setting the PTO force constraint to 50% of the maximum unconstrained PTO force reduces the total absorbed energy by only 10%, approximately.

4.2.3 A note on the residual term of the radiation convolution integral

In section 4.2.2, it is shown that the convolution integral describing the radiation force can be solved analytically when the state (velocity) is approximated by using a truncated Fourier series, thus the numerical integration of the convolution integral can be avoided when solving the equation of motion. It should be noted that whenever the velocity is approximated by a linear combination of basis functions, the numerical integration of the convolution integral can be done offline, for a given hydrodynamic problem and a given choice of basis functions. In fact, considering the expansion for the velocity in eq. (4.30), that is

$$v_i(t) \approx v_i^N(t) = \sum_{k=1}^{N} x_{ik}^v \, \phi_k(t) \qquad i = 1, \dots, n$$

the term of the residual of the dynamic equation involving the convolution integral in (4.37) is

$$\sum_{j=1}^{n} \int_0^t \mathrm{K}_{ij}(t-\tau) v_j^N(\tau)\, d\tau = \sum_{j=1}^{n} \sum_{k=1}^{N} x_{ik}^v \int_0^t \mathrm{K}_{ij}(t-\tau)\, \phi_k(\tau)\, d\tau.$$

The minimisation of the residual by means of the mean weighted residual method results in the inner products $\langle r_i^v, \psi_j \rangle$ in (4.39); because of linearity, that is $\langle f+g, h\rangle = \langle f, h\rangle + \langle g, h\rangle$, each of the inner products corresponding to the convolution integral can be considered separately, and they are

$$\langle \int_0^t \mathrm{K}_{ij}(t-\tau)\, \phi_k(\tau)\, d\tau, \psi_l(t)\rangle = \int_0^T \int_0^t \mathrm{K}_{ij}(t-\tau)\, \phi_k(\tau)\, d\tau\, \psi_l(t)\, dt = \kappa_{ijkl}.$$

The elements κ_{ijkl} are not functions of time; they only depends on the basis functions ϕ_k, the test functions ψ_k and the radiation impulse responses K_{ij}. Consequently, the terms of the inner products $\langle r_i^v, \psi_j \rangle$ in (4.39) can be written as

$$\langle \sum_{j=1}^{n} \int_0^t \mathrm{K}_{ij}(t-\tau) v_j^N(\tau)\, d\tau, \psi_l(t)\rangle = \sum_{j=1}^{n} \sum_{k=1}^{N} x_{ik}^v \kappa_{ijkl}.$$

The coefficients κ_{ijkl} can be calculated either analytically, if possible, or by numerical integration once the basis functions, test functions and the hydrodynamics have been chosen. In other words, by applying the mean weighted residual method for the approximation of the equation of motion, all the computation involving the integration of the convolution integral can be carried out offline, reducing the computational load when solving the NLP problem of the approximated optimal control problem.

4.3 Nonlinear optimal control of wave energy converters

In this section, the transcription of the optimal control problem of a WEC is carried out using the pseudospectral method. The WEC considered is a flap-type, seabed referenced pitching device, and it is modelled with the linear equation used in the previous section (eq. (4.23)), with the addition of a nonlinear term describing viscous effects. Section 4.3.1 provides a detailed description of the WEC model, while sec. 4.3.2 illustrates the general concept of pseudospectral optimal control, in greater detail than presented in sec. 4.1.2.1. The derivation of the NLP problem resulting from the application of the pseudospectral method to the control of a WEC is provided in sec. 4.3.3, with simulation results presented in sec. 4.3.4.

4.3.1 WEC dynamical model

The device considered in this section is depicted in fig. 4.10. It is a flap-type WEC hinged on the y axis at a depth h=15m, with a width W=30m, thickness D=1m and a uniform material density ρ_b= 250kg/m^3. The equation of motion is derived from Euler's second law, which says that the rate of change of the angular momentum is equal to the sum of the external moments of force about the axis y:

$$I_y \ddot{\theta} = \gamma_w(t) + \gamma_p(t).$$

I_y is the moment of inertia of the body with respect to the the axis y, γ_p is the torque applied by the PTO, and γ_w is the resultant of the moments due to the interaction between water and

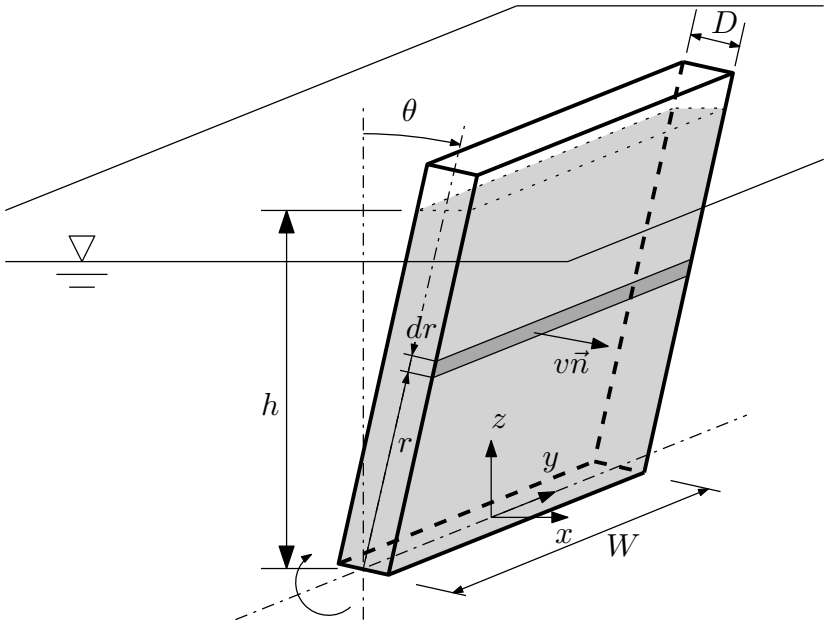

Figure 4.10: Flap-type wave energy converter. The shaded area indicates the submerged region.

the oscillating body, which is composed of four terms, as described by [15]:

$$\gamma_w(t) = \gamma_h(t) + \gamma_d(t) + \gamma_r(t) + \gamma_e(t).$$

The hydrostatic restoring moment γ_h is assumed to be linearly proportional to the pitch angle ($\gamma_h = S_h\theta$), where S_h is the hydrostatic restoring coefficient. The excitation moment γ_e, due to the effect of the incident waves, is calculated as (see sec.2.2.2) $\gamma_e(t) = \mathrm{H} * \zeta$, where ζ is the wave elevation and $*$ denotes the convolution operator

$$f * g = \int_{-\infty}^{-\infty} f(t-\tau)g(\tau)d\tau.$$

The radiation moment γ_r is due to the motion of the body which causes waves to be radiated away, and it depends on the velocity and acceleration of the oscillating body described in section 2.2.2.3, that is

$$\gamma_r = -I_\infty \ddot{\theta} - \mathrm{K} * \dot{\theta}$$

The functions H and K are, respectively, the impulse responses of the excitation and radiation, while I_∞ is the asymptotic value of the added inertia at infinite frequency. The values of H, K and I_∞ have been calculated by means of the boundary element software WAMIT [226].

The nonlinear part of the dynamic model is due to the moment of the drag force (f_d), which is generally modelled as proportional to the square of the fluid velocity normal to the surface of the body [227]:

$$f_d = -(1/2)\rho C_d A v|v|,$$

where ρ is the density of the water, C_d is the drag coefficient, A is the area normal to the direction of the relative fluid flow and v is the velocity normal to the surface (fig. 4.10). When the body is in the vertical position ($\theta = 0$), for small oscillations, the normal velocity on the vertical surface is related to the angular velocity as $v \approx r\dot{\theta}$, where r is the vertical distance between the hinge and the point of the surface where the velocity is considered. The contribution to the drag force of the infinitesimal surface at a distance r from the hinge, of width W and height dr (fig. 4.10) is $df_d \approx -(1/2)\rho C_d W r^2 \dot{\theta}|\dot{\theta}|dr$. The infinitesimal moment of the drag force applied with respect to the axis y is $d\gamma_v = r\,df_d$; by integrating $d\gamma_v$ from 0 to h, the total moment of the drag force applied to the hinge is:

$$\gamma_v = -\frac{1}{2}\int_0^h \rho C_d W r^3 \dot{\theta}|\dot{\theta}|dr = -B_v\dot{\theta}|\dot{\theta}|$$

where $B_v = (1/8)\rho C_d W h^4$. According to [228], the drag coefficient of a plate orthogonal to

the direction of the flow is $C_d = 1.9$. The resulting equation of motion is

$$I_t \ddot{\theta} = -B_{v_1}\dot{\theta} - B_{v_2}\dot{\theta}|\dot{\theta}| - k * \dot{\theta} - S_h\theta + \gamma_p + \gamma_e. \tag{4.76}$$

where $I_t = \left(I_y + I_\infty\right)$, and B_{v_1} is the coefficient of a linear dissipative term, which models additional losses occurring at small velocities, when the effect of the quadratic term is negligible [227].

4.3.2 Pseudospectral optimal control

This section provides a general overview of the pseudospectral optimal control. To do so, let us consider, for example, the optimal control problem presented in sec. 4.1: determine the control $\boldsymbol{u}(t) \in \mathbb{R}^m$, that minimises, or maximises, the cost functional in the Lagrange form [210]:

$$J = \int_0^T g(\boldsymbol{x}, \boldsymbol{u}, t)\, dt, \qquad g : \mathbb{R}^n \times \mathbb{R}^m \times \mathbb{R} \to \mathbb{R} \tag{4.77}$$

subject to the dynamic constraint

$$\dot{\boldsymbol{x}} = \boldsymbol{f}(\boldsymbol{x}, \boldsymbol{u}, t) \quad t \in [0, T], \tag{4.78}$$

where $\boldsymbol{x}(t) \in \mathbb{R}^n$ and $\boldsymbol{f} : \mathbb{R}^n \times \mathbb{R}^m \times \mathbb{R} \to \mathbb{R}^n$.

Analogous to the Galerkin method (sec. 4.2.2), the first step is to approximate the state and control variables by considering, for the i-th components, the following expansion:

$$x_i(t) \approx x_i^N(t) := \sum_{k=1}^{N} \hat{x}_{ik}\phi_k(t) = \Phi(t)\hat{\boldsymbol{x}}_i \tag{4.79}$$

$$u_i(t) \approx u_i^N(t) := \sum_{k=1}^{N} \hat{u}_{ik}\phi_k(t) = \Phi(t)\hat{\boldsymbol{u}}_i \tag{4.80}$$

where

$$\hat{\boldsymbol{x}}_i = \left[\hat{x}_{i1}, \hat{x}_{i2}, \ldots, \hat{x}_{iN}\right]^T,$$
$$\hat{\boldsymbol{u}}_i = \left[\hat{u}_{i1}, \hat{u}_{i2}, \ldots, \hat{u}_{iN}\right]^T,$$

and

$$\Phi(t) = \left[\phi_1(t), \phi_2(t), \ldots, \phi_N(t)\right]$$

form a basis for an N-dimensional vector space, on which the state and control variables are

approximated. It is also convenient to define the vectors $\boldsymbol{X} \in \mathbb{R}^{Nn}$ and $\boldsymbol{U} \in \mathbb{R}^{Nm}$:

$$\boldsymbol{X} = \begin{bmatrix} \hat{\boldsymbol{x}}_1 \\ \vdots \\ \hat{\boldsymbol{x}}_n \end{bmatrix} \qquad \boldsymbol{U} = \begin{bmatrix} \hat{\boldsymbol{u}}_1 \\ \vdots \\ \hat{\boldsymbol{u}}_n \end{bmatrix}.$$

As the result of the approximations, the cost functional (4.77) depends only on the $N(n+m)$ coefficients in $\boldsymbol{X}$ and $\boldsymbol{U}$, thus the optimisation problem is finite dimensional.

To illustrate the effect of the approximation on the dynamic equation, the derivative of the approximated state variable is considered first, that is:

$$\dot{x}_i^N = \sum_{k=1}^{N} \hat{x}_{ik} \dot{\phi}_k(t) = \dot{\Phi}(t) \hat{\boldsymbol{x}}_i. \tag{4.81}$$

By substituting (4.79), (4.80) and (4.81) into (4.78), the approximated dynamic equation in the residual form is then

$$r_i(t) = \dot{x}_i^N(t) - f_i(\boldsymbol{x}^N(t), \boldsymbol{u}^N(t), t), \quad i = 1, \ldots, n \tag{4.82}$$

where $\boldsymbol{x}^N$ and $\boldsymbol{u}^N$ are, respectively, the vectors of the approximated state variables and control variables, the elements of which are x_i^N defined in (4.79) and u_i^N defined in (4.80). The coefficients $\hat{\boldsymbol{x}}_i$ and $\hat{\boldsymbol{u}}_j$ for which the n residuals (4.82) are minimised are calculated by using the pseudospectral method [229], also known as *collocation* method. The method consists of collocating the system dynamics at a number of discrete time points t_k, called *nodes*, meaning that the coefficients $\hat{\boldsymbol{x}}_i$ and $\hat{\boldsymbol{u}}_j$ are such that the dynamic equation is satisfied at a number of points t_k, or equivalently, the residuals r_i are zero at the N_c nodes:

$$r_i(t_j) = \dot{\Phi}(t_j) \hat{\boldsymbol{x}}_i - f_i\left(\boldsymbol{X}, \boldsymbol{U}, t_j\right) = 0 \tag{4.83}$$

which is a system of $n \times N_c$ equations because $j = 1, \ldots, N_c$ and $i = 1, \ldots, n$.

The functional $\boldsymbol{J}$ in (4.77) is also approximated by an appropriate quadrature formula with weights w_j, as

$$\boldsymbol{J}^N = \int_0^T g(\boldsymbol{X}, \boldsymbol{U}, t)\, dt \approx \sum_{j=0}^{N_c} g(\boldsymbol{X}, \boldsymbol{U}, t_j) w_j, \tag{4.84}$$

and the optimal control problem defined by the cost functional (4.77) and the dynamic constraint (4.78) is transformed into the finite dimensional optimisation problem: find $\boldsymbol{U}$ and $\boldsymbol{X}$ to maximise (or minimise) (4.84) subject to the constraints (4.83).

The collocation of the dynamic equation and of the cost functional, that is the choice of the nodes t_j, depend on a number of factors, including the expansions (4.79) and (4.80) [230, 231]

4.3.3 Optimal nonlinear WEC control

The optimal control problem that we are aiming to solve is the maximisation of the absorbed energy, which is equivalent to maximising the amount of work done by the PTO moment

$$J = \int_0^T \gamma_p(t)\,\dot{\theta}(t)\,dt, \tag{4.85}$$

subject to the constraint given by the dynamic model in (4.76). The first step is to choose the expansion for the state and control; as already described in sec.4.2.2, given the oscillatory nature of the problem, a zero-mean truncated Fourier series is again a sensible choice, thus:

$$x_i(t) \approx \sum_{k=1}^{N/2} x_{ik}^c \cos(k\omega_0 t) + x_{ik}^s \sin(k\omega_0 t) = \Phi(t)\hat{\boldsymbol{x}}_i \tag{4.86}$$

$$u(t) \approx \sum_{k=1}^{N/2} u_k^c \cos(k\omega_0 t) + u_k^s \sin(k\omega_0 t) = \Phi(t)\hat{\boldsymbol{u}} \tag{4.87}$$

where

$$\hat{\boldsymbol{x}}_i = \left[x_{i1}^c, x_{i1}^s, \dots, x_{i\frac{N}{2}}^c + x_{i\frac{N}{2}}^s\right]^T$$

$$\hat{\boldsymbol{u}} = \left[u_1^c, u_1^s, \dots, u_{\frac{N}{2}}^c + u_{\frac{N}{2}}^s\right]^T$$

$$\Phi(t) = \left[\cos(\omega_0 t), \sin(\omega_0 t), \dots, \cos\left(\frac{N}{2}\omega_0 t\right), \sin\left(\frac{N}{2}\omega_0 t\right)\right]$$

and the fundamental frequency is $\omega_0 = 2\pi/T$. A previous application of the Fourier pseudospectral method, not related to wave energy conversion, can be found in [232].

By substituting the state (4.86) and control (4.87) expansions into the cost function (4.85), the approximated absorbed energy is

$$J^N = \int_0^T \hat{\boldsymbol{u}}^T \Phi^T(t)\,\Phi(t)\hat{\boldsymbol{x}}_2\,dt = \frac{T}{2}\hat{\boldsymbol{u}}^T\hat{\boldsymbol{x}}_2, \tag{4.88}$$

because of the orthogonality of the basis Φ, that is $\langle \phi_i, \phi_j \rangle = \delta_{ij} T/2$, where δ_{ij} is the Kronecker delta.

The derivative of the state variables in (4.81), given the approximation of the state in (4.86), becomes

$$\dot{x}_i^N = \dot{\Phi}(t)\hat{\boldsymbol{x}}_i = \Phi(t)\,\mathrm{D}_\phi\,\hat{\boldsymbol{x}}_i \tag{4.89}$$

where the differentiation matrix $\mathrm{D}_\phi \in \mathbb{R}^{N\times N}$ is the same as the one for the Galerkin method in

sec. 4.2.2, that is a block diagonal matrix, with the k-th block is defined as

$$\mathrm{D}_{\phi}^{k} = \begin{bmatrix} 0 & k\,\omega_0 \\ -k\,\omega_0 & 0 \end{bmatrix}.$$

The state vector is composed of the angular position and velocity, that is, $\boldsymbol{x} = [x_1, x_2]^T = [\theta, \dot{\theta}]^T$, and the control input is the PTO moment ($u = \gamma_p$), thus $n = 2$ and $m = 1$. Consequently, the dynamic equation (4.76) can be transformed into the system of equations:

$$\dot{x}_1 = x_2 \tag{4.90}$$

$$I_t\,\dot{x}_2 = -B_{v_1} x_2 - B_{v_2} x_2 |x_2| - \mathrm{K} * x_2 - S_h x_1 + u - \gamma_e \tag{4.91}$$

By applying the approximations (4.86) and (4.89) to the first state equation (4.90), the result is

$$\Phi(t)\,\mathrm{D}_{\phi}\,\hat{\boldsymbol{x}}_1 - \Phi(t)\,\hat{\boldsymbol{x}}_2 = 0 \quad \Leftrightarrow \quad \mathrm{D}_{\phi}\,\hat{\boldsymbol{x}}_1 - \hat{\boldsymbol{x}}_2 = 0. \tag{4.92}$$

because the elements of Φ form a basis.

The residuals of the second state equation (4.91), collocated at the nodes t_j are

$$r_j = \mathrm{I}_t\,\Phi_j\,\mathrm{D}_{\phi}\,\hat{\boldsymbol{x}}_2 + B_{v_1}\Phi_j\,\hat{\boldsymbol{x}}_2 + B_{v_2}\Phi_j\,\hat{\boldsymbol{x}}_2|\Phi_j\,\hat{\boldsymbol{x}}_2| + S_h\Phi_j\,\hat{\boldsymbol{x}}_1 + (\mathrm{K} * \Phi)_{t_j}\,\hat{\boldsymbol{x}}_2 - \Phi_j\,\hat{\boldsymbol{u}} - \gamma_e(t_j). \tag{4.93}$$

where $\Phi_j = \Phi(t_j)$. The convolution term can be simplified by substituting the approximation (4.86) into the convolution integral; after some basic manipulations involving trigonometric identities and the definition of the sine and cosine transforms, which follow the same steps described in (4.58)–(4.59) , the result is

$$(k * \Phi)_{t_j}\,\hat{\boldsymbol{x}}_2 = \int_{-\infty}^{+\infty} \mathrm{K}(t_j - \tau)\,x_2^N(\tau)\,d\tau \tag{4.94}$$

$$= \Phi_j\left(\mathrm{G} - I_{\infty}\mathrm{D}_{\Phi}\right)\hat{\boldsymbol{x}}_2, \tag{4.95}$$

where the matrix $\mathrm{G} \in \mathbb{R}^{N\times N}$ is block diagonal, and the k-th block is

$$\mathrm{G}_k = \begin{bmatrix} B(k\,\omega_0) & k\,\omega_0 A(k\,\omega_0) \\ -k\,\omega_0 A(k\,\omega_0) & B(k\,\omega_0) \end{bmatrix}.$$

The frequency domain coefficients A and B are related to the impulse responses by means of the Cummins relations [36], and they are provided directly by [226].

Substituting (4.95) into (4.93), the residuals simplify to

$$r_j = I_y \Phi_j \, \mathrm{D}_\phi \, \hat{\boldsymbol{x}}_2 + B_{v_1} \Phi_j \, \hat{\boldsymbol{x}}_2 + B_{v_2} \Phi_k \, \hat{\boldsymbol{x}}_2 |\Phi_j \, \hat{\boldsymbol{x}}_2| + \Phi_j \, \mathrm{G} \, \hat{\boldsymbol{x}}_2 + S_h \Phi_j \, \hat{\boldsymbol{x}}_1 - \Phi_j \, \hat{\boldsymbol{u}} - \gamma_e(t_j) = 0. \quad (4.96)$$

The nodes t_j are uniformly spaced between 0 and $T - \Delta t$:

$$t_j = j \, \Delta t, \quad \text{with } \Delta t = T/(N+1) \quad \text{and } j = 0, \ldots, N.$$

The vectors $\boldsymbol{U}$ and $\boldsymbol{X}$ that give the optimal profile for the PTO moment and the motion of the flap, respectively, are the solutions of the nonlinear program which maximises the absorbed energy (4.88), subject to the $2N$ equality constraints due to the dynamic equations (4.92) and (4.96).

4.3.4 Sample results

Simulations have been carried out in Matlab and the algorithm used for solving the optimisation problem is the Sequential Quadratic Programming implemented by the *fmincon* function included in the Optimization Toolbox.

Figure 4.11 presents simulation results for an incident wave of amplitude $|\zeta|$=2m and period T=10s, where the state variables $(\theta, \dot{\theta})$ and the control input (γ_p) have been approximated using seven frequency components each (N=14). Figure 4.11a clearly shows that the controller aims to limit the angular velocity of the device, as the time profile of $\dot{\theta}$ resembles a "flattened" sinusoid and time profile of the angular position seems to approach a motion of constant speed in the time intervals $t \in [1.5, 3]$ and $t \in [6, 8]$. The PTO and the excitation moments are depicted in fig. 4.11b while the instantaneous absorbed power is shown in fig. 4.11c. Comparison of figs. 4.11a and 4.11b also shows that the controller tries to keep the velocity in phase with the excitation, as happens in the linear case [5].

Figure 4.12 shows the frequency contents of the state and control variables, in addition to the absorbed power. The amplitude of the frequency components decays quickly as the frequency increases, meaning that only a few components are necessary for a good approximation. This is confirmed by looking at table 4.1, where the average absorbed power (P_u), defined as

$$P_u = \frac{1}{T} J^N = \frac{1}{2} \hat{\boldsymbol{u}}^T \hat{\boldsymbol{x}},$$

is listed for different values of the expansion order N, and for different values of the wave period. The computation times of the optimisation problems, using a laptop computer with a Core i7 processor working at 2.8GHz are listed in brackets (seconds), and this confirms the suitability of this method for real time control. Based on the results given in table 4.1, the value of $N = 10$ has been used for the simulations presented in the rest of this section as

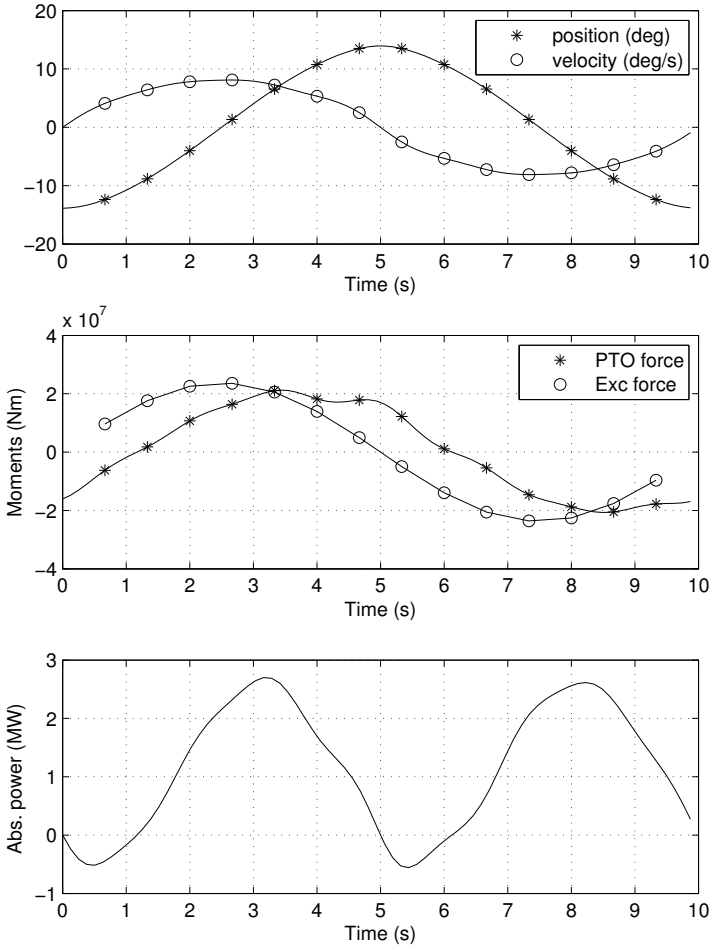

Figure 4.11: Motion, forces and absorbed power for $T = 10s$, $\zeta_a = 2m$ and for $N = 14$.

the best trade-off between speed and accuracy. Thus, position, velocity and PTO force are each approximated with a trigonometric polynomial with five frequency components, and the resulting approximate optimal control problem is a nonlinear program with 30 variables and 20 constraints.

In fig. 4.13, the average absorbed power is depicted as function of the wave period and wave amplitude. It is interesting to note that, where the model includes a quadratic viscous damping term, the absorbed power increases with $|\zeta|^{\frac{3}{2}}$ rather than $|\zeta|^2$, as for the linear case [5]. This fact is highlighted in fig. 4.14, where the solid curve is the absorbed power as a function of the wave amplitude $|\zeta|$, when only the linear dissipative term is present ($B_{v_2} = 0$); in this case, P_u is proportional to the square of the wave amplitude ($P_u \propto |\zeta|^2$). The dashed curve is the absorbed power when the nonlinear damping term is also included ($B_{v_1} \neq 0$, $B_{v_2} = 0$), and P_u

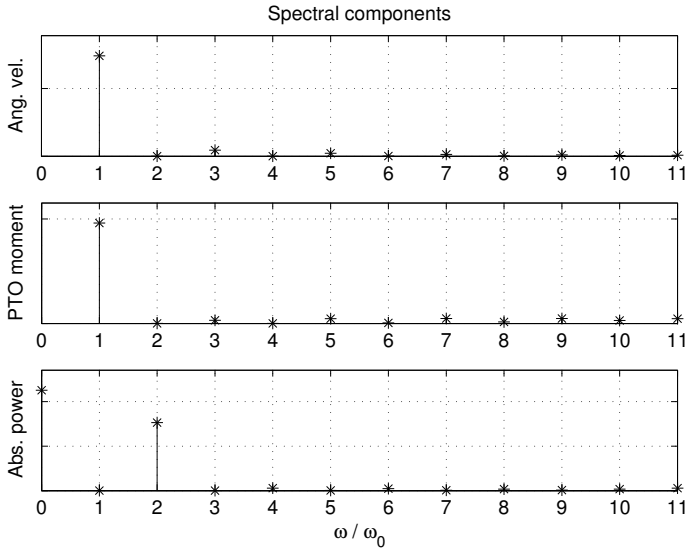

Figure 4.12: Spectral components of the velocity, the PTO moment and the absorbed power for $T = 10s$ and $\zeta_a = 2m$

increases with the wave amplitude as $P_u \propto |\zeta|^{\frac{3}{2}}$.

Of particular interest is fig. 4.15, which depicts the ratio of the average absorbed power over the sum of the power radiated and the power dissipated by the linear and quadratic terms, P_u/P_d, where

$$P_d = \frac{1}{T}\int_0^T \left(B_{v_1}\dot{\theta} + B_{v_2}\dot{\theta}|\dot{\theta}| + k * \dot{\theta}\right)\dot{\theta}dt.$$

Note that the ratio P_u/P_d is always greater than one, which is the value of P_u/P_d when the model is linear [5]. This fact does not imply that more energy is being absorbed, but only that a larger fraction of the total power flowing through the device is being converted, as the overall absorbed power is smaller because it increases with $|\zeta|^{\frac{3}{2}}$. This result is consistent with the linear absorption theory; in fact, when the amplitude of the incident wave is small, the linear dissipative term is dominant with respect to the quadratic term, and the ratio $P_u/P_d \to 1$, which is what happens in the linear case. The ratio P_u/P_d becomes close to 1 also when the wave period is close to $T = 5s$, for which the linear radiation damping B becomes the dominant term (fig. 4.16).

An additional significant difference with the linear case can be observed in fig.4.17, which depicts the ratio of the average reactive power to the absorbed power, where the average reactive power is defined as the power that the PTO returns to the oscillating body:

$$P_{reac} = -\frac{1}{T}\int_0^T \min\left[P(t), 0\right] dt, \text{ where } \quad P(t) = \dot{\theta}\ \gamma_p.$$

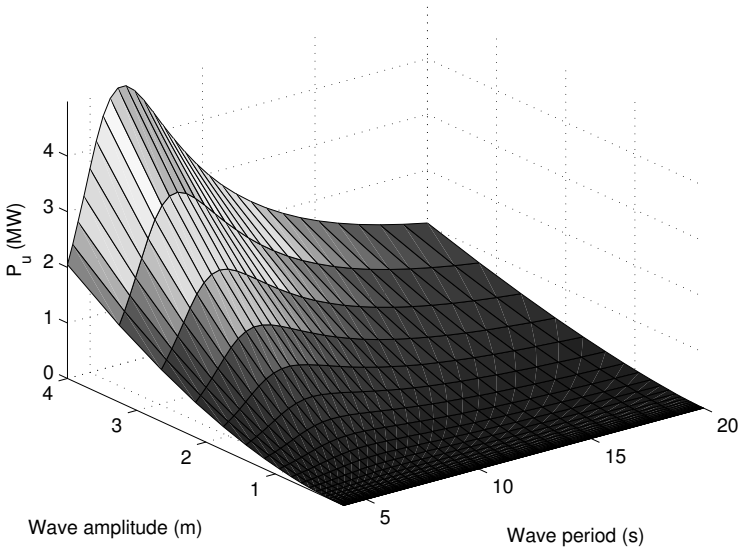

Figure 4.13: Average absorbed power (P_u).

The ratio P_{reac}/P_u is generally small for the range of wave periods and amplitudes considered, when the quadratic term becomes dominant, which is a favourable characteristic when designing a wave energy converter, because PTOs that are unable to return power to the oscillating body are generally less expensive. The consistency with the linear model can also be observed from the results in fig.4.17 when considering small wave amplitudes, where the amount of reactive power compared to the absorbed power increases considerably. It is well known that, with an optimal linear controller, the amount of reactive power is large when the period of the incident wave is far away from the resonance period [5].

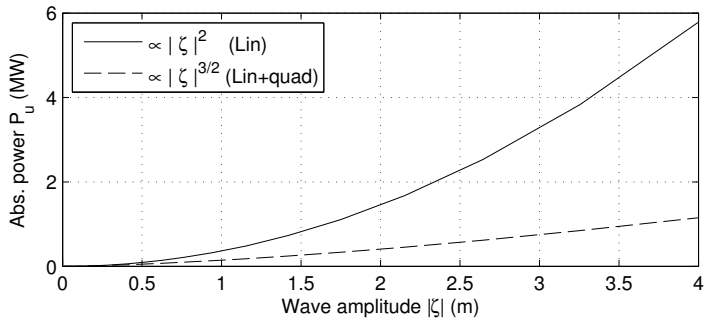

Figure 4.14: Absorbed power as function of the wave amplitude for the linear and nonlinear models (T=20s).

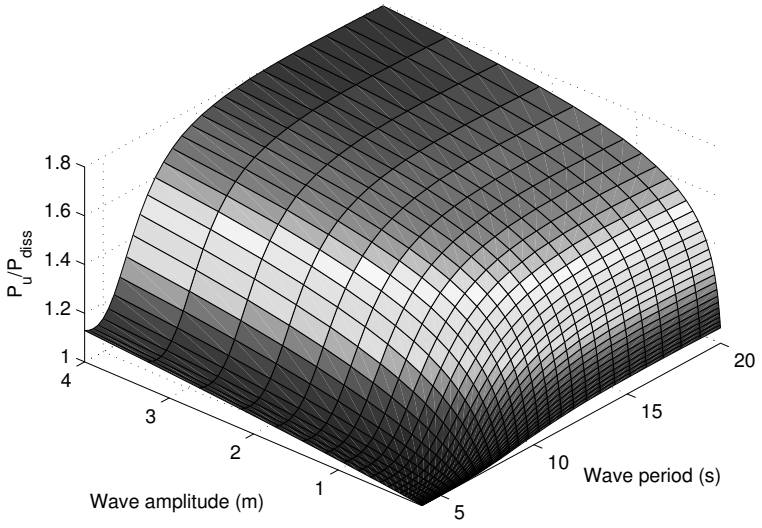

Figure 4.15: Ratio of the average absorbed power (P_u) over the dissipated and radiated power

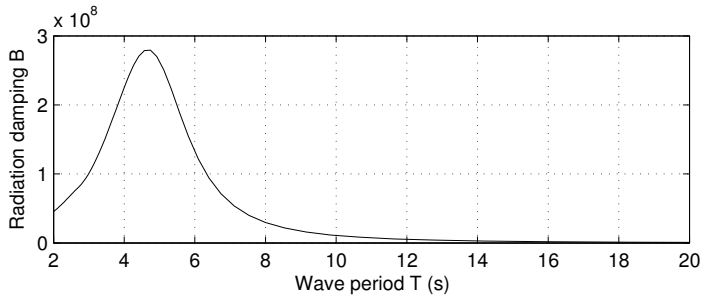

Figure 4.16: Radiation damping B.

Table 4.1: Absorbed energy (kW) and computing time (in brackets), as function of the order of the approximation (N) and of the wave period (T) for a wave amplitude of $|\zeta| = 2m$.

N	T=4s	T=8s	T=14s	T=20s
6	563.7 (0.16)	1463 (0.19)	685.5 (0.14)	399.8 (0.18)
10	564.5 (0.43)	1472 (0.31)	687.5 (0.32)	401.5 (0.37)
14	654.6 (0.89)	1473 (0.64)	687.7 (0.58)	401.6 (0.56)
18	N/A	1473 (1.17)	687.7 (0.98)	401.6 (0.79)

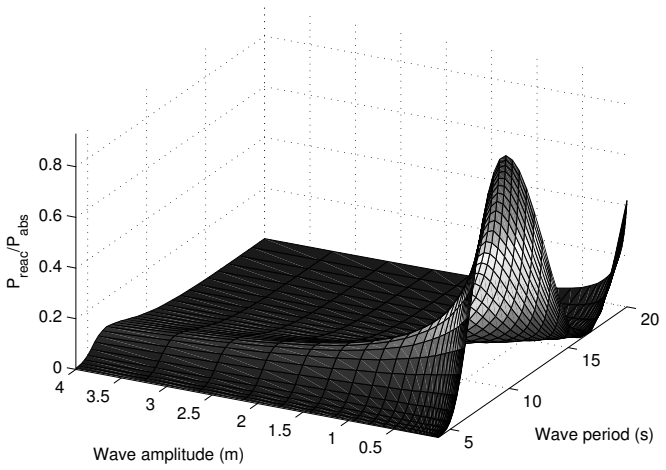

Figure 4.17: Ratio of the average reactive power over the average absorbed power

4.4 Chapter summary and discussion

This chapter has presented the approximation of the linear and nonlinear optimal control problems of WECs by means of spectral and pseudospectral methods. At first, the discretisation has been framed in the setting of the mean weighted residuals method, which includes, as special cases, both spectral and pseudospectral methods. It has been shown that, by using the mean weighted residuals, the convolution integral describing the radiation force can be simplified, and numerical integration can be carried out offline, thus reducing the computational load and the time for solving the NLP problem of the approximated control problem.

An illustrative example of a spectral method, that is the Galerkin method with approximation of state and control by means of Fourier series, has been presented in sec. 4.2.2. The derivation of the quadratic program approximating the optimal control of a single body WEC has been described in detail, and it has been shown that the resulting NLP problem is convex. Both PTO force and position constraints have also been considered, in addition to a discussion on the effects of PTO force constraints on the total absorbed energy. Spectral methods are generally more accurate than pseudospectral methods [216]; however, in the case of a nonlinear system the implementation of spectral methods is more difficult and computationally expensive, because they require online integration of the inner product integrals [220].

An application of pseudospectral methods for a nonlinear WEC model is presented in sec. 4.3; it is shown that the optimal behaviour of the nonlinear flap-type WEC is considerably different when compared to the linear case. In fact, the controller tends to prevent the device from moving with high velocity and, most importantly, the ratio of the total absorbed energy over the dissipated plus radiated energy is larger than one, which is the value resulting from the appli-

cation of an optimal controller when the model is linear. The direct consequence of this fact is that, by using a more accurate nonlinear model with a nonlinear optimal controller, a smaller, thus less expensive, PTO is required. In sec. 4.3 it is also shown that few frequency components are required for a good approximation of the optimal solution, resulting in a small NLP problem which can be solved quickly, and making this technique a suitable candidate for real time implementation.

The results presented in this chapter are the foundations on which the applications presented in the following chapters are based. In particular, chapter 5 uses the Fourier-Galerkin formulation for the control of arrays of WECs, while chapter 6 presents a geometrical interpretation of force and position constraints which is also based on the Fourier Galerkin formulation.

Chapter 5

Global and Independent control of arrays of wave energy converters

The previous chapter has provided the fundamental contribution of this thesis, which is the formulation of the optimal control problem of WECs in the framework of spectral and pseudospectral optimal control, in addition to two examples involving single-bodies WECs.

In this chapter, the Fourier-Galerkin spectral method introduced in sec. 4.2.2 is used for the direct transcription of optimal control problems of arrays of WECs. The objective of this chapter is twofold: to illustrate an additional application of the direct transcription method presented in sec. 4.2 to a more complex system composed of multiple WECs, and to analyse the benefit of coordinated control of arrays of WECs.

Wave energy converters in an array interact by means of radiation and diffraction forces, as already described in the theoretical background chapter (sec. 2.2); however, the control system can only affect the radiation component, which is the one that depends on the motion of the oscillating body. Because of the interaction, as discussed in 3.6, the optimal PTO force on each device depends on the motion of all the other devices in the array, and the stronger the hydrodynamic interaction the stronger the dependency of the optimal PTO force on the motion of the other devices.

The control strategy that takes into account the entire configuration of the array is called, in this thesis, Global Control (GC). It is evident that such a control strategy requires communication between devices and a centralised processing unit, with additional cost associated with the

infrastructure for data transmission (fig. 5.1). Global control also has a reduced fault tolerance because a malfunction of the central processing unit will cause the suspension of the whole array operation, if redundancy is not introduced, at additional cost. However, the great benefit of implementing a GC strategy is that it allows the maximum energy absorption[1].

In some situations, if the interaction between the WECs composing the array is not strong, a suboptimal control strategy, which obviates some of the drawbacks of the GC, may be more suitable. In particular, the Independent Control (IC) strategy considered in this chapter consists of implementing an optimal controller on each device which uses a control model that completely neglects the hydrodynamic interactions between the WECs (fig. 5.1). The IC obviates the necessity of data transmission between the devices and improves the fault tolerance of the system at the expenses of a reduced amount of total absorbed energy.

This chapter is composed of two main parts: in the first part, secs. 5.1 to 5.5, the comparison between GC and IC is carried out without control or state constraints. In particular, sec. 5.1 provides a description of the dynamical model used for the simulation of the array. The implementation of the control systems is described in sec. 5.2, with sec. 5.2.1 illustrating the discretisation of the equation of motion; sec. 5.2.2 and sec. 5.2.3 detail the implementation of the GC and IC, respectively. Simulation results are provided in sec. 5.3 for a number of scenarios: different array layouts with a range of inter-device distances, different WEC geometries, several sea states and a range of incident wave heading angles.

Since GC uses the model of the entire array for the calculation of the optimal PTO force while the IC completely neglects the hydrodynamic interactions, and even though the GC is capable of absorbing the the maximum amount of energy, it relies strongly on the accuracy of the system model. Section 5.4 considers the sensitivity of the relative performance between the GC and the IC with respect to position offsets of the WECs; in particular, the comparison is carried out in the situation where a device is allowed to move from its nominal position without the control knowing the actual displacement.

Section 5.5 provides a discussion on the interaction between WECs due to the control system as function of the inter-device distance while, in sec. 5.6, constraints on the state and control have been introduced into the formulation of both control problems. The PTO force constraints are described in sec. 5.6.1; the oscillation amplitude constraints are described in sec. 5.6.2 for the GC and, in sec. 5.6.3, for independent control. Simulation results showing the effects of both types of constraints on the relative performance between GC and IC are then discussed in sec. 5.7.

[1] Within the limits of validity of the linear model

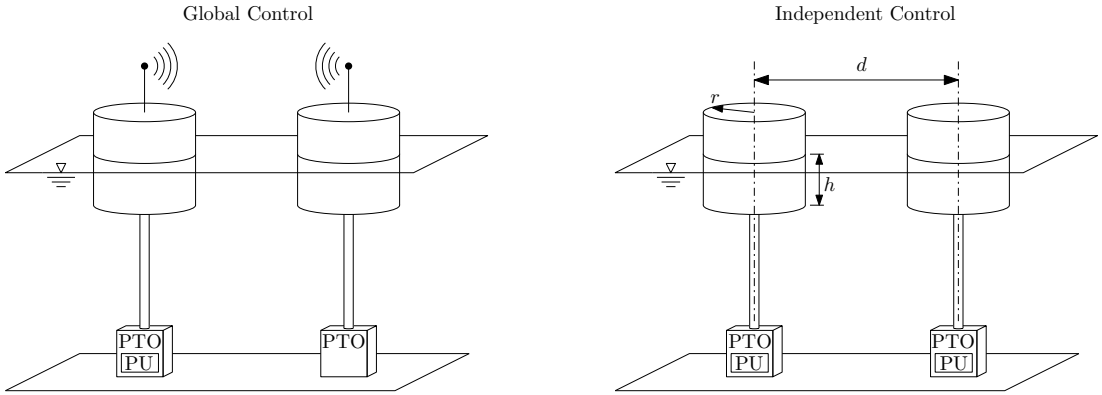

Figure 5.1: Conceptual differences between GC and IC for a 2-body array; GC has a centralised Processing Unit (PU) and a data transmission infrastructure whereas IC does not require communication between WECs and each device has its own PU.

5.1 Array simulation model

The WECs composing the arrays considered in this chapter are vertical cylinders of radius r, draught h and the distance between their vertical axis is denoted with d, as depicted in fig. 5.1 for the particular case of a two-body array. The motion of each WEC is assumed to be restricted to heave only, and the system dynamic is modelled, in the time domain, by the linear Cummins equation in (4.23), that is:

$$\mathbf{M}_t\,\ddot{\boldsymbol{z}}(t) + \mathbf{B}\,\dot{\boldsymbol{z}}(t) + \int_{t_0}^{t} \mathbf{K}(t-\tau)\dot{\boldsymbol{z}}(\tau)\,d\tau + \mathbf{S}\,\boldsymbol{z}(t) = \boldsymbol{f}_e(t) + \boldsymbol{f}_{pto}(t). \tag{5.1}$$

Equation (5.1), in contrast to the models used in sec. 4.2.2 and sec. 4.3 for the single WEC, is a systems of n integro-differential equations, where n is the number of WECs composing the array. Consistent with the notation adopted in the rest of this thesis, $\boldsymbol{z}(t) \in \mathbb{R}^n$ is the vector of the vertical positions of the WECs; $\mathbf{M}_t$ is the total mass matrix defined as $\mathbf{M}_t = \mathbf{M} + \mathbf{m}_\infty$ where $\mathbf{M} \in \mathbb{R}^{n\times n}$ is the generalised mass matrix and $\mathbf{m}_\infty \in \mathbb{R}^{n\times n}$ is the asymptotic values of the added mass at infinite frequency; $\mathbf{B} \in \mathbb{R}^{n\times n}$ is the viscous damping term; $\mathbf{S} \in \mathbb{R}^{n\times n}$ is the hydrodynamic stiffness and $\mathbf{K}(t) \in \mathbb{R}^{n\times n}$ is the matrix of the radiation impulse responses. The PTO configuration matrix has been omitted since, for this configuration, $\mathbf{F}_p$ is the identity matrix of size n (see sec. 4.2.1.2), that is $\mathbf{F}_p = \mathbf{I}_n$.

The excitation force is calculated from the wave elevation, as described in section 2.2.2.3; that is $\boldsymbol{f}_e(t) = \mathscr{F}^{-1}\{\mathbf{X}(\omega)\eta(\omega)\}$, where $\eta(\omega)$ is the Fourier transform of the wave elevation and $\mathbf{X}(\omega)$ is the frequency domain exciting force transfer function. The radiation coefficients $\mathbf{m}_\infty$ and $\mathbf{K}(t)$ are calculated from the frequency domain radiation impedance matrix $\mathbf{Z}(\omega)$ by applying Ogilvie's relations in (2.59)–(2.62), and the matrices $\mathbf{X}(\omega)$, $\mathbf{Z}(\omega)$ and $\mathbf{S}$ are then computed using the boundary element solver WAMIT® [226].

The viscous effect of a fluid on a body has been described in sec. 4.3.1 as a force proportional to the square of the relative velocity between the body and the fluid surrounding the body; i.e. $f_d = (1/2)C_d\rho\dot{z}|\dot{z}|A$, where ρ is the fluid density, A is the area of the body projected onto the plane orthogonal to the velocity $\dot{z}$, and C_d is the drag coefficient, which is obtained experimentally (see for example appendix 2 in [233]). The two control strategies presented in this chapter are based on linear models for an array of WECs, thus the viscous effects have been approximated by a force $\hat{f}_d$ which is *linearly* proportional to the velocity and that dissipates the same amount of energy as the force f_d. This procedure is known as Lorentz linearisation [234], and it has been previously used in the case of WECs by Folley *et al.* [15]. The approximation is carried out by equating the work done by the nonlinear drag force f_d with the work done by the linear approximation $\hat{f}_d = \mathrm{B}\dot{z}$, which results in

$$\int_0^T f_d \dot{z} dt = \int_0^T \hat{f}_d \dot{z} dt.$$

By means of simple manipulation, the linear damping coefficient B can be expressed as

$$\mathrm{B} = \frac{C_d \rho A \int_0^T \dot{z}^2(t)|\dot{z}(t)|\, dt}{2\int_0^T \dot{z}^2(t)\, dt} \tag{5.2}$$

Knowledge of the velocity is required to calculate the coefficient B, but the velocity itself also depends on B, thus an iterative procedure has been implemented. The procedure is initiated by setting B to an initial value B^0, which is not critical for the convergence because the relation between B and the velocity $\dot{z}$ is monotonic ($\dot{z}$ decreases when B increases). The i-th iteration of the procedure is composed of two steps, which are:

1. Calculate the velocity $\dot{z}^i$ using the value of B^{i-1}
2. Calculate B^i using the velocity $\dot{z}^i$ and the formula (5.2).

The procedure is stopped when the difference between two subsequent values of B is smaller than a threshold δ, that is $|\mathrm{B}^i - \mathrm{B}^{i-1}| < \delta$. For any given geometry, controller type and sea state, the coefficient B is calculated by simulating an isolated device and the matrix $\mathbf{B} = \mathrm{B}\mathbf{I}_n$.

5.2 Energy maximising control

The control problem, as usual (see chapter 4), is defined as: find the optimal PTO forces which maximises the total energy absorbed by the array, described by the equation of motion (5.1) over a time interval of length T.

In the ideal case, assuming the wave excitation is known completely into the future, the optimisation is performed over an infinitely long time interval, that is for $T \to +\infty$; however, it has

been shown [86] that a limited horizon suffices to achieve close to optimal energy absorption. As a consequence, the real-time implementation of the control algorithm can be performed in a receding horizon fashion, as described in [225], where future knowledge of either wave elevation or excitation force, up to time T ahead, is obtained by prediction. The focus of *this* chapter is on the *control of arrays of WECs*, and for this the effects of prediction have been neglected by applying the separation principle [235], which is a standard approach in control engineering, allowing the design of the optimal control to be separated from the design of the predictor; thus perfect knowledge of future wave elevation is assumed, in order to isolate the effects of control on the total energy produced.

5.2.1 Discretisation of the equation of motion

Direct transcription of control problems have been performed by means of spectral methods, more precisely, by using the Fourier-Galerkin transcription described in sec. 4.2.2. However, in this case, the system is not single-dimensional, but the number of DoF is n. The starting point, as usual, is the approximation of the state and control; thus, the velocity and the PTO force on the i-th device are:

$$v_i(t) \approx \sum_{k=1}^{N/2} x_{ik}^c \cos(k\omega_0 t) + x_{ik}^s \sin(k\omega_0 t) \tag{5.3}$$

$$f_{pto_i}(t) \approx \sum_{k=1}^{N/2} u_{ik}^c \cos(k\omega_0 t) + u_{ik}^s \sin(k\omega_0 t). \tag{5.4}$$

In analogy with the single WEC case, described in sec. 4.2.2, by assuming no drift, that is zero-mean velocities and positions, the differentiation matrix is invertible, and the position can be expressed in terms of the velocity as in (4.60). Following the same derivation leading to the discretised equation of motion for the single body in (4.61), the discretised equation of motion for the array, is:

$$\mathbf{G}\boldsymbol{X} = \boldsymbol{U} + \mathbf{E}. \tag{5.5}$$

For an array of three WECs, for example, $\boldsymbol{X}$, $\boldsymbol{U}$ and $\mathbf{E}$ are defined as

$$\boldsymbol{X} = \begin{bmatrix} \hat{\boldsymbol{x}}_1 \\ \hat{\boldsymbol{x}}_2 \\ \hat{\boldsymbol{x}}_3 \end{bmatrix} \qquad \boldsymbol{U} = \begin{bmatrix} \hat{\boldsymbol{u}}_1 \\ \hat{\boldsymbol{u}}_2 \\ \hat{\boldsymbol{u}}_3 \end{bmatrix} \qquad \mathbf{E} = \begin{bmatrix} \hat{\boldsymbol{e}}_1 \\ \hat{\boldsymbol{e}}_2 \\ \hat{\boldsymbol{e}}_3 \end{bmatrix}, \tag{5.6}$$

where $\hat{\boldsymbol{x}}_i$ and $\hat{\boldsymbol{u}}_i$ are the vectors of the Fourier coefficients of the velocity and PTO force of the

i-th device, respectively, and are arranged as

$$\hat{\boldsymbol{x}}_i = \left[x^c_{i1}, x^s_{i1}, x^c_{i2}, x^s_{i2}, \dots, x^c_{i\frac{N}{2}}, x^s_{i\frac{N}{2}}\right]^T$$
$$\hat{\boldsymbol{u}}_i = \left[u^c_{i1}, u^s_{i1}, u^c_{i2}, u^s_{i2}, \dots, u^c_{i\frac{N}{2}}, u^s_{i\frac{N}{2}}\right]^T.$$

The elements of the vectors $\hat{\boldsymbol{e}}_i$ are the Fourier coefficients of the excitation force on the i-th device and are arranged in the same manner as the vectors $\hat{\boldsymbol{x}}_i$ and $\hat{\boldsymbol{u}}_i$.

In contrast to the single body case in (4.62), the matrix $\mathbf{G}$ is not block diagonal; in fact

$$\mathbf{G} = \begin{bmatrix} \mathrm{G}_{11} & \mathrm{G}_{12} & \mathrm{G}_{13} \\ \mathrm{G}_{21} & \mathrm{G}_{22} & \mathrm{G}_{23} \\ \mathrm{G}_{31} & \mathrm{G}_{32} & \mathrm{G}_{33} \end{bmatrix}, \tag{5.7}$$

where the matrices $\mathrm{G}_{jk} \in \mathbb{R}^{N\times N}$ are block diagonal, and they are built from the hydrodynamic coefficients as

$$\mathrm{G}_{jk} = \begin{bmatrix} \mathrm{D}^1_{\mathrm{jk}} & \mathrm{M}^1_{\mathrm{jk}} & 0 & \cdots & 0 & 0 \\ -\mathrm{M}^1_{\mathrm{jk}} & \mathrm{D}^1_{\mathrm{jk}} & 0 & \cdots & 0 & 0 \\ 0 & 0 & \ddots & & \vdots & \vdots \\ \vdots & \vdots & & \ddots & 0 & 0 \\ 0 & 0 & \cdots & 0 & \mathrm{D}^{N/2}_{jk} & \mathrm{M}^{N/2}_{jk} \\ 0 & 0 & \cdots & 0 & -\mathrm{M}^{N/2}_{jk} & \mathrm{D}^{N/2}_{jk} \end{bmatrix}, \tag{5.8}$$

where

$$\mathrm{D}^l_{jk} = \mathrm{R}_{jk}(l\omega_0) + \mathrm{B}_{jk}$$
$$\mathrm{M}^l_{jk} = l\omega_0\left(\mathrm{M}_{jk} + \mathrm{m}_{jk}(l\omega_0)\right) - \mathrm{S}_{jk}/(l\omega_0) \qquad \text{for } l = 1, \dots, N/2.$$

B_{jk}, M_{jk} and S_{jk} are, respectively, the elements of the matrices $\mathbf{B}$, $\mathbf{M}$ and $\mathbf{S}$, while $\mathrm{R}_{jk}(\omega)$ and $\mathrm{m}_{jk}(\omega)$ are the elements of the radiation impedance matrix $\mathbf{Z}(\omega) = \mathbf{R}(\omega) + i\omega\,\mathbf{m}(\omega)$. Figure 5.2 depicts the sparsity pattern of the matrix $\mathbf{G}$ (i.e. the non-zero elements) for the example case of a three-WEC array with 10 frequency components ($N = 20$). The matrix $\mathbf{G}$ is 60×60 while each G_{jk} is 20×20 and is block diagonal with 2×2 blocks. Additionally, fig. 5.2 highlights the particular "multi-diagonal" structure of $\mathbf{G}$ which is due to the orthogonality of the basis functions.

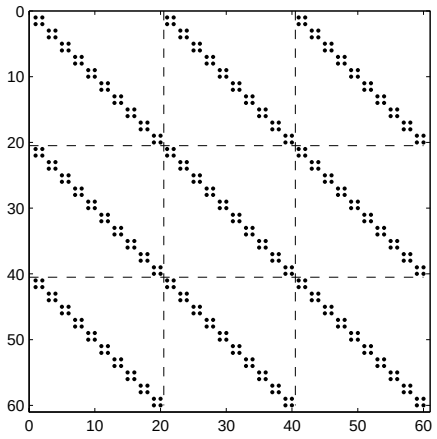

Figure 5.2: Sparsity pattern of the matrix $\mathbf{G}$ for a three-WECs array and $N = 20$.

5.2.2 Global control

The Global Control strategy is aware of the complete configuration of the array; thus, the control model is the discretised equation of motion in (5.5). The total energy absorbed by the array is considered to be the sum of the mechanical work done by each of the PTO forces, i.e.

$$J = -\sum_{i=1}^{n} \int_0^T v_i(t)\, f_{pto_i}(t)\, dt = \int_0^T \boldsymbol{v}(t)^T\, \boldsymbol{f}_{pto}(t)\, dt, \tag{5.9}$$

where $v_i(t)$ and $f_{pto_i}(t)$ are, respectively, the heave velocity and the PTO force of the i-th device; they are also the i-th elements of the vectors $\boldsymbol{v}$ and $\boldsymbol{f}_{pto}$, respectively, where $\boldsymbol{v} = \dot{\boldsymbol{z}}$.

By substituting the approximated velocity in (5.3) and PTO force in (5.4) into the the definition of the total absorbed energy (5.9), in analogy with the result for the single-WEC in (4.51), the finite dimensional cost function $\boldsymbol{J}^N$ is

$$\boldsymbol{J}^N = -\frac{T}{2}\boldsymbol{U}^T\boldsymbol{X}.$$

If $\mathbf{G}$ is non-singular, by solving (5.5) with respect to $\boldsymbol{X}$, that is

$$\boldsymbol{X} = \mathbf{G}^{-1}\boldsymbol{U} + \mathbf{G}^{-1}\mathbf{E},$$

$\boldsymbol{J}^N$ can be expressed as a function of the vector $\boldsymbol{U}$ only. Consequently, the optimal control vector $\boldsymbol{U}^*$, which describes the PTO forces maximising the absorbed energy for the array, is

obtained by solving the optimisation problem[2]

$$\boldsymbol{U}^* = \arg\max_{\boldsymbol{U}} \boldsymbol{J}^N = \arg\max_{\boldsymbol{U}} -\boldsymbol{U}^T\mathbf{G}^{-1}\boldsymbol{U} - \boldsymbol{U}^T\mathbf{G}^{-1}\mathbf{E}, \tag{5.10}$$

which is the equivalent of equation (4.64) for the single-WEC case.

5.2.3 Independent control

For the IC case, it is assumed that no communication occurs between the devices, and each controller uses the model of a single isolated device. That is, the control system of each device uses the model (5.1) where the variables z, f_{pto} and f_e are scalars; also M_t, B, K(t) and S are scalars, and they are the parameters of a single isolated device with the same shape and dimensions as the devices composing the corresponding array.

To illustrate the procedure for calculation of the IC, let's consider the example case of an array composed of two WECs (as shown in Fig.5.1). In this case, the discretised equation of motion (5.5) can be written as:

$$\begin{bmatrix} \mathrm{G}_{11} & \mathrm{G}_{12} \\ \mathrm{G}_{21} & \mathrm{G}_{22} \end{bmatrix} \begin{bmatrix} \hat{\boldsymbol{x}}_1 \\ \hat{\boldsymbol{x}}_2 \end{bmatrix} = \begin{bmatrix} \hat{\boldsymbol{u}}_1 \\ \hat{\boldsymbol{u}}_2 \end{bmatrix} + \begin{bmatrix} \hat{\boldsymbol{e}}_1 \\ \hat{\boldsymbol{e}}_2 \end{bmatrix}$$

which is equivalent to

$$\mathrm{G}_{11}\hat{\boldsymbol{x}}_1 = \hat{\boldsymbol{u}}_1 + \hat{\boldsymbol{e}}_1 - \mathrm{G}_{12}\hat{\boldsymbol{x}}_2 \tag{5.11}$$

$$\mathrm{G}_{22}\hat{\boldsymbol{x}}_2 = \hat{\boldsymbol{u}}_2 + \hat{\boldsymbol{e}}_2 - \mathrm{G}_{21}\hat{\boldsymbol{x}}_1. \tag{5.12}$$

Instead of the correct model in (5.11)–(5.12), the IC controllers of devices 1 and 2 use, respectively, the discretised model

$$\mathrm{G}_s\hat{\boldsymbol{x}}_1 = \hat{\boldsymbol{u}}_1 + \bar{\boldsymbol{e}}_1 \tag{5.13}$$

$$\mathrm{G}_s\hat{\boldsymbol{x}}_2 = \hat{\boldsymbol{u}}_2 + \bar{\boldsymbol{e}}_2, \tag{5.14}$$

where $\mathrm{G}_s \in \mathbb{R}^{N\times N}$ is analogous to the matrix $\mathbf{G}$ in the approximated equation of motion of the array in (5.5). However, in this case, G_s is calculated using the hydrodynamic coefficients of a single isolated device. In particular, G_s is a block diagonal matrix with square blocks of size two, and it is constructed in the same manner as the diagonal blocks G_{jj} of the matrix $\mathbf{G}$, as described in (5.8) for $i = j$, with the difference being that the elements D^l_{jk} and M^l_{jk} of G_s are calculated using the radiation impedance matrix of a single isolated device, as in (4.62).

[2]The term $T/2$ is a positive scaling factor that can be neglected for the calculation of the optimal PTO force because the vector $\boldsymbol{U}^*$ which maximises $\boldsymbol{J} = -(T/2)\boldsymbol{U}^T\boldsymbol{X}$ also maximises the cost function $\overline{J} = -\boldsymbol{U}^T\boldsymbol{X}$

The elements of the vectors $\bar{\boldsymbol{e}}_1$ and $\bar{\boldsymbol{e}}_2$ are the Fourier coefficients of the total excitation forces measured by the estimator on WEC 1 and 2, respectively, which are given by

$$\bar{\boldsymbol{e}}_1 = \hat{\boldsymbol{e}}_1 - \mathrm{G}_{12}\hat{\boldsymbol{x}}_2,$$
$$\bar{\boldsymbol{e}}_2 = \hat{\boldsymbol{e}}_2 - \mathrm{G}_{21}\hat{\boldsymbol{x}}_1.$$

In fact, it is assumed that the excitation force estimator on each device is not capable of discerning the excitation force due to incoming waves (Froude-Krylov and diffraction forces) from the radiation generated by other bodies; therefore, the estimator provides a signal which is the sum of the radiation force caused by other bodies ($\mathrm{G}_{12}\hat{\boldsymbol{x}}_2$ and $\mathrm{G}_{21}\hat{\boldsymbol{x}}_1$) and excitation from incoming waves ($\hat{\boldsymbol{e}}_1$ and $\hat{\boldsymbol{e}}_2$).

Each of the independent controllers calculates the optimal PTO force that maximises the energy absorbed by the corresponding WEC, using the models in (5.13) and (5.14). The optimal PTO forces ($\hat{\boldsymbol{u}}_1^*$ and $\hat{\boldsymbol{u}}_2^*$) are the solutions to the optimisation problems

$$\hat{\boldsymbol{u}}_1^* = \arg\max_{\hat{\boldsymbol{u}}_1} J_1 = \arg\max_{\hat{\boldsymbol{u}}_1} -\hat{\boldsymbol{u}}_1^T \mathrm{G}_s^{-1}\hat{\boldsymbol{u}}_1 - \hat{\boldsymbol{u}}_1^T \mathrm{G}_s^{-1}\bar{\boldsymbol{e}}_1 \tag{5.15}$$

$$\hat{\boldsymbol{u}}_2^* = \arg\max_{\hat{\boldsymbol{u}}_2} J_2 = \arg\max_{\hat{\boldsymbol{u}}_2} -\hat{\boldsymbol{u}}_2^T \mathrm{G}_s^{-1}\hat{\boldsymbol{u}}_2 - \hat{\boldsymbol{u}}_2^T \mathrm{G}_s^{-1}\bar{\boldsymbol{e}}_2 \tag{5.16}$$

the cost functions of which are the energy absorbed by each device, that is $J_1 = -\hat{\boldsymbol{u}}_1^T\hat{\boldsymbol{x}}_1$ and $J_2 = -\hat{\boldsymbol{u}}_2^T\hat{\boldsymbol{x}}_2$. The solutions to the optimisation problems in (5.15) and (5.16) are coupled because $\hat{\boldsymbol{u}}_1^*$ depends on $\bar{\boldsymbol{e}}_1$ which, in turns, is function of the velocity of body 2 ($\hat{\boldsymbol{x}}_2$), and vice versa; the problem is then effectively solved iteratively.

The initial condition is considered to be the situation where all the PTOs are switched off (i.e. $\hat{\boldsymbol{u}}_1 = \hat{\boldsymbol{u}}_2 = \mathbf{0}$). The velocities $\hat{\boldsymbol{x}}_1$ and $\hat{\boldsymbol{x}}_2$ are then calculated by means of the equation of motion (5.5) and the controller calculates the PTO forces by solving the optimisation problems (5.15) and (5.16). When the PTO forces are applied to the WECs, the new velocities are calculated again, using (5.5), and the process is repeated. The computations performed by the controller at the j-th step of the iteration are :

$$\boldsymbol{X}^j = \mathbf{G}^{-1}\left(\boldsymbol{U}^{*j-1} + \mathbf{E}\right) \tag{5.17}$$

$$\hat{\boldsymbol{u}}_1^{*j} = \arg\max_{\hat{\boldsymbol{u}}_1} -\hat{\boldsymbol{u}}_1^T \mathrm{G}_s^{-1}\hat{\boldsymbol{u}}_1 - \hat{\boldsymbol{u}}_1^T \mathrm{G}_s^{-1}\left(\hat{\boldsymbol{e}}_1 - \mathrm{G}_{12}\hat{\boldsymbol{x}}_2^j\right) \tag{5.18}$$

$$\hat{\boldsymbol{u}}_2^{*j} = \arg\max_{\hat{\boldsymbol{u}}_2} -\hat{\boldsymbol{u}}_2^T \mathrm{G}_s^{-1}\hat{\boldsymbol{u}}_2 - \hat{\boldsymbol{u}}_2^T \mathrm{G}_s^{-1}\left(\hat{\boldsymbol{e}}_2 - \mathrm{G}_{21}\hat{\boldsymbol{x}}_1^j\right), \tag{5.19}$$

where $j > 1$, $\boldsymbol{U}^0 = \mathbf{0}$ and $\boldsymbol{U}^{*j}$, $\boldsymbol{X}^j$, $\mathbf{E}$ are built from the vectors $\hat{\boldsymbol{u}}_1^{*j}$, $\hat{\boldsymbol{u}}_2^{*j}$, $\hat{\boldsymbol{x}}_1^j$, $\hat{\boldsymbol{x}}_2^j$, $\hat{\boldsymbol{e}}_1$, $\hat{\boldsymbol{e}}_2$ according to (5.6). The first step of each iteration in (5.17) calculates the actual velocities of the WECs using the correct model of the array in (5.5), using the (sub)optimal PTO forces $\hat{\boldsymbol{u}}_1^{*j}$ and $\hat{\boldsymbol{u}}_2^{*j}$,

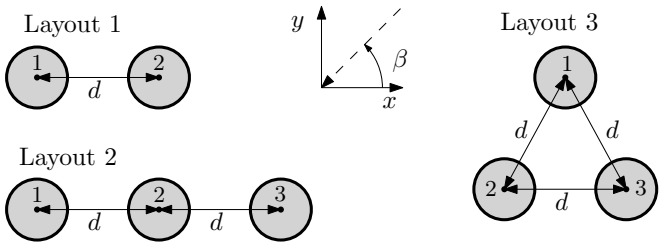

Figure 5.3: Top view of array layouts and of incident waves angle β

which are then calculated in the following steps (5.18)–(5.19) with the updated velocities and radiation forces from the other devices. The iteration stops when the PTO forces approach their asymptotic values, which is implemented by the condition $\left\|\boldsymbol{U}^{*j} - \boldsymbol{U}^{*j-1}\right\| < \varepsilon$.

The extension of the IC to a three-WEC array is immediate once the equation of motion (5.5) is written explicitly as in (5.11)–(5.12), that is:

$$\begin{aligned}
\mathrm{G}_{11}\hat{\boldsymbol{x}}_1 &= \hat{\boldsymbol{u}}_1 + \hat{\boldsymbol{e}}_1 - \mathrm{G}_{12}\hat{\boldsymbol{x}}_2 - \mathrm{G}_{13}\hat{\boldsymbol{x}}_3 \\
\mathrm{G}_{22}\hat{\boldsymbol{x}}_2 &= \hat{\boldsymbol{u}}_2 + \hat{\boldsymbol{e}}_2 - \mathrm{G}_{21}\hat{\boldsymbol{x}}_1 - \mathrm{G}_{23}\hat{\boldsymbol{x}}_3 \\
\mathrm{G}_{33}\hat{\boldsymbol{x}}_3 &= \hat{\boldsymbol{u}}_3 + \hat{\boldsymbol{e}}_3 - \mathrm{G}_{31}\hat{\boldsymbol{x}}_1 - \mathrm{G}_{32}\hat{\boldsymbol{x}}_2
\end{aligned}$$

where the definition of $\mathbf{G}$ in (5.7) has been used. The j-th step of the iteration is then

$$\begin{aligned}
\boldsymbol{X}^j &= \mathbf{G}^{-1}\left(\boldsymbol{U}^{*j-1} + \mathbf{E}\right) \\
\hat{\boldsymbol{u}}_1^{*j} &= \arg\max_{\hat{\boldsymbol{u}}_1} -\hat{\boldsymbol{u}}_1^T \mathrm{G}_s^{-1}\hat{\boldsymbol{u}}_1 - \hat{\boldsymbol{u}}_1^T \mathrm{G}_s^{-1}\left(\hat{\boldsymbol{e}}_1 - \mathrm{G}_{12}\hat{\boldsymbol{x}}_2^j - \mathrm{G}_{13}\hat{\boldsymbol{x}}_3^j\right) \\
\hat{\boldsymbol{u}}_2^{*j} &= \arg\max_{\hat{\boldsymbol{u}}_2} -\hat{\boldsymbol{u}}_2^T \mathrm{G}_s^{-1}\hat{\boldsymbol{u}}_2 - \hat{\boldsymbol{u}}_2^T \mathrm{G}_s^{-1}\left(\hat{\boldsymbol{e}}_2 - \mathrm{G}_{21}\hat{\boldsymbol{x}}_1^j - \mathrm{G}_{23}\hat{\boldsymbol{x}}_3^j\right) \\
\hat{\boldsymbol{u}}_3^{*j} &= \arg\max_{\hat{\boldsymbol{u}}_3} -\hat{\boldsymbol{u}}_3^T \mathrm{G}_s^{-1}\hat{\boldsymbol{u}}_3 - \hat{\boldsymbol{u}}_3^T \mathrm{G}_s^{-1}\left(\hat{\boldsymbol{e}}_2 - \mathrm{G}_{21}\hat{\boldsymbol{x}}_1^j - \mathrm{G}_{12}\hat{\boldsymbol{x}}_2^j\right),
\end{aligned}$$

and the vectors $\boldsymbol{U}^{*j}$, $\boldsymbol{X}^j$, $\mathbf{E}$ are defined according to (5.6).

5.3 Sample results

Three array layouts have been considered (fig. 5.3): layout 1 is composed of two heaving cylinders; layout 2 is a linear array of three WECs, while layout 3 is composed of three WECs placed at the vertices of an equilateral triangle. For each layout, twenty-four values of the inter-body spacing d have been chosen, logarithmically spaced between $2.2r$ to $10r$. Three device geometries for the WECs composing each array have been simulated, each of which has approximately the same volume ($\approx 160\pi\ m^3$) but different resonant periods; table 5.1 lists the radii r, draughts h and resonant period T_r for each device.

Table 5.1: WECs dimensions and resonance period

WEC Geometry	1	2	3
Radius r (m)	4	5	6.25
Draught h (m)	10	6	4
Resonance T_r (s)	7.1	5.9	5.4

The optimal control laws for each WEC, in the case of IC, are obtained by iteration, and it is assumed that, between consecutive iterations, there is enough time for the waves radiated from a device to reach all the other devices, and enough time for the estimator and predictor on each WEC to build a reliable forecast of the incoming waves (i.e. reach quasi steady state). While this is not feasible in practice, it provides a *best-case scenario* for IC case, providing an upper performance bound for the IC. However, the comparison between the GC and the IC is also carried out by considering only the first iteration of the IC, which starts from an initial condition where each PTO is switched off. The comparison of the GC with the first iteration of the IC is interesting from a practical point of view, since it highlights the effect of the PTO (and therefore the control system) on the interaction between devices.

Each of the three array layouts depicted in fig. 5.3 has been simulated for all three WEC geometries in table 5.1. Both GC and IC have been computed for each of the resulting nine possible arrays with inter-body spacing ranging between $2.2r$ and $10r$, and considering four Bretschneider spectra with $H_s = 1m$ and $T_p = \{6, 8, 10, 12\}$s. The parameters ω_0 and N for the discretisation of the control problem are $N = 160$ and $\omega_0 = 2\pi/200$ rad/s, respectively, while the thresholds δ and ε for the adaptive approximation of the viscous damping and the calculation of the IC (sec. 5.2.3), respectively, are $\delta = 1$ and $\varepsilon = 10$.

The patterns exhibited by the results are illustrated by the representative cases depicted in figs. 5.4–5.6, which show the ratio between the energy absorbed using IC and GC (E_i/E_g). In addition, table 5.2 summarises the results for the different geometries, with the table entries representing Δ_{GI}, which is the integral of the difference between the (ideal) IC and GC cases, that is

$$\Delta_{GI} = \int_{2.2}^{10} 1 - \frac{E_i}{E_g} \, \mathrm{d}\,(d/r),$$

and it is highlighted by the shaded area in fig.5.4. In figs. 5.4–5.6, the asterisk marks denote curves corresponding to the asymptotic behaviour of the IC, that is, when the control algorithm reaches (the ideal situation of) convergence in the calculation of the control law, while the circle marks denote the curves corresponding to the first iteration. As expected, the GC always performs better than the IC in terms of absorbed energy, with the difference decreasing monotonically with an increase in the separation distance between the bodies. Although the difference between GC and IC, for the asymptotic IC case, is generally smaller than 5-10%, the

relative performance is considerably larger when comparison is made with the first iteration of the IC. In addition, the performance of the IC degrades when the number of bodies in the array increases.

Comparing figs. 5.4-5.6, it is evident that IC suffers a degradation in performance for devices with stronger radiative properties. In fact, at any distance d, the ratio E_i/E_g for geometry 3 (fig. 5.6) is smaller than E_i/E_g for geometry 2 (fig. 5.5), which is a flatter device compared to geometry 3; in turn, E_i/E_g for geometry 2 is smaller than E_i/E_g for geometry 1 (fig. 5.4), which is flatter than geometry 2. By flatter, it is meant that the ratio r/h is larger, with resulting stronger radiative properties. Tables 5.2 show how the relative behaviours of the GC and IC are affected by the sea state, for different geometries. For layout 1, composed of two WECs, the relative performance of the asymptotic value of the IC case with respect to the GC case is not significantly affected by sea state, while more significant variations exist for layouts 2 and 3.

For layouts 2 and 3, the patterns in the E_i/E_g curves are still similar to the case of layout 1; however, the dependency on the heading angle emerges for layout 2, especially when considering the first iteration of the IC. This phenomenon shows that the performance of the IC is affected by the wave heading angle only in the case of an extended linear array (layout 2).

5.4 Sensitivity analysis

One potential drawback of the GC is the reliance on a more complex model, with particular emphasis on inter-device interactions. It could be expected, therefore, that variations in inter-device separation (e.g. for slack-moored devices) might introduce a modelling error which may impact the performance of the GC.

Table 5.2: Values of Δ_{GI} for geometry 1, 2 and 3

Geometry 1	$T_p = 6s$	$T_p = 8s$	$T_p = 10s$	$T_p = 12s$
Layout 1	0.072	0.068	0.064	0.054
Layout 2	0.113	0.122	0.130	0.121
Layout 3	0.200	0.188	0.188	0.170
Geometry 2	$T_p = 6s$	$T_p = 8s$	$T_p = 10s$	$T_p = 12s$
Layout 1	0.132	0.135	0.123	0.102
Layout 2	0.217	0.225	0.219	0.200
Layout 3	0.310	0.313	0.307	0.279
Geometry 3	$T_p = 6s$	$T_p = 8s$	$T_p = 10s$	$T_p = 12s$
Layout 1	0.190	0.207	0.191	0.160
Layout 2	0.324	0.335	0.312	0.281
Layout 3	0.429	0.433	0.420	0.387

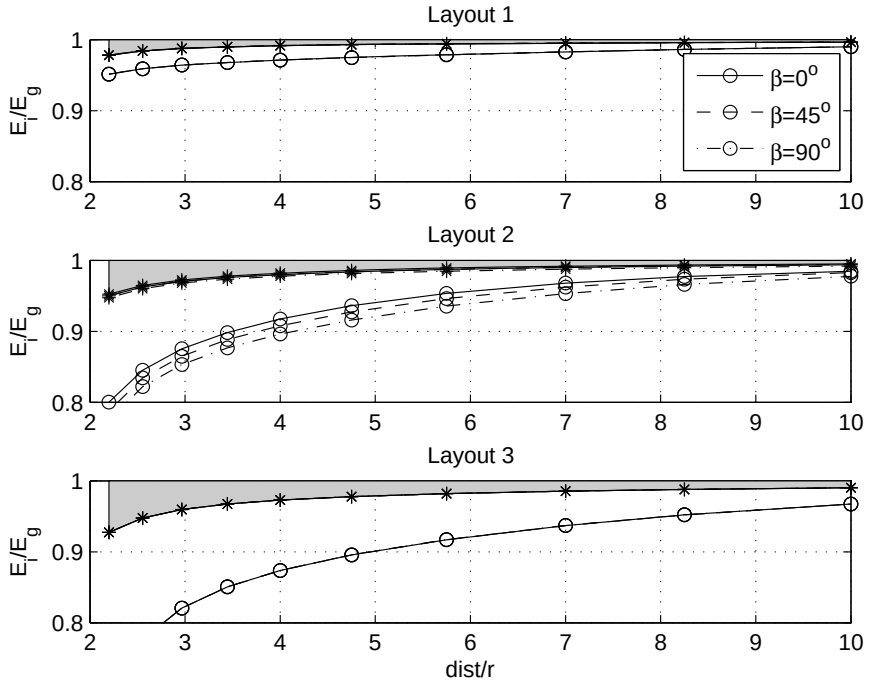

Figure 5.4: Relative performance of IC and GC for geometry 1, $T_p = 12s$ ($\lambda = 225m$). The mark $*$ identifies the asymptotic values of E_i/E_g; the mark $\circ$ identifies the first iteration E_i^1/E_g; the shaded area denotes Δ_{GI}.

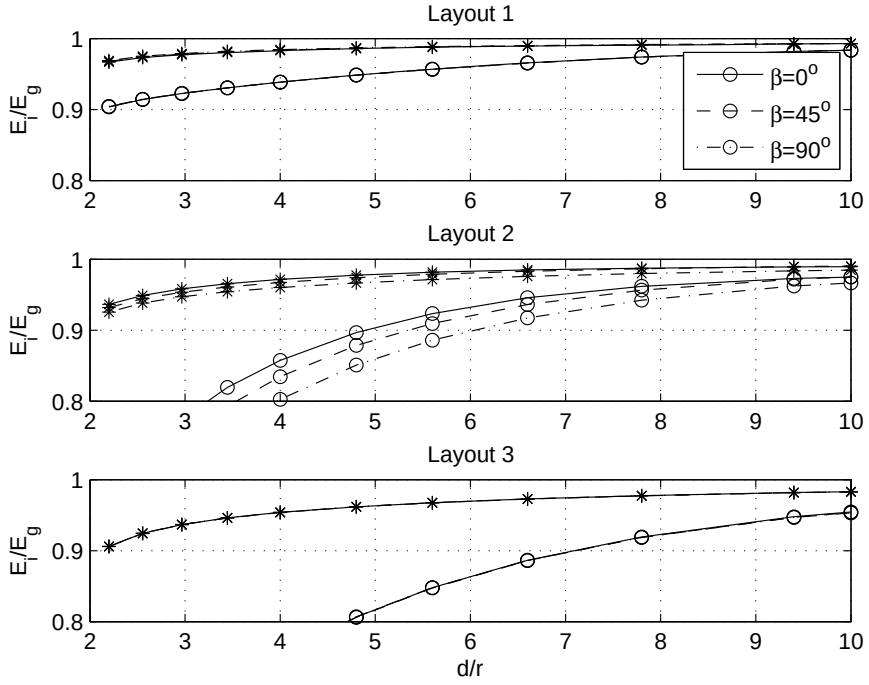

Figure 5.5: Relative performance of IC and GC for geometry 2, $T_p = 12s$ ($\lambda = 225m$)

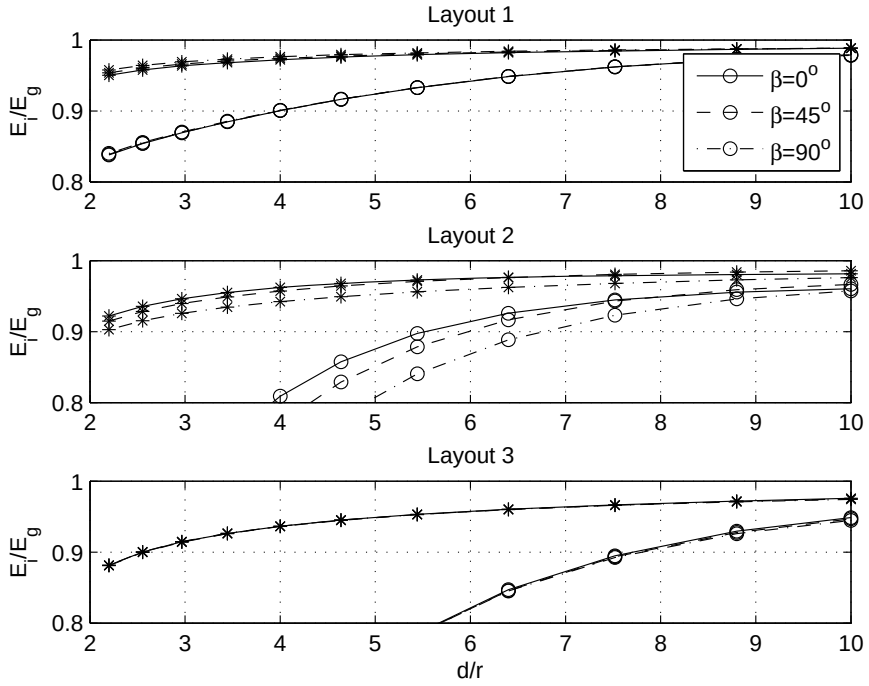

Figure 5.6: Relative performance of IC and GC for geometry 3, $T_p = 12s$ ($\lambda = 225m$)

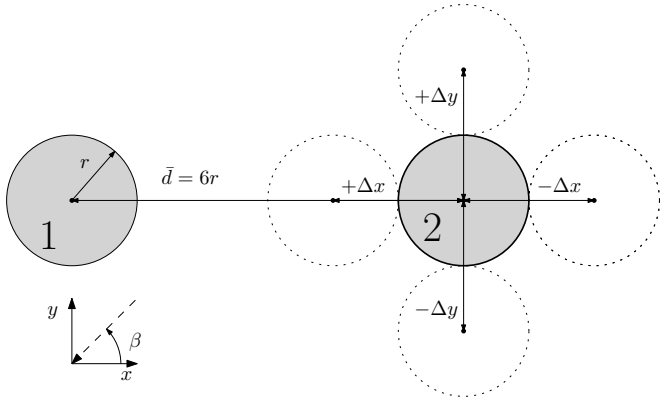

Figure 5.7: Top view of the array layout for the sensitivity analysis. The nominal distance $\bar{d}$ between the devices is $\bar{d} = 6r$. The devices in the nominal position are coloured in grey, while the dotted white circles denote the positions of the devices corresponding to the maximum offsets ($\pm\Delta x, \pm\Delta y = 2r$)

While some sensitivity analysis has been previously performed for WEC arrays, these studies mainly concerned sensitivity of suboptimal control to mis-tuning of the damping [188, 195], or the sensitivity of the sub-optimal damping to sea state. In [236], the effect of the uncertainty in the position of WECs on the interaction factor for an array has been considered from a probabilistic point of view, using individual linear damping. However, these studies do not employ a "fully-aware" global hydrodynamic model, where off-diagonal damping terms form an integral part of the control model.

In this section, the sensitivity of the relative IC vs GC performance with respect to position variation of an array element is examined; in particular, we consider layout 1, which is composed of two WECs, and we study the relative performance of the GC compared to the IC in terms of absorbed energy, that is E_i/E_g. Figure 5.7 depicts the configuration used for the sensitivity analysis; body 1 is held fixed while body 2 is displaced around its nominal position, for which $\bar{d} = 6r$. The offsets Δx and Δy have been chosen as uniformly distributed between $-2r$ and $2r$, for a total of 21 values including zero, with an increment of $0.2r$.

IC, by design, is not concerned with the position of the WECs, thus the calculation of the optimal profile of the PTO forces and energy absorbed is performed as described in section 5.2.3. Two cases have been considered for GC, depending on the availability of correct estimation of the excitation force. In the first case, the optimal profile of the PTO force is calculated using correct values of the excitation force; this can be the situation, for example, where the estimation of the excitation forces are performed using sensors on board of the WEC. Although the real position of the device is unknown, the excitation forces are correctly estimated (neglecting other phenomena) because the measurements used for the estimation are taken at the correct location. The second case introduces an error in the estimation of the excitation force which can be due to the fact, for example, that the wave field is measured using *wave data buoys* located at a certain known distance from the nominal position of the WECs. In this situation, the algorithm for the estimation of the excitation forces can only provide values related to the nominal positions of the WECs.

The sensitivity results are displayed using some indicative detailed plots (fig. 5.8 for the case of correct excitation force estimation and fig. 5.9 for the case of incorrect excitation force estimation) while summary results are presented in tables 5.3–5.5 for the case of incorrect estimation of the excitation force. The table entries show the maximum deviation of E_i/E_g due to the perturbation (normally achieved at $\Delta x/2r = 1$) and only variations in Δx are shown, due to the virtual symmetry between the cases of $[\beta = 0^\circ\,, \Delta x \neq 0]$ and $[\beta = 90^\circ\,, \Delta y \neq 0]$. Significant symmetry also for $\beta = 45^\circ$.

5.4.1 Correct estimation of the excitation force

The optimal PTO force profile calculated by the GC when WEC 2 is in a displaced position is obtained using (5.5) as the controller model. However, the excitation force vector $\mathbf{E}$ is replaced by $\mathbf{E}_o$, which is the correct value of the excitation force at the exact location of the device. Thus, in this case, the error is only in the matrix $\mathbf{G}$, which is built using hydrodynamic coefficients of the devices in their nominal position, instead of using the exact position. The optimal profile for the PTO force ($\boldsymbol{U}_o^*$) is then the solution of the quadratic optimisation problem defined by (5.10), where $\mathbf{E}$ is replaced by $\mathbf{E}_o$, that is

$$\boldsymbol{U}_o^* = \arg\max_{\boldsymbol{U}} -\boldsymbol{U}^T\mathbf{G}^{-1}\boldsymbol{U} - \boldsymbol{U}^T\mathbf{G}^{-1}\mathbf{E}_o, \tag{5.20}$$

and the energy absorbed by the array is calculated as

$$J_o = \boldsymbol{U}_o^{*T}\boldsymbol{X}_o.$$

The vector of the exact velocities of the devices ($\boldsymbol{X}_o$) is calculated using (5.5) as

$$\boldsymbol{X}_o = \mathbf{G}_o^{-1}\left(\boldsymbol{U}_o^* + \mathbf{E}_o\right),$$

where $\mathbf{G}_o$ is built using the hydrodynamic coefficients of the WECs in their exact locations.

The relative performance of GC with respect to IC, measured with the ratio E_i/E_g, is not sensitive to variations in the position along the y axis, i.e to position variations when the WEC moves orthogonally to the plane passing through the axes of the cylinders (the xz plane). In general, it has been found that the relative performance of GC with respect to IC is less sensitive to position offsets when the sea state has a larger T_p.

It has also been observed that, for all the sea states and geometries, GC and IC perform similarly when the incident wave angle is 45°; in fact, for any value of Δx, the line corresponding to $\beta = 45^\circ$ is always close to the value that E_i/E_g takes for $\Delta x = 0$.

5.4.2 Incorrect estimation of the excitation force

When the estimation of the excitation force is not correct, the GC optimal PTO profile $\boldsymbol{U}_{oe}$ is calculated by solving the quadratic optimisation problem (5.10), with both $\mathbf{E}$ and $\mathbf{G}$ referred to the nominal position of the devices. The energy absorbed by the array is then calculated as

$$J_{oe} = \boldsymbol{U}_{oe}^{*\,T}\boldsymbol{X}_{oe},$$

where

$$\boldsymbol{X}_{oe} = \mathbf{G}_o^{-1}\left(\boldsymbol{U}_{oe}^* + \mathbf{E}_o\right),$$

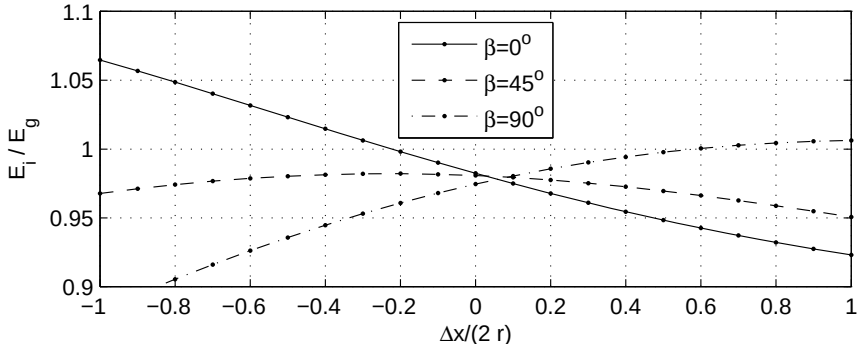

Figure 5.8: Sensitivity to offset along x for geometry 3, with $T_p = 6s$, $\lambda = 56m$. Correct excitation force estimation.

with $\mathbf{G}_o$ and $\mathbf{E}_o$ defined as in sec 5.4.1.

Figure 5.9 shows the comparison of performance between GC and IC, for Geometry 3, with $T_p = 6s$. GC performs progressively worse than IC with increasing device displacement, as the curves E_i/E_g, for any heading angle β, always reach their minimum for $\Delta x = 0$ and $\Delta y = 0$, that is the nominal position. Similarly to the case where the estimation of the excitation force is correct, the degradation in performance of GC with respect to IC is smaller for longer wavelengths (see table 5.3–5.5) and for devices with smaller radiation characteristics (compare Geometry 1 to Geometry 3 in table 5.3–5.5).

Table 5.3: Geometry 1; $\max_{\Delta x}(E_i/E_g)$ - $E_i/E_g|_{\Delta x=0}$

Geometry 1	$T_p = 6s$	$T_p = 8s$	$T_p = 10s$	$T_p = 12s$
$\beta = 0°$	0.096	0.035	0.018	0.011
$\beta = 45°$	0.039	0.016	0.009	0.006
$\beta = 90°$	0.003	0.002	0.002	0.002

Table 5.4: Geometry 2; $\max_{\Delta x}(E_i/E_g)$ - $E_i/E_g|_{\Delta x=0}$

	$T_p = 6s$	$T_p = 8s$	$T_p = 10s$	$T_p = 12s$
$\beta = 0°$	0.211	0.067	0.031	0.018
$\beta = 45°$	0.092	0.030	0.015	0.009
$\beta = 90°$	0.012	0.007	0.005	0.003

When the estimation of the excitation force is affected by the error due to the position offset of one device, the relative performance of GC with respect to IC degrades significantly when the offset is in the direction of the incoming waves. Figure 5.9, for example, shows that when $\beta = 0°$, E_i/E_g is not affected by offsets along y , but is notably sensitive to displacements along

Table 5.5: Geometry 3; $\max_{\Delta x}(E_i/E_g)$ - $E_i/E_g|_{\Delta x=0}$

	$T_p = 6s$	$T_p = 8s$	$T_p = 10s$	$T_p = 12s$
$\beta = 0^\circ$	0.390	0.119	0.049	0.027
$\beta = 45^\circ$	0.200	0.057	0.024	0.014
$\beta = 90^\circ$	0.026	0.013	0.008	0.005

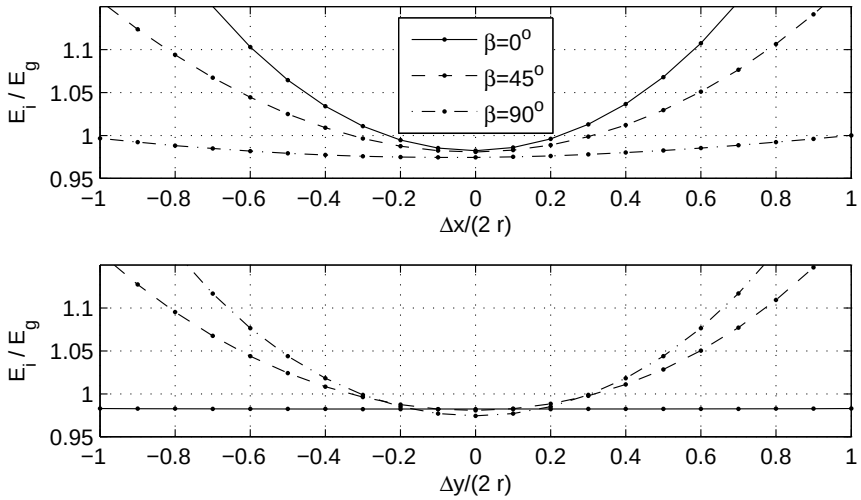

Figure 5.9: Sensitivity to offset along x and y for geometry 3 for $T_p = 6s$, $\lambda = 56m$. Incorrect excitation force estimation.

x. Conversely, when $\beta = 90^\circ$, E_i/E_g is strongly affected by variation of position along y and it is not sensitive along the x direction. The explanation of this effect can be related to the fact that a displacement of the body in the direction of the incoming waves corresponds to a phase shift in the excitation force, while a displacement in the direction orthogonal to the incoming waves only affect the diffraction component. In particular, the Froude-Krylov force is constant on a direction orthogonal to the wave direction (plane wave case), while the diffraction force depends on the layout of the array and on the geometry of the devices. The effect of a small displacement along y on the diffraction component is negligible because the distance d between the bodies remains unaltered, that is $d \approx \bar{d}$.

Figure 5.9 allows us to discern between the effects of the diffraction and the Froude-Krylov forces on the relative performance between GC and IC. In particular, the curve corresponding to $\beta = 0^\circ$ is perfectly horizontal when the displacement occurs along y, where variations of both diffraction and Froude-Krylov forces are negligible. For $\beta = 90^\circ$, the curve corresponding to displacements along y is not constant, and its variation is due to diffraction only because, in this case, the Froude-Krylov component is constant along y.

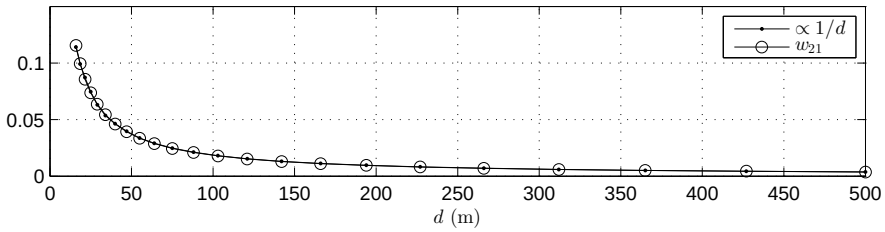

Figure 5.10: Interaction factor w_{21} for geometry 3 as a function of d

5.5 Interaction analysis

One striking feature of the results is the characteristic 'asymptotic' convergence of E_i/E_g to 1, as d/r becomes large. This can be explained by the reduction in interaction effects as the separation distance between array elements increases.

In [237], Babarit showed that, for a two-body array of heaving or surging WECs aligned with the direction of the incoming waves and large d, *when radiation is negligible*, the alteration of the energy absorption due to wave interaction effects decreases asymptotically with the square root of the separating distance. A similar discussion is carried out in [236], where further development accounts for the effects of radiation at closer distances. Although the authors provide a model for the approximation of the interaction factor as function of the separating distance, the effect of radiation on the interaction between WECs is not isolated from the effect of diffraction. Separation between the effects of diffraction and radiation on the energy absorption have been considered in Babarit *et al.* [196], where the problem has been studied by considering a two-body array and keeping one device fixed, inhibiting radiation.

In this section, the case of a two-body array with no incoming waves is considered, with the first device (WEC 1) induced to oscillate by means of a pre-specified PTO force ($\hat{\boldsymbol{u}}_1$), and the second device (WEC 2) to be optimally controlled so as to absorb the maximum amount of energy radiated by the first device. As expected, from analytical considerations, the maximum amount of energy transferred from the first device to the second is inversely proportional to the distance d. The first step to show this effect is to define $\mathbf{H}$, if $\mathbf{G}$ is non-singular, as

$$\mathbf{H} = \mathbf{G}^{-1} = \begin{bmatrix} \mathrm{H}_{11} & \mathrm{H}_{12} \\ \mathrm{H}_{21} & \mathrm{H}_{22} \end{bmatrix}$$

From the discretised equation of motion (5.5), the energy absorbed by WEC 2, denoted as J_2, is:

$$J_2 = -\hat{\boldsymbol{u}}_2^T \hat{\boldsymbol{x}}_2 = -\hat{\boldsymbol{u}}_2^T \mathbf{H}_{22} \hat{\boldsymbol{u}}_2 - \hat{\boldsymbol{u}}_2^T \mathbf{H}_{21} \hat{\boldsymbol{u}}_1 \tag{5.21}$$

For this two-body case, it can be seen numerically that the symmetric part[3] of H_{22} is positive

[3] the symmetric part of $\mathbf{H}$ is $(\mathbf{H} + \mathbf{H}^T)/2$

definite, thus equation (5.21) is a convex quadratic function of $\hat{\boldsymbol{u}}_2$. Therefore, for any given value of the PTO force $\hat{\boldsymbol{u}}_1$, the optimal value of the PTO force $\hat{\boldsymbol{u}}_2$ that maximises J_2 is

$$\hat{\boldsymbol{u}}_2^* = (\mathbf{H}_{22} + \mathbf{H}_{22}^T)^{-1}\mathbf{H}_{21}\hat{\boldsymbol{u}}_1.$$

The "radiation interaction factor" w_{21}, defined as the ratio of the energy delivered to the system by means of the mechanical work done by the PTO on WEC 1 and the energy recovered by means of the optimally controlled WEC 2, is $w_{21} = J_2/J_1 = \hat{\boldsymbol{u}}_2^T\hat{\boldsymbol{x}}_2/\hat{\boldsymbol{u}}_1^T\hat{\boldsymbol{x}}_1$. Using (5.5) and (5.6), and some further manipulation, w_{21} can be evaluated as:

$$w_{21} = \frac{\hat{\boldsymbol{u}}_1^T\mathbf{H}_{21}^T\left(\bar{\mathbf{H}}_2^T\mathbf{H}_{22}\bar{\mathbf{H}}_2 + \bar{\mathbf{H}}_2^T\right)\mathbf{H}_{21}\hat{\boldsymbol{u}}_1}{\hat{\boldsymbol{u}}_1^T\left(\mathbf{H}_{11} + \mathbf{H}_{12}\bar{\mathbf{H}}_2\mathbf{H}_{21}\right)\hat{\boldsymbol{u}}_1}$$

where $\bar{\mathbf{H}}_2 = \left(\mathbf{H}_{22} + \mathbf{H}_{22}^T\right)^{-1}$.

Figure 5.10 shows that w_{21} is inversely proportional to the inter-body distance d. In particular, the curve marked with circles ($\circ$) depicts the values of w_{21} for an array composed of two devices of geometry 3 as a function of the inter-body distance d, where $\hat{\boldsymbol{u}}_1$ has been chosen as a random vector. The curve marked with dots ($\cdot$) is obtained by fitting the values of w_{21} with a function $f(d) = \alpha/d$, where the value of α is obtained using least squares.

5.6 Constraints

Physical limitations of the WECs components are taken into account by introducing constraints on state and control. Similarly to the single-body case described in sec. 4.2.2.2, PTO force and oscillation amplitude constraints are applied for both the GC and IC.

5.6.1 PTO force constraint

Consistent with the notation introduced in sec. 4.2.2.2, the maximum available force on PTO of the i-th device is

$$|f_{pto_i}(t)| \leq \mathrm{F}_{max}.$$

By using the vector of basis functions $\Phi(t)$, defined in (4.50), that is

$$\Phi(t) = \left[\cos(\omega_0 t), \sin(\omega_0 t), \ldots, \cos\left(\frac{N}{2}\omega_0 t\right), \sin\left(\frac{N}{2}\omega_0 t\right)\right],$$

the PTO force approximation in (5.4) can be written as

$$f_{pto_i}(t) \approx \Phi(t)\,\hat{\boldsymbol{u}}_i.$$

Thus, the constraint of the approximated force is

$$|\Phi(t)\,\hat{\boldsymbol{u}}_i| \leq \mathrm{F}_{max},$$

or equivalently

$$\begin{cases} \Phi(t)\hat{\boldsymbol{u}}_i \leq \mathrm{F}_{max} \\ -\Phi(t)\hat{\boldsymbol{u}}_i \leq \mathrm{F}_{max}. \end{cases}$$

As in (4.71) and (4.73), the PTO force constraint is then enforced at the time instants t_k, for $k = 0, \ldots, N_c$, by introducing the system of $2(N_c + 1)n$ linear inequalities

$$\begin{bmatrix} \boldsymbol{\Theta} \\ -\boldsymbol{\Theta} \end{bmatrix} \hat{\boldsymbol{u}}_i \leq \mathbf{1}_{2(N_c+1)\times 1}\,\mathrm{F}_{max} \tag{5.22}$$

where $\mathbf{1}_{2(N_c+1)\times 1}$ is the vector of all ones of size $2(N_c + 1)$, the matrix $\boldsymbol{\Theta}$ is

$$\boldsymbol{\Theta} = \begin{bmatrix} \Phi_0 \\ \Phi_1 \\ \vdots \\ \Phi_{N_c} \end{bmatrix}$$

and $\Phi_k = \Phi(t_k)$.

5.6.2 Oscillation amplitude constraints for global control

The oscillation amplitude constraint for the i-th device is defined as

$$|z_i(t)| \leq \mathrm{Z}_{max}.$$

Following the same steps carried out for the PTO force constraints, and by using the relation between the Fourier coefficients of the velocity and position in (4.60), the oscillation amplitude constraint on the approximated position can be written as

$$|\Phi(t)\mathrm{D}_{\phi}^{-1}\hat{\boldsymbol{x}}_i| \leq \mathrm{Z}_{max}.$$

Finally, the constraints can be enforced at the time instant t_k, by means of the system of $2(N_c + 1)n$ linear inequalities

$$\begin{cases} \Xi\,\mathbf{G}^{-1}\boldsymbol{U} \leq \mathbf{1}_{(N_k\times 1)n}\mathrm{Z}_{max} - \Xi\,\mathbf{G}^{-1}\mathbf{E} \\ -\Xi\,\mathbf{G}^{-1}\boldsymbol{U} \leq \mathbf{1}_{(N_k\times 1)n}\mathrm{Z}_{max} + \Xi\,\mathbf{G}^{-1}\mathbf{E}. \end{cases} \tag{5.23}$$

where the matrix Ξ is block diagonal as

$$\Xi = \begin{bmatrix} \boldsymbol{\Theta} \mathrm{D}_{\phi}^{-1} & \mathbf{0} & \dots & \mathbf{0} \\ \mathbf{0} & \boldsymbol{\Theta} \mathrm{D}_{\phi}^{-1} & \dots & \mathbf{0} \\ \vdots & \vdots & \ddots & \vdots \\ \mathbf{0} & \mathbf{0} & \dots & \boldsymbol{\Theta} \mathrm{D}_{\phi}^{-1} \end{bmatrix}.$$

5.6.3 Adaptive constraints for independent control

The control models in (5.13) and (5.14) used by IC are not accurate because they neglect part of the hydrodynamic interaction between the WECs. This fact does not influence the definition of the PTO force constraint because equation (5.22) does not depends on the dynamics of the device; however, the definition of the oscillation amplitude constraints in equation (5.23) does depend on the matrix $\mathbf{G}$, which embeds the (hydro)dynamics of system. Therefore, the oscillation amplitude constraints for the IC case have been defined, on the i-th device, using the control models (5.13) and (5.14), resulting in the linear inequalities

$$\begin{bmatrix} \boldsymbol{\Theta} \\ -\boldsymbol{\Theta} \end{bmatrix} \mathrm{D}_{\phi}^{-1} \mathrm{G}_{s}^{-1} \hat{\boldsymbol{u}}_i \leq \mathbf{1}_{2(N_k \times 1)} \mathrm{Z}_{max_i} - \begin{bmatrix} \boldsymbol{\Theta} \\ -\boldsymbol{\Theta} \end{bmatrix} \mathrm{D}_{\phi}^{-1} \mathrm{G}_{s}^{-1} \bar{\boldsymbol{e}}_i. \tag{5.24}$$

Consequently, the solution of the IC constrained optimal control problem given by (5.15) and (5.16), subject to the linear constraints (5.22) and/or (5.24), may produce a motion that violates one of the amplitude constraints. The constrained optimal control problem for IC is approached by first solving the optimal control problems defined in (5.15) and (5.16), with constraints (5.22) and (5.24). If the motion of any of the devices violates a constraint, the optimal control problem is solved again, but with a more restrictive constraint. In practice, if the motion of the i-th device violates the amplitude constraint Z_{max_i}, the control problem is solved again, but the new amplitude constraint $\widetilde{\mathrm{Z}}_{max_i}$ is $\widetilde{\mathrm{Z}}_{max_i} = \alpha \, \mathrm{Z}_{max_i}$ with $0 < \alpha < 1$. The sequence is then repeated by decreasing α until all constraints are satisfied.

5.6.4 Solving the optimisation problem

The optimisation problems for GC and IC are convex quadratic programs. In fact, it can be verified that the matrices G and G_s of the quadratic cost functions (5.10), (5.15) and (5.16) are positive definite and the constraints (5.22) (5.23) and (5.23) are linear. The active set algorithm [222] is used to solve the optimisation problems, which is implemented in Matlab by the function `quadprog`.

5.7 Sample results (with constraints)

Simulations for the constrained case are carried out for the same layouts (fig. 5.3) and geometries (table 5.1) described in section 5.3. The inter-body spacing d is logarithmically spaced between $2.2r$ to $10r$, and four Bretschneider spectra are considered, with $H_s = 1m$ and $T_p = \{6, 8, 10, 12\}$s. The parameters ω_0 and N for the discretisation of the control problem are $N = 160$ and $\omega_0 = 2\pi/200$ rad/s respectively, while the thresholds δ and β for the adaptive approximation of the viscous damping (sec. 5.1) and the IC iteration procedure (sec.5.2.3), respectively, are $\delta = 1$ and $\epsilon = 10$.

The patterns exhibited by the results are illustrated by the representative cases depicted in figs. 5.11–5.13, which show the ratio between the energy absorbed using IC and GC (E_i/E_g), with respect to the normalized amplitude constraint $\bar{\mathrm{Z}}$ and normalized force constraint $\bar{\mathrm{F}}$, defined as

$$\bar{\mathrm{Z}} = \frac{\mathrm{Z}_{max}}{\max|z_u^1|} \qquad \bar{\mathrm{F}} = \frac{\mathrm{F}_{max}}{\max|f_{pto_u}^1|},$$

where z_u^1 is the oscillation amplitude of a single isolated and unconstrained device, and $f_{pto_u}^1$ is the optimal PTO force of a single isolated and unconstrained device.

It can be immediately noticed that the relative performance of IC with respect to GC is more sensitive to the force constraint than the oscillation amplitude constraint. In particular, when restricting the maximum allowed PTO force, the performance of IC approaches the performance of GC ($E_i/E_g \to 1$). On the other hand, the relative performance of IC degrades when imposing a more restrictive the oscillation amplitude constraint (i.e. when decreasing $\bar{\mathrm{Z}}$). These observations about the behaviour of the ratio E_i/E_g with respect to $\bar{\mathrm{Z}}$ and $\bar{\mathrm{F}}$ are consistent for the three layouts, across several sea states and wave heading angles, as can be seen by comparing figures 5.11, 5.12 and 5.13.

Tables 5.6 and 5.7 provide a wider range of results for E_i/E_g, as a function of the peak period and the wave heading angle, for array layouts 2 and 3, respectively. For each T_p and β, tables 5.6 and 5.7 list three entries: the first, denoted by Unc, is the ratio E_i/E_g for the unconstrained case; the entry denoted by $(\overline{\nabla E_{ig}})_{\bar{\mathrm{Z}}}$ is the average gradient of E_i/E_g in the direction of the amplitude constraints, while $(\overline{\nabla E_{ig}})_{\bar{\mathrm{F}}}$ is the average gradient in the direction of the force constraint. Tables 5.6 and 5.7 confirm that the relative performance of IC is more sensitive to the force constraint than the oscillation amplitude constraint and that, by reducing the maximum allowed PTO force, the ratio $E_i/E_g \to 1$. However, there seems to be an exception for the case of the smallest peak period ($T_p = 6s$), where a restriction of the maximum PTO force causes, on average, a degradation of the relative performance of the IC. In particular, by looking at table 5.6, which lists the simulation results for array layout 2 composed of WECs of geometry 2, when $T_p = 6s$, the sensitivity of E_i/E_g decreases in magnitude when the heading angle β increases; thus,

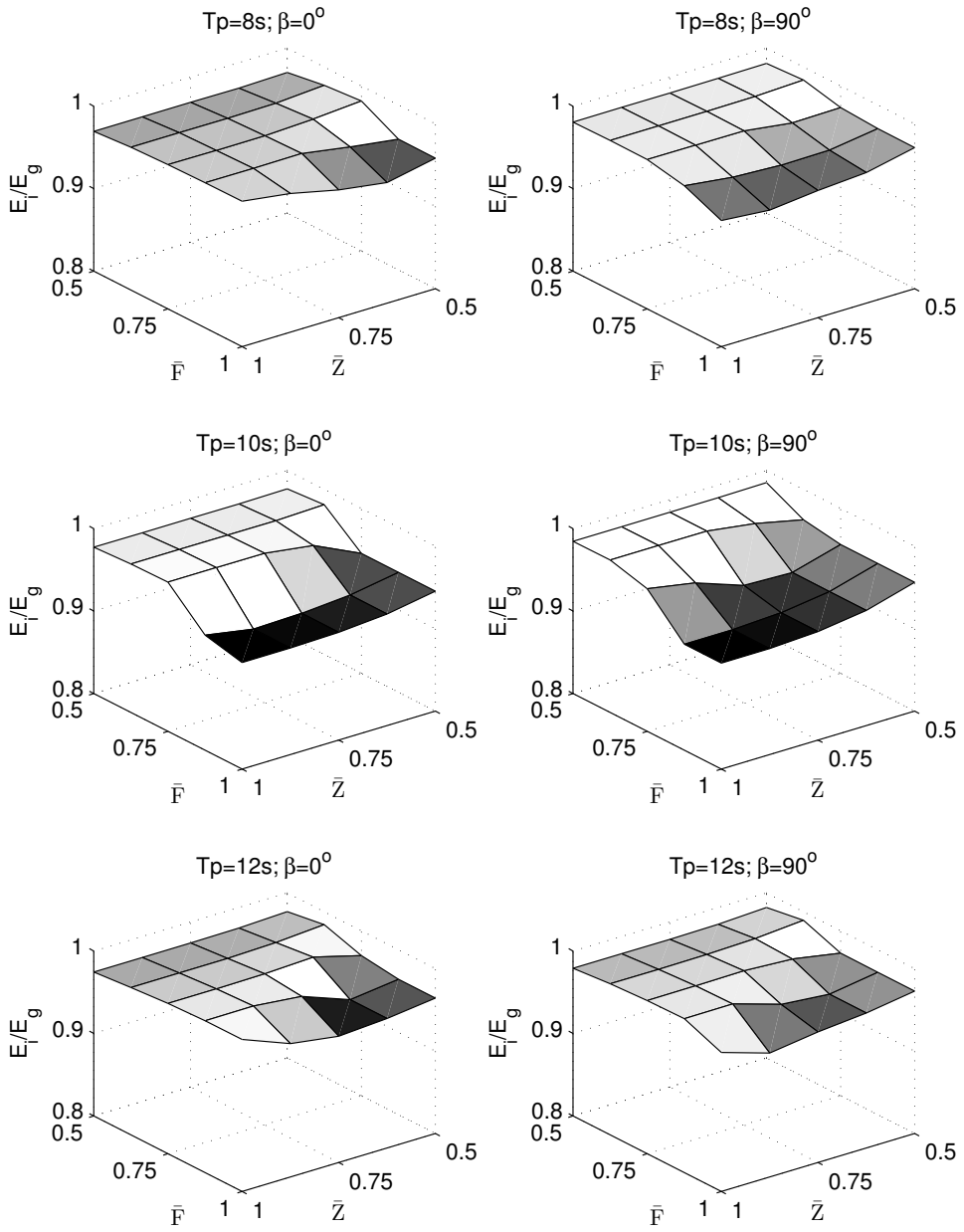

Figure 5.11: Layout 1; Geometry 2; $d = 20m$

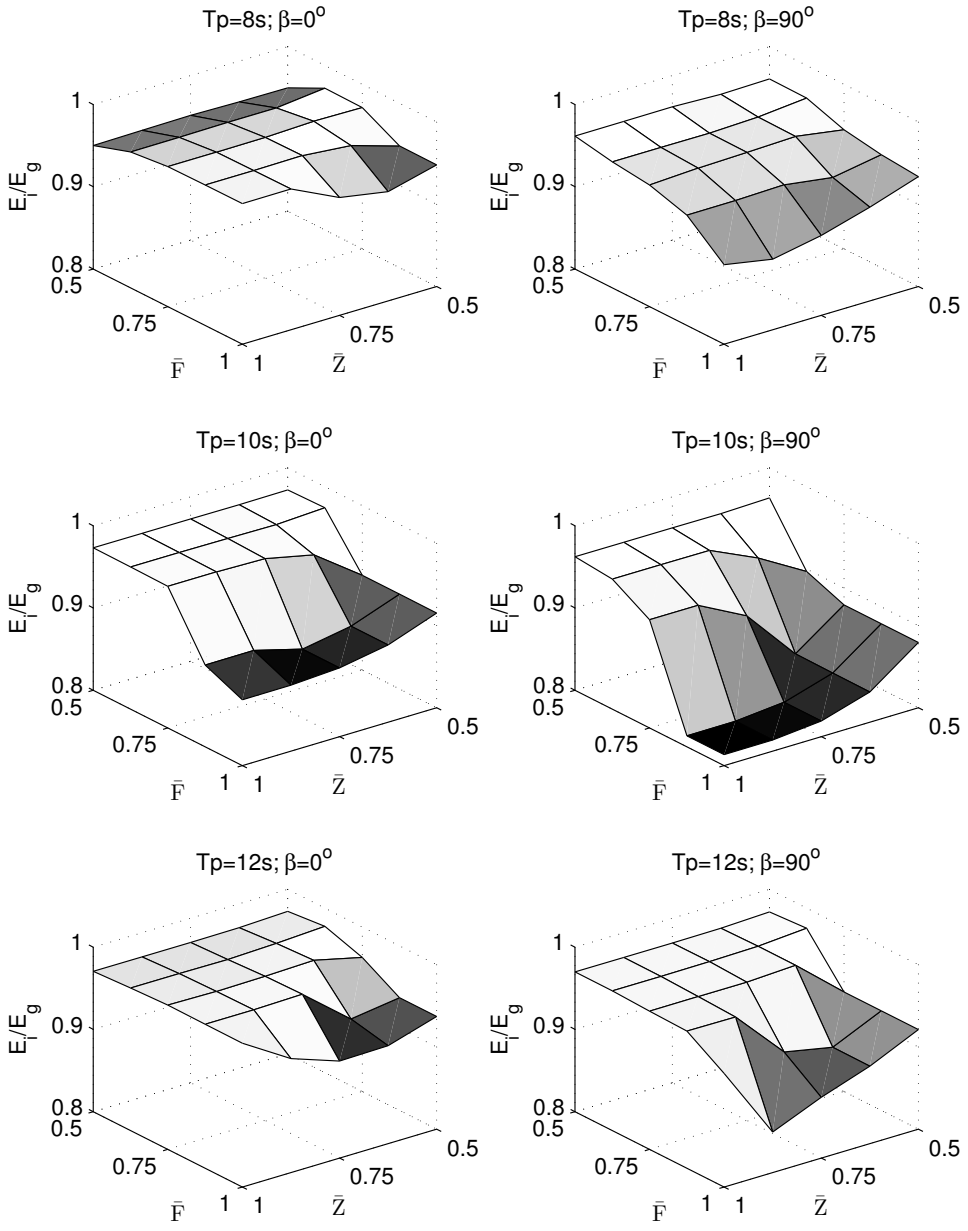

Figure 5.12: Layout 2; Geometry 2; $d = 20m$

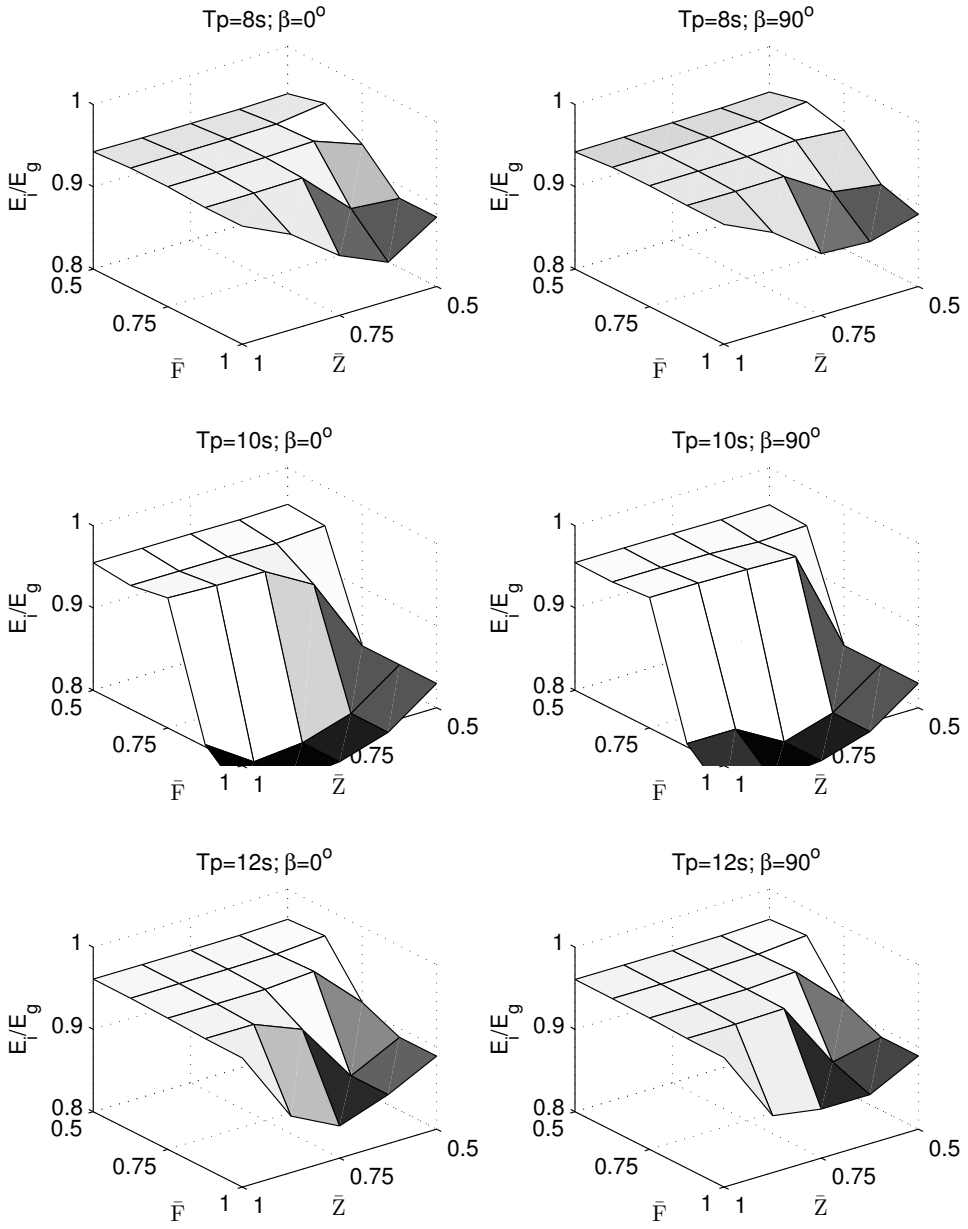

Figure 5.13: Layout 3; Geometry 2; $d = 20m$

Table 5.6: Layout 2; Geometry 2; $d = 20m$

		T_p=6s	T_p=8s	T_p=10s	T_p=12s
β=0°	Unc	0.953	0.971	0.880	0.975
	$(\overline{\nabla E_{ig}})_{\bar{Z}}$	0.007	-0.015	-0.002	-0.032
	$(\overline{\nabla E_{ig}})_{\bar{F}}$	-0.050	-0.005	0.165	0.068
β=30°	Unc	0.963	0.971	0.867	0.974
	$(\overline{\nabla E_{ig}})_{\bar{Z}}$	0.004	-0.014	0.002	-0.039
	$(\overline{\nabla E_{ig}})_{\bar{F}}$	-0.036	0.027	0.184	0.087
β=45°	Unc	0.962	0.954	0.852	0.972
	$(\overline{\nabla E_{ig}})_{\bar{Z}}$	0.008	-0.008	-0.005	-0.041
	$(\overline{\nabla E_{ig}})_{\bar{F}}$	-0.021	0.066	0.209	0.097
β=60°	Unc	0.957	0.914	0.834	0.919
	$(\overline{\nabla E_{ig}})_{\bar{Z}}$	0.010	0.011	0.029	-0.028
	$(\overline{\nabla E_{ig}})_{\bar{F}}$	-0.011	0.099	0.235	0.145
β=90°	Unc	0.945	0.897	0.813	0.938
	$(\overline{\nabla E_{ig}})_{\bar{Z}}$	0.014	0.017	0.008	-0.041
	$(\overline{\nabla E_{ig}})_{\bar{F}}$	-0.016	0.111	0.260	0.151

Table 5.7: Layout 3; Geometry 2; $d = 20m$

		T_p=6s	T_p=8s	T_p=10s	T_p=12s
β=0°	Unc	0.930	0.944	0.764	0.957
	$(\overline{\nabla E_{ig}})_{\bar{Z}}$	0.005	-0.051	-0.013	-0.072
	$(\overline{\nabla E_{ig}})_{\bar{F}}$	-0.015	0.098	0.344	0.158
β=30°	Unc	0.933	0.942	0.763	0.957
	$(\overline{\nabla E_{ig}})_{\bar{Z}}$	-0.005	-0.054	0.017	-0.071
	$(\overline{\nabla E_{ig}})_{\bar{F}}$	-0.022	0.133	0.345	0.160
β=45°	Unc	0.924	0.942	0.763	0.957
	$(\overline{\nabla E_{ig}})_{\bar{Z}}$	0.000	-0.047	-0.014	-0.072
	$(\overline{\nabla E_{ig}})_{\bar{F}}$	-0.015	0.110	0.345	0.159
β=60°	Unc	0.922	0.944	0.764	0.957
	$(\overline{\nabla E_{ig}})_{\bar{Z}}$	0.009	-0.050	-0.015	-0.071
	$(\overline{\nabla E_{ig}})_{\bar{F}}$	-0.014	0.109	0.344	0.158
β=90°	Unc	0.927	0.946	0.765	0.957
	$(\overline{\nabla E_{ig}})_{\bar{Z}}$	0.011	-0.037	-0.016	-0.071
	$(\overline{\nabla E_{ig}})_{\bar{F}}$	-0.025	0.087	0.343	0.149

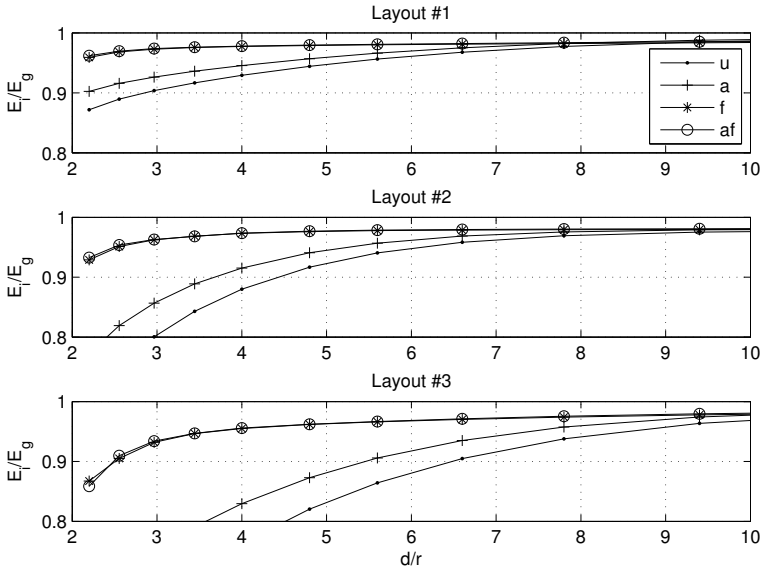

Figure 5.14: Geometry 2; $T_p = 10s$; $\beta = 0^\circ$

the results suggest that the performance degradation of the IC is reduced when the array is in terminator position ($\beta = 90^\circ$). When $T_p = 6s$, the negative values of the gradient $(\overline{\nabla E_{ig}})_{\bar{\mathrm{F}}}$ for both layouts 2 and 3 (tables 5.6 and 5.7, respectively) could be due to the fact that the corresponding peak wavelength is approximately $56m$ (in infinite water depth), which is slightly less than three times the inter-body distance $d = 20m$. Thus, the small ratio between the wavelength and d may cause strong inter-body interference, which penalises IC.

In all cases, the magnitude of $(\overline{\nabla E_{ig}})_{\bar{\mathrm{F}}}$ is larger than the magnitude of $(\overline{\nabla E_{ig}})_{\bar{\mathrm{Z}}}$; that is, E_i/E_g is more sensitive to variations in the force constraint than variations in the amplitude constraint, no matter whether the variation is positive or negative.

The effect of the inter-body distance on E_i/E_g, in conjunction with the wave heading angle and for the three layouts, is shown in figs. 5.14, 5.15 and 5.16. Each plot contains four curves, corresponding to different constraint configurations: the curve labelled "u" depicts E_i/E_g as function of the inter-body distance for the unconstrained case; the curves labelled "a" and "f" correspond the the cases where only one type of constraint is active and it is set to its minimum value considered in this paper, the normalized value of which is 0.5. In particular, the curve labelled as "a" is obtained by imposing $\bar{\mathrm{Z}} = 0.5$ and leaving the PTO force unconstrained, while the curve "f" is obtained by setting $\bar{\mathrm{F}} = 0.5$. The last curve ("af") is obtained by simulating the system when both the normalized PTO force and normalized oscillation amplitude constraints are set to 0.5 ($\bar{\mathrm{F}} = 0.5$ and $\bar{\mathrm{Z}} = 0.5$).

As expected, IC behaves similarly to GC in terms of total absorbed energy (the ratio $E_i/E_g \rightarrow 1$) for large inter-body spacing. In fact, the inter-body hydrodynamic interactions (both radiation

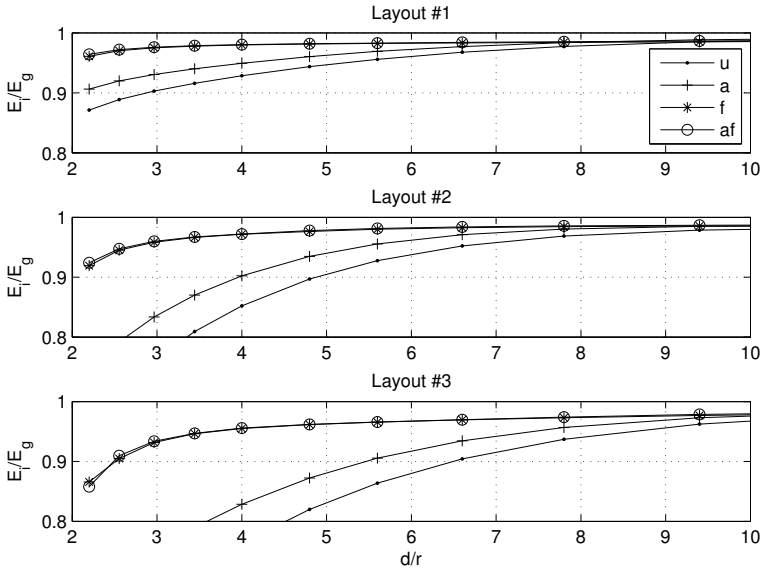

Figure 5.15: Geometry 2; $T_p = 10s$; $\beta = 45^\circ$

and diffraction) decrease with increasing distance, and the error introduced in the control model used by IC becomes negligible.

Figures 5.14–5.16 also highlight how restrictions in the motion and PTO force causes the performance of the IC to improve when compared to GC, since the curves corresponding to any constrained configuration ("a", "f", "af") are always above the curve corresponding to the unconstrained motion and force ("u"). It is also evident, from figs. 5.14–5.16, that the effect of the PTO force constraint on E_i/E_g is larger than the effect of the motion constraint, as the curves "f" and 'af" are always overlapped. This means that an additional reduction in the oscillation amplitude constraint has no effect on E_i/E_g when the normalized force constraint is already set to $\bar{\text{F}}$=0.5.

Figures 5.14–5.16 correspond to simulations performed with the same geometry of the WEC (G 2) and same sea state (T_p=10s), and to different wave heading angles β. By comparing all these figures, it can be noted that E_i/E_g for layout 2 (linear array with three WECs) is the most sensitive to β, while for the layout 1, which is composed of two devices, is less sensitive. When considering layout 3, E_i/E_g is practically unaffected by the wave heading angle. The behaviour of E_i/E_g with respect to the heading angle and the array layout is confirmed by the data in tables 5.8 and 5.9, which list the values of E_i/E_g and their gradients for additional values of β and for two sea states ($T_p = 8s$ for table 5.8 and $T_p = 10s$ for table 5.9).

The effect of the WEC geometry on the relative performance of IC compared to GC can be inferred from the data in tables 5.10 and 5.11, which list the values of E_i/E_g, $(\overline{\nabla E_{ig}})_{\bar{\text{Z}}}$ and $(\overline{\nabla E_{ig}})_{\bar{\text{F}}}$ for the three layouts and the three WEC geometries; both tables refer to the same wave

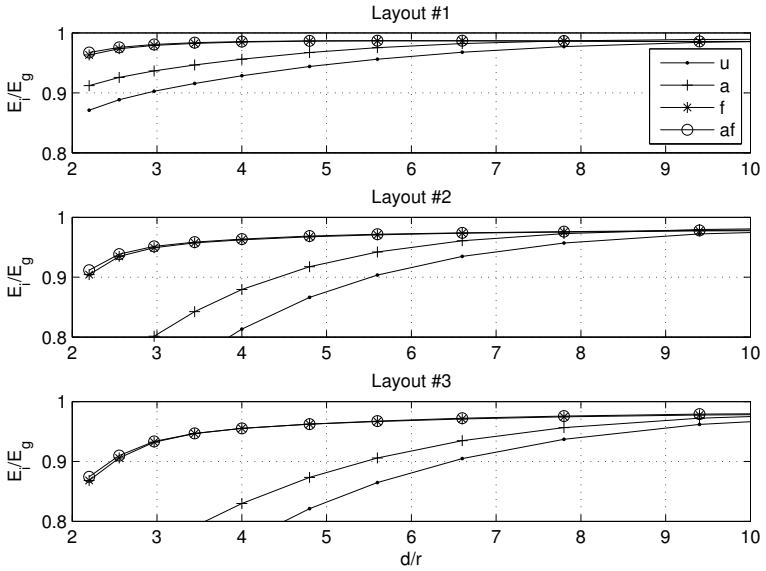

Figure 5.16: Geometry 2; $T_p = 10s$; $\beta = 90^\circ$

heading angle $\beta = 90^\circ$ and normalized distance $d/r = 4$. The IC performs worse for the device with the strongest radiative properties (geometry 3) in all the situations; this observation was expected, since a stronger interaction implies a larger effect of the error in the control model used by the IC, with the consequent degradation in relative performance.

Table 5.8: $d = 20m$; $T_p = 8s$; Geometry 2

		L 1	L 2	L 3
β=0°	Unc	0.976	0.971	0.944
	$(\overline{\nabla E_{ig}})_{\bar{Z}}$	-0.009	-0.015	-0.051
	$(\overline{\nabla E_{ig}})_{\bar{Z}}$	0.018	-0.005	0.098
β=30°	Unc	0.977	0.971	0.942
	$(\overline{\nabla E_{ig}})_{\bar{Z}}$	-0.011	-0.014	-0.054
	$(\overline{\nabla E_{ig}})_{\bar{Z}}$	0.022	0.027	0.133
β=45°	Unc	0.977	0.954	0.942
	$(\overline{\nabla E_{ig}})_{\bar{Z}}$	-0.014	-0.008	-0.047
	$(\overline{\nabla E_{ig}})_{\bar{Z}}$	0.023	0.066	0.110
β=60°	Unc	0.969	0.914	0.944
	$(\overline{\nabla E_{ig}})_{\bar{Z}}$	-0.006	0.011	-0.050
	$(\overline{\nabla E_{ig}})_{\bar{Z}}$	0.032	0.099	0.109
β=90°	Unc	0.953	0.897	0.946
	$(\overline{\nabla E_{ig}})_{\bar{Z}}$	0.005	0.017	-0.037
	$(\overline{\nabla E_{ig}})_{\bar{Z}}$	0.048	0.111	0.087

Table 5.9: $d = 20m$; $T_p = 10s$; Geometry 2

		L 1	L 2	L 3
β=0°	Unc	0.929	0.880	0.764
	$(\overline{\nabla E_{ig}})_{\bar{Z}}$	-0.005	-0.002	-0.013
	$(\overline{\nabla E_{ig}})_{\bar{Z}}$	0.087	0.165	0.344
β=30°	Unc	0.929	0.867	0.763
	$(\overline{\nabla E_{ig}})_{\bar{Z}}$	-0.003	0.002	0.017
	$(\overline{\nabla E_{ig}})_{\bar{F}}$	0.088	0.184	0.345
β=45°	Unc	0.929	0.852	0.763
	$(\overline{\nabla E_{ig}})_{\bar{Z}}$	0.004	-0.005	-0.014
	$(\overline{\nabla E_{ig}})_{\bar{F}}$	0.090	0.209	0.345
β=60°	Unc	0.928	0.834	0.764
	$(\overline{\nabla E_{ig}})_{\bar{Z}}$	0.008	0.029	-0.015
	$(\overline{\nabla E_{ig}})_{\bar{F}}$	0.092	0.235	0.344
β=90°	Unc	0.928	0.813	0.765
	$(\overline{\nabla E_{ig}})_{\bar{Z}}$	0.007	0.008	-0.016
	$(\overline{\nabla E_{ig}})_{\bar{F}}$	0.096	0.260	0.343

Table 5.10: $T_p = 8s$; d/r=4; $\beta = 90°$

		L 1	L 2	L 3
G 1	Unc	0.966	0.925	0.975
	$(\overline{\nabla E_{ig}})_{\bar{Z}}$	0.005	0.009	-0.015
	$(\overline{\nabla E_{ig}})_{\bar{F}}$	0.017	0.083	0.015
G 2	Unc	0.953	0.897	0.946
	$(\overline{\nabla E_{ig}})_{\bar{Z}}$	0.005	0.017	-0.037
	$(\overline{\nabla E_{ig}})_{\bar{F}}$	0.048	0.111	0.087
G 3	Unc	0.924	0.868	0.917
	$(\overline{\nabla E_{ig}})_{\bar{Z}}$	0.025	0.031	-0.030
	$(\overline{\nabla E_{ig}})_{\bar{F}}$	0.063	0.113	0.119

Table 5.11: $T_p = 10s$; d/r=4; $\beta = 90°$

		L 1	L 2	L 3
G 1	Unc	0.965	0.896	0.875
	$(\overline{\nabla E_{ig}})_{\bar{Z}}$	0.009	0.021	0.006
	$(\overline{\nabla E_{ig}})_{\bar{F}}$	0.037	0.145	0.175
G 2	Unc	0.928	0.813	0.765
	$(\overline{\nabla E_{ig}})_{\bar{Z}}$	0.007	0.008	-0.016
	$(\overline{\nabla E_{ig}})_{\bar{F}}$	0.096	0.260	0.343
G 3	Unc	0.897	0.761	0.690
	$(\overline{\nabla E_{ig}})_{\bar{Z}}$	0.021	0.033	-0.041
	$(\overline{\nabla E_{ig}})_{\bar{F}}$	0.139	0.307	0.439

5.8 Summary and discussion

This chapter has two main purposes, which are to provide an additional illustrative example of the direct Fourier-Galerkin transcription presented in sec. 4.2.2 applied to a more complex configuration of WECs and, in doing so, to compare the performance of two approaches for the control of a system of oscillating bodies.

With regard to the first objective, the systems considered are arrays composed of two and three devices, for a total of three layouts. Section 5.1 describes the dynamical model of the system while sec. 5.2.1 details its discretisation by means of the Fourier-Galerkin method.

The two approaches for the control of arrays of WECs that have been compared in this chapter are Global Control, which calculates the optimal control law using the full model of the array, and the Independent Control which, on the other hand, completely neglects the hydrodynamic interactions when calculating the solution to the optimal control problem.

The two control strategies have been compared in terms of the total absorbed energy, and the simulations have been carried out for a broad range of scenarios, obtained by considering several array layouts and inter-body distances, different geometries for the oscillating bodies, various sea states and wave incidence angles. As expected, GC always outperforms the IC, although they have similar performances when the hydrodynamic interaction between the devices are small, as in the case of large separation distances.

In real situations, it is often the case that the parameters of the control model change with time. Section 5.4 examines the sensitivity of the relative performance between the two control strategies with respect to position offsets for a system composed of two WECs where one device has been displaced from its nominal position. Simulation results have shown that GC is more sensitive to position offsets the the IC, with a significant reduction in performance in some situations.

The last part of this chapter details how to implement the constraints for both the GC and the IC strategies (sec. 5.6), and the simulation results in sec. 5.7 show that a restriction on the PTO force reduces the difference between the performance of the two controllers, on average, more than a restriction of the same relative magnitude on the oscillation amplitude. This could be due to the fact that the power radiated from a device depends on the total force applied to the device and its velocity; thus, a smaller force results in a smaller radiated power which, in turns, results in a smaller interaction that reduces the disadvantage of the IC.

Chapter 6

Geometrical interpretation of PTO constraints

The central theme of this thesis is the numerical optimal control of Wave Energy Converters. It has been shown in chapter 4 that the direct transcription of an optimal control problem results in a NLP problem, which is composed of a cost function describing the total absorbed energy and a set of constraints that model the dynamic of the WEC. Additional constraints have also been considered in chapters 4 and 5 to take into account of physical limitations of the mechanical components, such as the maximum oscillation amplitude and the maximum force which can be exerted by the PTO.

If the optimal control problem only includes one type of constraint (force or position), it is easy to see that a solution to the constrained NLP exists[1]; however, if both force and position constraints are included in the formulation of the optimal control problem, the feasibility is not guaranteed, i.e. it may not be possible to find a PTO force and the corresponding motion of the device which satisfy both the force and position constraints.

This chapter presents a procedure for the study of the feasibility problem which introduces a geometrical interpretation of force and position constraints, and of the expression for the total absorbed energy. Additionally, the approach presented here gives, in a particular case, a graphical answer which provides some insight into the interplay between the constraints and

[1] If only the force constraint is considered, then a feasible solution (non necessarily optimal), for any value of the maximum force $F_{max} > 0$, is $f_{pto}(t) = 0$ for $t \in [0, T]$. On the other hand, if only position constraints are considered, a feasible solution, for any value of the maximum oscillation amplitude Z_{pto}, is the PTO force that cancels the excitation force ($f_{pto} = -f_e$).

the excitation forces (i.e. the wave climate), placed against the background of the absorbed energy, providing a basis for the sensitivity analysis of the total absorbed energy with respect to each of the constraints.

The first step of the procedure consists of redefining the *hard* constraints on force and position (see sec. 4.2.2.2) with *soft* constraints using the 2-norm. The newly defined constraints, by means of Parseval's identity and properties relating different norms, can be interpreted as geometrical objects that bound the original constraints from above and below. The result is a set of expressions stating necessary/sufficient conditions for feasibility/infeasibility of the energy maximisation problem.

Section. 6.1 describes the model of the two body WEC used to illustrate the procedure, in addition to the direct transcription of the optimal control problem using the Fourier-Galerkin formulation; The derivation of the procedure, that is the main result of this chapter, is illustrated in sec. 6.2 , while a summary of the theoretical results is given in sec. 6.3. In sec. 6.4, the feasibility problem for a single body WEC is illustrated as a special case of the two body WEC; additionally, it is shown how the method can be applied to both types of device by using a unified formulation. When considering only one frequency at a time (sec. 6.5), the method gives a graphical perspective of the feasibility problem, which is illustrated in sec. 6.6 for both single and two body WECs.

6.1 Model of a self-reacting point absorber

The first device considered is a two body self-reacting point absorber, the motion of which is restricted to heave only, as depicted in fig. 6.1. The WEC is described in the time domain by Cummins equation in (4.23), which can be rewritten, for ease of reference, as the system

$$\mathrm{m}_1 \ddot{z}_1(t) - f_{r_1}(t) + \mathrm{B}_1 \dot{z}_1(t) + \mathrm{S}_1 z_1(t) = f_{e_1}(t) - f_{pto}(t) \tag{6.1}$$

$$\mathrm{m}_2 \ddot{z}_2(t) - f_{r_2}(t) + \mathrm{B}_2 \dot{z}_2(t) + \mathrm{S}_2 z_2(t) = f_{e_2}(t) + f_{pto}(t), \tag{6.2}$$

where (6.1) is the equation of motion of body 1 and (6.2) is the equation of motion of body 2. The vertical position of the i-th body is z_i ($i \in \{1, 2\}$), while, consistent with the notation adopted in this thesis, S_i is the hydrostatic stiffness coefficient, B_i is the linear friction coefficient, m_i is the mass, and f_{e_i} is the excitation force. The radiation forces f_{r_1} and f_{r_2} are

$$f_{r_1}(t) = -\mathrm{m}_{\infty_{11}} \ddot{z}_1(t) - \mathrm{K}_{11}(t) * \dot{z}_1(t) - \mathrm{m}_{\infty_{12}} \ddot{z}_2(t) - \mathrm{K}_{12}(t) * \dot{z}_2(t)$$

$$f_{r_2}(t) = -\mathrm{m}_{\infty_{22}} \ddot{z}_2(t) - \mathrm{K}_{22}(t) * \dot{z}_2(t) - \mathrm{m}_{\infty_{21}} \ddot{z}_1(t) - \mathrm{K}_{21}(t) * \dot{z}_1(t),$$

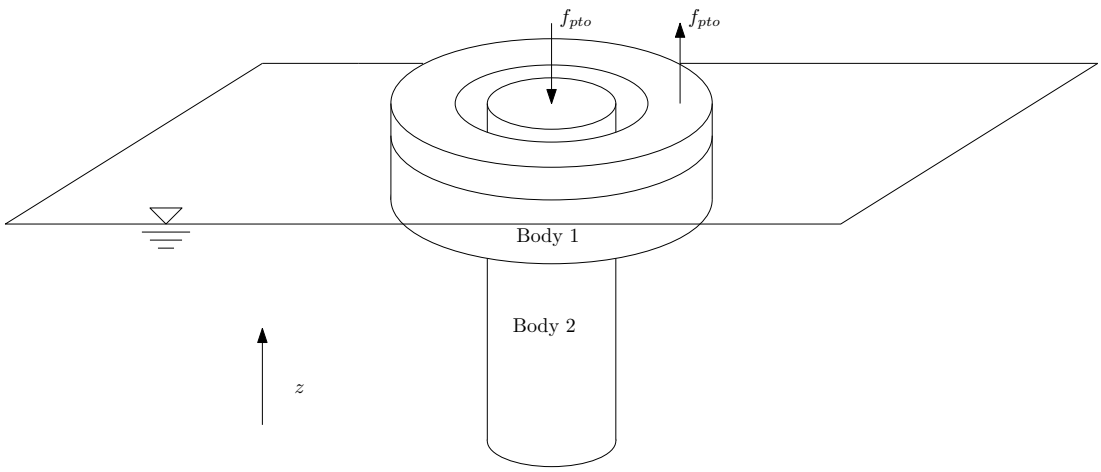

Figure 6.1: Self-reacting point absorber.

where the symbol $*$ denotes the convolution operator[2] and the coefficients K_{ij} and $\mathrm{m}_{\infty ij}$, with $i, j \in \{1, 2\}$, are, respectively, the radiation impulse responses and the asymptotic values of the added mass for $\omega \to \infty$. The PTO applies a force on both bodies with the same magnitude and opposite direction (see fig. 6.1), thus the same force f_{pto} appears in both equations (6.1) and (6.2) with the same magnitude and opposite sign.

As in the remainder of this thesis, the energy absorbed in the interval $[0, T]$, neglecting losses, corresponds to the work done by the PTO force , that is

$$J = -\int_0^T \left(v_2(t) - v_1(t)\right) f_{pto}(t)\, dt = -\int_0^T \boldsymbol{v}^T \mathbf{F}_p\, f_{pto}\, dt \tag{6.3}$$

where $\boldsymbol{v} = [v_1\ v_2]^T = [\dot{z}_1\ \dot{z}_2]^T$, and the PTO configuration matrix $\mathbf{F}_p$ is (see sec. 4.2.1.2)

$$\mathbf{F}_p = \begin{bmatrix} -1 \\ 1 \end{bmatrix}.$$

6.1.1 Discretisation

Since the discretisation of the equations of motion (6.1)– (6.2) is carried out by means of the Fourier-Galerkin method (sec. 4.2.2), the first step is to approximate the state variables, position and velocity, and the PTO force, using zero-mean truncated Fourier series with $N/2$ frequency components as

$$v_1(t) \approx v_1^N(t) = \Phi(t)\, \hat{\boldsymbol{x}}_1 \qquad\qquad v_2(t) \approx v_2^N(t) = \Phi(t)\, \hat{\boldsymbol{x}}_2 \tag{6.4}$$

$$f_{pto}(t) \approx f_{pto}^N(t) = \Phi(t)\, \hat{\boldsymbol{u}}. \tag{6.5}$$

[2] $f * g = \int_{-\infty}^{+\infty} f(t-\tau) g(\tau)\, d\tau$

where

$$\Phi(t) = \left[\cos(\omega_0 t), \sin(\omega_0 t), \dots, \cos\left(\frac{N}{2}\omega_0 t\right), \sin\left(\frac{N}{2}\omega_0 t\right)\right],$$

For the practical implementation of the method, it is also convenient to represent the excitation forces with a truncated Fourier series containing $N/2$ frequency components as

$$f_{e_1}(t) \approx f_{e_1}^N(t) = \Phi(t)\,\hat{\boldsymbol{e}}_1 \qquad f_{e_2}(t) \approx f_{e_2}^N(t) = \Phi(t)\,\hat{\boldsymbol{e}}_2. \tag{6.6}$$

The vectors $\hat{\boldsymbol{x}}_1, \hat{\boldsymbol{x}}_2 \in S^V \subseteq \mathbb{R}^N$, $\hat{\boldsymbol{u}} \in S^P \subseteq \mathbb{R}^N$ and $\hat{\boldsymbol{e}}_1, \hat{\boldsymbol{e}}_2 \in \mathbb{R}^N$ are defined as

$$\hat{\boldsymbol{x}}_1 = \left[x_{11}^c, x_{11}^s, x_{12}^c, x_{12}^s, \dots, x_{1\frac{N}{2}}^c, x_{1\frac{N}{2}}^s\right]^T \qquad \hat{\boldsymbol{x}}_2 = \left[x_{21}^c, x_{21}^s, x_{22}^c, x_{22}^s, \dots, x_{2\frac{N}{2}}^c, x_{i\frac{N}{2}}^s\right]^T$$
$$\hat{\boldsymbol{e}}_1 = \left[e_{11}^c, e_{11}^s, e_{12}^c, e_{12}^s, \dots, e_{1\frac{N}{2}}^c, e_{1\frac{N}{2}}^s\right]^T \qquad \hat{\boldsymbol{e}}_2 = \left[e_{21}^c, e_{21}^s, e_{22}^c, e_{22}^s, \dots, e_{2\frac{N}{2}}^c, e_{i\frac{N}{2}}^s\right]^T$$

$$\hat{\boldsymbol{u}} = \left[u_1^c, u_1^s, u_2^c, u_2^s, \dots, u_{\frac{N}{2}}^c, u_{\frac{N}{2}}^s\right]^T.$$

Since the differentiation matrix D_ϕ is invertible (see sec. 4.2.2), then the approximated positions can be expressed in terms of the velocity coefficients $\hat{\boldsymbol{x}}_1$ and $\hat{\boldsymbol{x}}_2$ as

$$z_1(t) \approx z_1^N(t) = \Phi(t)\,\mathrm{D}_\phi^{-1}\,\hat{\boldsymbol{x}}_1 \qquad z_2(t) \approx z_2^N(t) = \Phi(t)\,\mathrm{D}_\phi^{-1}\,\hat{\boldsymbol{x}}_2,$$

and the approximated equations of motion (6.1)– (6.2) in residual form are

$$\begin{aligned} r_1^N = &\left(\left(\mathrm{m}_1 + \mathrm{m}_{\infty_{11}}\right)\Phi\mathrm{D}_\phi + \mathrm{B}_1\Phi + \mathrm{S}_1\Phi\mathrm{D}_\phi^{-1} + \mathrm{K}_{11} * \Phi\right)\hat{\boldsymbol{x}}_1 - \Phi\hat{\boldsymbol{e}}_1 + \Phi\hat{\boldsymbol{u}} \\ &+ \left(\mathrm{m}_{\infty_{12}}\Phi\mathrm{D}_\phi\hat{\boldsymbol{x}}_+ \mathrm{K}_{12}(t) * \Phi\right)\hat{\boldsymbol{x}}_2 \\ r_2^N = &\left(\left(\mathrm{m}_2 + \mathrm{m}_{\infty_{22}}\right)\Phi\mathrm{D}_\phi + \mathrm{B}_2\Phi + \mathrm{S}_2\Phi\mathrm{D}_\phi^{-1} + \mathrm{K}_{22} * \Phi\right)\hat{\boldsymbol{x}}_2 - \Phi\hat{\boldsymbol{e}}_2 - \Phi\hat{\boldsymbol{u}} \\ &+ \left(\mathrm{m}_{\infty_{21}}\Phi\mathrm{D}_\phi\hat{\boldsymbol{x}}_+ \mathrm{K}_{21}(t) * \Phi\right)\hat{\boldsymbol{x}}_1. \end{aligned}$$

By applying the Galerkin method, that is by requiring the residuals r_1^N and r_2^N to be orthogonal to all the elements ϕ_j of the basis vector Φ as

$$\begin{aligned} &\langle r_1^N, \phi_j\rangle = 0 \\ &\langle r_2^N, \phi_j\rangle = 0, \qquad\qquad j = 1, \dots, N \end{aligned}$$

the result is the linear system

$$\begin{bmatrix} \mathbf{G}_{11} & \mathbf{G}_{22} \\ \mathbf{G}_{21} & \mathbf{G}_{22} \end{bmatrix} \begin{bmatrix} \hat{\boldsymbol{x}}_1 \\ \hat{\boldsymbol{x}}_2 \end{bmatrix} = \begin{bmatrix} -\mathbf{I}_N \\ \mathbf{I}_N \end{bmatrix} \hat{\boldsymbol{u}} + \begin{bmatrix} \hat{\boldsymbol{e}}_1 \\ \hat{\boldsymbol{e}}_2 \end{bmatrix}, \tag{6.7}$$

where $\mathbf{I}_N$ is the identity matrix of size N. The matrices $\mathbf{G}_{ij}$ are given by

$$\mathbf{G}^{ij} = \begin{bmatrix} \mathrm{D}_{ij}^1 & \mathrm{M}_{ij}^1 & 0 & \cdots & 0 & 0 \\ -\mathrm{M}_{ij}^1 & \mathrm{D}_{ij}^1 & 0 & \cdots & 0 & 0 \\ 0 & 0 & \ddots & & \vdots & \vdots \\ \vdots & \vdots & & \ddots & 0 & 0 \\ 0 & 0 & \cdots & 0 & \mathrm{D}_{ij}^{N/2} & \mathrm{M}_{ij}^{N/2} \\ 0 & 0 & \cdots & 0 & -\mathrm{M}_{ij}^{N/2} & \mathrm{D}_{ij}^{N/2} \end{bmatrix}, \tag{6.8}$$

with $i, j=\{1, 2\}$, and where

$$\begin{cases} \mathrm{D}_{ii}^l = \mathrm{R}_{ii}(l\omega_0) + \mathrm{B}_i \\ \mathrm{M}_{ii}^l = l\omega_0 \left(\mathrm{m}_i + \mathrm{m}_{ii}(l\omega_0)\right) - \mathrm{S}_i/(l\omega_0) \end{cases} \quad \text{for } i = j$$

$$\begin{cases} \mathrm{D}_{ii}^l = \mathrm{R}_{ii}(l\omega_0) \\ \mathrm{M}_{ii}^l = l\omega_0 \mathrm{m}_{ii}(l\omega_0) \end{cases} \quad \text{for } i \neq j.$$

for $l = 1, \ldots, N/2$. It has to be noted that $\mathbf{G}_{12} = \mathbf{G}_{21}$ because the radiation impedance matrix is symmetric (see sec. 2.2.2.2).

The sparsity pattern of the matrix $\mathbf{G}$ is depicted in fig. 6.2; as for the case of arrays of WECs described in sec. 5.2.1, $\mathbf{G}$ has a *multi-diagonal* structure. The matrix $\mathbf{G}$ can be transformed into the equivalent block diagonal matrix $\bar{\mathbf{G}}$, the sparsity pattern of which is depicted in fig. 6.3, by rearranging rows and columns. The rows and columns of $\mathbf{G}$ can be rearranged by pre- and post-multiplication to a suitable permutation matrix $\mathbf{P}$ [238], that is $\bar{\mathbf{G}} = \mathbf{P}\,\mathbf{G}\,\mathbf{P}^T$, and each of the 4×4 blocks on the diagonal of $\bar{\mathbf{G}}$ is of the form

$$\bar{\mathbf{G}}^l = \begin{bmatrix} \mathrm{D}_{11}^l & \mathrm{M}_{11}^l & \mathrm{D}_{12}^l & \mathrm{M}_{12}^l \\ \mathrm{D}_{11}^l & -\mathrm{M}_{11}^l & \mathrm{D}_{12}^l & -\mathrm{M}_{12}^l \\ \mathrm{D}_{21}^l & \mathrm{M}_{21}^l & \mathrm{D}_{22}^l & \mathrm{M}_{22}^l \\ \mathrm{D}_{21}^l & -\mathrm{M}_{21}^l & \mathrm{D}_{22}^l & -\mathrm{M}_{22}^l \end{bmatrix}. \tag{6.9}$$

The benefit of this transformation is that each matrix $\bar{\mathbf{G}}^l$ corresponds to the frequency $l\omega_0$ and, since permutation matrices are nonsingular, the matrix $\mathbf{G}$ is invertible if all the blocks $\bar{\mathbf{G}}^l$ are nonsingular. In other words, the singularity of the matrix $\mathbf{G}$ can be checked independently for each frequency $l\omega_0$ by checking the singularity of the blocks $\bar{\mathbf{G}}^l$; this procedure could be useful to verify, for example, the presence of resonance-related issues, as a nearly singular $\mathbf{G}$ indicates that very large velocities are obtained by small forces.

The inverse of $\mathbf{G}$, if it exists, can be calculated by inverting $\mathbf{G}_{22}$ and its Schur complement,

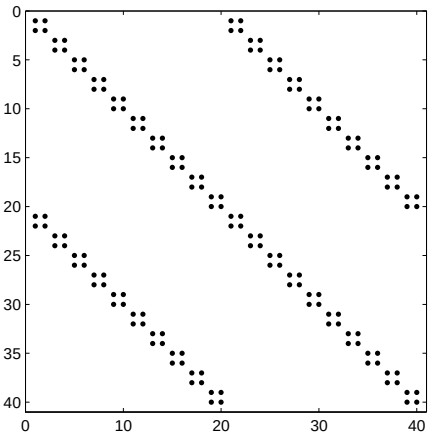

Figure 6.2: Sparsity pattern of the matrix $\mathbf{G}$ with 10 frequency components ($N = 20$).

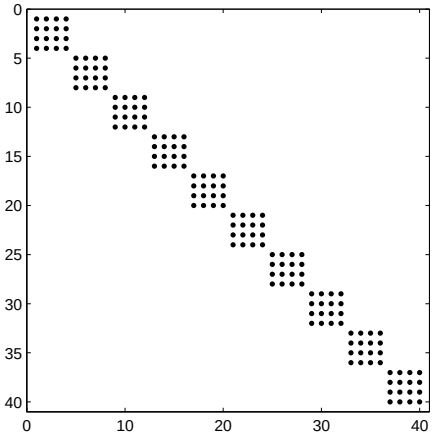

Figure 6.3: Sparsity pattern of the matrix $\bar{\mathbf{G}}$.

which is $\left(\mathbf{G}_{11} - \mathbf{G}_{12}\mathbf{G}_{22}^{-1}\mathbf{G}_{21}\right)$, as [238]

$$\begin{aligned}\mathbf{G}^{-1} &= \begin{bmatrix} \left(\mathbf{G}_{11} - \mathbf{G}_{12}\mathbf{G}_{22}^{-1}\mathbf{G}_{21}\right)^{-1} & -\left(\mathbf{G}_{11} - \mathbf{G}_{12}\mathbf{G}_{22}^{-1}\mathbf{G}_{21}\right)^{-1}\mathbf{G}_{12}\mathbf{G}_{22}^{-1} \\ -\mathbf{G}_{22}^{-1}\mathbf{G}_{21}\left(\mathbf{G}_{11} - \mathbf{G}_{12}\mathbf{G}_{22}^{-1}\mathbf{G}_{21}\right)^{-1} & \mathbf{G}_{22}^{-1} + \mathbf{G}_{22}^{-1}\mathbf{G}_{21}\left(\mathbf{G}_{11} - \mathbf{G}_{12}\mathbf{G}_{22}^{-1}\mathbf{G}_{21}\right)^{-1}\mathbf{G}_{12}\mathbf{G}_{22}^{-1} \end{bmatrix} \\ &= \begin{bmatrix} \mathbf{H}_{11} & \mathbf{H}_{12} \\ \mathbf{H}_{21} & \mathbf{H}_{22} \end{bmatrix} \end{aligned} \tag{6.10}$$

The total absorbed energy in (6.3), using the approximations in (6.4)– (6.6), becomes

$$\begin{aligned} J &= -\int_0^T \Phi(t)\begin{bmatrix}\hat{\boldsymbol{x}}_1 & \hat{\boldsymbol{x}}_2\end{bmatrix}\mathbf{F}_p\,\hat{\boldsymbol{u}}^T\,\Phi(t)^T\,dt = -\int_0^T \left(\hat{\boldsymbol{x}}_1 - \hat{\boldsymbol{x}}_2\right)^T\Phi(t)^T\Phi(t)\,\hat{\boldsymbol{u}}\,dt \\ &= -\left(\hat{\boldsymbol{x}}_1 - \hat{\boldsymbol{x}}_2\right)^T\boldsymbol{\Gamma}\,\hat{\boldsymbol{u}} \\ &= -\frac{T}{2}\left(\hat{\boldsymbol{x}}_1 - \hat{\boldsymbol{x}}_2\right)^T\,\hat{\boldsymbol{u}}, \end{aligned} \tag{6.11}$$

where the matrix $\boldsymbol{\Gamma}$, defined in (4.52), is $\boldsymbol{\Gamma} = \frac{T}{2}\mathbf{I}_N$. The vector $\hat{\boldsymbol{x}}_1 - \hat{\boldsymbol{x}}_2$ can be expressed in terms of the excitation and the PTO forces by using the definition of the inverse of $\mathbf{G}$ in (6.10) (for the WECs considered in this chapter it has been verified that $\mathbf{G}^{-1}$ exists). Multiplying both sides of (6.7) by $\mathbf{G}^{-1}$, the result is

$$\begin{bmatrix}\hat{\boldsymbol{x}}_1 \\ \hat{\boldsymbol{x}}_2\end{bmatrix} = \begin{bmatrix}\mathbf{H}_{11} & \mathbf{H}_{12} \\ \mathbf{H}_{21} & \mathbf{H}_{22}\end{bmatrix}\left(\begin{bmatrix}-\mathbf{I}_N \\ \mathbf{I}_N\end{bmatrix}\hat{\boldsymbol{u}} + \begin{bmatrix}\hat{\boldsymbol{e}}_1 \\ \hat{\boldsymbol{e}}_2\end{bmatrix}\right). \tag{6.12}$$

Once again, by multiplying both sides of (6.12) by the matrix $[\mathbf{I}_N \ -\mathbf{I}_N]$, that is

$$\begin{bmatrix}\mathbf{I}_N & -\mathbf{I}_N\end{bmatrix}\begin{bmatrix}\hat{\boldsymbol{x}}_1\\ \hat{\boldsymbol{x}}_2\end{bmatrix} = \begin{bmatrix}\mathbf{I}_N & -\mathbf{I}_N\end{bmatrix}\begin{bmatrix}\mathbf{H}_{11} & \mathbf{H}_{12}\\ \mathbf{H}_{21} & \mathbf{H}_{22}\end{bmatrix}\left(\begin{bmatrix}-\mathbf{I}_N\\ \mathbf{I}_N\end{bmatrix}\hat{\boldsymbol{u}} + \begin{bmatrix}\hat{\boldsymbol{e}}_1\\ \hat{\boldsymbol{e}}_2\end{bmatrix}\right),$$

the vector $\hat{\boldsymbol{x}}_1 - \hat{\boldsymbol{x}}_2$ is

$$\begin{aligned}\hat{\boldsymbol{x}}_1 - \hat{\boldsymbol{x}}_2 &= -\left(\mathbf{H}_{11} + \mathbf{H}_{22} - \mathbf{H}_{12} - \mathbf{H}_{21}\right)\hat{\boldsymbol{u}} + \left(\mathbf{H}_{11} - \mathbf{H}_{12}\right)\hat{\boldsymbol{e}}_1 + \left(\mathbf{H}_{22} - \mathbf{H}_{21}\right)\hat{\boldsymbol{e}}_2\\ &= -\mathbf{H}\,\hat{\boldsymbol{u}} + \mathbf{Q}_1\hat{\boldsymbol{e}}_1 - \mathbf{Q}_2\hat{\boldsymbol{e}}_2\\ &= -\mathbf{H}\,\hat{\boldsymbol{u}} + \mathbf{Q},\end{aligned} \tag{6.13}$$

where

$$\mathbf{H} = \mathbf{H}_{11} + \mathbf{H}_{22} - \mathbf{H}_{12} - \mathbf{H}_{21} \tag{6.14}$$

$$\mathbf{Q}_1 = \mathbf{H}_{11} - \mathbf{H}_{12} \qquad\qquad \mathbf{Q}_2 = \mathbf{H}_{22} - \mathbf{H}_{21}$$

and

$$\mathbf{Q} = \left(\mathbf{H}_{11} - \mathbf{H}_{12}\right)\hat{\boldsymbol{e}}_1 + \left(\mathbf{H}_{22} - \mathbf{H}_{21}\right)\hat{\boldsymbol{e}}_2. \tag{6.15}$$

The total absorbed energy in (6.11) , by using (6.13), becomes the quadratic function of the variable $\hat{\boldsymbol{u}}$:

$$J = -\frac{T}{2}\hat{\boldsymbol{u}}^T\,\mathbf{H}\hat{\boldsymbol{u}} + \frac{T}{2}\hat{\boldsymbol{u}}^T\left(\mathbf{Q}_1\hat{\boldsymbol{e}}_1 - \mathbf{Q}_2\hat{\boldsymbol{e}}_2\right) = -\frac{T}{2}\hat{\boldsymbol{u}}^T\,\mathbf{H}\hat{\boldsymbol{u}} + \frac{T}{2}\hat{\boldsymbol{u}}^T\mathbf{Q}. \tag{6.16}$$

It can be verified numerically, for the devices considered in this chapter, that the symmetric part of the matrix $\mathbf{H}$ (i.e. $(\mathbf{H}+\mathbf{H}^T)/2$) is positive definite; therefore, the quadratic cost function in (6.16) is concave and the global maximum of the total absorbed energy, for the unconstrained problem, is obtained for the control vector $\hat{\boldsymbol{u}}^*$ calculated as

$$\hat{\boldsymbol{u}}^* = \left(\mathbf{H}+\mathbf{H}^T\right)^{-1}\left(\mathbf{Q}_1\hat{\boldsymbol{e}}_1 - \mathbf{Q}_2\hat{\boldsymbol{e}}_2\right) = \left(\mathbf{H}+\mathbf{H}^T\right)^{-1}\mathbf{Q}. \tag{6.17}$$

6.2 Specification and approximation of constraints

In this chapter, the constraints on the PTO force and on the oscillation amplitude are defined in a slightly different manner than the definitions provided in sec. 4.2.2.2. In particular, the

constraints are specified in terms of the maximum (max)-norm[3] $\|\cdot\|_\infty$, defined as

$$\left\|g\right\|_\infty = \max_{t\in[0,T]} |g(t)|; \tag{6.18}$$

thus the PTO force constraint is defined as

$$\left\|f_{pto}^N\right\|_\infty \leq \mathrm{F}_{max}, \tag{6.19}$$

while the constraint on the relative oscillation amplitude is

$$\left\|z_1^N - z_2^N\right\|_\infty = \left\|\Delta z^N\right\|_\infty \leq \Delta \mathrm{Z}_{max}. \tag{6.20}$$

It is immediate to verify that the definitions in (6.19) and (6.20) are equivalent to the definitions stated previously in sec. 4.2.2.2, specifically in (4.67) and in (4.68).

6.2.1 Constraint approximation

While the max-norm describes how the constraints are actually specified, i.e. in terms of absolute limits, the max-norm is not the easiest to manipulate mathematically and does not easily lead to geometric interpretation. The following results allows the redefinition of the constraint conditions in terms of the 2-norm, which is more convenient to use. In particular, the 2-norm $\|g\|_2$ of a function $g(t)$ is defined as

$$\left\|g\right\|_2 = \left(\int_0^T |g(t)|^2 dt\right)^{1/2}. \tag{6.21}$$

A general property relating the 2-norm and the max-norm of a function g, for which the norms defined by eq. (6.18) and eq. (6.21) exists, is [239] (p.229)

$$\left\|g\right\|_2 \leq \sqrt{T}\left\|g\right\|_\infty. \tag{6.22}$$

Additionally, for a zero mean Fourier series with $N/2$ frequency components (g^N) and a fundamental frequency $\omega_0 = 2\pi/T$, the inequality [239]

$$\left\|g^N\right\|_\infty \leq \sqrt{\frac{N}{T}}\left\|g^N\right\|_2 \tag{6.23}$$

provides an upper bound for the max-norm as a function of the 2-norm.

By using the inequality in (6.23), it is possible to find sufficient conditions for the *satisfac-*

[3]This norm is also called maximum norm, supremum norm and uniform norm. The general definition of the norm is specified in with the supremum (sup) in place of the maximum (max); however, the velocity and the PTO forces are assumed to be continuous in $[0, T]$ (they are Fourier series), thus the maximum replaces the supremum.

tion of the inequalities in (6.19) and (6.20) in terms of the 2-norm, (6.21), namely

$$\left\|f_{pto}^{N}\right\|_{\infty} \leq \sqrt{\frac{N}{T}}\left\|f_{pto}^{N}\right\|_{2} \leq \mathrm{F}_{max}, \tag{6.24}$$

$$\left\|\Delta z^{N}\right\|_{\infty} \leq \sqrt{\frac{N}{T}}\left\|\Delta z^{N}\right\|_{2} \leq \Delta \mathrm{Z}_{max}. \tag{6.25}$$

Inequalities (6.24) and (6.25) specify the 2-norm scaled by $\sqrt{N/T}$ as an upper bound for the max-norm, meaning that if the 2-norm of the force or oscillation amplitude is smaller than the maximum allowed value (F_{max} and $\Delta\mathrm{Z}_{max}$, respectively), then the original constraint in (6.19) or in (6.20) (defined in terms of the max-norm) is also satisfied.

Sufficient conditions for the *violation* of at least one of the constraints, also in terms of the 2-norm, can be obtained using the inequality in (6.22), that is

$$\left\|f_{pto}^{N}\right\|_{\infty} \geq 1/\sqrt{T}\left\|f_{pto}^{N}\right\|_{2} \geq \mathrm{F}_{max} \tag{6.26}$$

$$\left\|\Delta z^{N}\right\|_{\infty} \geq 1/\sqrt{T}\left\|\Delta z^{N}\right\|_{2} \geq \Delta \mathrm{Z}_{max}. \tag{6.27}$$

Thus, the inequalities (6.26) and (6.27) show that the 2-norm, scaled by $1/\sqrt{T}$, provides a lower bound for the max-norm; in other words, if the 2-norm multiplied by $1/\sqrt{T}$ violates a constraint, then the max-norm also violates it.

6.2.2 Calculation of the approximated constraints

The 2-norm of the PTO force constraint is immediately calculated by applying Parseval's identity, resulting in

$$\left\|f_{pto}^{N}\right\|_{2}^{2} = \int_{0}^{T}\left(f_{pto}^{N}(t)\right)^{2}\,dt = \frac{T}{2}\sum_{k=1}^{N/2}\left(u_{k}^{c}\right)^{2} + \left(u_{k}^{c}\right)^{2} = \frac{T}{2}\hat{\boldsymbol{u}}^{T}\hat{\boldsymbol{u}}. \tag{6.28}$$

By noting that

$$\Delta z^{N} = z_{1}^{N} - z_{2}^{N} = \Phi(t)\mathrm{D}_{\phi}^{-1}\hat{\boldsymbol{x}}_{1} - \Phi(t)\mathrm{D}_{\phi}^{-1}\hat{\boldsymbol{x}}_{2} = \Phi(t)\mathrm{D}_{\phi}^{-1}\left(\hat{\boldsymbol{x}}_{1} - \hat{\boldsymbol{x}}_{2}\right),$$

the 2-norm of the relative oscillation amplitude constraint is,

$$\begin{aligned}
\left\|\Delta z^{N}\right\|_{2}^{2} &= \int_{0}^{T}\left(z^{N}(t)\right)^{2}\,dt = \int_{0}^{T}\left(\Phi(t)\mathrm{D}_{\phi}^{-1}\left(\hat{\boldsymbol{x}}_{1} - \hat{\boldsymbol{x}}_{2}\right)\right)^{T}\left(\Phi(t)\mathrm{D}_{\phi}^{-1}\left(\hat{\boldsymbol{x}}_{1} - \hat{\boldsymbol{x}}_{2}\right)\right)\,dt \\
&= \left(\hat{\boldsymbol{x}}_{1} - \hat{\boldsymbol{x}}_{2}\right)^{T}\mathrm{D}_{\phi}^{-T}\int_{0}^{T}\Phi(t)^{T}\Phi(t)\,dt\mathrm{D}_{\phi}^{-1}\left(\hat{\boldsymbol{x}}_{1} - \hat{\boldsymbol{x}}_{2}\right) \\
&= \left(\hat{\boldsymbol{x}}_{1} - \hat{\boldsymbol{x}}_{2}\right)^{T}\mathrm{D}_{\phi}^{-T}\boldsymbol{\Gamma}\,\mathrm{D}_{\phi}^{-1}\left(\hat{\boldsymbol{x}}_{1} - \hat{\boldsymbol{x}}_{2}\right)
\end{aligned}$$

$$= \frac{T}{2} \left(\hat{\boldsymbol{x}}_1 - \hat{\boldsymbol{x}}_2 \right)^T \mathbf{W}^2 \left(\hat{\boldsymbol{x}}_1 - \hat{\boldsymbol{x}}_2 \right), \tag{6.29}$$

where $\boldsymbol{\Gamma} = \frac{T}{2}\mathbf{I}_N$ and the matrix $\mathbf{W} = \mathrm{D}_{\phi}^{-T}\,\boldsymbol{\Gamma}\,\mathrm{D}_{\phi}^{-1}$ is:

$$\mathbf{W} = \begin{bmatrix} 1/\omega_0 & 0 & \cdots & 0 & 0 \\ 0 & 1/\omega_0 & \cdots & 0 & 0 \\ \vdots & \vdots & \ddots & \vdots & \vdots \\ 0 & 0 & \cdots & 2/N\omega_0 & 0 \\ 0 & 0 & \cdots & 0 & 2/N\omega_0 \end{bmatrix}. \tag{6.30}$$

Using equation (6.13), the 2-norm of the amplitude constraint in (6.29) can be written as a function of the vector $\hat{\boldsymbol{u}}$:

$$\begin{aligned} \left\| \Delta z^N \right\|_2^2 &= \frac{T}{2} \left(-\mathbf{H}\,\hat{\boldsymbol{u}} + \mathbf{Q} \right)^T \mathbf{W} \left(-\mathbf{H}\,\hat{\boldsymbol{u}} + \mathbf{Q} \right) \\ &= \frac{T}{2} \Big(\hat{\boldsymbol{u}}^T \mathbf{H}^T \mathbf{W}^2 \mathbf{H}\,\hat{\boldsymbol{u}} - 2\,\mathbf{Q}^T \mathbf{W}^2 \mathbf{H}\,\hat{\boldsymbol{u}} + \mathbf{Q}^T \mathbf{W}^2 \mathbf{Q} \Big). \end{aligned} \tag{6.31}$$

Equations (6.28) and (6.31) show the main reason why the 2-norm is more tractable than the max-norm: the 2-norm of both the PTO force and the relative position can be written as quadratic functions of the sole variable $\hat{\boldsymbol{u}}$.

Substituting equations (6.28) and (6.31) into inequalities (6.24) and (6.25) and rearranging, sufficient conditions for satisfaction of the constraints are:

$$\hat{\boldsymbol{u}}^T \hat{\boldsymbol{u}} \leq \frac{2}{N} \mathrm{F}_{max}^2, \tag{6.32}$$

and

$$\hat{\boldsymbol{u}}^T \mathbf{H}^T \mathbf{W}^2 \mathbf{H}\,\hat{\boldsymbol{u}} - 2\,\mathbf{Q}^T \mathbf{W}^2 \mathbf{H}\,\hat{\boldsymbol{u}} + \mathbf{Q}^T \mathbf{W}^2 \mathbf{Q} \leq \frac{2}{N} \Delta \mathrm{Z}_{max}^2, \tag{6.33}$$

while the sufficient conditions for violation of the constraints are:

$$\hat{\boldsymbol{u}}^T \hat{\boldsymbol{u}} \geq 2\mathrm{F}_{max}^2 \tag{6.34}$$

and

$$\hat{\boldsymbol{u}}^T \mathbf{H}^T \mathbf{W}^2 \mathbf{H}\,\hat{\boldsymbol{u}} - 2\,\mathbf{Q}^T \mathbf{W}^2 \mathbf{H}\,\hat{\boldsymbol{u}} + \mathbf{Q}^T \mathbf{W}^2 \mathbf{Q} \geq 2\Delta \mathrm{Z}_{max}^2. \tag{6.35}$$

Inequalities (6.32)–(6.35) describe the constraints as a function of the PTO force only, in terms of the vector $\hat{\boldsymbol{u}}$, for given excitations $\hat{\boldsymbol{e}}_1$ and $\hat{\boldsymbol{e}}_2$, contained in the vector $\mathbf{Q}$.

6.2.3 Geometrical interpretation

The expressions of both the absorbed energy and the constraints can be viewed as geometric entities. In fact, the energy absorbed by the WEC in (6.16) can be considered as a paraboloid in an $N+1$ dimensional space centred in $\hat{\boldsymbol{u}}^*$ (6.17). Furthermore, the feasibility of the constrained energy maximisation problem can be studied by first defining the sets

$$S_f(R_f) = \left\{\hat{\boldsymbol{u}} : \hat{\boldsymbol{u}}^T\hat{\boldsymbol{u}} \leq R_f\right\}$$

and

$$S_z(R_z) = \left\{\hat{\boldsymbol{u}} : \hat{\boldsymbol{u}}^T\mathbf{H}^T\mathbf{W}^2\mathbf{H}\hat{\boldsymbol{u}} - 2\,\mathbf{Q}^T\mathbf{W}^2\mathbf{H}\hat{\boldsymbol{u}} + \mathbf{Q}^T\mathbf{W}^2\mathbf{Q} \leq R_z\right\}. \tag{6.36}$$

It follows that a sufficient condition for the satisfaction of both the force and the amplitude constraints described by inequalities (6.19) and (6.20) is

$$S_f\left(\frac{2}{N}\mathrm{F}_{max}^2\right) \cap S_z\left(\frac{2}{N}\Delta\mathrm{Z}_{max}^2\right) \neq \varnothing, \tag{6.37}$$

which means that, if the (2-norm) lower bounds on the force and amplitude constraints intersect, then there is a feasible solution for force and amplitude within the constraints. Clearly, from eq. (6.24)–(6.25), the condition in (6.37) is slightly conservative, since the sets corresponding to the max-norms may intersect, even if those corresponding to the 2-norms do not.

From the upper bound on the max-norm in (6.22), it is possible to specify a sufficient condition for the violation of at least one of the constraints in (6.19) or (6.20) as

$$S_f\left(2\mathrm{F}_{max}^2\right) \cap S_z\left(2\Delta\mathrm{Z}_{max}^2\right) = \varnothing. \tag{6.38}$$

The force constraint defined by the set $S_f(R_f)$ can be interpreted as the region of the N-dimensional space S^P enclosed by the *hypersphere* centred at the origin and of radius $\sqrt{R_f}$. The amplitude constraint $S_z(R_z)$ is the region of the space enclosed by the *hyperellipsoid* with axes parallel to the elements of the basis of S^P, because the matrix $\mathbf{H}^T\mathbf{W}^2\mathbf{H}$ is diagonal and has all positive elements. The centre $\boldsymbol{z}_c$ of the hyperellipsoid is

$$\boldsymbol{z}_c = \mathbf{H}^{-1}\mathbf{Q} = \mathbf{H}^{-1}\left(\mathbf{Q}_1\hat{\boldsymbol{e}}_1 - \mathbf{Q}_2\hat{\boldsymbol{e}}_2\right), \tag{6.39}$$

while the radii r_i are given by

$$r_i = \sqrt{\frac{R_z}{\lambda_i}}, \tag{6.40}$$

and λ_i are the eigenvalues of $\mathbf{H}^T\mathbf{W}^2\mathbf{H}$, i.e. the diagonal elements.

Equation (6.37) states that if the intersection between the hypersphere describing the force

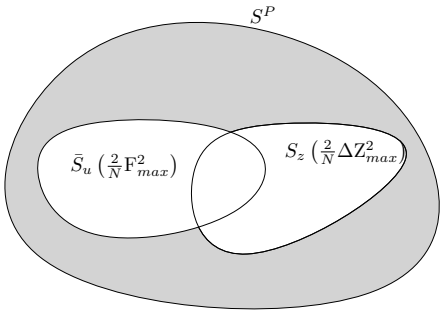

Figure 6.4: Sufficient condition for feasibility

constraint and the hyperellipsoid describing the amplitude constraint is not the empty set, then, for the given excitation forces, the device is able to satisfy both the amplitude and the force constraints. Conversely, equation (6.38) states that if the intersection between the two sets is the empty set, then at least one constraint will be violated.

6.3 Summary of the theoretical results

6.3.1 Sufficient condition for feasibility

The sufficient condition for feasibility of the energy maximisation problem is stated as: there exists a $\hat{\boldsymbol{u}} \in S^P$ such that $\hat{\boldsymbol{u}}$ satisfies both force and relative position constraints, which is equivalent to say that there is some $\hat{\boldsymbol{u}}$ that satisfies both inequalities

$$\begin{cases} \hat{\boldsymbol{u}}^T\hat{\boldsymbol{u}} \leq \dfrac{2}{N}\mathrm{F}^2_{max} \\ \hat{\boldsymbol{u}}^T\mathbf{H}^T\mathbf{W}^2\mathbf{H}\hat{\boldsymbol{u}} - 2\,\mathbf{Q}^T\mathbf{W}^2\mathbf{H}\hat{\boldsymbol{u}} + \mathbf{Q}^T\mathbf{W}^2\mathbf{Q} \leq \dfrac{2}{N}\Delta Z^2_{max}. \end{cases} \tag{6.41}$$

The sufficient condition in (6.41) can be expressed using sets, by saying that the intersection between the sets

$$S_f\left(\frac{2}{N}\mathrm{F}^2_{max}\right) = \left\{\hat{\boldsymbol{u}} : \hat{\boldsymbol{u}}^T\hat{\boldsymbol{u}} \leq \frac{2}{N}\mathrm{F}^2_{max}\right\}$$

and

$$S_z\left(\frac{2}{N}\Delta Z^2_{max}\right) = \left\{\hat{\boldsymbol{u}} : \hat{\boldsymbol{u}}^T\mathbf{H}^T\mathbf{W}^2\mathbf{H}\hat{\boldsymbol{u}} - 2\,\mathbf{Q}^T\mathbf{W}^2\mathbf{H}\hat{\boldsymbol{u}} + \mathbf{Q}^T\mathbf{W}^2\mathbf{Q} \leq \frac{2}{N}\Delta Z^2_{max}\right\}$$

is not empty, that is

$$\boxed{S_f\left(\frac{2}{N}\mathrm{F}^2_{max}\right) \cap S_z\left(\frac{2}{N}\Delta Z^2_{max}\right) \neq \varnothing \qquad \Rightarrow \qquad \text{Feasible}}, \tag{6.42}$$

which is also illustrated by fig. 6.4.

6.3.2 Necessary condition for infeasibility

The law of contraposition says that the two statements "$A \Rightarrow B$" and "$\neg A \Leftarrow \neg B$" are equivalent, i.e.

$$A \Rightarrow B \qquad \equiv \qquad \neg A \Leftarrow \neg B \tag{6.43}$$

where $\neg$ is the logic negation. By applying the equivalence (6.43) to the statement in (6.42), it is possible to find the necessary condition for infeasibility, which is

$$\neg \left(S_f \left(\frac{2}{N} \mathrm{F}_{max}^2 \right) \cap S_z \left(\frac{2}{N} \Delta \mathrm{Z}_{max}^2 \right) \neq \varnothing \right) \qquad \Leftarrow \qquad \neg \, \text{Feasible}$$

resulting in

$$\boxed{S_f \left(\frac{2}{N} \mathrm{F}_{max}^2 \right) \cap S_z \left(\frac{2}{N} \Delta \mathrm{Z}_{max}^2 \right) = \varnothing \qquad \Leftarrow \qquad \text{Non feasible}}.$$

In other words, if the problem is not feasible, then no $\hat{\boldsymbol{u}}$ exists which belongs to $S_f \left(\frac{2}{N} \mathrm{F}_{max}^2 \right)$ and $S_z \left(\frac{2}{N} \Delta \mathrm{Z}_{max}^2 \right)$ at the same time.

6.3.3 Sufficient condition for infeasibility

The sufficient condition for infeasibility is that any vector $\hat{\boldsymbol{u}} \in S^P$ violates at least one constraint, and it can be specified by saying that at least one of the inequalities

$$\hat{\boldsymbol{u}}^T \hat{\boldsymbol{u}} > 2 \, \mathrm{F}_{max}^2$$

or

$$\hat{\boldsymbol{u}}^T \mathbf{H}^T \mathbf{W}^2 \mathbf{H} \hat{\boldsymbol{u}} - 2 \, \mathbf{Q}^T \mathbf{W}^2 \mathbf{H} \hat{\boldsymbol{u}} + \mathbf{Q}^T \mathbf{W}^2 \mathbf{Q} > 2 \, \Delta \mathrm{Z}_{max}^2$$

are true. Using sets, the sufficient condition for infeasibility can be reformulated by saying that the union between the sets

$$\bar{S}_f \left(2 \, \mathrm{F}_{max}^2 \right) = \left\{ \hat{\boldsymbol{u}} \, : \, \hat{\boldsymbol{u}}^T \hat{\boldsymbol{u}} > 2 \, \mathrm{F}_{max}^2 \right\}$$

and

$$\bar{S}_z \left(2 \, \Delta \mathrm{Z}_{max}^2 \right) = \left\{ \hat{\boldsymbol{u}} \, : \, \hat{\boldsymbol{u}}^T \mathbf{H}^T \mathbf{W}^2 \mathbf{H} \hat{\boldsymbol{u}} - 2 \, \mathbf{Q}^T \mathbf{W}^2 \mathbf{H} \hat{\boldsymbol{u}} + \mathbf{Q}^T \mathbf{W}^2 \mathbf{Q} > \, 2 \, \Delta \mathrm{Z}_{max}^2 \right\}$$

is the set S^P, that is:

$$\bar{S}_f \left(2 \, \mathrm{F}_{max}^2 \right) \cup \bar{S}_z \left(2 \, \Delta \mathrm{Z}_{max}^2 \right) = S^P \qquad \Rightarrow \qquad \text{Non feasible;}$$

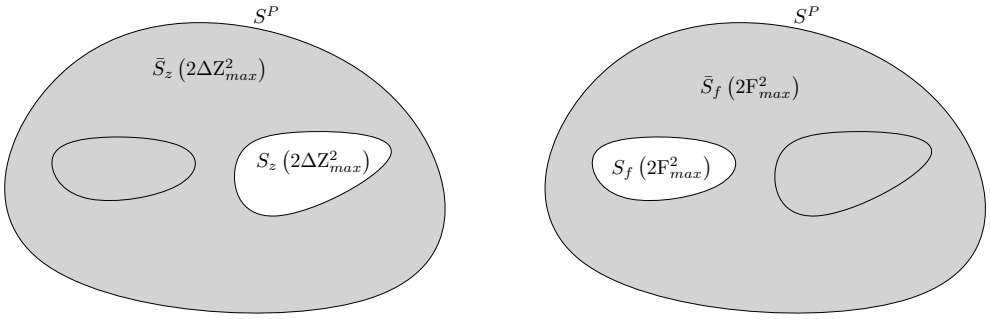

Figure 6.5: Sufficient condition for non feasibility

figure 6.5 graphically illustrates the situation. Using De Morgan's law ($\overline{A \cup B} = \bar{A} \cap \bar{B}$), the previous expression becomes:

$$\overline{S_f\left(2\,\mathrm{F}^2_{max}\right) \cap S_z\left(2\,\Delta\mathrm{Z}^2_{max}\right)} = S^P \qquad \Rightarrow \qquad \text{Infeasibility}$$

which is equivalent to

$$\boxed{S_f\left(2\,\mathrm{F}^2_{max}\right) \cap S_z\left(2\,\Delta\mathrm{Z}^2_{max}\right) = \varnothing \qquad \Rightarrow \qquad \text{Infeasibility}}, \tag{6.44}$$

where

$$S_f\left(2\,\mathrm{F}^2_{max}\right) = \left\{\hat{\boldsymbol{u}} : \hat{\boldsymbol{u}}^T\hat{\boldsymbol{u}} \leq 2\,\mathrm{F}^2_{max}\right\}$$

and

$$S_z\left(2\,\Delta Z^2_{max}\right) = \left\{\hat{\boldsymbol{u}} : \hat{\boldsymbol{u}}^T\mathbf{H}^T\mathbf{W}^2\mathbf{H}\hat{\boldsymbol{u}} - 2\,\mathbf{Q}^T\mathbf{W}^2\mathbf{H}\hat{\boldsymbol{u}} + \mathbf{Q}^T\mathbf{W}^2\mathbf{Q} \leq 2\Delta Z^2_{max}\right\}.$$

6.3.4 Necessary condition for feasibility

Applying the rule (6.43) to eq. (6.44), it follows that the necessary condition for feasibility is:

$$\boxed{S_f\left(2\,\mathrm{F}^2_{max}\right) \cap S_z\left(2\,\Delta\mathrm{Z}^2_{max}\right) \neq \varnothing \qquad \Leftarrow \qquad \text{Feasibility}}. \tag{6.45}$$

In other words, if the problem is feasible, then there exists a $\hat{\boldsymbol{u}}$ which belongs to both sets $S_f\left(2\,\mathrm{F}^2_{max}\right)$ and $S_z\left(2\,\Delta\mathrm{Z}^2_{max}\right)$ at the same time.

6.4 Special case of single body

A single body heaving buoy is now considered as a special case of the self-reacting point absorber described in sec. 6.1. The time domain model for a single body WEC has been presented

already in sec. 4.2.2, and it is given by eq. (4.44), i.e.

$$(\mathrm{m} + \mathrm{m}_\infty)\ddot{z}(t) + \mathrm{K}(t) * \dot{z}(t) + \mathrm{B}\,\dot{z}(t) + \mathrm{S}\,z(t) = f_e(t) - f_{pto}(t), \tag{6.46}$$

while the energy absorbed by the PTO, neglecting losses, is (see eq. (4.45)

$$J(T) = -\int_0^T f_{pto}(t)\,v(t)\,dt.$$

The energy maximization problem is then discretised by following the same steps performed for the case of a self-reacting device (sec. 6.1.1), and described already with the same notation in sec. 4.2.2. The discretised equation of motion is the linear system

$$\mathbf{G}\,\hat{\boldsymbol{x}} = \hat{\boldsymbol{e}} - \hat{\boldsymbol{u}}, \tag{6.47}$$

where the matrix $\mathbf{G}$ is exactly the one in (4.62). If the matrix $\mathbf{G}$ is invertible, the converted energy is

$$J = \hat{\boldsymbol{u}}^T\hat{\boldsymbol{x}} = -\hat{\boldsymbol{u}}^T\mathbf{G}^{-1}\hat{\boldsymbol{u}} - \hat{\boldsymbol{u}}^T\mathbf{G}^{-1}\hat{\boldsymbol{e}}. \tag{6.48}$$

Since the symmetric part of the matrix $\mathbf{G}^{-1}$ is positive definite, the quadratic function J is concave and the PTO force $\hat{\boldsymbol{u}}^*$ that maximises J in (6.48) is

$$\hat{\boldsymbol{u}}^* = (\mathbf{G}^{-T} + \mathbf{G}^{-1})^{-1}\mathbf{G}^{-1}\hat{\boldsymbol{e}}. \tag{6.49}$$

The force constraint is defined as in the case of the two body WEC; thus the 2-norm of the force constraint is given by (6.28). The constraint on the oscillation amplitude, on the other hand, is specified on the absolute position of the oscillating body rather than the relative position between body 1 and body 2; therefore, the 2-norm of the amplitude constraint becomes

$$\left\|z^N\right\|_2^2 = \frac{T}{2}\left(\hat{\boldsymbol{u}}^T\mathbf{G}^{-T}\mathbf{W}^2\mathbf{G}^{-1}\hat{\boldsymbol{u}} - 2\,\hat{\boldsymbol{e}}^T\mathbf{G}^{-T}\mathbf{W}^2\mathbf{G}^{-1}\hat{\boldsymbol{u}} + \hat{\boldsymbol{e}}^T\mathbf{G}^{-T}\mathbf{W}^2\mathbf{G}^{-1}\hat{\boldsymbol{e}}\right).$$

Using set notation, the oscillation amplitude constraint is described by

$$S_z'(R_z) = \left\{\hat{\boldsymbol{u}} : \hat{\boldsymbol{u}}^T\mathbf{G}^{-T}\mathbf{W}^2\mathbf{G}^{-1}\hat{\boldsymbol{u}} - 2\,\hat{\boldsymbol{e}}^T\mathbf{G}^{-T}\mathbf{W}^2\mathbf{G}^{-1}\hat{\boldsymbol{u}} + \hat{\boldsymbol{e}}^T\mathbf{G}^{-T}\mathbf{W}^2\mathbf{G}^{-1}\hat{\boldsymbol{e}} \le R_z\right\}, \tag{6.50}$$

where the set $S_z'(R_z)$ is the region of the vector space S^P enclosed by a hyperellipsoid centred at $\boldsymbol{z}_c = \hat{\boldsymbol{e}}$. The principal axes of the hyperellipsoid are parallel to the elements of the basis because the matrix $\mathbf{G}^{-T}\mathbf{W}^2\mathbf{G}^{-1}$ is diagonal, and the radii are

$$r_i' = \sqrt{\frac{R_z}{\lambda_i'}}, \tag{6.51}$$

where λ_i' are the eigenvalues of $\mathbf{G}^{-T}\mathbf{W}^2\mathbf{G}^{-1}$.

All the results described in this section can be translated into the results obtained for the two body WEC, summarised in sec. 6.3, by defining the matrix $\mathbf{H}$ and the vector $\mathbf{Q}$ as

$$\mathbf{H} = \mathbf{G}^{-1} \tag{6.52}$$

$$\mathbf{Q} = \mathbf{G}^{-1}\hat{e}. \tag{6.53}$$

In fact, with the definitions of $\mathbf{H}$ in (6.52) and $\mathbf{Q}$ in (6.53), the set $S_z'(R_z)$ in (6.50) becomes equal to the set $S_z(R_z)$ in (6.36), which specifies the constraint on the relative oscillation amplitude for the two body WEC.

6.5 Special case of single frequency analysis

If only one frequency at the time is considered, the sufficient conditions for feasibility are also necessary. In fact, a Fourier series g^N with one frequency component ($N = 2$) is

$$\begin{aligned} g^N(t) &= a\cos(\omega_0 t) + b\sin(\omega_0 t) \\ &= A\cos(\omega_0 t + \vartheta) \end{aligned}$$

with $A = \sqrt{a^2 + b^2}$ and $\vartheta = -\tan^{-1} b/a$. The max-norm of g^N, for $N = 2$, can be calculated explicitly as

$$\left\|g^N\right\|_\infty = \max_{t\in[0,T]} |g^N(t)| = \max_{t\in[0,T]} |\cos(\omega_0 t + \vartheta)|A = A = \sqrt{a^2 + b^2} = \sqrt{\boldsymbol{y}^T\boldsymbol{y}},$$

where $\boldsymbol{y} = [a, b]^T$. By using (6.28), the 2-norm of g^N is

$$\left\|g^N\right\|_2 = \sqrt{\frac{T}{2}\boldsymbol{y}^T\boldsymbol{y}},$$

thus, for $N = 2$,

$$\left\|g^N\right\|_2 = \sqrt{\frac{T}{2}}\left\|g^N\right\|_\infty.$$

Finally, the force and position constraints are

$$\left\|f_{pto}^N\right\|_\infty = \sqrt{\frac{2}{T}}\left\|f_{pto}^N\right\|_2 \leq \mathrm{F}_{max},$$

$$\left\|z^N\right\|_\infty = \sqrt{\frac{2}{T}}\left\|z^N\right\|_2 \leq \mathrm{Z}_{max};$$

furthermore, the sufficient condition for feasibility in (6.42) is also necessary, and it can be

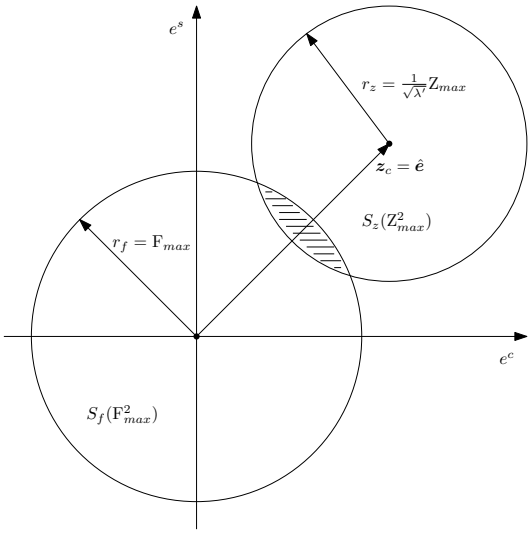

Figure 6.6: Feasible problem

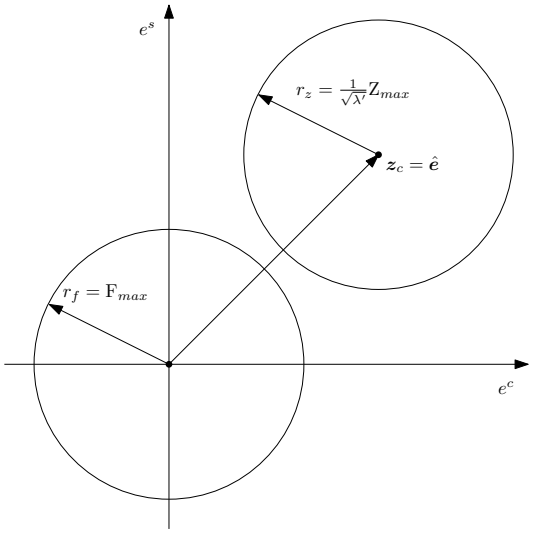

Figure 6.7: Non feasible problem

summarised by the system of inequalities

$$\begin{cases} \hat{\boldsymbol{u}}^T \hat{\boldsymbol{u}} \leq \mathrm{F}^2_{max} \\ \hat{\boldsymbol{u}}^T \mathbf{H}^T \mathbf{W}^2 \mathbf{H} \hat{\boldsymbol{u}} - 2\,\mathbf{Q}^T \mathbf{W}^2 \mathbf{H} \hat{\boldsymbol{u}} + \mathbf{Q}^T \mathbf{W}^2 \mathbf{Q} \leq \mathrm{Z}^2_{max}. \end{cases} \tag{6.54}$$

The inequalities in (6.54) are valid for both the single body WEC using the definition of $\mathbf{H}$ and $\mathbf{Q}$ in (6.52) and in (6.53), and for the two body WEC using the definitions of $\mathbf{H}$ and $\mathbf{Q}$ in (6.14) and in (6.15).

Additionally, for $N = 2$ the matrix $\mathbf{G}$ for the single body WEC is of the form

$$\mathbf{G} = \begin{bmatrix} \mathrm{D} & \mathrm{M} \\ -\mathrm{M} & \mathrm{D} \end{bmatrix}, \tag{6.55}$$

while the matrix $\mathbf{G}$ for the two body device is simply the 4×4 block $\bar{\mathbf{G}}$ in (6.9), for $l = 1$. It follows that, in both cases (single and two body WECs), the matrix $\mathbf{H}^T \mathbf{W}^2 \mathbf{H} = \lambda \mathbf{I}_2$, i.e. it is a diagonal matrix with equal values on the main diagonal, thus there are two coincident eigenvalues $\lambda_1 = \lambda_2 = \lambda$. Consequently, the geometrical entities describing both force and position constraints are discs; in particular the PTO force constraint is the disc centred at the origin with radius $r_f = \mathrm{F}_{max}$ ($S_f(\mathrm{F}^2_{max})$), while the oscillation amplitude constraint ($S_z(\mathrm{Z}^2_{max})$) is the disc with radius $r_z = \frac{1}{\sqrt{\lambda}}\mathrm{Z}_{max}$ and centred at

$$\boldsymbol{z}_c = \mathbf{H}^{-1}\mathbf{Q}.$$

It is interesting to note that, for the single body WEC, the disc describing the oscillation

amplitude constraint is centred on the vector $\boldsymbol{z}_c$, which is equal to the vector of the coefficient of the excitation force. In fact, using (6.52) and (6.53),

$$\boldsymbol{z}_c = \mathbf{H}^{-1}\mathbf{Q} = \left(\mathbf{G}^{-1}\right)^{-1}\mathbf{G}^{-1} = \hat{\boldsymbol{e}},$$

and this expression gives an explicit relation between the feasibility of the energy maximisation problem and the excitation force. In particular, the relation shows that for more violent sea states, there is a lower likelihood of simultaneously satisfying position and amplitude constraints, as expected, because $\boldsymbol{z}_c$ will move far away from the origin as $\hat{\boldsymbol{e}}$ becomes large (see for example fig 6.7).

For the two body WEC, the centre $\boldsymbol{z}_c$ of the disc representing the relative oscillation amplitude constraint depends on a *weighted* difference between the excitation forces experienced by the two bodies; in fact, using the definition of $\mathbf{Q}$ in (6.15),

$$\boldsymbol{z}_c = \mathbf{H}^{-1}\mathbf{Q} = \mathbf{H}^{-1}\left(\left(\mathbf{H}_{11} - \mathbf{H}_{12}\right)\hat{\boldsymbol{e}}_1 + \left(\mathbf{H}_{22} - \mathbf{H}_{21}\right)\hat{\boldsymbol{e}}_2\right). \tag{6.56}$$

A graphical illustration of the results described in this section is given in fig. 6.6 for a feasible energy maximisation problem (the intersection between the discs is not empty, i.e. $S_f(\mathrm{F}^2_{max}) \cap S_z(\mathrm{Z}^2_{max}) \neq \varnothing$), and in fig. 6.7 for a non feasible problem ($S_f(\mathrm{F}^2_{max}) \cap S_z(\mathrm{Z}^2_{max}) = \varnothing$), where the axes of the diagrams are enumerated in terms of the sine and cosine components of the PTO force, i.e. e^s and e^c, respectively.

A broad conclusion, from fig. 6.6, is that if the circle centred at $\boldsymbol{z}_c$ contains the origin, no PTO force is required to limit the motion in order to satisfy the amplitude constraint, i.e. the wave excitation force can always be contained within the amplitude range of the device; however, in this situation no energy will be extracted from waves because the PTO force is not doing mechanical work.

Considering that the intersection between the two disks ($S_f(\mathrm{F}^2_{max})$ and $S_z(\mathrm{Z}^2_{max})$) is non-empty if the sum of the radii is larger that the distance between the centres, it follows that the necessary and sufficient condition for feasibility, eq. (6.54), can be simplified to:

$$\mathrm{F}_{max} + \frac{\mathrm{Z}_{max}}{\sqrt{\lambda'}} \geq \left\|\hat{\boldsymbol{e}}\right\|_2. \tag{6.57}$$

6.6 Sample numerical results

Two illustrative examples are presented in this section: a single body WEC, which is a vertical cylinder (fig. 4.1) of 10m diameter and 25m draught, and the self-reacting heaving WEC composed of two coaxial bodies, a torus and a cylinder, depicted in fig. 6.1, the dimensions of

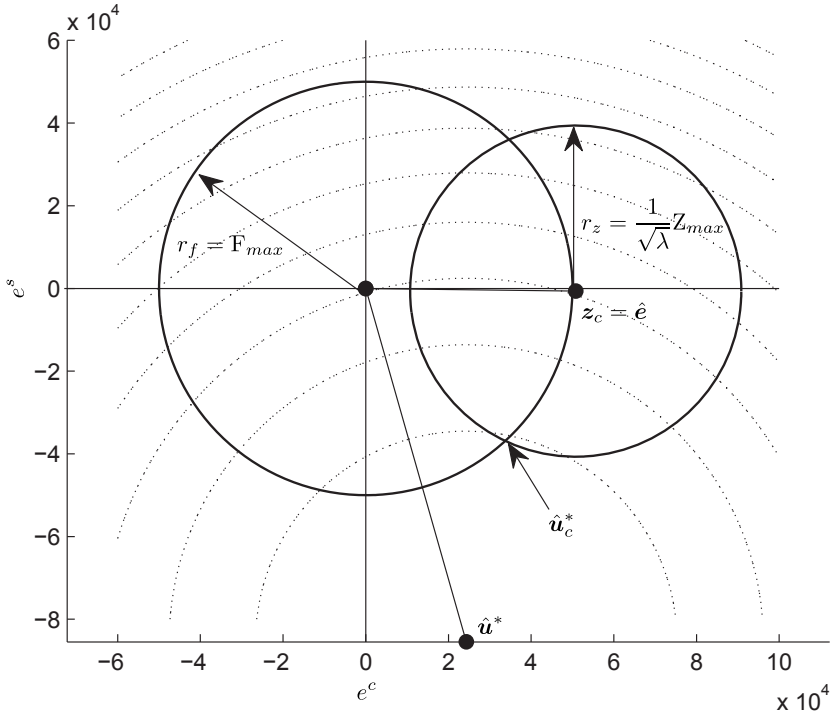

Figure 6.8: Single body device in a monochromatic sea: $\mathrm{F}_{max} = 50\,\mathrm{kN}$, $\mathrm{Z}_{max} = 3\mathrm{m}$.

which are listed in table 6.1.

Initially, the single body device will be considered and a constraint analysis will be performed for a monochromatic sea. This will allow the development of some insight into the use of the geometrical tool, and to consider the tool from a design perspective. While monochromatic analysis might seem restrictive, appropriate choice of the frequency, such as the resonant frequency of the device, or the peak energy frequency of the incident sea, could be sufficient to determine the peak loading condition. However, a polychromatic approach, for the single body case, is also considered in sec. 6.6.2. The last part of the section will illustrate the results for the multi-body device with a polychromatic sea spectrum. In all the cases considered, the hydrodynamic parameters have been calculated using the WAMIT hydrodynamic software.

Table 6.1: Dimensions of the two body WEC

Body 1 (Torus)	
Outer diameter	20m
Inner diameter	10m
Draught	8m

Body 2 (Cylinder)	
Diameter	8m
Draught	30m

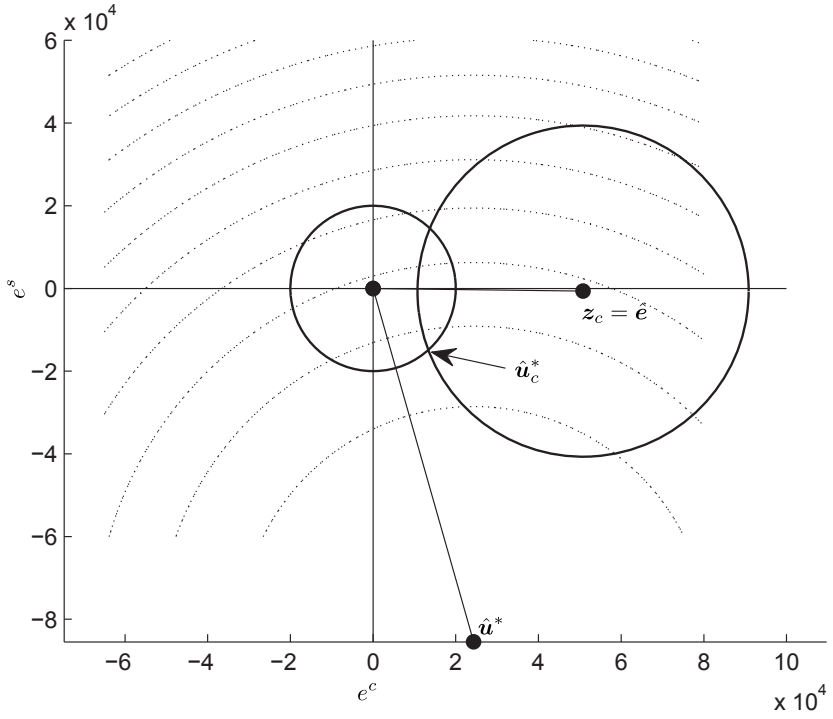

Figure 6.9: Single body device in a monochromatic sea: $\mathrm{F}_{max} = 20\,\mathrm{kN}$, $\mathrm{Z}_{max} = 3\mathrm{m}$.

6.6.1 Single frequency analysis

Figures 6.8 and 6.9 depict the force and position constraint for a monochromatic incident wave at a period of $T_w = 9\mathrm{s}$ and with an amplitude $\eta = 3\mathrm{m}$. The oscillation amplitude constraint is set to $\mathrm{Z}_{max} = 3\mathrm{m}$, while the PTO force constraint is set to $\mathrm{F}_{max} = 50\,\mathrm{kN}$ for the diagram in fig. 6.8, and to $\mathrm{F}_{max} = 20\,\mathrm{kN}$ for the diagram in fig. 6.9.

The force constraint is described by the circle centred at the origin ($[u^s, u^c] = [0, 0]$) with radius $r_f = \mathrm{F}_{max}$ ($r_f = 5\,10^4$ in fig. 6.8 and $r_f = 2\,10^4$ in fig. 6.9), while the oscillation amplitude constraint is the circle centred in $\boldsymbol{z}_c = \hat{\boldsymbol{e}}$ with radius $r_z = \sqrt{1/\lambda}\,\mathrm{Z}_{max}$. Both fig. 6.8 and fig. 6.9 show a feasible energy maximisation problem, because the intersection between the discs is not empty ($S_f(\mathrm{F}_{max}^2) \cap S_z(\mathrm{Z}_{max}^2) \neq \varnothing$); as discussed in sec. 6.5, the intersection between the two discs is both necessary and sufficient for feasibility when $N = 2$.

The procedure described in this chapter allows us not only to analyse the feasibility of the constrained energy maximisation problem, but also to study the effect of constraints on the energy absorbed by the PTO. To do so, fig. 6.8 and fig. 6.9 include the level curves of the function $\boldsymbol{J}$ in (6.48), which is the elliptic paraboloid describing the total energy absorbed by the WEC. The level curves are the dotted circles centred at the optimal unconstrained control vector $\hat{\boldsymbol{u}}^*$; in fact, the paraboloid has a circular section because $\mathbf{H}$ is of the form of (6.55), thus $\mathbf{H}$ has two coincident eigenvalues. Additionally, fig. 6.8 and fig. 6.9 also include the point

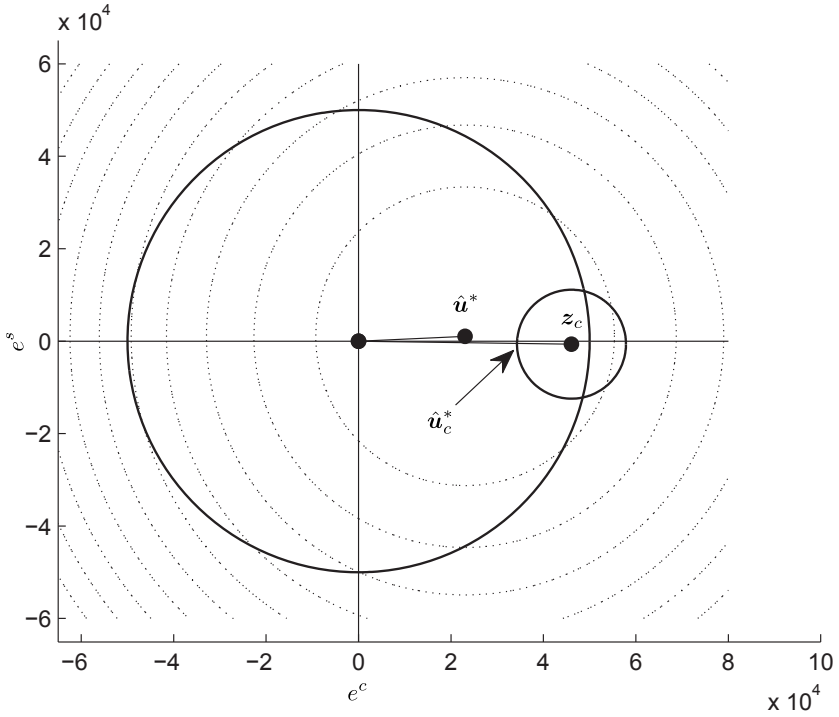

Figure 6.10: Single body device at resonance ($T_w \approx 10s$).

labelled $\hat{\boldsymbol{u}}_c^*$, which is the optimal PTO force satisfying both force and amplitude constraints.

Let us consider the situation in fig. 6.8 first: a relaxation of the force constraint, that is an increase in F_{max}, will provide a small increase on the total absorbed energy, because $\hat{\boldsymbol{u}}_c^*$ will move along the circle that describes the position constraint, and the tangent to the position constraint circle at $\hat{\boldsymbol{u}}_c^*$ is almost parallel to the tangent to the contour line passing through $\hat{\boldsymbol{u}}_c^*$. On the other hand, by relaxing the position constraint, i.e. by increasing Z_{max}, the total absorbed energy will increase by a larger amount because $\hat{\boldsymbol{u}}_c^*$ will move along the circle describing the force constraint, the tangent of which at $\hat{\boldsymbol{u}}_c^*$ is almost orthogonal to the contour lines, i.e. in the direction of the gradient of $\boldsymbol{J}$. By applying the same analysis to the situation in fig. 6.9, the result is diametrically opposite, where the larger increase in the absorbed energy is caused by relaxing the PTO force constraint, i.e. by increasing F_{max}.

The situation in fig. 6.10 corresponds to the resonance frequency of the vertical cylinder, which can be calculated with the formula $\omega_r = \sqrt{\frac{g}{draught}}$, because the ratio $\frac{radius}{draught} << 1$ [5], where g is the gravitational acceleration; the resonant period T_r is then $T_r = 2\pi/\omega_r \approx 10s$. By definition [5], a single body WEC is at resonance when the imaginary part of the mechanical impedance vanishes, that is

$$\mathrm{m} + \mathrm{m}(\omega_r) - \frac{S}{\omega_r^2} = 0.$$

The matrix $\mathbf{G}$, then, becomes diagonal because the terms M_{ii}^l in (6.8) and in (4.62) are zero;

consequently, the optimal PTO force in (6.49) is

$$\hat{\boldsymbol{u}}^* = (\mathbf{G}^{-T} + \mathbf{G}^{-1})^{-1}\mathbf{G}^{-1}\hat{\boldsymbol{e}} = (2\mathbf{G}^{-1})^{-1}\mathbf{G}^{-1}\hat{\boldsymbol{e}} = \frac{1}{2}\hat{\boldsymbol{e}}. \tag{6.58}$$

By substituting $\hat{\boldsymbol{u}}^*$ into the discretised equation of motion, it yields the optimal velocity

$$\hat{\boldsymbol{x}}^* = \frac{1}{2}\mathbf{G}^{-1}\hat{\boldsymbol{e}} = \frac{1}{2\left(\mathrm{R}(\omega_r) + \mathrm{B}\right)}\hat{\boldsymbol{e}},$$

which is exactly the velocity when reactive control is applied (see eq. 2.86). Figure 6.10 depicts the relation between the optimal PTO force and the excitation force in eq. (6.58); in fact $\hat{\boldsymbol{u}}^*$ and $\hat{\boldsymbol{e}}$ are in phase and the length of $\hat{\boldsymbol{u}}^*$ is half the length of $\hat{\boldsymbol{e}}$, showing consistency with the classical frequency domain approach known in the literature [5].

Additionally, fig. 6.10 shows that, for the given choice of the constraints, the optimal constrained PTO force $\hat{\boldsymbol{u}}_c^*$ is not on the boundary of the set $S_f(\mathrm{F}_{max}^2)$ (the force constraint), but it is inside; thus an increase in F_{max} will not affect the optimal absorbed energy, as the point $\hat{\boldsymbol{u}}_c^*$ will not move following a relaxation of the force constraint. Conversely, the point $\hat{\boldsymbol{u}}_c^*$ is on the boundary of the set $S_z(\mathrm{Z}_{max}^2)$, and a relaxation of the position constraint will cause an increase in the absorbed energy, as the optimal PTO force $\hat{\boldsymbol{u}}_c^*$ will move in the direction of the gradient of the absorbed energy function $\boldsymbol{J}$ (i.e. orthogonally to the level curves).

6.6.2 Multiple frequency analysis

While the analysis at a single frequency of sec. 6.6.1 has some useful design features, real seas contain multiple frequency components and designers need to ensure that physical constraints are satisfied for *all* active frequencies. In fig. 6.11, the same heaving cylinder is considered in a sea state corresponding to a Bretschneider wave spectrum with parameters $H_{mo} = 6.5m$ and $T_p = 10s$. In essence, the plane of figs. 6.8–6.10 is extended to a 3rd dimension, with the addition of a frequency axis.

This increase in dimension brings a corresponding reduction in the clarity of interpretation; however, fig. 6.11 can be effectively projected onto a 2 dimensional plane by using equation (6.57) for the frequency range of interest. Figure 6.12 shows the projection, and the necessary and sufficient condition for feasibility becomes

$$\frac{\left\|\hat{\boldsymbol{e}}\right\|_2}{\left(\mathrm{F}_{max} + \dfrac{\mathrm{Z}_{max}}{\sqrt{\lambda'}}\right)} \leq 1.$$

For the polychromatic case considered in this section, two sets of constraints have been studied:

1. $\mathrm{Z}_{max} = 2m$, $\mathrm{F}_{max} = 450kN$

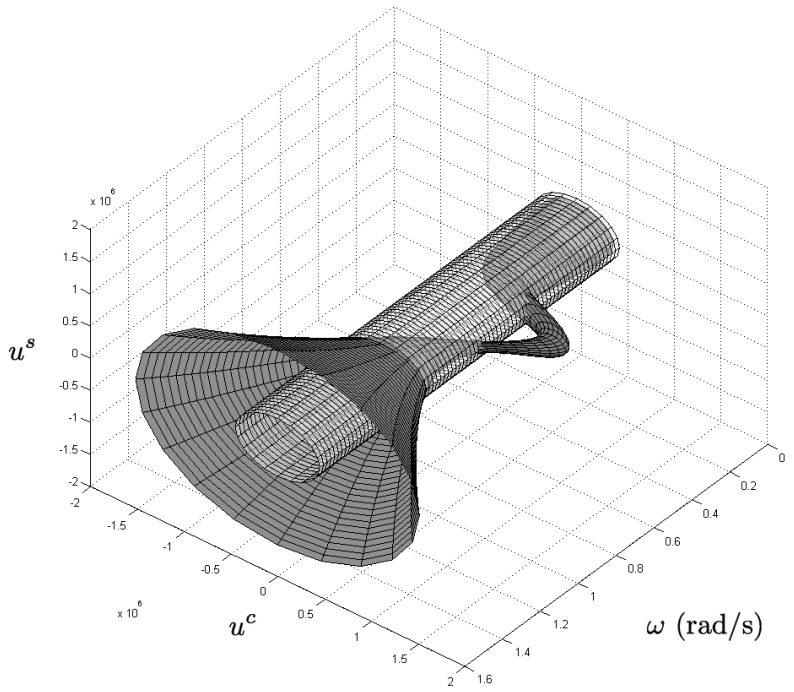

Figure 6.11: Single body device with Bretschneider spectrum

2. $Z_{max} = 4m$, $F_{max} = 700kN$

From fig. 6.12, case (1) above violates the constraints, while case (2) satisfies the constraints. Further, detailed, examination can now proceed by focussing on the single frequency ω^* and using plots similar to that of figs. 6.8–6.10, thereby improving the insight into individual constraint satisfaction and manipulation.

The two-body case differs only from the single body case in that the oscillation amplitude constraint is relative rather than absolute (relative position between body 1 and body 2). However, by using the appropriate definition for the matrix **H**, in (6.14) and (6.53), and for the vector **Q**, in (6.15) and (6.53), the formulation of the problem is independent of the type of WEC considered and, for $N = 2$, the necessary and sufficient condition in (6.54) is identical for both the single and two body case. Consequently, the general form of the diagrams in figs. 6.8– 6.10 is followed also for the two body WEC, with a noteworthy difference that the centre $\boldsymbol{z}_c$ of the amplitude constraint set $S_z(Z_{max})$ is not the excitation force vector $\hat{\boldsymbol{e}}$, but the weighted difference between the excitations on body 1 and body 2 in eq. (6.56).

Figure 6.13 shows the situation for 4 different sets of constraints, where constraint satisfaction is only guaranteed for $\Delta Z_{max} = 0.1m$, $F_{max} = 0.45kN$. Again, a more detailed examination can be obtained by resorting to the u^c versus u^s plane (as in figs. 6.8– 6.10), with a focus on

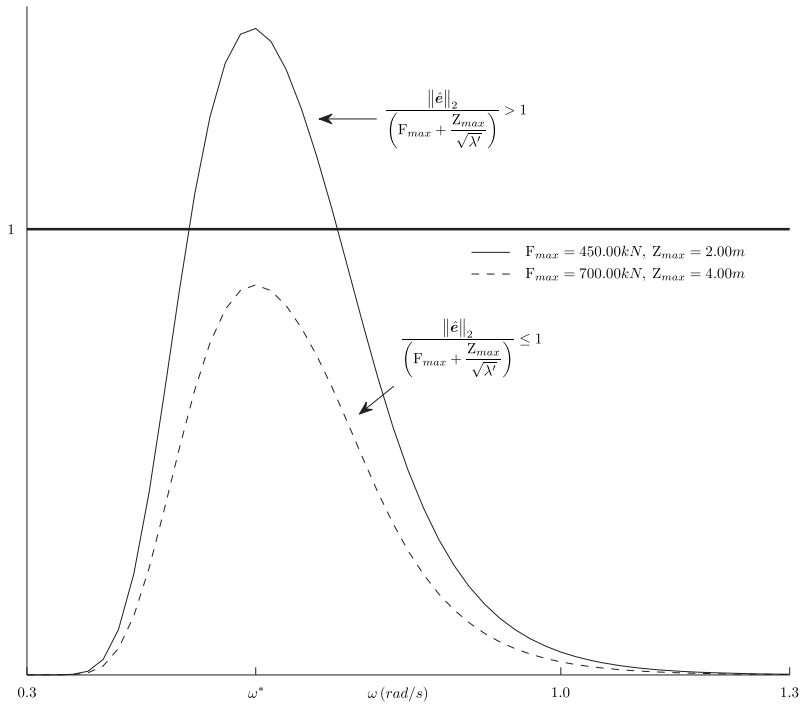

Figure 6.12: Single body device with Bretschneider spectrum, using 2D projection

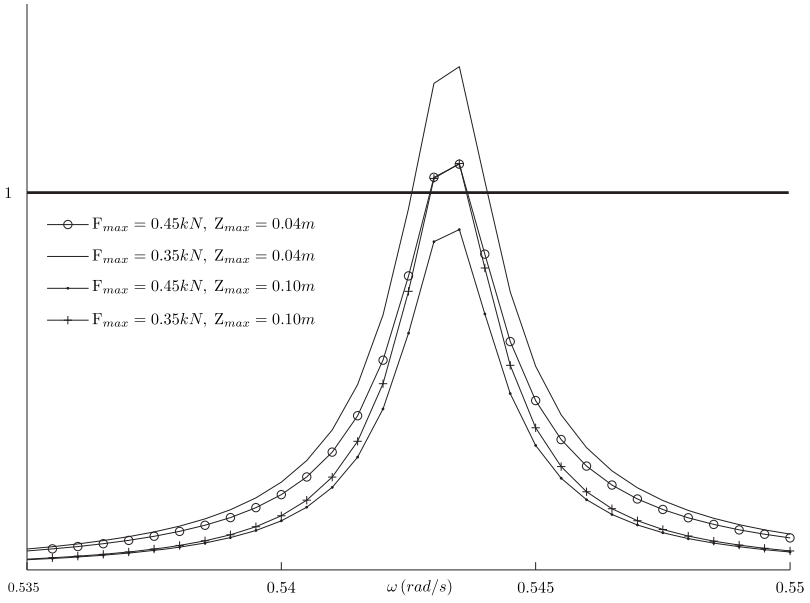

Figure 6.13: Two-body device with Bretschneider sea spectrum

the peak frequency. A characteristic difference between fig. 6.13 and fig. 6.12 is that the bandwidth of the two-body system is significantly narrower, reflecting the significant difference in dynamics for the single and two body cases, for the range of parameters considered.

6.7 Summary and discussion

This chapter has presented a methodology for the study of the feasibility of the constrained optimal control of WECs. The approach is based on the geometrical interpretation of the expressions describing the force and position constraints, and the energy absorbed by the device.

Force and position constraints are naturally defined using the max-norm when they describe the maximum value that such a quantity can take; however, this formulation is more difficult to manipulate analytically than, for example, the 2-norm. In fact, thanks to the Fourier-Galerkin transcription and to the Parseval's identity (see sec. 6.2.2), the 2-norm of both the position and the PTO force are quadratic functions of the vector $\hat{\boldsymbol{u}}$, i.e. the Fourier coefficients of the PTO force (control signal). The geometrical interpretation comes into play by interpreting the quadratic functions as geometrical entities in an N-dimensional vector space ($S^P \in \mathbb{R}^N$).

Two inequalities, relating the 2-norm and the max-norm, have been used to bound from above and below the original constraints (defined using the max-norm) with the 2-norm of the force and positions. By combining the inequalities and the geometrical interpretation of the 2-norms, the result is a set of necessary and sufficient conditions of the feasibility for the energy maximisation problem. In particular, the feasibility is guaranteed by verifying the intersections of a (hyper-)sphere enclosing the region of the space S^P which contains vectors $\hat{\boldsymbol{u}}$ for which the force constraint is satisfied, with an (hyper-)ellipsoid enclosing the region of the space S^P which contains the vectors $\hat{\boldsymbol{u}}$ satisfying the position constraint. Conversely, the non-feasibility is determined by the intersection of two complementary regions described by the same shapes with appropriately larger radii.

The merit of the approach presented in this chapter, besides the feasibility analysis, is also to highlight, by means of a visual feedback due to the geometrical interpretation, the interplay between the wave climate (excitation force) and the constraints, keeping in the background the energy absorbed by the WEC. Thus, the procedure can be the basis for a design tool used for the *balanced dimensioning* and techno-economical optimisation of WECs; in particular, the cost of a particular device is generally positively correlated with the values of the maximum force (F_{max}) and oscillation amplitude (Z_{max}), since larger devices and larger forces require more expensive components. On the other hand, the amount of absorbed energy is positively correlated with the revenues generated by the WEC, if the device is rewarded by the amount of energy it is capable of producing. Therefore, this procedure can be useful at the deign stage of WECs, to make informed decisions on the optimal dimension of a given device concept and for a given

wave climate, by following the analysis discussed in sec. 6.6.

Altogether, the work presented in this chapter could also be considered as an extension of the work present by Evans in [170], where the author studied the energy absorption of WECs under motion constraints in the frequency domain. In fact, when considering one frequency at a time, the results are in agreement with the classical frequency domain theory of wave energy conversion, as described in sec. 6.5 and illustrated with the numerical results of sec. 6.6. Moreover, the formulation presented in this chapter also includes force constraints, and provides the basis for a tool for the sensitivity analysis of the absorbed energy with respect to force and position constraints, in addition to the intuitive aspects provided by their geometrical interpretation.

Chapter 7

Conclusions

This thesis has presented the formulation of the optimal control problem for WECs in the framework of direct transcription methods known as spectral and pseudospectral optimal control. The major benefit provided by this approach is the possibility to formulate complex control problems where realistic scenarios can be taken into account, such as physical limitations and nonlinearities in the behaviour of the devices. Direct transcription methods transform continuous time optimal control problems into Non Linear Programming (NLP) problems, for which the literature (and the market) offer a large number of standard algorithms (and software packages). The major contribution of this thesis is, therefore, the study and implementation of a method which allows difficult control problems of WECs to be transformed into problems that can be solved by standard and well developed finite dimensional optimisation techniques.

A significant distinction with previous approaches for the nonlinear constrained optimal control of WECs is the capability of spectral and pseudospectral methods to provide an approximation of the optimal solution directly from sampled frequency and impulse responses models of the radiation forces, obviating the need for finite order approximations (state space). To this end, it has been shown in sec. 4.2.3 that any of the discretisation methods belonging to the family of mean weighted residuals, not only spectral and pseudospectral methods, transform the convolution integral describing the radiation forces into a linear combination of the basis functions used to approximate the velocity of the WEC. Although the result was to be expected since the convolution is a linear operator, sec. 4.2.3 illustrates how to carry out the discreti-

sation and, most importantly, highlights the fact that the necessary numerical integration for the calculation of the convolution integral can be carried out offline, considerably reducing the computational load. The advantage of being able to design the controller from the sampled impulse or frequency response is to avoid an additional level of approximation introduced when fitting the sampled data with a parametric model.

The approach presented in this thesis is also modular; in fact, sec. 4.2.1.2 describes how the energy maximisation problem can be formulated for a number of multi body/multi device configurations by the simple definition of the PTO configuration matrix, which is also illustrated by the examples in chapter 5 (arrays of WECs) and in chapter 6 (two body WEC). Furthermore, indirect transcription methods based for example on Pontryagin's Minimum Principle, as discussed in sec. 4.1, require the manual derivation the necessary condition for optimality from which the NLP is built; on the other hand, direct transcription methods allows the construction of the NLP problem automatically from the definition of the continuous time optimal control problem. As a result, the combination of all these properties make the direct transcription methods presented in this thesis ideal candidates for being implemented in software packages for the simulation and optimisation of WECs, which include automated controller design.

This thesis also presents a number of simulation results obtained from the implementation of spectral and pseudospectral optimal control. Section 4.2 demonstrates that the energy absorbed by a single body WEC is described by a convex quadratic function, when the direct transcription of the optimal control problem is carried out by means of the Fourier-Galerkin method. A noteworthy practical implication of convexity is that it ensures the existence and uniqueness of the optimal solution, also when constraints on the PTO force and oscillation amplitude are introduced (sec.4.2.2.2). Moreover, convexity of the quadratic program guarantees faster converge towards the optimal solution compared to a non-convex problem, which is of particular relevance in real-time applications.

Simulation results for the device considered in sec. 4.2also show that a considerable restriction in the maximum allowed PTO force causes a relatively small reduction in the amount of absorbed energy. The analysis is consequential for the techno-economical optimisation of the device, as the PTO rating is directly related to the cost of the components, whereas the absorbed energy is related to the revenue generated by selling electricity to the grid.

In this respect, chapter 6 illustrates an approach for the study of the effects of the PTO force and oscillation amplitude constraints on the total absorbed energy. The procedure has originally been developed for the study of the feasibility of the constrained energy maximisation problem, and it provides an intuitive framework for the design of WECs, thanks to the geometrical interpretation of the functions describing both the total absorbed energy and the constraints. The monochromatic analysis, in particular, provides a visual feedback that highlights the interplay between the device specifications (PTO force and position constraints), the device characteristics

(the function describing the absorbed energy) and the wave climate (excitation force).

The plots constructed by following the procedure in ch. 6 give an immediate overview of the feasibility problem, and they also give clear indications regarding the effects produced by altering the specification of the constraints. In more detail, it shows whether a relaxation of a constraints produces an increase in the absorption, or if does not have any effect all. In practice, the procedure can be used to quickly verify if the dimensioning of a WEC is suitable for a given wave climate, and, if possible, to provide a guidance for the improvement of its performance.

Chapter 5 presents the comparison of two antithetical control strategies for arrays of WECs. The Global Control strategy computes the optimal motion by taking into account the complete model of the array and it provides the global optimum for the absorbed energy; however, it is a centralised control strategy by nature and requires a data transmission infrastructure between WECs for its implementation. On the opposite end, the Independent Control strategy consists of implementing a control system on each device which is independent from all the others, and it is assumed that no communication occurs between devices.

It has been shown by simulation results that the GC strategy always performs better in terms of absorbed energy than the IC, as expected, with the difference in performance increasing when reducing the inter-body distance, and when increasing the number of devices.

Besides the observations obtained by simulation results, the essence of the work in chapter 5 is the procedure itself: in fact, it is envisaged by the author that the approach presented can be used in the design stage of a WEC array as a support for the decision regarding the control strategy to be adopted. Nevertheless, the procedure can also be used for the analysis of an existing array of WECs not equipped with the necessary infrastructure for the implementation of a GC strategy, to evaluate the benefit in terms of absorbed energy (which could be significant in some situations e.g. $>10\%$), against the additional cost of implementing a data transmission system (which can be relatively inexpensive compared to the overall cost of the array).

The results discussed so far in this conclusion chapter have been obtained by applying spectral optimal control to WECs and arrays of WECs described by linear models. Although spectral methods provide great accuracy for the approximation of the solutions of differential equations, they are difficult to implement when the system includes nonlinearities; in this case pseudospectral methods are suitable alternatives because they exhibits similar accuracy and have straightforward implementation.

Thanks to pseudospectral methods, sec. 4.3 reports the first results of optimal control of WECs which include a nonlinear viscous (dissipative) terms. The optimal behaviour of the WEC is considerably different form the case where the device is described by a linear model. It is known that reactive control is difficult, if not impractical to implement because, besides non-causality, it forces large and often unrealistic oscillation amplitudes on the device. Additionally, large oscillation amplitudes are obtained by using a large amount of reactive power, that is

by returning energy from the PTO to the oscillating body, thus requiring highly efficient and expensive components.

Simulation results in sec. 4.3 show that the optimal control, in presence of quadratic viscous dissipative terms, tends to limit the displacement and the velocity of the oscillating body. Furthermore, the optimal motion requires a much smaller quantity of reactive power compared to the linear case, and the ratio of useful absorbed energy over the sum of the radiated and dissipated energy is larger than one, which is the value obtained when reactive control is implemented.

The practical implication of the simulation results are important for the real time control of WECs because a linear optimal controller (i.e. reactive control) under a sinusoidal oscillation will force the device to oscillate sinusoidally by using large amount of reactive power. If the quadratic viscous terms are negligible compared to the linear radiative and dissipative terms, then the reactive power will produce an increase in the total absorption. However, by forcing the device to oscillate with large motion and velocity, the quadratic viscous terms may become relevant with the consequent dissipation of a large amount of energy.

Most importantly, the results in sec. 4.3 have a significant influence on the device design; in fact, smaller optimal oscillation amplitudes implies a smaller device, and a smaller amount of reactive power with respect to the total absorbed power lowers the efficiency requirements and produces less stress on the PTO components, extending their lifetime. Furthermore, simulation results also shows that the maximum amount of absorbed energy is proportional to $|\zeta|^{\frac{3}{2}}$, where ζ is the wave amplitude, when the quadratic viscous terms are dominant, rather than being proportional to $|\zeta|^2$ as in the linear case. Consequently, the design of WECs solely based on linear theory is likely to produce devices which are over specified and with an overestimated energy production, if nonlinear viscous terms become relevant.

7.1 Future work

The work presented in this thesis has been based on the model of WEC commonly known as Cummins equations, with the addition of a term describing a generic PTO force and, in sec. 4.3, a nonlinear term describing viscous forces. However, a more realistic model of a WEC should include several additional (nonlinear) components, such as the PTO dynamic, the moorings and hydrostatic forces. Moreover, a WEC generally oscillates in several modes of motion, including combinations of translations and rotations, and it is often composed of multiple bodies, introducing nonlinear kinematic equations in the model. Clearly, by considering additional nonlinear terms (dynamics and kinematics), the energy absorption properties may change considerably, as shown for example in sec. 4.3, thus affecting the device design.

Pseudospectral optimal control is widely used in trajectory planning and flight control,

which is an area of research that shares many similarities to wave energy conversion, as both fields are concerned with rigid bodies moving in a fluid. Therefore, it would be ideal, as future research, to implement pseudospectral methods for solving optimal WEC control problems which also include combinations of nonlinear kinematics, moorings and PTO dynamics.

Such control problems would result in a large NLP problem, which would take considerable amount of computational resources and time to be solved. In this respect, it has been shown throughout this thesis that the cost function of the transcribed control problems have peculiar structures (see the **G** matrix definitions for the control problems in ch. 4–6), which depends, besides the geometry of the WECs configuration, on the choice of the basis functions used to approximate the state and control. Therefore, it could be relevant to carry out a study of the effect of the basis function on the structure of the NLP problem, such as sparsity patterns and numerical conditioning, for example, as an extension to the discussion regarding the dimensionality reduction reported in sec. 4.2.2.3. The result of such analysis may help to identify algorithms for solving the optimisation problem that take advantage of the particular structure to improve, for example, computational speed and memory usage, which are critical in real time control.

7.2 Concluding remarks

The control system has a significant impact on both technical and economical performance of WECs. The work presented in this thesis provides a framework which allows the design of WECs to be carried out while taking into account more realistic scenarios than the current practice, which include nonlinearities and physical limitations of the device components, with the benefit of improving both the device performance and the estimation of the final cost of energy.

Additionally, spectral and pseudospectral optimal control provide a direct and indirect contribution for the real time control of WECs. The direct contribution is their implementation in a receding horizon fashion (i.e. model predictive control), while the indirect contribution is their use as benchmarks for the development of simplified suboptimal control laws.

References

[1] P. W. Atkins, *Creation Revisited: The Origin of Space, Time and the Universe*. Penguin Science, 1994.

[2] J. Falnes, "A review of wave-energy extraction," *Marine Structures*, vol. 20, no. 4, pp. 185–201, Oct. 2007. [Online]. Available: http://www.sciencedirect.com/science/article/B6V41-4R1NN8K-1/1/88187d53cdf17e0ff5944e20596c96ff

[3] B. Drew, A. R. Plummer, and M. N. Sahinkaya, "A review of wave energy converter technology," *Proceedings of the Institution of Mechanical Engineers, Part A: Journal of Power and Energy*, vol. 223, no. 8, pp. 887–902, 2009. [Online]. Available: http://pia.sagepub.com/content/223/8/887.abstract

[4] A. F. d. O. Falcão, "Wave energy utilization: A review of the technologies," *Renewable and Sustainable Energy Reviews*, vol. 14, no. 3, pp. 899 – 918, 2010. [Online]. Available: http://www.sciencedirect.com/science/article/pii/S1364032109002652

[5] J. Falnes, *Ocean waves and oscillating systems: linear interactions including wave-energy extraction*. Cambridge University Press, 2002.

[6] K. Unneland, "Identification and order reduction of radiation force models of marine structures," Ph.D. dissertation, Norwegian University of Science and Technology, NTNU, 2007.

[7] Z. Yu and J. Falnes, "State-space modelling of a vertical cylinder in heave," *Applied Ocean Research*, vol. 17, no. 5, pp. 265–275, Oct. 1995. [Online]. Available: http://www.sciencedirect.com/science/article/B6V1V-3Y6PCTM-1/1/e3054b3f74f1daea10819282c94ef510

[8] E. Kristiansen and O. Egeland, "Frequency-dependent added mass in models for controller design for wave motion damping," in *6th IFAC Conference on Manoeuvering and Control of Marine Craft*, 2003.

[9] A. Babarit, J. Hals, M. Muliawan, A. Kurniawan, T. Moan, and J. Krokstad, "Numerical benchmarking study of a selection of wave energy converters," *Renewable Energy*, vol. 41, no. 0, pp. 44 – 63, 2012. [Online]. Available: http://www.sciencedirect.com/science/article/pii/S0960148111005672

[10] J.-C. Gilloteaux and R. J. V., "Control-informed geometric optimisation of wave energy converters," in *IFAC Conference on Control Applications in Marine Systems (CAMS)*, 2010.

[11] H. Engja and J. Hals, "Modelling and simulation of sea wave power conversion systems," in *7th European Wave and Tidal Energy Conference, EWTEC*, September 2007.

[12] G. Bacelli, J.-C. Gilloteaux, and R. J. V., "State space model of a hydraulic power take off unit for wave energy conversion employing bondgraphs," in *Proc. 10th World Renewable Energy Congress - WRECX, Glasgow*, 2008.

[13] J.-C. Gilloteaux, "Mouvements de grande amplitude d'un corps flottant en fluide parfait. application à la récupération de l'énergie des vagues," Ph.D. dissertation, Ecole Centrale de Nantes, France, 2007.

[14] A. Merigaud, J.-C. Gilloteaux, and R. J. V., "A nonlinear extension for linear boundary element methods in wave energy device modelling," in *Proc. of 31st International Conference on Ocean, Offshore and Arctic Engineering (OMAE2012)*, 2012.

[15] M. Folley, T. Whittaker, and J. van't Hoff, "The design of small seabed-mounted bottom-hinged wave energy converters," in *Proc. 7th European Wave and Tidal Energy Conference (EWTEC), Porto*, 2007.

[16] A. S. Zurkinden and M. Kramer, "Numerical time integration methods for a point absorber wave energy converter," in *Proc. of 27th International Workshop on Water Waves and Floating Bodies (IWWWFB), Copenhagen*, 2012.

[17] S. R. Nielsen, Q. Zhou, M. M. Kramer, B. Basu, and Z. Zhang, "Optimal control of nonlinear wave energy point converters," *Ocean Engineering*, vol. 72, no. 0, pp. 176 – 187, 2013. [Online]. Available: http://www.sciencedirect.com/science/article/pii/S0029801813002758

[18] N. Tom and R. W. Yeung, "Non-linear model predictive control applied to a generic ocean-wave energy extractor," in *Proc. of 32nd International Conference on Ocean, Offshore and Arctic Engineering (OMAE2013)*, 2013.

[19] M. Richter, M. Magana, O. Sawodny, and T. Brekken, "Nonlinear model predictive control of a point absorber wave energy converter," *Sustainable Energy, IEEE Transactions on*, vol. 4, no. 1, pp. 118–126, Jan. 2013.

[20] J. Betts, *Practical Methods for Optimal Control Using Nonlinear Programming*, ser. Advances in design and control. Society for Industrial and Applied Mathematics, 2001.

[21] H. Eidsmoen, "Optimum control of a floating wave-energy converter with restricted amplitude," *Journal of Offshore Mechanics and Arctic Engineering*, vol. 118, no. 2, pp. 96–102, 1996. [Online]. Available: http://link.aip.org/link/?JOM/118/96/1

[22] S. H. Salter, J. R. M. Taylor, and N. J. Caldwell, "Power conversion mechanisms for wave energy," *Proceedings of the Institution of Mechanical Engineers, Part M: Journal of Engineering for the Maritime Environment*, vol. 216, no. 1, pp. 1–27, 2002. [Online]. Available: http://pim.sagepub.com/content/216/1/1.2.abstract

[23] J. Cruz, M. Rea, A. Sarmento, G. Thomas, and R. Henderson, *Ocean Wave Energy*, J. Cruz, Ed. Springer, 2008. [Online]. Available: http://dx.doi.org/10.1007/978-3-540-74895-3_5

[24] B. Czech and P. Bauer, "Wave energy converter concepts : Design challenges and classification," *Industrial Electronics Magazine, IEEE*, vol. 6, no. 2, pp. 4 –16, June 2012.

[25] K. Mohamed, N. Sahoo, and T. Ibrahim, "A survey of technologies used in wave energy conversion systems," in *Energy, Automation, and Signal (ICEAS), 2011 International Conference on*, dec. 2011, pp. 1 –6.

[26] F. Farley, R. Rainey, and J. Chaplin [ed.], "The peaks and troughs of wave energy: the dreams and the reality," *Special issue of Philosophical Transactions of the Royal Society A: Mathematical, Physical and Engineering Sciences*, vol. 370, no. 1959, pp. 201–529, January 2012. [Online]. Available: http://rsta.royalsocietypublishing.org/content/370/1959.toc

[27] M. Durand, A. Babarit, B. Pettinotti, O. Quillard, J. Toularastel, and A. Clément, "Experimental validation of the performances of the searev wave energy converter with real time latching control," in *7th European Wave and Tidal Energy Conference, EWTEC*, 2007.

[28] A. F. d. O. Falcão, "Phase control through load control of oscillating-body wave energy converters with hydraulic pto system," *Ocean Engineering*, vol. 35, no. 3-4, pp. 358–366, Mar. 2008. [Online]. Available: http://www.sciencedirect.com/science/article/B6V4F-4PXM6KB-1/2/6c0c0c83e8f3dd0a6b54c58482749d71

[29] A. Babarit, M. Guglielmi, and A. H. Clément, "Declutching control of a wave energy converter," *Ocean Engineering*, vol. 36, no. 12-13, pp. 1015–1024, Sep. 2009. [Online]. Available: http://www.sciencedirect.com/science/article/B6V4F-4WBK7KN-1/2/cb4ec850dbab08dba6ae8e48a9db5aaf

[30] R. Costello, J. V. Ringwood, and J. Webber, "Comparison of two alternative hydraulic pto concepts for wave energy conversion," in *9th European Wave and Tidal Energy Conference, EWTEC*, 2011.

[31] T. Ogilvie, "Recent progress toward the understanding and prediction of ship motions," in *Proc. Fifth Symposium on Naval Hydrodynamics, Bergen, Norway*, 1964.

[32] J. N. Newman, *Marine Hydrodynamics*. The MIT press, 1977.

[33] M. St. Denis and J. W. Pierson, "On the motions of ships in confused seas," *Trans. The Society of Naval Architects and Marine Engineers – SNAME*, vol. 61, pp. 280 – 357, 1953.

[34] J. Newman, *The exciting forces on fixed bodies in waves*. Washington, D.C. :Dept. of the Navy, David Taylor Model Basin,, 1963, no. 1717, http://www.biodiversitylibrary.org/bibliography/47501. [Online]. Available: http://www.biodiversitylibrary.org/item/102114

[35] L. Tick, "Differential equations with frequency dependent coefficients," *Ship Research*, vol. 3, no. 2, pp. 45–46, 1959.

[36] W. Cummins, "The impulse response function and ship motions.technical report 1961," *Schiffstechnik*, vol. 9, pp. 101–109, 1962.

[37] J. Falnes, "On non-causal impulse response functions related to propagating water waves," *Applied Ocean Research*, vol. 17, no. 6, pp. 379–389, Dec. 1995. [Online]. Available: http://www.sciencedirect.com/science/article/B6V1V-40SFM6N-5/1/78f6159cb0fecd254701a7d0800d48b3

[38] E. Kristiansen, A. Hjulstad, and O. Egeland, "State-space representation of radiation forces in time-domain vessel models," *Ocean Engineering*, vol. 32, no. 17-18, pp. 2195–2216, Dec. 2005. [Online]. Available: http://www.sciencedirect.com/science/article/B6V4F-4GCX1VT-3/1/23d6368eb9b15c26af6ee8e916c9dd0a

[39] C. J. Damaren, "Time-domain floating body dynamics by rational approximation of the radiation impedance and diffraction mapping," *Ocean Engineering*, vol. 27, no. 6, pp. 687–705, Jun. 2000. [Online]. Available: http://www.sciencedirect.com/science/article/B6V4F-3XG84MD-6/2/3c3c23354931b1b68a5fa699a18d7466

[40] T. Perez and T. I. Fossen, "Time- vs. frequency-domain identification of parametric radiation force models for marine structures at zero speed," *Modeling, Identification and Control*, vol. 29, no. 1, pp. 1–19, 2008.

[41] T. Burton, *Volterra Integral and Differential Equations*, ser. Mathematics in Science and Engineering. Elsevier, 2006, vol. 202. [Online]. Available: http://www.sciencedirect.com/science/article/pii/S0076539205800190

[42] P. J. v. d. Houwen and H. J. J. t. Riele, "Linear multistep methods for volterra integral and integro-differential equations," *Mathematics of Computation*, vol. 45, no. 172, pp. pp. 439–461, 1985. [Online]. Available: http://www.jstor.org/stable/2008135

[43] H. Brunner, "A survey of recent advances in the numerical treatment of volterra integral and integro-differential equations," *Journal of Computational and Applied Mathematics*, vol. 8, no. 3, pp. 213 – 229, 1982. [Online]. Available: http://www.sciencedirect.com/science/article/pii/0771050X82900444

[44] G. Duclos, A. Clément, and G. Chatry, "Absorption of outgoing waves in a numerical wave tank using a self-adaptive boundary condition," *International Journal of Offshore and Polar Engineering*, vol. 11, no. 3, pp. 168–175, September 2001.

[45] E. Jefferys, "Simulation of wave power devices," *Applied Ocean Research*, vol. 6, no. 1, pp. 31–39, Jan. 1984. [Online]. Available: http://www.sciencedirect.com/science/article/B6V1V-4803127-6/2/06d68e2d96de90bba294eade90c6a0dc

[46] T. Perez and T. I. Fossen, "Joint identification of infinite-frequency added mass and fluid-memory models of marine structures," *Modeling, Identification and Control*, vol. 29, no. 3, pp. 93–102, 2008.

[47] R. Taghipour, T. Perez, and T. Moan, "Hybrid frequency-time domain models for dynamic response analysis of marine structures," *Ocean Engineering*, vol. 35, no. 7, pp. 685–705, May 2008. [Online]. Available: http://www.sciencedirect.com/science/article/B6V4F-4R5W09B-1/1/defc033ccd3cedb56b48e35eb965a780

[48] R. Taghipour, "Efficient prediction of dynamic response for flexible and multi-body marine structures," Ph.D. dissertation, Norwegian University of Science and Technology, Department of Marine Technology, 2008, paper III is reprinted with kind permission from Elsevier, sciencedirect.com. [Online]. Available: http://urn.kb.se/resolve?urn=urn:nbn:no:ntnu:diva-2321

[49] T. Perez and T. I. Fossen, "Practical aspects of frequency-domain identification of dynamic models of marine structures from hydrodynamic data," *Ocean Engineering*,

vol. 38, no. 2-3, pp. 426–435, Feb. 2011. [Online]. Available: http://www.sciencedirect.com/science/article/B6V4F-51MCPMW-2/2/c9d6c6b733bd6ac900716d02f481ccb4

[50] ——, "A matlab toolbox for parametric identification of radiation-force models of ships and offshore structures," *Modeling, Identification and Control*, vol. 30, no. 1, pp. 1–15, 2009.

[51] K. Budal and J. Falnes, "A resonant point absorber of ocean-wave power," *Nature*, vol. 256, no. 5517, pp. 478–479, aug 1975, (With corrigendum in Vol.257, p.626).

[52] D. V. Evans, "A theory for wave-power absorption by oscillating bodies," *Journal of Fluid Mechanics Digital Archive*, vol. 77, no. 01, pp. 1–25, 1976. [Online]. Available: http://journals.cambridge.org/action/displayAbstract?aid=374123

[53] J. N. Newman, "The interaction of stationary vessels with regular waves," in *Proc of the Eleventh Symposium on Naval Hydrodynamics*. Office of Naval Research, London, 1976, pp. 491–501.

[54] K. Budal and J. Falnes, "Interacting point absorbers with controlled motion," in *Power from sea waves*, B. Count, Ed. London, UK: Academic Press., 1980, pp. 381–399.

[55] S. H. Salter, "Wave power," *Nature*, vol. 249, no. 5459, pp. 720–724, Jun. 1974. [Online]. Available: http://dx.doi.org/10.1038/249720a0

[56] D. V. Evans, "Power from water waves," *Annu. Rev. Fluid Mech.*, vol. 13, no. 1, pp. 157–, Jan. 1981. [Online]. Available: http://dx.doi.org/10.1146/annurev.fl.13.010181.001105

[57] C. C. Mei, "Power extraction from water waves," *Journal of Ship Research*, vol. 20, pp. 63–66, Jun. 1976.

[58] B. M. Count, "On the dynamics of wave-power devices," *Proceedings of the Royal Society of London. Series A, Mathematical and Physical Sciences*, vol. 363, no. 1715, pp. pp. 559–579, 1978. [Online]. Available: http://www.jstor.org/stable/79730

[59] I. Glendenning, "Wave energy," *Physical Science, Measurement and Instrumentation, Management and Education - Reviews, IEE Proceedings A*, vol. 127, no. 5, pp. 301 – 307, june 1980.

[60] J. Falnes, "Optimum control of oscillation of wave-energy converters," in *Annex Report B1: Device fundamentals/Hydrodynamics of the "Wave Energy Converters: Generic Technical Evaluation Study"*. Danish Wave Power Aps, 1993.

[61] F. W. King, *Hilbert Transform vol. 1*. Cambridge University Press, 2009.

[62] D. Evans, "Some theoretical aspects of three-dimensional wave-energy absorbers," in *First Symposium on Wave Energy Utilization, Gothenburg*. Chalmers University of Technology, 1979.

[63] J. Falnes, "Radiation impedance matrix and optimum power absorption for interacting oscillators in surface waves," *Applied Ocean Research*, vol. 2, no. 2, pp. 75–80, Apr. 1980. [Online]. Available: http://www.sciencedirect.com/science/article/B6V1V-47YVV8H-4/2/65fc8b0ba1fd466dcee3c663f11b86f4

[64] ——, "Principles for capture of energy from ocean waves. phase control and optimum oscillation." NTNU, Tech. Rep., 1997. [Online]. Available: http://folk.ntnu.no/falnes/web_arkiv/InstFysikk/phcontrl.pdf

[65] ——, "Optimum control of oscillation of wave-energy converters," in *Eleventh International Offshore and Polar Engineering Conference*, 2001.

[66] U. Korde, "Control system applications in wave energy conversion," in *Proc. ot the OCEANS 2000 MTS/IEEE Conference and Exhibition*, vol. 3, 2000, pp. 1817–1824 vol.3.

[67] S. H. Salter, "Power conversion systems for ducks," in *International Conference on Future Energy Concepts*, 1979, pp. 100–108.

[68] P. Nebel, "Maximizing the efficiency of wave-energy plant using complex-conjugate control," *Proc. of the Institution of Mechanical Engineers, Part I: Journal of Systems and Control Engineering*, vol. 206, no. 49, pp. 225–236, Jun. 1992. [Online]. Available: http://dx.doi.org/10.1243/PIME_PROC_1992_206_338_02

[69] J. Hals, T. Bjarte-Larsson, and J. Falnes, "Optimum reactive control and control by latching of a wave-absorbing semisubmerged heaving sphere," *ASME Conf. Proc.*, vol. 2002, no. 36142, pp. 415–423, Jan. 2002. [Online]. Available: http://link.aip.org/link/abstract/ASMECP/v2002/i36142/p415/s1

[70] J. Shek, D. Macpherson, and M. Mueller, "Phase and amplitude control of a linear generator for wave energy conversion," in *Power Electronics, Machines and Drives, 2008. PEMD 2008. 4th IET Conference on*, 2008, pp. 66–70.

[71] J. Shek, D. Macpherson, M. Mueller, and J. Xiang, "Reaction force control of a linear electrical generator for direct drive wave energy conversion," *Renewable Power Generation, IET*, vol. 1, no. 1, pp. 17–24, 2007.

[72] U. A. Korde, "On providing a reaction for efficient wave energy absorption by floating devices," *Applied Ocean Research*, vol. 21, no. 5, pp. 235–248, Oct. 1999. [Online]. Available: http://www.sciencedirect.com/science/article/B6V1V-3XDHHKB-2/2/82737e41cef1a81d047cc5fabc227c6c

[73] ——, "Systems of reactively loaded coupled oscillating bodies in wave energy conversion," *Applied Ocean Research*, vol. 25, no. 2, pp. 79–91, Apr. 2003. [Online]. Available: http://www.sciencedirect.com/science/article/B6V1V-495VGY7-1/2/9c977fa4b6062e3c8282f8f8af3f718d

[74] J. Falnes, "Wave-energy conversion through relative motion between two single-mode oscillating bodies," *Journal of Offshore Mechanics and Arctic Engineering*, vol. 121, no. 1, pp. 32–38, 1999. [Online]. Available: http://link.aip.org/link/?JOM/121/32/1

[75] P. Beirão, D. Valério, and J. Sá Da Costa, "Comparison of control strategies applied to the archimedes wave swing," in *European Control Conference*, 2007.

[76] ——, "Identification and phase and amplitude control of the archimedes wave swing using a pid and imc," in *Second International Conference on Electrical Engineering, Coimbra, ISEC*, 2007.

[77] D. Valério, P. Beirão, and J. Sá Da Costa, "Optimisation of wave energy extraction with the archimedes wave swing," *Ocean Engineering*, vol. 34, no. 17-18, pp. 2330–2344, Dec. 2007. [Online]. Available: http://www.sciencedirect.com/science/article/B6V4F-4NWNCX0-1/2/7dc498d63538d07ef473d4405132c980

[78] ——, "Reactive control and phase and amplitude control applied to the archimedes wave swing," in *17th International Offshore and Polar Engineering Confrence, ISOPE*, 2007.

[79] F. Wu, X. P. Zhang, P. Ju, and M. Sterling, "Optimal control for AWS-based wave energy conversion system," *Power Systems, IEEE Transactions on*, vol. 24, no. 4, pp. 1747 – 1755, nov. 2009.

[80] E. Tedeschi, M. Molinas, M. Carraro, and P. Mattavelli, "Analysis of power extraction from irregular waves by all-electric power take off," in *Energy Conversion Congress and Exposition (ECCE), 2010 IEEE*, sept. 2010, pp. 2370 –2377.

[81] E. Tedeschi, M. Carraro, M. Molinas, and P. Mattavelli, "Effect of control strategies and power take-off efficiency on the power capture from sea waves," *Energy Conversion, IEEE Transactions on*, vol. 26, no. 4, pp. 1088 –1098, dec. 2011.

[82] H. Yavuz, S. Mıstıkoğlu, and T. Stallard, "Processing irregular wave measurements to enhance point absorber power capture performance," *Ocean Engineering*, vol. 38, no. 4, pp. 684 – 698, 2011. [Online]. Available: http://www.sciencedirect.com/science/article/pii/S0029801810002866

[83] F. Fusco, J.-C. Gilloteaux, and J. V. Ringwood, "A study on prediction requirements in time-domain control of wave energy converters," in *Proceedings of Control Applications in Marine Systems (CAMS)*, 2010.

[84] F. Fusco and J. Ringwood, "A model for the sensitivity of non-causal control of wave energy converters to wave excitation force prediction errors," in *9th European Wave and Tidal Energy Conference, EWTEC*, 2011.

[85] F. Fusco and J. V. Ringwood, "Quantification of the prediction requirements in reactive control of wave energy converters," in *18th World Congress of the International Federation of Automatic Control (IFAC)*, 2011.

[86] F. Fusco and J. Ringwood, "A study of the prediction requirements in real-time control of wave energy converters," *Sustainable Energy, IEEE Transactions on*, vol. 3, no. 1, pp. 176 –184, jan. 2012.

[87] J. Eder, J. Bretl, and K. Edwards, "Empirical demonstration of acausal control strategies for wave energy converters," in *Proc. of 32nd International Conference on Ocean, Offshore and Arctic Engineering (OMAE2013)*, Nantes, France, 2013.

[88] B. Li, D. E. Macpherson, and J. K. H. Shek, "Direct drive wave energy converter control in irregular waves," in *Renewable Power Generation (RPG 2011), IET Conference on*, sept. 2011, pp. 1 –6.

[89] B. Li, R. Crozier, and E. Macpherson, "Reactive causal control of a linear generator in irregular waves for wave power system," in *9th European Wave and Tidal Energy Conference, EWTEC*, 2011.

[90] D. Montoya Andrade, A. García Santana, and A. de la Villa Jaén, "Frequency-matching assessment under reactive control on wave energy converters," in *4th International Conference on Ocean Energy, ICOE*, 2012.

[91] R. H. Hansen and M. M. Kramer, "Modelling and control of the wavestar prototype," in *9th European Wave and Tidal Energy Conference, EWTEC*, 2011.

[92] F. Fusco and J. V. Ringwood, "Suboptimal causal reactive control of wave energy converters using a second order system model," in *21st International Offshore (Ocean) and Polar Engineering Conference (ISOPE)*, 2011.

[93] S. Lattanzio and J. Scruggs, "Maximum power generation of a wave energy converter in a stochastic environment," in *Control Applications (CCA), 2011 IEEE International Conference on*, sept. 2011, pp. 1125 –1130.

[94] J. Scruggs and S. Lattanzio, "Optimal causal control of an ocean wave energy converter in stochastic waves," in *9th European Wave and Tidal Energy Conference, EWTEC*, 2011.

[95] M. Vantorre, R. Banasiak, and R. Verhoeven, "Modelling of hydraulic performance and wave energy extraction by a point absorber in heave," *Applied Ocean Research*, vol. 26, no. 1-2, pp. 61–72, 2004. [Online]. Available: http://www.sciencedirect.com/science/article/B6V1V-4DDXS0W-1/2/007bce4d8bcba164f33a815bb495cd69

[96] G. De Backer, M. Vantorre, R. Banasiak, J. De Rouck, C. Beels, and H. Verhaeghe, "Performance of a point absorber heaving with respect to a floating platform," in *7th European Wave and Tidal Energy Conference, EWTEC*, 2007.

[97] H. Yavuz, T. J. Stallard, A. P. McCabe, and G. A. Aggidis, "Time series analysis-based adaptive tuning techniques for a heaving wave energy converter in irregular seas," *Proceedings of the I MECH E Part A Journal of Power and Energy*, vol. 221, pp. 77–90(14), 2007. [Online]. Available: http://www.ingentaconnect.com/content/pep/jpe/2007/00000221/00000001/art00010

[98] J. A. Oskamp and H. T. Özkan Haller, "Power calculations for a passively tuned point absorber wave energy converter on the oregon coast," *Renewable Energy*, vol. 45, no. 0, pp. 72 – 77, 2012. [Online]. Available: http://www.sciencedirect.com/science/article/pii/S0960148112001383

[99] A. de Andrés, R. Guanche, J. Armesto, F. del Jesus, C. Vidal, and I. Losada, "Time domain model for a two-body heave converter: Model and applications," *Ocean Engineering*, vol. 72, no. 0, pp. 116 – 123, 2013. [Online]. Available: http://www.sciencedirect.com/science/article/pii/S0029801813002655

[100] R. Waters, M. Stalberg, O. Danielsson, O. Svensson, S. Gustafsson, E. Stromstedt, M. Eriksson, J. Sundberg, and M. Leijon, "Experimental results from sea trials of an offshore wave energy system," *Appl. Phys. Lett.*, vol. 90, no. 3, pp. 034 105–3, Jan. 2007. [Online]. Available: http://link.aip.org/link/?APL/90/034105/1

[101] M. Eriksson, R. Waters, O. Svensson, J. Isberg, and M. Leijon, "Wave power absorption: Experiments in open sea and simulation," *J. Appl. Phys.*, vol. 102, no. 8, pp. 084 910–5, Oct. 2007. [Online]. Available: http://link.aip.org/link/?JAP/102/084910/1

[102] J. Engström, V. Kurupath, J. Isberg, and M. Leijon, "A resonant two body system for a point absorbing wave energy converter with direct-driven linear generator," *Journal of Applied Physics*, vol. 110, no. 12, p. 124904, 2011. [Online]. Available: http://link.aip.org/link/?JAP/110/124904/1

[103] M. Stålberg, R. Waters, O. Danielsson, and M. Leijon, "Influence of generator damping on peak power and variance of power for a direct drive wave energy converter," *J. Offshore Mech. Arct. Eng.*, vol. 130, no. 3, pp. 031 003–4, Aug. 2008. [Online]. Available: http://link.aip.org/link/?JOM/130/031003/1

[104] C. Bostrom, R. Waters, E. Lejerskog, O. Svensson, M. Stalberg, E. Stromstedt, and M. Leijon, "Study of a wave energy converter connected to a nonlinear load," *Oceanic Engineering, IEEE Journal of*, vol. 34, no. 2, pp. 123 –127, april 2009.

[105] K. Schlemmer, F. Fuchshumer, N. Böhmer, R. Costello, and C. Villegas, "Design and control of a hydraulic power take-off for an axi-symmetric heaving point absorber," in *9th European Wave and Tidal Energy Conference, EWTEC*, 2011.

[106] C. Cargo, "Optimal design of a wec hydraulic power take-off unit in irregular waves," in *9th European Wave and Tidal Energy Conference, EWTEC*, 2011.

[107] C. J. Cargo, A. R. Plummer, A. J. Hillis, and M. Schlotter, "Determination of optimal parameters for a hydraulic power take-off unit of a wave energy converter in regular waves," *Proceedings of the Institution of Mechanical Engineers, Part A: Journal of Power and Energy*, vol. 226, no. 1, pp. 98–111, 2012. [Online]. Available: http://pia.sagepub.com/content/226/1/98.abstract

[108] D. Guenther, D. Jones, and D. Brown, "An investigative study of a wave-energy device," in *(University of Illinois and U.S. Department of Energy, Midwest Energy Conference, Chicago, Ill., Nov. 19-21, 1978.) Energy (UK), vol. 4, Apr. 1979, p. 299-306.*, vol. 4, Apr. 1979, pp. 299–306.

[109] M. J. French, "A generalized view of resonant energy transfer," *Journal of Mechanical Engineering Science*, vol. 21, pp. 299–300, 1979.

[110] A. Babarit, G. Duclos, and A. Clément, "Comparison of latching control strategies for a heaving wave energy device in random sea," *Applied Ocean Research*, vol. 26, no. 5, pp. 227–238, Jul. 2004. [Online]. Available: http://www.sciencedirect.com/science/article/B6V1V-4GSC2JW-1/2/d660fd4605b9fe398b19a243cde3ac40

[111] A. Babarit and A. Clément, "Optimal latching control of a wave energy device in regular and irregular waves," *Applied Ocean Research*, vol. 28, no. 2, pp.

77–91, Apr. 2006. [Online]. Available: http://www.sciencedirect.com/science/article/B6V1V-4KFMMC8-1/2/ed3a41a3492e2df5d08728fd5d480993

[112] A. H. Clément and A. Babarit, "Discrete control of resonant wave energy devices," *Philosophical Transactions of the Royal Society A: Mathematical,Physical and Engineering Sciences*, vol. 370, no. 1959, pp. 288–314, 2012. [Online]. Available: http://rsta.royalsocietypublishing.org/content/370/1959/288.abstract

[113] J. A. M. Cretel, A. Lewis, G. Thomas, and G. Lightbody, "A critical assessment of latching as control strategy for wave-energy point absorbers," in *21st International Offshore and Polar Engineering Conference, ISOPE*, 2011.

[114] M. Greenhow and S. P. White, "Optimal heave motion of some axisymmetric wave energy devices in sinusoidal waves," *Applied Ocean Research*, vol. 19, no. 3-4, pp. 141–159, 1997. [Online]. Available: http://www.sciencedirect.com/science/article/B6V1V-3SNMR88-1/2/367d454746257cc937f89968fd7a2689

[115] T. Mundon, A. Murray, J. Hallam, and L. Patel, "Causal neural control of a latching ocean wave point absorber," *Artificial Neural Networks: Formal Models and Their Applications - ICANN 2005*, vol. 3697, pp. 423–429, 2005. [Online]. Available: http://dx.doi.org/10.1007/11550907_67

[116] M. Molinas, O. Skjervheim, P. Andreasen, T. Undeland, J. Hals, T. Moan, and B. Sorby, "Power electronics as grid interface for actively controlled wave energy converters," in *International Conference on Clean Electrical Power, 2007. ICCEP '07.*, O. Skjervheim, Ed., 2007, pp. 188–195.

[117] F. Kara, "Time domain prediction of power absorption from ocean waves with latching control," *Renewable Energy*, vol. 35, no. 2, pp. 423–434, Feb. 2010. [Online]. Available: http://www.sciencedirect.com/science/article/B6V4S-4WNGD7D-1/2/ff2eae72856314f8dca04d8105897c34

[118] A. F. d. O. Falcão, P. A. P. Justino, J. C. C. Henriques, and J. M. C. S. André, "Reactive versus latching phase control of a two-body heaving wave energy converter," in *European Control Conference*, 2009.

[119] J. J. Cândido and P. A. Justino, "Modelling, control and pontryagin maximum principle for a two-body wave energy device," *Renewable Energy*, vol. 36, no. 5, pp. 1545–1557, May 2011. [Online]. Available: http://www.sciencedirect.com/science/article/pii/S096014811000515X

[120] J. C. C. Henriques, M. F. P. Lopes, R. P. F. Gomes, L. L. M. Gato, and A. F. d. O. Falcão, "Performance evaluation of a two-body heaving wec with latching control using a new numerical method," in *9th European Wave and Tidal Energy Conference, EWTEC*, 2011.

[121] J. Henriques, M. Lopes, R. Gomes, L. Gato, and A. Falcão, "On the annual wave energy absorption by two-body heaving wecs with latching control," *Renewable Energy*, vol. 45, no. 0, pp. 31 – 40, 2012. [Online]. Available: http://www.sciencedirect.com/science/article/pii/S0960148112001322

[122] U. A. Korde, "Phase control of floating bodies from an on-board reference," *Applied Ocean Research*, vol. 23, no. 5, pp. 251–262, Oct. 2001. [Online]. Available: http://www.sciencedirect.com/science/article/B6V1V-44HXBXT-1/2/8aadbf7da7cda06bfca23649223b1457

[123] ——, "Latching control of deep water wave energy devices using an active reference," *Ocean Engineering*, vol. 29, no. 11, pp. 1343–1355, Sep. 2002. [Online]. Available: http://www.sciencedirect.com/science/article/B6V4F-44J697J-5/2/d13ab9d965f11040618515a6967f8c47

[124] J. Hals, R. Taghipour, and T. Moan, "Dynamics of a force-compensated two-body wave energy converter in heave with hydraulic power take-off subject to phase control," in *7th European Wave and Tidal Energy Conference, EWTEC*, September 2007.

[125] T. Bjarte-Larsson and J. Falnes, "Investigation of phase-controlled wave-power buoy," in *6th European Wave and Tidal Energy Conference, EWTEC*, 2005.

[126] J. Falnes and T. Bjarte-Larsson, "Theoretical and experimental investigation of wave energy conversion by a phase-controlled heaving body," *Proceedings of the I MECH E Part M*, vol. 220, pp. 175–183(9), 2006.

[127] T. Bjarte-Larsson and J. Falnes, "Laboratory experiment on heaving body with hydraulic power take-off and latching control," *Ocean Engineering*, vol. 33, no. 7, pp. 847–877, May 2006. [Online]. Available: http://www.sciencedirect.com/science/article/B6V4F-4HB4DNX-1/2/4c042dc080d4e021fb4fc676707bc51c

[128] J. Falnes and P. M. Lillebekken, "Budal's latching-controlled-buoy type wave-power plant," in *5th European Wave and Tidal Energy Conference, EWTEC*, 2003.

[129] H. Lendenmann, K.-C. Strømsem, M. Dai Pre, W. Arshad, A. Leirbukt, G. Tjensvoll, and T. Gulli, "Direct generation wave energy converters for optimized electrical power production," in *7th European Wave and Tidal Energy Conference, EWTEC*, 2007.

[130] P. Beirão, D. Valério, and J. Sá Da Costa, "Phase control by latching applied to the archimedes wave swing." in *Controlo 2006. Lisboa: 7th Portuguese Conference on Automatic Control*, 2006.

[131] D. Valério, P. Beirão, M. J. G. C. Mendes, and J. Sá Da Costa, "Robustness assessment of model-based control for the archimedes wave swing," in *European Control Conference*, 2009.

[132] A. Babarit and A. H. Clément, "Otpimal latching control of a wave energy converter," in *6th European Wave and Tidal Energy Conference, EWTEC*, 2005.

[133] M. Kamensky, M. Guglielmi, and A. Formal'skii, "Optimal switching control of an absorber ocean wave energy device," in *Control and Automation, 2008 16th Mediterranean Conference on*, 2008, pp. 785–790.

[134] A. Babarit, G. Duclos, A. Clément, and J. Gilloteaux, "Latching control of a power take off oscillator carried by a wave activated body," in *International Workshop on Water Waves and Floating Bodies, IWWWFB, Longyearbyen, Norway*, 2005.

[135] A. Babarit and A. Clément, "Application of the optimal command method to the control of searev wave energy converter : a study on the influence of time constants on the efficiency of latching control." in *European Control Conference*, 2009.

[136] H. Eidsmoen, "Simulation of a tight-moored amplitude limited heaving-buoy wave-energy converter with phase control," Norwegian University of Science and Technology, NTNU, Tech. Rep., 1996.

[137] ——, "Simulation of a slack-moored heaving-buoy wave- energy converter with phase control," Division of Physics, Norwegian University of Science and Technology NTNU, Trondheim, Norway, Technical report, 1996. [Online]. Available: http://folk.ntnu.no/falnes/web_arkiv/InstFysikk/simconve.pdf

[138] ——, "Tight-moored amplitude-limited heaving-buoy wave-energy converter with phase control," *Applied Ocean Research*, vol. 20, no. 3, pp. 157–161, Jun. 1998. [Online]. Available: http://www.sciencedirect.com/science/article/B6V1V-3TN44S4-4/2/39a291a2dd6f32a348cb1cbd6665a641

[139] A. Babarit, H. Mouslim, M. Guglielmi, and C. A.H., "Simulation of the searev wave energy converter with a by-pass control of its hydraulic power-take-off," in *Proc. World Renewable Energy Congress, Glasgow*, 2008.

[140] M. Folley and T. Whittaker, "The control of wave energy converters using active bipolar damping," *Proceedings of the Institution of Mechanical Engineers, Part M: Journal of Engineering for the Maritime Environment*, vol. 223, no. 4, pp. 479–487, Nov. 2009. [Online]. Available: http://dx.doi.org/10.1243/14750902JEME169

[141] K. J. Gunn, C. J. Taylor, and C. Lingwood, "An independent validation of the optimality of latching and de-clutching control by evolutionary methods," in *9th European Wave and Tidal Energy Conference, EWTEC*, 2011.

[142] G. A. Nolan, R. J. V., E. W. Leithead, and S. Butler, "Optimal damping profile for a heaving buoy wave energy converter," in *The Fifteenth International Offshore and Polar Engineering Conference*, 2005.

[143] B. Teillant, J.-C. Gilloteaux, and R. J. V., "Optimal damping profile for a heaving buoy wave energy converter," in *IFAC Conference on Control Applications in Marine Systems (CAMS)*, 2010. [Online]. Available: http://rian.ie/en/item/redirect/record_id/53391

[144] P. Beirão, M. J. G. C. Mendes, D. Valério, and J. Sá Da Costa, "Control of the archimedes wave swing using neural networks," in *7th European Wave and Tidal Energy Conference, EWTEC*, 2007.

[145] D. Valério, M. J. Mendes, P. Beirão, and J. S. da Costa, "Identification and control of the aws using neural network models," *Applied Ocean Research*, vol. 30, no. 3, pp. 178 – 188, 2008. [Online]. Available: http://www.sciencedirect.com/science/article/pii/S0141118708000679

[146] A. F. d. O. Falcão, "Modelling and control of oscillating-body wave energy converters with hydraulic power take-off and gas accumulator," *Ocean Engineering*, vol. 34, no. 14-15, pp. 2021–2032, Oct. 2007. [Online]. Available: http://www.sciencedirect.com/science/article/B6V4F-4NFXDRN-1/2/33fff3f7f03c02ce90f17ee04ab30454

[147] G. Duclos, A. Babarit, and A. H. Clement, "Optimizing the power take off of a wave energy converter with regard to the wave climate," *Journal of Offshore Mechanics and Arctic Engineering*, vol. 128, no. 1, pp. 56–64, 2006. [Online]. Available: http://link.aip.org/link/?JOM/128/56/1

[148] M. Schoen, J. Hals, and T. Moan, "Wave prediction and fuzzy logic control of wave energy converters in irregular waves," in *Control and Automation, 2008 16th Mediterranean Conference on*, 2008, pp. 767–772.

[149] ——, "Robust control of heaving wave energy devices in irregular waves," in *Control and Automation, 2008 16th Mediterranean Conference on*, 2008, pp. 779–784.

[150] ——, "Wave prediction and robust control of heaving wave energy devices for irregular waves," *Energy Conversion, IEEE Transactions on*, vol. 26, no. 2, pp. 627 –638, june 2011.

[151] T. R. Mundon, A. F. Murray, and R. Wallace, "Toward a biologically inspired, neural control mechanism for multiple degree of freedom wave energy converters," in *9th European Wave and Tidal Energy Conference, EWTEC*, 2011.

[152] K. Ahn, D. Truong, H. H. Tien, and J. I. Yoon, "An innovative design of wave energy converter," *Renewable Energy*, vol. 42, no. 0, pp. 186 – 194, 2012, <ce:title>International Symposium on Low Carbon and Renewable Energy Technology 2010 (ISLCT 2010)</ce:title>. [Online]. Available: http://www.sciencedirect.com/science/article/pii/S0960148111004642

[153] E. Ozkop, I. Altas, and A. Sharaf, "A novel fuzzy logic tansigmoid controller for wave energy converter-grid interface dc energy utilization farm," in *Electrical and Computer Engineering, 2009. CCECE '09. Canadian Conference on*, may 2009, pp. 1184 –1187.

[154] A. Sharaf and A. El-Gammal, "Optimal variable structure self regulating PSO-controller for stand-alone wave energy conversion scheme," in *Mathematical/Analytical Modelling and Computer Simulation (AMS), 2010 Fourth Asia International Conference on*, may 2010, pp. 438 –443.

[155] J. J. Cândido and P. A. P. Justino, "Frequency, stochastic and time domain models for an articulated wave power device," *ASME Conference Proceedings*, vol. 2008, no. 48234, pp. 633–643, 2008. [Online]. Available: http://link.aip.org/link/abstract/ASMECP/v2008/i48234/p633/s1

[156] J. J. Cândido and P. A. P. S. Justino, "Stochastic, time domain models and pontryagin maximum principle for a two body wave power device," in *8th European Wave and Tidal Energy Conference, EWTEC*, 2009.

[157] C. J. Taylor, M. A. Stables, P. Cross, K. Gunn, and G. A. Aggidis, "Linear and nonlinear modeling and control of a power take-off simulation for wave energy conversion," in *8th European Wave and Tidal Energy Conference, EWTEC*, 2009.

[158] P. Cross, C. J. Taylor, and G. A. Aggidis, "State dependent feed–forward control for wave energy conversion," in *9th European Wave and Tidal Energy Conference, EWTEC*, 2011.

[159] K. Gunn, C. J. Taylor, and C. Lingwood, "Evolutionary algorithms for the development and optimisation of wave energy converter control systems," in *8th European Wave and Tidal Energy Conference, EWTEC*, 2009.

[160] P. Ricci, J. Lopez, M. Santos, J. L. Villate, P. Ruiz-Minguela, F. Salcedo, and A. F. de O. Falcão, "Control strategies for a simple point-absorber connected to a hydraulic power take-off," in *8th European Wave and Tidal Energy Conference, EWTEC*, 2009.

[161] P. Ricci, J. Lopez, M. Santos, P. Ruiz-Minguela, J. Villate, F. Salcedo, and A. de O Falcã ando, "Control strategies for a wave energy converter connected to a hydraulic power take-off," *Renewable Power Generation, IET*, vol. 5, no. 3, pp. 234 –244, may 2011.

[162] E. Amon, A. Schacher, and T. Brekken, "A novel maximum power point tracking algorithm for ocean wave energy devices," in *Energy Conversion Congress and Exposition, 2009. ECCE 2009. IEEE*, sept. 2009, pp. 2635 –2641.

[163] B. Orazov, O. O'Reilly, and Ö. Savas, "On the dynamics of a novel ocean wave energy converter," *Journal of Sound and Vibration*, vol. 329, no. 24, pp. 5058–5069, Nov. 2010. [Online]. Available: http://www.sciencedirect.com/science/article/B6WM3-50KMVSW-2/2/20266b4d309484fdfb446de664956073

[164] P. R. Costa, P. B. Garcia-Rosa, and S. F. Estefen, "Phase control strategy for a wave energy hyperbaric converter," *Ocean Engineering*, vol. 37, no. 17–18, pp. 1483 – 1490, 2010. [Online]. Available: http://www.sciencedirect.com/science/article/pii/S002980181000168X

[165] C. Villegas and H. van der Schaaf, "Implementation of pitch stability control for a wave energy converter," in *9th European Wave and Tidal Energy Conference, EWTEC*, 2011.

[166] T. Lewis, A. von Jouanne, and T. Brekken, "Wave energy converter with wideband power absorption," in *Energy Conversion Congress and Exposition (ECCE), 2011 IEEE*, sept. 2011, pp. 3844 –3851.

[167] M. R. Belmont, "A lower bound estimate of the gains stemming from quiescent period predictive control using conventional sea state statistics," *Journal of Renewable and Sustainable Energy*, vol. 1, no. 6, p. 063104, 2009. [Online]. Available: http://link.aip.org/link/?RSE/1/063104/1

[168] M. Belmont, "Increases in the average power output of wave energy converters using quiescent period predictive control," *Renewable Energy*, vol. 35, no. 12, pp. 2812–2820, Dec. 2010. [Online]. Available: http://www.sciencedirect.com/science/article/B6V4S-50867J7-2/2/bc2e4600ef4e8abfed4f7e4619861727

[169] J. Newman, "Absorption of wave energy by elongated bodies," *Applied Ocean Research*, vol. 1, no. 4, pp. 189 – 196, 1979. [Online]. Available: http://www.sciencedirect.com/science/article/pii/0141118779900269

[170] D. Evans, "Maximum wave-power absorption under motion constraints," *Applied Ocean Research*, vol. 3, no. 4, pp. 200–203, Oct. 1981. [Online]. Available: http://www.sciencedirect.com/science/article/B6V1V-4816TBH-24/2/b81da13cab0165d97e4d81d93de23c41

[171] D. Pizer, "Maximum wave-power absorption of point absorbers under motion constraints," *Applied Ocean Research*, vol. 15, no. 4, pp. 227–234, 1993. [Online]. Available: http://www.sciencedirect.com/science/article/B6V1V-4816TFX-35/2/08c7b175b96395b9c6861b945d989ed9

[172] U. Korde, "Use of oscillation constraints in providing a reaction for deep water floating wave energy devices," *International Journal of Offshore and Polar Engineering*, vol. 11, no. 2, pp. 1473 – 1484, 2001.

[173] G. De Backer, "Hydrodynamic design optimization of wave energy converters consisting of heaving point absorbers," Ph.D. dissertation, Ghent University. Faculty of Engineering, 2009. [Online]. Available: https://biblio.ugent.be/publication/1006160

[174] J. Scruggs, "Multi-objective optimal causal control of an ocean wave energy converter in random waves," in *OCEANS 2011*, sept. 2011, pp. 1 –6.

[175] J. Hals, J. Falnes, and T. Moan, "Constrained optimal control of a heaving buoy wave-energy converter," *Journal of Offshore Mechanics and Arctic Engineering*, vol. 133, no. 1, p. 011401, 2011. [Online]. Available: http://link.aip.org/link/?JOM/133/011401/1

[176] J. A. M. Cretel, G. Lightbody, G. P. Thomas, and A. W. Lewis, "Maximisation of energy capture by a wave-energy point absorber using model predictive control," in *IFAC World Congress*, 2011.

[177] T. Brekken, "On model predictive control for a point absorber wave energy converter," in *PowerTech, 2011 IEEE Trondheim*, june 2011, pp. 1 –8.

[178] J. Newman, "The low-frequency limit for wave-power systems," *Applied Ocean Research*, vol. 5, no. 1, pp. 38–44, 1983. [Online]. Available: http://www.sciencedirect.com/science/article/pii/0141118783900561

[179] J. Falnes and K. Budal, "Wave-power absorption by parallel rows of interacting oscillating bodies," *Applied Ocean Research*, vol. 4, no. 4, pp. 194–207, 1982. [Online]. Available: http://www.sciencedirect.com/science/article/pii/S0141118782800266

[180] J. Falnes, "Wave-power absorption by an array of attenuators oscillating with unconstrained amplitudes," *Applied Ocean Research*, vol. 6, no. 1, pp. 16–22, 1984. [Online]. Available: http://www.sciencedirect.com/science/article/pii/0141118784900245

[181] C. Fitzgerald and G. P. Thomas, "A preliminary study of the optimal formation of an array of wave power devices," in *7th European Wave and Tidal Energy Conference, EWTEC*, 2007.

[182] P. A. Justino and A. Clément, "Hydrodynamic performance for small arrays of submerged spheres," in *5th European Wave and Tidal Energy Conference, EWTEC*, 2003, pp. 266–273.

[183] A. Z. Annuar, D. E. Macpherson, D. I. M. Forehand, and M. A. Mueller, "Optimum power control for arrays of direct drive wave energy converters," in *6th IET International Conference on Power Electronics, Machines and Drives, PEMD*, Mar. 2012, pp. 1–6.

[184] P. Ricci, J.-B. Saulnier, and A. F. de O. Falcão, "Point-absorber arrays: a configuration study off the portuguese west-coast," in *7th European Wave and Tidal Energy Conference, EWTEC*, 2007.

[185] J. Cruz, R. Sykes, P. Siddorn, and R. Eatock Taylor, "Wave farm design: Preliminary studies on the influences of wave climate, array layout and farm control," in *8th European Wave and Tidal Energy Conference, EWTEC*, 2009.

[186] J. Cruz, R. Sykes, P. Siddorn, and R. Taylor, "Estimating the loads and energy yield of arrays of wave energy converters under realistic seas," *Renewable Power Generation, IET*, vol. 4, no. 6, pp. 488–497, Nov. 2010.

[187] R. Antonutti and G. E. Hearn, "Optimisation of point-absorber arrays," in *9th European Wave and Tidal Energy Conference, EWTEC*, 2011.

[188] B. Child and V. Venugopal, "Non-optimal tuning of wave energy device arrays," in *2nd International Conference on Ocean Energy, ICOE*, 2008.

[189] ——, "Optimal configurations of wave energy device arrays," *Ocean Engineering*, vol. 37, no. 16, pp. 1402 – 1417, 2010. [Online]. Available: http://www.sciencedirect.com/science/article/pii/S0029801810001447

[190] P. C. Vicente, A. F. d. O. Falcão, and P. A. Justino, "A time domain analysis of arrays of floating point-absorber wave energy converters including the effect of nonlinear mooring forces," in *3rd International Conference on Ocean Energy, ICOE*, 2010.

[191] B. Borgarino, A. Babarit, and P. Ferrant, "Impact of wave interactions effects on energy absorption in large arrays of wave energy converters," *Ocean Engineering*, vol. 41, no. 0, pp. 79 – 88, 2012. [Online]. Available: http://www.sciencedirect.com/science/article/pii/S0029801812000054

[192] S. Bellew, T. Stallard, and P. Stansby, "Optimisation of a heterogeneous array of heaving bodies," in *8th European Wave and Tidal Energy Conference, EWTEC*, 2009.

[193] G. De Backer, M. Vantorre, C. Beels, J. De Rouck, and P. Frigaard, "Performance of closely spaced point absorbers with constrained floater motion," in *8th European Wave and Tidal Energy Conference, EWTEC*, 2009.

[194] ——, "Power absorption by closely spaced point absorbers in constrained conditions," *Renewable Power Generation, IET*, vol. 4, no. 6, pp. 579–591, Nov. 2010.

[195] M. Folley and T. Whittaker, "The effect of sub-optimal control and the spectral wave climate on the performance of wave energy converter arrays," *Applied Ocean Research*, vol. 31, no. 4, pp. 260 – 266, 2009, <ce:title>Renewable Energy: Leveraging Ocean and Waterways</ce:title> <ce:subtitle>Renewable Energy</ce:subtitle>. [Online]. Available: http://www.sciencedirect.com/science/article/pii/S0141118709000947

[196] A. Babarit, B. Borgarino, P. Ferrant, and A. Clément, "Assessment of the influence of the distance between two wave energy converters on energy production," *Renewable Power Generation, IET*, vol. 4, no. 6, pp. 592–601, Nov. 2010.

[197] A. Blavette, D. O'Sullivan, M. Egan, and A. Lewis, "Grid compliance of ocean energy converters: Control strategies and recommendations," in *9th European Wave and Tidal Energy Conference, EWTEC*, 2011.

[198] F. Wu, X.-P. Zhang, P. Ju, and M. Sterling, "Modeling and control of AWS-based wave energy conversion system integrated into power grid," *Power Systems, IEEE Transactions on*, vol. 23, no. 3, pp. 1196 –1204, aug. 2008.

[199] L. Alberti, E. Tedeschi, N. Bianchi, M. Santos, and A. Fasolo, "Effect of the generator sizing on a wave energy converter considering different control strategies," *COMPEL: The International Journal for Computation and Mathematics in Electrical and Electronic Engineering*, vol. 32, no. 1, pp. 233–247, 2013.

[200] V. C. Tai, P. C. See, S. Merle, and M. Molinas, "Sizing and control of the electric power take off for a buoy type point absorber wave energy converter," in *International Conference on Renewable Energies and Power Qualities ICREPQ'12*, 2012.

[201] M. Santos, E. Tedeschi, P. Ricci, M. Molinas, and J. Martín, "Grid connection improvements by control strategy selection for wave energy converters," in *INTERNATIONAL CONFERENCE ON RENEWABLE ENERGIES AND POWER QUALITY (ICREPQ'11)*, 2011.

[202] M. Santos, F. Salcedo, Tedeschi, E. Robles, and J. Villate, "Centralized control of a wave energy farm," in *Proc. International Conference on Renewable Energies and Power Quality (ICREPQ)*, Santiago de Compostela (Spain), 2012.

[203] E. Tedeschi, M. Santos, P. Ricci, M. Molinas, and J. L. Villate, "Control strategies for the grid integration of wave energy converters at the biscay marine energy platform," in *9th European Wave and Tidal Energy Conference, EWTEC*, 2011.

[204] J. Van den Berg, P. Ricci, E. Tedeschi, I. Touzon, and J. L. Villate, "Control strategies for improving power performance of two-body heaving wave energy devices," in *21st International Offshore and Polar Engineering Conference, ISOPE*, 2011.

[205] E. Tedeschi and M. Molinas, "Impact of control strategies on the rating of electric power take off for wave energy conversion," in *Industrial Electronics (ISIE), 2010 IEEE International Symposium on*, july 2010, pp. 2406 –2411.

[206] ——, "Tunable control strategy for wave energy converters with limited power takeoff rating," *Industrial Electronics, IEEE Transactions on*, vol. 59, no. 10, pp. 3838 –3846, oct. 2012.

[207] D. Valerio, P. Beirao, M. Mendes, and J. Sa da Costa, "Comparison of control strategies performance for a wave energy converter," in *Control and Automation, 2008 16th Mediterranean Conference on*, june 2008, pp. 773 –778.

[208] J. Hals, J. Falnes, and T. Moan, "A comparison of selected strategies for adaptive control of wave energy converters," *Journal of Offshore Mechanics and Arctic Engineering*, vol. 133, no. 3, p. 031101, 2011. [Online]. Available: http://link.aip.org/link/?JOM/133/031101/1

[209] A. S. Zurkinden, S. H. Lambertsen, L. Damkilde, Z. Gao, and T. Moan, "Fatigue analysis of a wave energy converter taking into account different control strategies," in *Proc. of 32nd International Conference on Ocean, Offshore and Arctic Engineering (OMAE2013)*. Nantes, France: ASME, 2013.

[210] R. Stengel, *Optimal Control and Estimation*, ser. Dover books on advanced mathematics. Dover Publications, 1986. [Online]. Available: http://books.google.ie/books?id=jDjPxqm7Lw0C

[211] H. Sussmann and J. Willems, "300 years of optimal control: from the brachystochrone to the maximum principle," *Control Systems, IEEE*, vol. 17, no. 3, pp. 32–44, 1997.

[212] R. Bellman, *Dynamic Programming*. Princeton University Press, 1957.

[213] I. M. Ross, *A Primer on Pontryagin's Principle in Optimal Control*. Collegiate Publishers, 2009.

[214] D. A. Benson, "A gauss pseudospectral transcription for optimal control," Ph.D. dissertation, Massachusetts Institute Of Technology, 2005.

[215] F. Fahroo and I. M. Ross, "Costate estimation by a legendre pseudospectral method," *Journal of Guidance, Control, and Dynamics*, vol. 24, no. 2, pp. 270–277, Mar. 2001. [Online]. Available: http://dx.doi.org/10.2514/2.4709

[216] J. P. Boyd, *Chebyshev and Fourier Spectral Methods*. Dover Publications, 2001.

[217] G. Hicks and W. Ray, "Approximation methods for optimal control systems," *Can. J. Chem. Engng.*, vol. 49, pp. 522–528, 1971.

[218] R. Sargent and G. Sullivan, "The development of an efficient optimal control package," in *Proc. of the 8th IFIP Conference on Optimization Techniques*, Heidelberg, 1977.

[219] H. Bock and K. Plitt, "A multiple shooting algorithm for direct solution of optimal control problems," in *Proc. of 9th IFAC World Congress, Budapest*, 1984.

[220] C. Canuto, Y. Hussaini, A. Quarteroni, and T. Zang, *Spectral Methods: Fundamentals in Single Domains*, ser. Scientific Computation. Springer, 2006.

[221] L. N. Trefethen, *Spectral Methods in MATLAB*. SIAM, Philadelphia, 2000.

[222] J. Nocedal and S. J. Wright, *Numerical Optimization*, 2nd ed. New York: Springer, 2006.

[223] S. Boyd and L. Vandenberghe, *Convex Optimization*. Cambridge University Press, 2004.

[224] I. M. Ross, "A roadmap for optimal control: The right way to commute," *Annals of the New York Academy of Sciences*, vol. 1065, no. 1, pp. 210–231, 2005. [Online]. Available: http://dx.doi.org/10.1196/annals.1370.015

[225] G. Bacelli, J. V. Ringwood, and J.-C. Gilloteaux, "A control system for a self-reacting point absorber wave energy converter subject to constraints," in *IFAC World Congress, Milan*, vol. 18, 2011, pp. 11 387–11 392.

[226] *WAMIT Inc. USA*, 2011. [Online]. Available: www.wamit.com

[227] J. Journée and W. Massie, *Offshore Hydromechanics*. Delft University of Technologyy, 2001.

[228] R. Blevins, *Applied Fluid Dynamics Handbook*. Krieger Publishing Company, 1992.

[229] G. Elnagar, M. Kazemi, and M. Razzaghi, "The pseudospectral legendre method for discretizing optimal control problems," *Automatic Control, IEEE Transactions on*, vol. 40, pp. 1793–1796, 1995.

[230] I. M. Ross and M. Karpenko, "A review of pseudospectral optimal control: From theory to flight," *Annual Reviews in Control*, vol. 36, no. 2, pp. 182 – 197, 2012. [Online]. Available: http://www.sciencedirect.com/science/article/pii/S1367578812000375

[231] D. Garg, M. Patterson, W. W. Hager, A. V. Rao, D. A. Benson, and G. T. Huntington, "A unified framework for the numerical solution of optimal control problems using pseudospectral methods," *Automatica*, vol. 46, no. 11, pp. 1843 – 1851, 2010. [Online]. Available: http://www.sciencedirect.com/science/article/pii/S0005109810002980

[232] G. N. Elnagar and M. A. Kazemi, "Nonlinear periodic optimal control: A pseudospectral fourier approach," *Numerical Functional Analysis and Optimization*, vol. 25, no. 7-8, pp. 707–724, 2005.

[233] J. F. Douglas, J. Gasiorek, and J. Swaffield, *Fluid Mechanics, 5th ed.* Pearson/Prentice Hall, 2005.

[234] G. M. Terra, W. J. van de Berg, and L. R. M. Maas, "Experimental verification of lorentz' linearization procedure for quadratic friction," *Fluid Dynamics Research*, vol. 36, pp. 175–188, 1995.

[235] H. Kwakernaak and R. Sivan, *Linear optimal control systems*. Wiley-Interscience New York, 1972, vol. 172.

[236] M. Folley and T. Whittaker, "The adequacy of phase-averaged models for modelling wave farms," in *30th International Conference on Ocean, Offshore and Arctic Engineering (OMAE2011)*, no. 44373. ASME, 2011, pp. 663–671. [Online]. Available: http://link.aip.org/link/abstract/ASMECP/v2011/i44373/p663/s1

[237] A. Babarit, "Impact of long separating distances on the energy production of two interacting wave energy converters," *Ocean Engineering*, vol. 37, no. 8–9, pp. 718–729, 2010.

[238] R. A. Horn and C. R. Johnson, *Matrix Analysis*. Cambridge University Press, 1990.

[239] A. F. Timan, *Theory Of Approximation Of Functions Of A Real Variable*. Courier Dover Publications, 1994.